UNIVERSITE SIDI MOHAMED BEN ABDELLAH
FACULTE DES SCIENCES ET TECHNIQUES - FES
Centre d'Etudes Doctorales : Sciences et Techniques de l'Ingénieur

Fès, le 03 décembre 2016

N° d'ordre 39/2016

THESE DE DOCTORAT

Dans le cadre d'une cotutelle entre l'Université Sidi Mohamed Ben Abdellah
&
l'Université de Lyon

Présentée par

Mr. ZERGOUNE Zakaria

Spécialité : Mécanique

Sujet de la thèse : Approche méso-macro pour la modélisation de la transmission acoustique des sandwiches

Thèse présentée et soutenue le samedi 03 décembre 2016 à 9h devant le jury composé de :

Nom & Prénom	Titre	Etablissement	
EL KADIRI Mounia	Professeur d'enseignement supérieur	EMI - Rabat	Présidente
ABOUTAJEDDINE Ahmed	Professeur d'enseignement supérieur	FST - Fès	Rapporteurs
BOJJI Chakib	Professeur d'enseignement supérieur	ENSET - Rabat	
BOUHADDI Noureddine	Professeur des universités	FEMTO-ST - France	
ZINE Abdelmalek	Maître de conférences	ECL - France	Examinateur
BAREILLE Olivier	Maître de conférences	ECL - France	Co-directeurs
BENAMAR Rhali	Professeur d'enseignement supérieur	EMI - Rabat	
HARRAS Bilal	Professeur d'enseignement supérieur	FST - Fès	Directeurs de thèse
ICHCHOU Mohamed	Professeur des universités	ECL - France	

Laboratoires d'accueil : Laboratoire de Génie mécanique

Laboratoire de Tribologie et Dynamique des Systèmes

Etablissements : Faculté des Sciences et Techniques de Fès

École centrale de Lyon

Acknowledgment

Firstly, I would like to express my sincere gratitude to my advisors Professor **Bilal Harras** and Professor **Mohamed Najib Ichchou** for the continuous support of my Ph.D study and related research, for their patience, motivation, and immense knowledge. Their guidance helped me in all the time of research and writing of this project thesis. I could not have imagined having better advisors and mentors for my Ph.D study.

I would like also to take this as an opportunity in expressing sincere gratitude for my co-advisors, Professor **Rhali Benamar** and Professor **Olivier Bareille** for their support and insightful suggestions which are invaluable. I would like to thank all the members of the jury, especially the three reviewers, for their precious advice on the correction of this dissertation.

I would like to thank all the members of the jury, Professor **Mounia El Kadiri** and especially the three reviewers, Professor **Aboutajeddine Ahmed**, Professor **Bojji Chakib** and Professor **Bouhaddi Noureddine** for their precious advice on the correction of this dissertation.

My sincere appreciation also goes to my colleagues that I worked with, **Omar Baho, Jean-Loup chritien, Christophe Droz, Changwei Zhou**, for the particularly useful discussions and the pleasant moments we spent together during all these years.

Most of all, I would like to thank my family for their unconditional love and encouragement. I am truly grateful to my father, mother and brothers for their supports, sacrifices and motivation to pursue my education. I am indebted to them for being by my side throughout my life, without whose support I would not have achieved anything in my education.

شكر وتقدير

الحمد لله رب العالمين والصلاة والسلام على المبعوث رحمة للعالمين سيدنا محمد وعلى آله وصحبه أجمعين

عملا بقوله تعالى:

وَإِذْ تَأَذَّنَ رَبُّكُمْ لَئِن شَكَرْتُمْ لَأَزِيدَنَّكُمْ ..... ﴿٧﴾

نشكر الله عز وجل على نعمه التي لا تقدر ولا تحصى ومنها توفيقه تعالى على إتمام هذا العمل. نتقدم بجزيل الشكر والامتنان وخالص العرفان والتقدير إلى الأستاذين المؤطرين **بلال الهراس** و**محمد نجيب إيشو**، الذين شرفاني بقبولهما الإشراف على رسالة الدكتوراه وعلى دعمهما وتوجيهاتهما القيمة فجزاهما الله خير الجزاء.

كما يسرنا أن نوجه أسمى آيات التقدير والعرفان إلى أساتذتنا الكرام على إرشاداتهم وأراءهم ونخص بالذكر الأستاذ **الرحال ابن عمر** والأستاذ **أليفيي باغي** والأستاذ **عبد المالك الزين.**

كما نتقدم بخالص الشكر والعرفان إلى باقي أعضاء لجنة التحكيم المكونة من الأساتذة الكرام: الأستاذ **أحمد أبو تاجدين**، الأستاذ **شكيب البوجي**، الأستاذة **منية القادري**، الأستاذ **نور الدين بوهدّي** ونتقدم بالشكر الخالص كذلك إلى كل من ساعدنا في إنجاز هذا العمل.

وقبل وبعد فالشكر لله ولله الحمد في الأولى والأخير

Dedication

I dedicate my dissertation work to my whole family. First of all, A special feeling of gratitude to my lovely parents, **Mohamed Zergoune** and **Chama El Ouardi** whose words of encouragement and push for tenacity ring in my ears. My brother and my sisters have never left my side and are very special.

I also dedicate this dissertation to my friends and my colleagues who have supported me throughout the process.

Abstract

Prediction of the flexural vibroacoustic behavior of honeycomb sandwich structures in the low-mid frequency is nowadays becoming of high interest in different industrial sectors. This trend is mainly owing to the advantageous mechanical properties of the sandwich structures. One of the main advantages of this kind of structures lies principally in the high stiffness-to-weight ratio. Even though, acoustically the decrease of the panel mass with a high stiffness leads to an unsuitable acoustic comfort. For this reason, there is an increasing demand for approaches modeling the vibroacoustic behavior of the sandwich structures with a maximum accuracy.

The present thesis deals with a meso-macro approach based on a numerical method for modeling the vibroacoustic behavior of sandwich structures. The modeling description is mainly used to address the acoustic insulation problem considered in the thesis. The presented work focuses on the topology of the sandwich core to treat the addressed problem. The main advantage of the proposed model is that it takes into account the core shear and panel orthotropic effects.

The modeling approach suggested here is based on the wave finite element method (WFE method), which combines the standard finite element method and the periodic structure theory. The sandwich structure has been modeled as a tridimensional waveguide which holds absolutely the meso-scale information of the modeled panel. The transition frequency, which indicates the frequency at which the core shear becomes important, was identified via two different numerical methods. An expression of the acoustic transmission for an equivalent isotropic sandwich panel was also derived. A parametric study was then conducted with a goal of revealing the effect of the geometric parameters of the sandwich core on the vibroacoustic indicators.

Keywords : Sandwich panels, Honeycomb, Vibro-acoustic behavior, Transition frequency, Sound transmission loss.

Résumé

La modélisation du comportement vibroacoustique en flexion des structures sandwich est devenue aujourd'hui de plus en plus d'un grand intérêt dans les différents secteurs industriels. Cette tendance est principalement due aux propriétés mécaniques avantageuses des structures sandwich. L'un des principaux avantages de ce type de structures réside principalement dans le rapport rigidité-poids élevé. En revanche, acoustiquement la diminution de la masse du panneau avec une rigidité élevée conduit à un confort acoustique insatisfait. Pour cette raison, il y a une demande croissante pour des approches de modélisation du comportement vibroacoustique des structures sandwich avec une précision maximale.

La présente thèse propose une approche méso-macro basée sur une méthode numérique pour la prédiction des caractéristiques dynamiques des structures sandwich. La méthode est principalement utilisée pour résoudre le problème de transparence acoustique considéré dans ce projet de thèse. Le travail présenté porte principalement sur la topologie du coeur du sandwich pour traiter le problème abordé. Le principal avantage du modèle proposé réside dans les effets du coeur prises en compte telle que l'effet du cisaillement et celle de l'orthotropie du panneau sandwich.

L'approche de modélisation proposée est basée sur la méthode des éléments finis ondulatoire, qui combine la méthode des éléments finis classique et la théorie des structures périodiques. La structure sandwich a été modélisée comme un guide des ondes tridimensionnelles qui garde absolument les informations à l'échelle mésoscopique du panneau modélisé. La fréquence de transition définie la fréquence à laquelle le cisaillement du coeur devient important. Cette fréquence spéciale a été identifié via deux méthodes numériques. Une expression de transmission acoustique à travers un panneau sandwich a également été dérivée. Ensuite, une étude paramétrique a été menée dans le but de révéler l'effet des différents paramètres géométriques sur les indicateurs vibroacoustiques.

Mots-clés : Panneaux sandwichs, Nid d'abeille, Comportement vibro-acoustique, Frèquence de transition, Indice d'affaiblissement acoustique.

TABLE OF CONTENTS

List of Figures

List of Tables

Table **Page**

List of Abbreviations

Short form	Signification
ESL theories	: Equivalent single layer theories
LW theory	: Layer Wise theory
PVD	: Principle of Virtual Displacement
CLPT	: Classical Laminate Plate Theory
FSDT	: First-order Shear Deformation Theory
TSDT	: Third-order Shear Deformation Theory
HSDT	: High-order Shear Deformation Theory
SEA	: Statistical Energy Analysis
PST	: Periodic Structures Theory
FEM	: Finite Element Method
WFEM	: Wave Finite Element Method
TL	: Sound Transmission Loss
SEA	: Statistical Energy Analysis
DLF	: Damping Loss Factor
CLF	: Coupling Loss Factor
TMM	: Transfer Matrix Method
FTMM	: Finite Transfer Matrix Method
MOR	: Model order reduction
IWC	: Inhomogeneous Wave Correlation
WSFEM	: Wave spectral finite element model
DLM	: Discrete laminate model

INTRODUCTION

Industrial and scientific context

Over the last few decades, the acoustic comfort issue has become a topical subject of great interest to scientific and industrial communities. Noise pollution caused by road or air traffic, for example, are less and less tolerated by society and subject to more stringent European standards. Furthermore, the acoustic comfort in transportation means (cars, trains, planes, launchers, etc.) is considered currently an important quality criterion. Faced with these challenges, the relevant mechanical industries must develop reliable vibroacoustic analysis means even at the preliminary project stage.

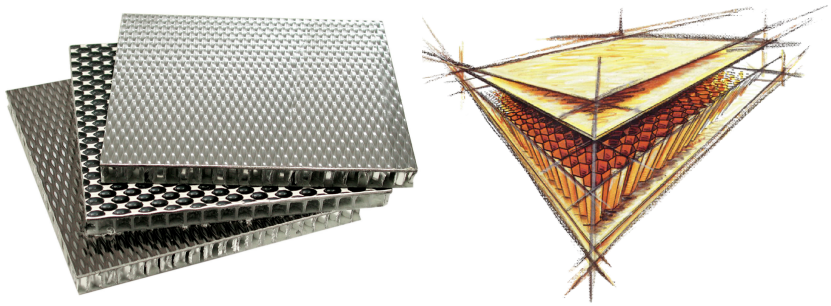

Figure 0.1: Honeycomb sandwich panels.

The honeycomb sandwich structures represent a special interest in the industry, due to their very low mass for very high equivalent stiffness, especially in compression. They are commonly used in automotive manufacturing, aerospace and so on. Specifically, most modern transportation means (cars, planes,...) use the sandwiches because they provide real benefits in terms of dynamic behavior vibration and weight. The sandwich material consists of a lightweight, thick core bonded by a pair of stiff, thin facesheets which offers an extremely high stiffness-to-mass ratio. However, from the vibroacoustic point of view, increasing stiffness-weight ratio could have a harmful effect on the vibroacoustic performance of the structure. this drawback can be often avoided with

a weight-increasing solution which is considered as an undesirable idea for the transportation engineering.

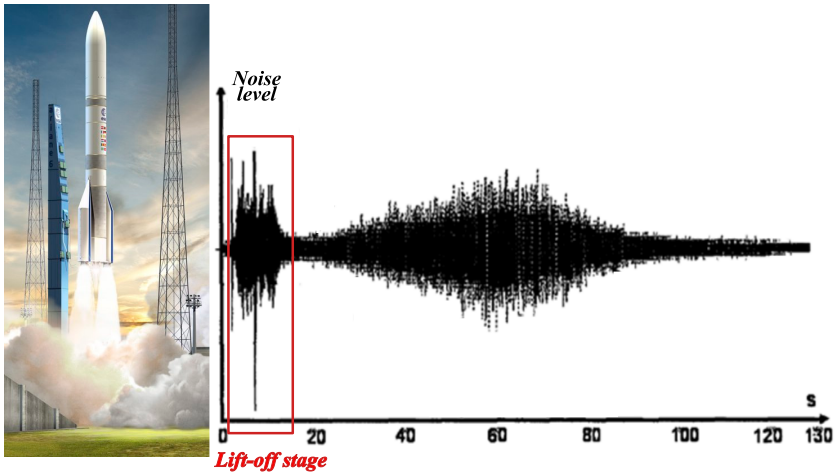

Figure 0.2: Noise level over time in the bottom of the launcher [144].

In the space industry, the launch vehicle and its payload, made of sandwich structures, have to endure at the launch and lift-off stage a harmful acoustic environment induced by the engine exhaust noise and its reverberation on the launch pad which can exceed 160 decibels. As shown in figure 0.2, the lift-off is the stage at which the launcher should be sized to support the generated noise characterized by a diffuse field. The payload may be, for instance, an electronics system, a person, or some other suitable object that should be carried into outer space. In general, there are mainly three source types of aero-acoustic excitation [37, 143, 144] that the payload may be exposed to during the flight of the launch vehicle:

- The diffuse noise due to the interaction of sound waves generated by the supersonic jet engine rocket on the launch pad during the lift-off phase;
- The noise of supersonic jet rocket engine due to the transformation of kinetic energy of the jet into sound energy propagating along the launcher via the ambient air;
- The noise of aerodynamic origin due to the cruise speed of the launch which reaches 8000 km/h during atmospheric flight phase;

These noise types can generate vibration and noise inside the launcher which might damage the fragile structures and components, including the electronics on-board equipment whose the first vibration modes are at mid-high frequencies. For this reason, it is

necessary to create a predictive model of induced vibrations in order to avoid damages of the structure and transporting equipment.

Many noise control treatments were proposed and attached to the fairing to reduce the noise inside of the fairing at which the payload is located. Among them, it can be found sound-absorbing materials placed on the walls of the fairing. These sound absorbing materials can be insulating sandwich panels. Additionally, some fairings can involve multiple layers of shells in which damping materials are located between the shells of the fairing. Furthermore, foam blankets can also be used within the fairing.

On the other hand, these types of noise control treatments require space and increase the weight of the launch vehicle. As a result, the size and/or weight of the payload should be reduced. Moreover, these components can also increase the manufacturing cost of a launch vehicle. Therefore, it would be advantageous to have other innovative alternatives and methods that take into account one or more of the issues discussed above, as well as possibly other issues.

Research Objectives

The research conducted in this thesis has been aimed to propose a modeling process with a goal of improving the acoustic insulation performance of the sandwich panel. The enhancement is conditioned by keeping the key benefit of the sandwich structure, the high stiffness with a low mass. So, the whole work can be related to three main axes :

- Conduct a systematic literature review including the theoretical and experimental approaches developed to treat the insulation performance of the sandwich panel;
- Implement a numerical vibroacoustic model which can consider all the variety of scales and materials of the sandwich structures;
- Perform an experimental test to validate the developed models and the obtained and deduced results;

Thesis outline

Throughout the present thesis, the analysis of the wave propagation and the sound insulation performance of the sandwich structures have been modeled using a meso-macro approach based mainly on the 2D wave finite element method. The main part of the project thesis consists of six chapters dealing with increasing complexity problems.

In view of consistency, each of these chapters can be treated at full length and can be considered, to a certain extent, as a separate, self-contained account.

Chapter 1 has been devoted entirely to present the theoretical published developments carried out to model the vibroacoustic behavior of the sandwich panels. Then, experimental attempts have been cited showing the performed work to enhance the acoustic performance of the sandwich structures. After that, experimental techniques to measure the vibroacoustic indicators have been described.

In **chapter 2**, the meso-macro approach proposed to describe the wave propagation through the sandwich panel has been developed with a reduction strategy. An extension of the developed approach for curved sandwich structures has been given.

Chapter 3 addresses the identification of the transition frequency which separating the global bending panel and the core shear. Two numerical methods have been proposed which are accounted the orthotrapic effect of the sandwich panel. The obtained results have been validated and compared with analytical methods presented in the first chapter.

Chapter 4 has been devoted to evaluate the effects of different core shapes on the bending-shear transition and on the modal density. The transition frequency was identified by the bisection method presented in chapter 3. Parametric analyses of different core configurations have been provided.

Throughout **chapter 5**, a proposed modeling strategy has been applied to investigate the acoustic performance of the sandwich panels. The proposed strategy was based on the meso-macro approach developed in the second chapter. The validation of the obtained results and a parametric study have been given.

Chapter 6 presents the Inhomogeneous Wave Correlation (IWC) method applied to identify experimentally the transition frequency of two sandwich panels with different cell size. The obtained results have been compared to bring out the effect of the cell size on the transition frequency.

Chapter 7 has been devoted to investigate the nonlinear free vibration of symmet-

rical rectangular composite plates with C-C-SS-SS boundaries.

Finally, **conclusions** and discussions related to the perspective work were drawn after chapter 6.

CHAPTER 1

LITERATURE SURVEY : THEORETICAL MODELS AND EXPERIMENTAL METHODS FOR SANDWICH STRUCTURES

Contents

THe first chapter summarizes the most important methods found out at the beginning stage of the project's thesis (state of the art) concerning the vibroacoustic behavior of the sandwich structures. On the whole, this chapter starts with a general review of works published about theoretical models predicting the dynamic behavior of the sandwich panels. It is followed by a definition of the transition frequencies for a typical sandwich panel and then a literature review of existing studies employed to identify these transitions. A particular attention is paid throughout this survey to the transition frequency separating the global panel bending and the core shear. Afterward, some studies discussing the development of the sound transmission loss for sandwich panels are briefly presented. Finally, the last section of the chapter was devoted to introducing the experimental methods existing in the literature for determining the dispersion characteristics.

1.1 Introduction

In the last decades, Several applications using composite structures are steadily increasing. This trend is dictated by the requirements of the industrial manufacturers looking for more performances. These latter results in a higher load capacity as well as reduced fuel consumption.

Sandwich panel refers here to a structure consisting of two thin face-sheets of high stiffness material surrounding a lightweight, low-stiffness and thick core. The face-sheets are made typically of a composite laminate or aluminum, have good stretch properties and carry the tensile and compressive stresses in the sandwich. The central layer of the sandwich panel called the core can be made of a light foam or a honeycomb structure or another configuration (see figure 1.1) with good compression properties. The core has several important functions, in particular, it keeps a constant distance between the top and bottom face-sheets and also avoids that, during the panel bending, the face-sheets slide over each other.

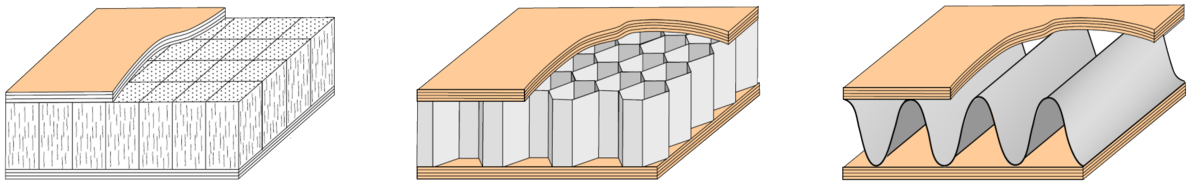

Figure 1.1: Different core configurations of a sandwich panel

The investigation of the vibroacoustic behavior issue for the plates goes back to the early eighteenth century. The German physicist Ernst Chladni (1787) is the founder of the modern acoustics, labeled as the father of acoustics. He was the first to observe experimentally the modes of a square thin plate. Since then, there has been a considerable interest among researchers for the plate vibration. Among the published studies, it can be cited the early works of Kirchhoff [75], Rayleigh [137], love [87], performed in the late nineteenth century, which involved the study of thin plates. They were followed by the works of Reissner [120], Uflyand [145] Mindlin [99] in the mid-twentieth century, adapted to moderately thick homogeneous plate. Simultaneously, the behavior of multilayer anisotropic plates was studied by Lekhnitskii [81] and Ambartsumyan [7].

After World War II, the sandwich structures have become an important element in the aircraft construction. Therefore, several studies have focused on the dynamic behavior of composite plates with the bending behavior. Among this research, we can point out the study Kerwin [73] who analyzed the damping of flexural waves in composites with viscoelastic layers and the work of Rao and Nakra [127] who analyzed the vibrations sandwiches asymmetric beams with a particular attention to the effects of inertia.

In the next sections, a literature review of the most relevant studies published throughout the previous decades are briefly introduced. The review presents theoretical models able to predict the dynamic characteristics and the vibroacoustic performance of sandwich panels. Afterwards, some of interesting experimental attempts dealing with the improvement of the acoustic performance of sandwich panels are presented.

1.2 Overview of wave propagation models for sandwich panels

1.2.1 Classical 2D approximation models

The classical 2D approximation models are based mainly on the development in Taylor series of the displacement field. The approximation allows determining the global response of the layered structure. They are involved, for instance, the critical buckling loads, the fundamental vibration frequencies and the associated mode. The global behavior can often be determined relatively via simple laminated theories, especially for very thin layered structures.

1.2.1.1 Equivalent single layer (ESL)

The ESL theories reduced the laminated structure to an equivalent single layer. These theories are obtained from the 3D elasticity theory by making appropriate assumptions concerning the kinematics of the strain or the stress field through the thickness of the laminate. These assumptions reduce the three-dimensional problem to a two-dimensional problem.

The ESL theories are developed assuming that the shape of the displacement or stress field is a linear combination of unknown functions of the thickness coordinate [75, 99, 120]. The partial differential equations result from this development are resolved by the principle of virtual displacement (PVD) [117]. So, it is supposed that the displacement or stress field is expressed as:

$$\varphi_i(x,y,z,t) = \sum_{j=0}^{N} (z)^j \varphi_i^j(x,y,t), \tag{1.1}$$

where ϕ_i is the i_{th} component of displacement or stress field and ϕ_i^j are functions of x, y and t to determine.

The application of ESL models is limited to the analysis of the global response of the laminate [107, 118]. In general, these models often provide a sufficiently accurate description of the global response of thin to moderately thick laminates. However, models of equivalent single layer (ESL) have several serious limitations that prevent them from being used to solve all the problems related to laminated composites. First, the accuracy of the global response predicted by these models deteriorates as the laminate becomes thick. Second, these models are often unable to describe accurately the state of stress or strain near intense loading areas which are needed most. Finally, these models can not represent the kinematics of delamination [118].

Classical laminated plate theory (CLPT)

The most simple theory of equivalent single layer (ESL) for laminated plates is called the classical theory of laminated plates theory (CLPT) [39, 121, 135, 156, 160] is an extension of the classical theory for isotropic thin plate developed by Kirchhoff [75] in 1850. It is based on the Kirchhoff-Love assumptions for the displacement field where the bending deformation are assumed linear and all transverse deformation effects are neglected [76].

The assumptions of Kirchhoff-Love are the following:

- The plate assumes to be thin. However, this theory does not cover the thick plates for which the effects of the shear deformation are more important;
- The deformation of transverse shear is neglected ($\gamma_{xz} = \gamma_{yz} = 0$);
- The in-plane displacement varies linearly through the thickness of the plate;

$$U = U_0 + z.\phi_x \quad and \quad V = V_0 + z.\phi_y$$

- The thickness of the laminate does not change during the deformation ($\epsilon_{zz} = 0$);
- The transverse normal stress is very low compared to other constraints (it was neglected : $\sigma_z \approx 0$);

↬ The adopted stress state is a state of plane stress (2D).

To take into account the previous assumptions, the displacement field is formulated as follows:

$$\begin{cases} U(x,y,z,t) = U_0(x,y,t) - z\dfrac{\partial W_0(x,y,t)}{\partial x} \\ V(x,y,z,t) = V_0(x,y,t) - z\dfrac{\partial W_0(x,y,t)}{\partial y} \\ W(x,y,z,t) = W_0(x,y,t) \end{cases} \tag{1.2}$$

where U_0, V_0, and W_0 are respectively the components of displacements field along the x-, y- and z-directions of a current point in the mid-plane (i.e. z = 0).

U, V, and W are the components of the displacements field of any point of the plate in the x, y, and z directions respectively. x and y are two local coordinates tangents to the mid-plane, while z is the coordinate normal to the surface of the plate, measured from the mid-surface.

So, the displacement field (eq. 1.2) implies that the straight lines perpendicular to the xy plane before deformation remain straight and perpendicular to the mid-plane after deformation (see figure 1.2).

The deformation field is then deduced simply from the expression of the displacement field (eq. 1.2) by the classical linear theory of continuous media, its expression is:

$$\epsilon = \epsilon_m + \epsilon_f = \epsilon_m + zk(x,y) = \begin{pmatrix} \epsilon^0_{xx} \\ \epsilon^0_{yy} \\ \gamma^0_{xy} \end{pmatrix} + z\begin{pmatrix} k_x \\ k_y \\ k_{xy} \end{pmatrix} = \begin{pmatrix} \frac{\partial U_0}{\partial x} \\ \frac{\partial V_0}{\partial y} \\ \frac{\partial U_0}{\partial y} + \frac{\partial V_0}{\partial x} \end{pmatrix} + z\begin{pmatrix} -\frac{\partial^2 W_0}{\partial x^2} \\ -\frac{\partial^2 W_0}{\partial y^2} \\ -2\frac{\partial^2 W_0}{\partial x \partial y} \end{pmatrix}, \tag{1.3}$$

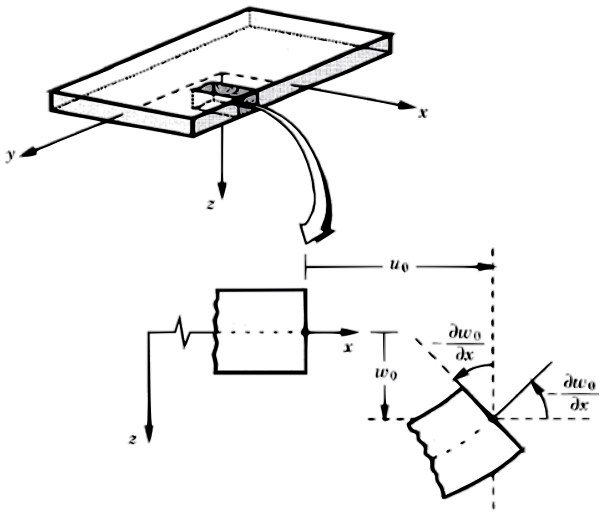

Figure 1.2: Undeformed and deformed shape of a plate edge under the Kirchhoff-Love assumptions.

where ϵ_m is the membrane deformation. ϵ_f is the deformation in bending and torsion. k(x,y) is the matrix of the curvatures of the plate subject to bending.

$$\begin{pmatrix} U_0 \\ V_0 \\ W_0 \end{pmatrix} = \begin{pmatrix} U \\ V \\ W \end{pmatrix} . e^{j(k_x x + k_y y - \omega t)}. \tag{1.4}$$

By developing the equation of motion determined using Hamilton's principle, taking into account the assumptions of this theory and considering the harmonic displacement field (eq. 1.4), the following system is obtained:

$$\begin{cases} \left[(A_{11}.(i.\cos\theta)^2 + 2.A_{16}.(i.\cos\theta).(i.\sin\theta) + A_{66}.(i.\sin\theta)^2).k^2 - \rho_s.(-i.\omega)^2\right].U \\ + \left[(A_{16}.(i.\cos\theta)^2 + (A_{12}+A_{66}).(i.\cos\theta).(i.\sin\theta) + A_{26}.(i.\sin\theta)^2).k^2\right].V \\ - \left[(B_{11}.(i.\cos\theta)^3 + 3.B_{16}.(i.\cos\theta)^2.(i.\sin\theta) + (B_{12}+2.B_{66}).(i.\cos\theta).(i.\sin\theta)^2 \right. \\ \left. + B_{26}.(i.\sin\theta)^3).k^3\right].W = 0 \\ \\ \left[(A_{16}.(i.\cos\theta)^2 + (A_{12}+A_{66}).(i.\cos\theta).(i.\sin\theta) + A_{26}.(i.\sin\theta)^2).k^2\right].U \\ + \left[(A_{66}.(i.\cos\theta)^2 + 2.A_{26}.(i.\cos\theta).(i.\sin\theta) + A_{22}.(i.\sin\theta)^2).k^2 - \rho_s.(-i.\omega)^2\right].V \\ - \left[(B_{16}.(i.\cos\theta)^3 + (B_{12}+2.B_{66}).(i.\cos\theta)^2.(i.\sin\theta) + 3.B_{26}.(i.\cos\theta).(i.\sin\theta)^2 \right. \\ \left. + B_{22}.(i.\sin\theta)^3).k^3\right].W = 0 \end{cases} \tag{1.5}$$

The dispersion relation is achieved by computing the roots of the determinant of the previous system (1.5).

$$\begin{vmatrix} a_1.k^2+a_2 & a_3.k^2 & a_4.k^3 \\ a_3.k^2 & a_5.k^2+a_2 & a_6.k^3 \\ a_4.k^3 & a_6.k^3 & a_7.k^4-a_2 \end{vmatrix} = 0. \tag{1.6}$$

The development of the above equation (1.6) gives the following dispersion relation:

$$\zeta_1.k^8+\zeta_2.k^6+\zeta_3.k^4+\zeta_4.k^2+\zeta_5=0 \tag{1.7}$$

in which the coefficients ζ_i $(i=1,...,5)$ are written as follows:

$$\begin{cases} \zeta_1 = a_1.a_5.a_7 - a_1.a_6^2 - a_3^2.a_7 + 2.a_3.a_4.a_6 - a_4^2.a_5 \\ \zeta_2 = a_2.a_5.a_7 + a_1.a_2.a_7 - a_2.a_6^2 - a_2.a_4^2 \\ \zeta_3 = a_2^2.a_7 + a_3^2.a_2 - a_1.a_5.a_2 \\ \zeta_4 = -a_2^2.a_5 - a_1.a_2^2 \\ \zeta_5 = -a_2^3 \end{cases} \tag{1.8}$$

where the previous coefficients a_i (with $i = 1,,7$) are defined in **appendix A**.

First-order shear deformation theory (FSDT)

The FSDT is also known under the name of Mindlin theory. It is considered as an extension of the classical laminated plates theory (CLPT) obtained by including the transverse shear deformation (γ_{xz} and γ_{yz}) in the kinematic assumption (the transverse shear deformation is assumed to be constant with respect to the thickness coordinate).

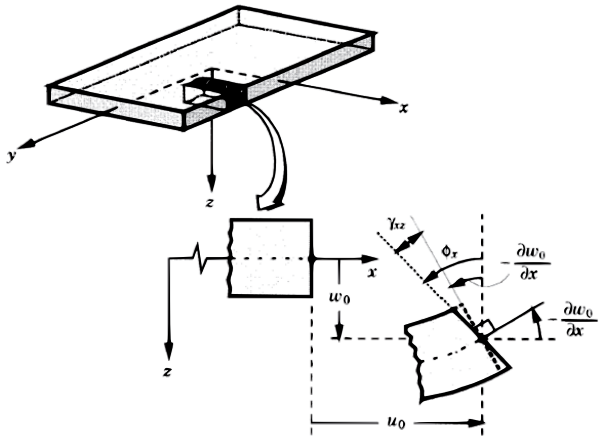

Figure 1.3: Undeformed and deformed shape of a plate edge under the Mindlin-Reissner assumptions.

This theory is based on a kinematics model originally proposed by Reissner and Mindlin [99, 120] which states that straight lines perpendicular to the undeformed mid-plane remain straight but not necessarily perpendicular to the deformed mid-plane (see figure 1.3).

The displacement field based on the present theory is defined by the following relationships:

$$\begin{cases} U(x,y,z,t) = U_0(x,y,t) + z\phi_x(x,y,t) \\ V(x,y,z,t) = V_0(x,y,t) + z\phi_y(x,y,t) \\ W(x,y,z,t) = W_0(x,y,t) \end{cases} \tag{1.9}$$

where ϕ_x and ϕ_y functions to be determined.

This theory gives good results for the prediction of the global response for a layered structure (bending load, buckling and natural frequencies). However, it is unable to predict with reasonable accuracy the stresses across the thickness, especially in areas of discontinuity such as the boundaries of layers. In 1970, Pipes and Pagano showed that near the borders of laminated structures, transverse stresses increase dramatically. This was referred to as "the boundary layer effect". Therefore, a model that can accurately predict the transverse shear stress is necessary to detect the causes of delamination. Later, higher order theories have been developed to overcome this problem.

High-order Shear Deformation Theory (HSDT)

The second-order and higher-order laminated plates use higher order polynomials (i.e. N > 1 in equation (1.1) to develop the displacements field components as a function of the thickness coordinate of the laminate (see [86, 101, 102, 139])). the higher-order theories introduce additional unknowns that are often difficult for a physical interpretation.

For instance, there are many papers on the third-order theories [40, 84, 138] and their applications [20, 74, 85, 130]. So, the displacement field based on third-order shear deformation theory (TSDT) is defined by the following relationships:

$$\begin{cases} U(x,y,z,t) = U_0(x,y,t) + z\phi_x(x,y,t) + z^3 \dfrac{-4}{3h^2}\left(\phi_x + \dfrac{\partial W_0}{\partial x}\right) \\ V(x,y,z,t) = V_0(x,y,t) + z\phi_y(x,y,t) + z^3 \dfrac{-4}{3h^2}\left(\phi_y + \dfrac{\partial W_0}{\partial y}\right) \\ W(x,y,z,t) = W_0(x,y,t) \end{cases} \tag{1.10}$$

where ϕ_x and ϕ_y are respectively the rotations of a vector normal to the surface around the x- and y-axes. h is the total thickness of the laminated plate.

It is clear that the higher-order theories for laminated plates provide a better representation of transverse shear stresses with respect to the CLPT and the FSDT. However, they involve stress resultants of a higher-order which are difficult to give a physical interpretation and they require significantly more computational effort. Therefore, these theories should be used only when necessary.

1.2.1.2 Layer-wise theory

Unlike ESL theories, the layer-wise theories (LW) are developed on the assumption that the displacement field is only continuous across the thickness of the laminate C^0 [107]. The layer-wise theories provide a more accurate representation of the moderate to hard cross section warping associated with the thick laminate deformation. The layer-wise theories can be divided into two classes:

- The partial layer-wise theories at which an approximation for the in-plane displacements (U and V) of the laminate is used only. This formulation provides discrete deformations of transverse shear (γ_{xz} and γ_{yz}) through the different layers;

- The full layer-wise theories that use an approximation development for all the three components of the displacement field;

Comparing with the ESL theories, the partial layer-wise theories provide a more realistic description of the kinematic laminated composites by introducing discrete transverse shear effects of the layer through the assumed displacement field.

The displacement field of the k^{th} layer using the layer-wise assumptions can be written as follows:

$$\begin{cases} U^k(x,y,z,t) = \sum_{j=1}^{n} U_j^k(x,y,t)\phi_j^k(z) \\ V^k(x,y,z,t) = \sum_{j=1}^{n} V_j^k(x,y,t)\phi_j^k(z) \\ W^k(x,y,z,t) = \sum_{j=1}^{m} W_j^k(x,y,t)\phi_j^k(z) \end{cases} \tag{1.11}$$

where U^k, V^k and W^k are respectively the components of the total displacement in the x-, y- and z-directions. U_j^k,V_j^k and W_j^k are the displacement components at the node j computed from the interpolation of displacements in the xy plane. $\varphi_j^k(z)$ and $\phi_j^k(z)$ are the continuous functions of the thickness coordinate. They may be chosen as one-dimensional interpolation Lagrange functions of the thickness coordinate. n represents the number of nodes used in the in-plane displacement discretization. m represents the number of nodes used in the out-of-plane displacement discretization.

However, it has been noticed that the final results contain parasitic shear modes when using the layer-wise theories for the thin structures.

1.2.2 Kurtz & Watters' model

Kurtz & Watters' model [77], based on the impedance method, permits to predict the dynamic propagation characteristics across the sandwich panel. The developed model can consider the behavior cases of the sandwich core (a) and (b) illustrated in figure 1.4. It is assumed that the bending of the core has a negligible contribution to the bending stiffness of the global composite plate. This is due to the Young's modulus of the core material, which is most of the time so much smaller than that of the face-sheet material.

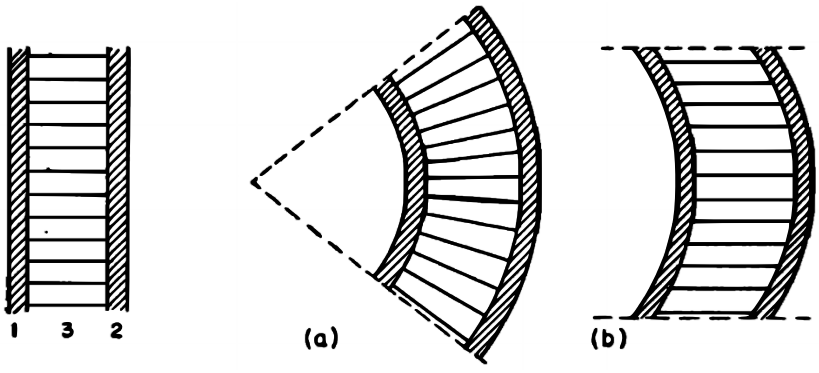

Figure 1.4: Bending of a sandwich plate by (a) bending and (b) shearing of the core layer [77].

The wave impedance Z_B for bending waves, in the present model, is expressed as follows:

$$Z_B = j\omega\rho_p + \frac{D\omega^3}{jc^4}. \tag{1.12}$$

where ρ_p is the total mass per unit area. $D = \frac{E_f I}{\left(1-\nu_f^2\right)}$ is the bending stiffness of the panel with I is the moment inertia of the cross section, E_f and ν_f are respectively the Young's modulus and Poisson's ratio of the sandwich face-sheets. While, the shear wave impedance Z_S for sandwich panel with equal face-sheets is then expressed as follows:

$$Z_S = j\omega\left(2\rho_f + \rho_c\right) + \frac{2D_f\omega^3}{jc^4} + \frac{S\omega}{jc^2}, \tag{1.13}$$

where ρ_f and ρ_c are respectively the face-sheet and core mass per unit area. S is the transverse shear stiffness. $D_f = \frac{E_f h_f}{\left(1-\nu_f^2\right)}$ is the bending stiffness of the sandwich face-sheet with h_f is the thickness of the top and bottom face-sheet.

Thus, the total impedance for the sandwich panel is obtained by using the equivalent electric circuit shown in figure 1.6. Where $L = \rho_p$, $C_1 = \frac{X^2}{D}$, $C_2 = \frac{X^2}{2D_f}$ and $C_3 = \frac{X}{S}$ with $X = \frac{c^2}{\omega^2}$. So that, the total impedance is given by :

$$Z_T = j\omega\rho_p + \frac{D}{j\omega X^2}\frac{\frac{2D_f}{j\omega X^2} + \frac{S}{j\omega X}}{\frac{D}{j\omega X^2} + \frac{2D_f}{j\omega X^2} + \frac{S}{j\omega X}}. \tag{1.14}$$

The below dispersion relation (eq. 1.15) is found by assuming the absence of energy dissipation (e.g. The total impedance Z_T 1.14 equal to zero). The relation is expressed in terms of the speed c of the exciting wave.

$$\frac{c_S^2}{c_b^4}c^6 + c_S^2c^4 - c_S^4c^2 - c_D^4c_S^2 = 0, \tag{1.15}$$

where

$$\begin{cases} c_b = \sqrt[4]{\omega^2 \dfrac{D}{\rho_p}}\,; & \text{The full panel flexural wave speed.} \\ c_S = \sqrt{\dfrac{S}{\rho_p}}\,; & \text{The core shear wave speed.} \\ c_D = \sqrt[4]{\dfrac{2D_f\omega^2}{\rho_p}}\,; & \text{The face-sheet bending wave speed.} \end{cases} \tag{1.16}$$

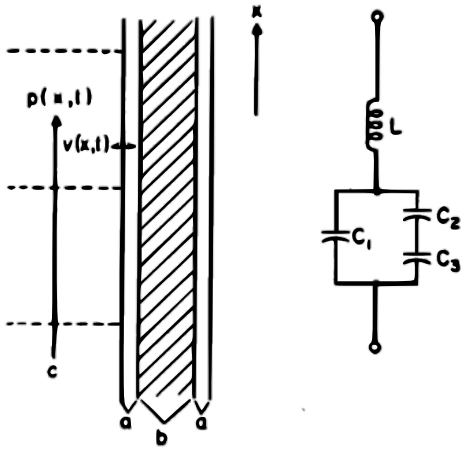

Figure 1.5: Equivalent electric circuit of the total impedence [77].

The present model is among the first models which concluded that the shear wave propagation in such structures is possible if the Young's modulus of the sandwich core is smaller than that of the sandwich face-sheets, which is the case of the most industrial sandwich panel.

1.2.3 Ford, Lord & Walker's model

The model proposed by Ford, Lord and Walker [53] is restricted to sinusoidal deformations that are flexible enough to describe accurately all modes of vibration may occur. L_1 and L_2 is considered as the dimensions of the panel as shown in figure 1.6. The displacement field using the present model for the sandwich core is written as follows:

$$\begin{cases} U.\sin(\omega t) = \left\{\dfrac{(B_1+B_2)}{2} + \dfrac{(B_1-B_2).z}{d} + D_1.\cos\dfrac{\pi z}{d}\right\}\cos(k_1 x).\sin(k_2 y).\sin(\omega t) \\ V.\sin(\omega t) = \left\{\dfrac{(C_1+C_2)}{2} + \dfrac{(C_1-C_2).z}{d} + D_1.\cos\dfrac{\pi z}{d}\right\}\sin(k_1 x).\cos(k_2 y).\sin(\omega t) \\ W.\sin(\omega t) = \left\{\dfrac{(A_1+A_2)}{2} + \dfrac{(A_1-A_2).z}{d}\right\}\sin(k_1 x).\sin(k_2 y).\sin(\omega t) \end{cases} \tag{1.17}$$

where $A_1, A_2, B_1, B_2, C_1, C_2, D_1$ and D_2 are the generalized coordinates.

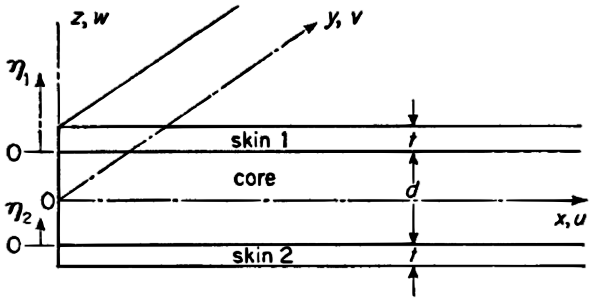

Figure 1.6: Coordinate system [53].

The displacement field for the top face-sheet of the sandwich panel is described as follows:

$$\begin{cases} U_T.\sin(\omega t) = B_1\cos(k_1 x).\sin(k_2 y).\sin(\omega t) - \eta_1\dfrac{\partial W_1}{\partial x}\sin(\omega t) \\ V_T.\sin(\omega t) = C_1\sin(k_1 x).\cos(k_2 y).\sin(\omega t) - \eta_1\dfrac{\partial W_1}{\partial y}\sin(\omega t) \\ W.\sin(\omega t) = A_1\sin(k_1 x).\sin(k_2 y).\sin(\omega t) \end{cases} \tag{1.18}$$

Whilst, the displacement field of the bottom face-sheet of is expressed as follows :

$$\begin{cases} U_B.\sin(\omega t) = B_2\cos(k_1 x).\sin(k_2 y).\sin(\omega t) - \eta_2\dfrac{\partial W_2}{\partial x}\sin(\omega t) \\ V_B.\sin(\omega t) = C_2\sin(k_1 x).\cos(k_2 y).\sin(\omega t) - \eta_2\dfrac{\partial W_2}{\partial y}\sin(\omega t) \\ W.\sin(\omega t) = A_2\sin(k_1 x).\sin(k_2 y).\sin(\omega t) \end{cases} \tag{1.19}$$

Applying the Rayleigh-Ritz method [149] to minimize the energy and using the previous displacement field assumptions, the following derivatives must be zero:

$$\frac{\partial(U-T)}{\partial A_1};\ \frac{\partial(U-T)}{\partial A_2};\ \frac{\partial(U-T)}{\partial B_1};\ etc. = 0 \tag{1.20}$$

The desired dispersion relation achieves then by solving eight equations. These eight equations are gotten By developing the previous equations (1.20).

1.2.4 Small-deflection theory

The small-deflection theory [47, 83, 136] is developed to consider the orthotropic plate and the deflexions due to the shear in the elastic behavior. The sandwich panel deformation is described in this theory by means of seven known physical constants:

↬ The flexural stiffness $D_x = -\dfrac{M_x}{\partial^2 W/\partial x^2}$ and $D_y - \dfrac{M_y}{\partial^2 W/\partial y^2}$ along x- and y-directions respectively;

↬ The cross-bending stiffness $D_{xy} = \dfrac{M_{xy}}{\partial^2 W/\partial x \partial y}$;

↬ The transverse shear stiffness $S_x = \dfrac{Q_x}{\gamma_x}$ and $S_y \dfrac{Q_y}{\gamma_y}$ along x- and y-directions respectively;

↬ The Poisson ratios $\nu_x = \dfrac{\partial^2 W/\partial y^2}{\partial^2 W/\partial x^2}$ and $\nu_y = \dfrac{\partial^2 W/\partial x^2}{\partial^2 W/\partial y^2}$;

From reference [83], the corresponding relations between resultant moments and curvatures and twist are written as follows :

$$\begin{cases} M_x = -\dfrac{D_x}{1-\nu_x\nu_y}\left[\dfrac{\partial}{\partial x}\left(\dfrac{\partial W}{\partial x} - \dfrac{Q_x}{S_x}\right) + \nu_y \dfrac{\partial}{\partial y}\left(\dfrac{\partial W}{\partial y} - \dfrac{Q_y}{S_y}\right)\right] \\ M_y = -\dfrac{D_y}{1-\nu_x\nu_y}\left[\dfrac{\partial}{\partial y}\left(\dfrac{\partial W}{\partial y} - \dfrac{Q_y}{S_y}\right) + \nu_x \dfrac{\partial}{\partial x}\left(\dfrac{\partial W}{\partial x} - \dfrac{Q_x}{S_x}\right)\right] \\ M_{xy} = -\dfrac{1}{2} D_{xy}\left[\dfrac{\partial}{\partial x}\left(\dfrac{\partial W}{\partial y} - \dfrac{Q_y}{S_y}\right) + \dfrac{\partial}{\partial y}\left(\dfrac{\partial W}{\partial x} - \dfrac{Q_x}{S_x}\right)\right] \end{cases} \tag{1.21}$$

The differential equations 1.22 governing the panel behavior is obtained by substituting the previous relations 1.21 into the last three moment equilibrium equation presented in [136].

$$\begin{cases} \dfrac{\partial Q_x}{\partial x} + \dfrac{\partial Q_y}{\partial y} - \rho_p \dfrac{\partial^2 W}{\partial t^2} = 0 \\ -\dfrac{\partial^3 W}{\partial x \partial y^2} - \dfrac{\partial^3 W}{\partial x^3} - \dfrac{Q_x}{D} + \dfrac{1}{S_x}\left(\dfrac{\partial^2 Q_x}{\partial x^2} + \dfrac{(1-\nu)}{2}\dfrac{\partial^2 Q_x}{\partial y^2}\right) + \dfrac{1}{S_y}\dfrac{(1+\nu)}{2}\dfrac{\partial^2 Q_y}{\partial x \partial y} + \dfrac{I}{D}\dfrac{\partial^2}{\partial t^2}\left(\dfrac{\partial w}{\partial x} - \dfrac{Q_x}{S_x}\right) = 0 \\ -\dfrac{\partial^3 W}{\partial x^2 \partial y} - \dfrac{\partial^3 W}{\partial y^3} - \dfrac{Q_y}{D} + \dfrac{1}{S_y}\left(\dfrac{\partial^2 Q_y}{\partial y^2} + \dfrac{(1-\nu)}{2}\dfrac{\partial^2 Q_y}{\partial x^2}\right) + \dfrac{1}{S_x}\dfrac{(1+\nu)}{2}\dfrac{\partial^2 Q_x}{\partial x \partial y} + \dfrac{I}{D}\dfrac{\partial^2}{\partial t^2}\left(\dfrac{\partial w}{\partial y} - \dfrac{Q_y}{S_y}\right) = 0 \end{cases} \tag{1.22}$$

So that, the dispersion relation for the sandwich panel is determined by solving the differential equations 1.22 and assuming harmonic solutions.

1.2.5 Renji's model

The model developed by Renji et al. [123] is an improved model of the classical plate theory [70] in which the transverse shear core of the sandwich panel is not considered. So, the differential equation, in which the shear effect is included, was derived as follows:

$$D_{11}\frac{\partial^4 w}{\partial x^4}+2(D_{12}+2D_{66})\frac{\partial^4 w}{\partial x^2\partial y^2}+D_{22}\frac{\partial^4 w}{\partial y^4}=-\frac{\rho_p}{S}\frac{\partial^2}{\partial t^2}\left(D_{11}\frac{\partial^2 w}{\partial x^2}+D_{22}\frac{\partial^2 w}{\partial y^2}\right)-\rho_p\frac{\partial^2 w}{\partial t^2}. \tag{1.23}$$

where D_{11}, D_{22}, D_{12} and D_{66} are the coefficients of the bending stiffness matrix of the sandwich panel. ρ_p is the mass per unit area of the sandwich panel and S is the equivalent shear modulus defined as: $S=G_c h_c\left(1+\frac{h_f}{h_c}\right)^2$ with G_c is the effective shear modulus of the sandwich core, h_f and h_c are respectively the face-sheet and core thicknesses.

After solving the differential equation 1.23, the dispersion relation obtained using the present model can then be written as:

$$D_{11}k_x^4+2(D_{12}+2D_{66})k_x^2k_y^2+D_{22}k_y^4-\frac{\omega\rho_p}{S}\left(D_{11}k_x^2+D_{22}k_y^2\right)=\rho_p\omega^2. \tag{1.24}$$

Supposing $r\cos\theta=\sqrt[4]{D_{11}k_x}$ and $r\sin\theta=\sqrt[4]{D_{22}k_y}$, The dispersion relation 1.24 can then be expressed in terms of the polar system in the following form:

$$f_1(\theta)r^4-\left(\frac{\rho\omega^2}{S}\right)\sqrt[4]{D_{11}D_{22}}f_2(\theta)r^2-\rho\omega^2=0, \tag{1.25}$$

where

$$\begin{cases} f_1(\theta)=1-\dfrac{1}{2}\left\{1-\dfrac{(D_{12}+2D_{66})}{\sqrt{D_{11}D_{22}}}\right\}\sin^2(2\theta) \\ \\ f_2(\theta)=\sqrt[4]{\dfrac{D_{11}}{D_{22}}}\cos^2\theta+\sqrt[4]{\dfrac{D_{22}}{D_{11}}}\sin^2\theta \end{cases} \tag{1.26}$$

For a typical sandwich panel, Renji et al. have pointed out in their work [123] that neglecting the transverse shear effect or considering the sandwich panel to be isotropic can lead to large errors in the vibroacoustic behavior prediction.

1.2.6 Improved ordinary sandwich panel theory (IOSPT)

The improved ordinary sandwich panel theory [61, 62] is an improved version of the full layer-wise theory presented in subsection 1.2.1.2. The improvement brought in the present model with respect to the original theory [114] lies in the fact that the in-plan rigidity of the sandwich core is accounted and also the orthotropic effect of the core and face-sheet materials is considered.

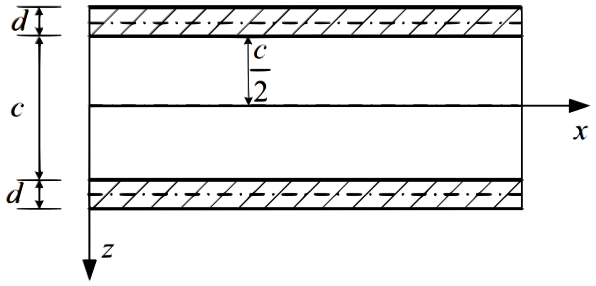

Figure 1.7: A symmetric sandwich panel [61].

The assumptions of the IOSPT can be summarized as the following:

- The sandwich panel is symmetric about the mid-plane of the sandwich panel;
- Since the face-sheet is thin with respect to the core, the classical thin plate theory is used for face-sheets;
- The normal stress in the thickness direction can be neglected. Thus, the anti-symmetric deformation is only considered;
- The panel core is assumed to be relatively soft. So, the transverse shear deformation and the in-plan rigidity are not neglected;
- The mass of the adhesive at the face-core interface are ignored;

According to the above assumptions, the displacement field along x- and y-directions for the top face-sheet is written as :

$$\begin{cases} U_t(x,y,z,t) = \dfrac{c+d}{2}\Phi_x - \left(z + \dfrac{c+d}{2}\right)\dfrac{\partial W}{\partial x} \\ V_t(x,y,z,t) = \dfrac{c+d}{2}\Phi_y - \left(z + \dfrac{c+d}{2}\right)\dfrac{\partial W}{\partial y} \end{cases} \tag{1.27}$$

Similarly, the displacement field along x- and y-directions for the bottom face-sheet is written as :

$$\begin{cases} U_b(x,y,z,t) = -\dfrac{c+d}{2}\Phi_x - \left(z - \dfrac{c+d}{2}\right)\dfrac{\partial W}{\partial x} \\ V_b(x,y,z,t) = \dfrac{c+d}{2}\Phi_y - \left(z - \dfrac{c+d}{2}\right)\dfrac{\partial W}{\partial y} \end{cases} \tag{1.28}$$

While, the displacements field of any point at the face/core interface along x- and y-directions was shown as:

$$\begin{cases} U\left(x,y,z = \pm\dfrac{c}{2},t\right) = \pm\dfrac{c+d}{2}\Phi_x \mp \dfrac{d}{2}\dfrac{\partial W}{\partial x} \\ V\left(x,y,z = \pm\dfrac{c}{2},t\right) = \pm\dfrac{c+d}{2}\Phi_y \mp \dfrac{d}{2}\dfrac{\partial W}{\partial y} \end{cases} \tag{1.29}$$

Assumed that the displacement field along x- and y-directions of the panel core are linear along the thickness direction, the in-plane displacement field of the panel core is written as:

$$\begin{cases} U_c(x,y,z,t) = -z\left(\dfrac{c+d}{c}\Phi_x - \dfrac{d}{c}\dfrac{\partial W}{\partial x}\right) \\ V_c(x,y,z,t) = -z\left(\dfrac{c+d}{c}\Phi_y - \dfrac{d}{c}\dfrac{\partial W}{\partial y}\right) \end{cases} \tag{1.30}$$

The characteristic wave-number equation is obtained by substituting the previous displacement fields in the total kinetic and strain energies and using the Hamilton's principle.

$$b_4 r^8 + b_3 r^6 + b_2 r^4 + b_1 r^2 + b_0 = 0, \tag{1.31}$$

in which b_i (with $i = 0,...,4$) are functions in terms of the angular frequency ω and the heading angle θ. r represents the polar wave-number of the sandwich panel with $k_x = r\cos\theta$ and $k_y = r\sin\theta$.

1.2.7 Discrete laminate model (DLM)

The discrete laminate model [56] allows modeling the dynamic behavior for thick laminates and sandwich panels. The displacement field of i^{th} layer of the panel is controlled by the Mindlin assumptions:

$$\begin{cases} U^i(x,y,z) = U_0^i(x,y) + z\varphi_x^i(x,y) \\ V^i(x,y,z) = V_0^i(x,y) + z\varphi_y^i(x,y) \\ W^i(x,y,z) = W_0^i(x,y) \end{cases} \tag{1.32}$$

The Flüge theory is used to describe the displacement-constraint relationships. In each layer, The rotational inertia, the in-plane, bending displacements as well as the transverse shear are taken into account in this model. In addition, the orthotropic ply's direction is considered for any lamina composing a layer.

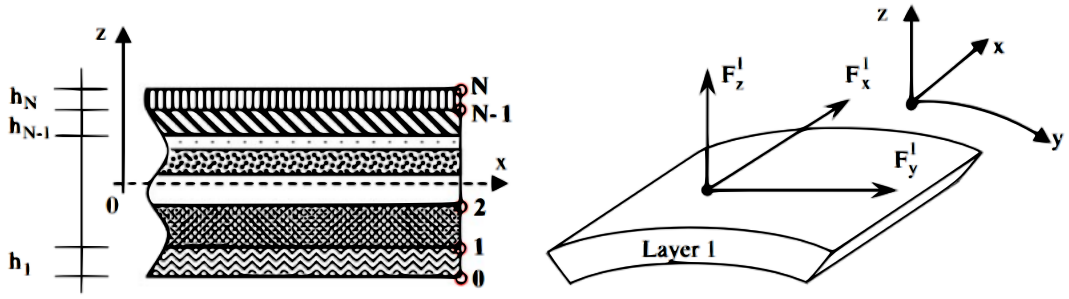

Figure 1.8: The interlayer forces considred in the DLM.

For the sandwich panel case, the discrete laminate model is based on the following assumptions [55]:

- The core thickness is considered higher than of the face-sheets;
- The sandwich core contributes only by transversal shear stresses;
- The transversal shear stresses are neglected in the face-sheets;
- The sandwich core and face-sheets are assumed incompressible through the panel thickness;

The dynamic equilibrium equations of the sandwich panel is expressed in the form of a polynomial complex eigenvalue problem, in terms of an in-plane and bending displacementrotation vector $\{e\}$:

$$k_c^2[A_2]\{e\} - ik_c[A_1]\{e\} - [A_0]\{e\} = 0, \tag{1.33}$$

where $k_c = \sqrt{k_x^2 + k_y^2}$, $\{e\} = \{U,\ V,\ W,\ \varphi_x,\ \varphi_y\}$ and $[A_0]$, $[A_1]$, $[A_2]$ are real matrices of dimension 5X5 defined in detail in the appendix of reference [55].

1.2.8 Wave spectral finite element model (WSFEM)

The wave spectral finite element model (WSFEM) [97] recently developed by Mejdi et al. is an improvement of the discrete laminate model presented previously. The present

model can predict the symmetric and anti-symmetric motion with either thin or thick face-sheets and a stiff or soft core.

The governing equation described the vibroacoustic behavior of the sandwich panel along the thickness direction, assuming k_x and k_y are known, is given by the following:

$$\left(k_z^2[K_2] + k_z[K_1] + [K_0] - \omega^2[M]\right)\{e\} = \{0\}, \tag{1.34}$$

in which $\{e\} = \{U,\ V,\ W\}^T$ is the displacement field with ^{T} stands for the vector transpose operator. $[K_2]$, $[K_1]$, $[K_0]$ and $[M]$ are 3x3 matrices given in [97].

1.2.9 Wave finite element method (WFE)

A large number of structures in the industrial and scientific fields are periodic along certain or all directions. The Floquet theory [22], which is considered as one of the basic theories of wave propagation in periodic structures, is recommended to analyze these kind of structures. The theory considers that the wave propagation properties in a periodic structure can be obtained from the propagation constant.

Knowing the wave propagation characteristics in periodic structures, such as the dispersion curve and the propagation speed, are of great interest to simplify the vibroacoustic behavior analysis of a such structure. Theoretically, the understanding of wave propagation provides the necessary basis for a successful implementation of numerous scientific and industrial techniques (e.g. the Statistical Energy Analysis (SEA)).

Among the methods very used in the literature for identifying the expressions of wave propagation characteristics, there are the wave finite element method (WFE method). The stated method combines the theory of periodic structures (PST) introduced by Mead [96] and the classical finite element method (FEM). The method was chosen due primarily to the fact that it is simple to implement and can predict the structure behavior over a wide frequency band particularly at mid and high frequencies where the size of the structure is large compared to the length of wave.

1.3 Transition frequency for sandwich panels

The transition frequency is an important vibroacoutic indicator among others which can provide information about the macro behavior of the structure. It is by definition the frequency at which the structure switches its current behavior type to an other behavior one.

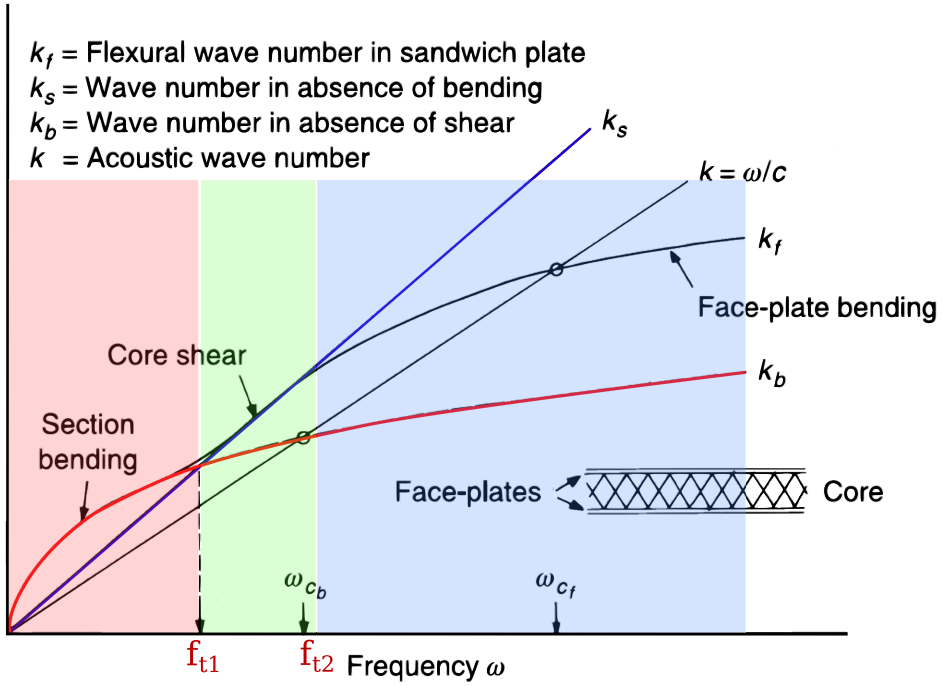

Figure 1.9: Typical dispersion curves for a sandwich panel [50].

As shown in figure 1.9 quoted from [50], a typical dispersion curve for a sandwich panel shows three dominant behavior regions. The first region (red zone) is controlled by the total section bending stiffness of the sandwich panel which is carried out in the low frequency range. The whole panel is acting in this region as a homogeneous panel. The second region (green zone) is controlled by the core shear stiffness at mid frequencies. Whilst in the last region (blue zone), the vibroacoustic behavior is controlled by the individual face-sheet bending stiffness at very high frequencies.

The first two regions are separated by the first transition frequency f_{t1} which has great interest in this project's thesis due to the fact that this spacial frequency defines the frequency at which the core shear becomes important with respect to the panel bend-

ing. While, the second transition frequency f_{t2} represents the switch of shearing core to the individual bending face-sheets.

Rindel's survey

Rindel, in his work [126], has pointed out three analytic expressions of the transition frequencies, called in his work cross-over frequency. The values of the transition frequencies depend on the dispersion characteristics chosen to define them. These three expressions describe the shift from the global bending of the thick plate to the core shear.

Based on the dispersion equation 1.15 set up by Kurtz and Walter, the transition frequency f_t^s is identified by equating the expression of the face-sheets bending wave speed and the core shear wave speed.

$$f_t^s = f_c \left(\frac{c_s}{c}\right)^2. \tag{1.35}$$

where $f_c = \frac{c^2}{2\pi}\sqrt{\frac{\rho_p}{D}}$ is the critical frequency which is the frequency at which the effective phase speed C_{Deff} equals the speed of sound in the surrounding media. The effective phase speed is expressed as the following form:

$$C_{Deff} = \frac{c_D^2}{c_S}\sqrt{-\frac{1}{2}+\frac{1}{2}\sqrt{1+4\left(\frac{c_S}{c_D}\right)^4}}. \tag{1.36}$$

with the expressions of c_D and c_S are presented in subsection 1.2.2 in equation 1.16.

It is shown from the development of the modal density expression that the modal density is constant in the low frequency range, but increases with frequency above the transition frequency f_t^n. It is noticed that the transition frequency f_t^n obtained using the modal density is the half of the one f_t^s obtained using the dispersion relation developed by Kurtz and watter $\left(f_t^n = \frac{f_t^s}{2}\right)$.

Evan's work

Evan has developed in his work [48] two formulations of the transition frequencies which separate the three regions previously mentioned. As has been stated, the first one

f_{t1} presents the transition from the plate bending to core shear. The other f_{t2} defines the shift from the shear core to the individual face-sheets bending.

$$\begin{cases} f_{t1} = \dfrac{1}{\pi\left(h_f + h_c\right)}\sqrt{\dfrac{\left(\rho_c h_c\right)^2}{2\rho_f h_f \rho_p}}\left(\dfrac{G}{\rho_c}\sqrt{\dfrac{\rho_f\left(1-\nu^2\right)}{E_f}}\right) \\ f_{t2} = \dfrac{\sqrt{3}}{\pi h_f}\sqrt{\dfrac{\left(\rho_c h_c\right)^2}{2\rho_f h_f \rho_p}}\left(\dfrac{G}{\rho_c}\sqrt{\dfrac{\rho_f\left(1-\nu^2\right)}{E_f}}\right) \end{cases} \tag{1.37}$$

where ρ_c and ρ_f are respectively the mass density of the panel core and face-sheets. G is the shear modulus of the core.

It should be noted that the development of the two transitions in Evan's study is based on Krutze and watters presented in subsection 1.2.2.

Guillaumie's work

Guillaumie's work [59] is based on Renji's model presented in subsection 1.2.5. The analytical expression of the transition frequency is developed using the inverse infinite mechanical impedance of the sandwich panel.

$$Z_\infty^{-1} = \frac{n(\omega)}{4\rho_p A} = \frac{\omega}{8S}\left(1 + \left(\rho_p\omega^2 + \frac{2S^2}{D}\right)\sqrt{\rho_p^2\omega^4 + \frac{4\rho_p\omega^2 S^2}{D}}\right). \tag{1.38}$$

The global bending and shear impedances are then deduced from the above formulation of the mechanical impedance.

$$\begin{cases} \left(Z_\infty^D\right)^{-1} = \dfrac{1}{8\sqrt{D\rho_p}} \\ \left(Z_\infty^S\right)^{-1} = \dfrac{\omega}{4S} \end{cases} \tag{1.39}$$

where $(Z_\infty^D)^{-1}$ and $(Z_\infty^S)^{-1}$ represent respectively the inverse infinite mechanical impedances below and above transition frequency. So, the first transition frequency is given by equating the two equations:

$$f_t = \frac{S}{4\pi}\sqrt{\frac{1}{\rho_p D}}. \tag{1.40}$$

The developed expression of the transition frequency separates the classical isotropic behavior of the sandwich panel and the out-of-plane shear core. It is worth mentioning that the previous transition formulation is the same as the one developed by Rindel using the modal density.

1.4 Modal density for sandwich panels

The modal density is by definition the distribution of the modal natural frequencies in the frequency domain. It should be mentioned that there are two alternative forms of the modal density; a modal density in terms of frequency $n(f)$ and another in terms of angular frequency $n(\omega)$ which are related by $n(\omega) = 2\pi n(f)$. So, the mathematical definition of the modal density is the differentiation of the mode count $N(\omega)$ with respect to the frequency.

$$n(\omega) = \frac{dN(\omega)}{d\omega}, \tag{1.41}$$

For a panel with dimension $a \times b$, the mode counts can be expressed by:

$$N(\omega) = \frac{ab}{2\pi^2} \int_0^{\frac{\pi}{2}} r^2 d\theta, \tag{1.42}$$

The first analytical development of modal density for honeycomb sandwich panels or shells was carried out by Wilkinson [157]. It is assumed that the face-sheets have the same thickness and are much thinner than the sandwich core; the face-sheets have a negligible bending stiffness about their mid-plane; the sandwich core makes a negligible contribution to the bending stiffness and it is considered to be isotropic. So, the modal density expression presented in the Wilkinson's work for a flat plate is given as follows:

$$n(f) = \frac{ab}{\pi S h_c^2} \frac{\Omega^2}{f} \left\{ 1 + \frac{\Omega^2 + 2\left(1-\nu^2\right)S^2}{\sqrt{\Omega^4 + 4\left(1-\nu^2\right)S^2\Omega^2}} \right\}, \tag{1.43}$$

where $S = \dfrac{Gh_c}{2E_f h_f}$ and $\Omega^2 = \dfrac{h_c^2\pi^2}{h_f E_f} f^2 \left\{ \dfrac{rho_c h_c}{2} + \rho_f h_f \right\}$. a, b are the panel dimensions. In the very high frequency range, the approximate model needs to include the bending of the face-sheets and the bending and shear of the sandwich core.

The effect of orthotropic sandwich core has then been accounted by Erickson [47]. The bending stiffness of the sandwich core is ignored but its shear effect was included in the analytic model via the insertion of the shear modulus G_x and G_y. The model has included the bending stiffness of the face-sheets and the rotary inertia of the sandwich panel.

Clarkson and Ranky [31] present in their paper an analytical development of the modal density for honeycomb sandwich plates. The development is based on the Erickson's model but the rotary inertia and the bending stiffness of the core are neglected. The proposed formula is expressed as follows:

$$n(f) = \frac{\pi^2}{2\omega_0}\frac{a}{b}\left\{ r\left(\frac{\omega}{\omega_0}\right) + \frac{1+\frac{1}{2}r^2\left(\frac{\omega}{\omega_0}\right)}{\sqrt{1+\frac{1}{4}r^2\left(\frac{\omega}{\omega_0}\right)}} \right\}, \tag{1.44}$$

in which $\omega_0 = \left(\frac{\pi}{b}\right)^2\sqrt{\frac{D}{\rho_p}}$ and $r\left(\frac{\omega}{\omega_0}\right) = 2\pi f\sqrt{\frac{D\rho_p}{D_{Qx}D_{Qy}}}$ with $D = \frac{E_f h_f h_c^2\left(1+\frac{h_f}{h_c}\right)^2}{2\left(1-\nu^2\right)}$ is the bending stiffness of the sandwich panel, $D_{Qx} = G_x h_c\left(1+\frac{h_f}{h_c}\right)^2$ and $D_{Qy} = G_y h_c\left(1+\frac{h_f}{h_c}\right)^2$ are the shear stiffness of the sandwich panel.

Afterwords, Renji [123] has developed an analytical formulation of the modal density of the sandwich panel in which the orthotropic effect of the sandwich panel as well as the shear core and the stiffness bending of the face-sheets are included. The modal density in the Renji's model is expressed in the following form:

$$\begin{aligned} n(f) = \frac{2ab\rho_p f}{S}\int_0^{\frac{\pi}{2}} \Bigg\{ & \frac{f_2(\theta)}{f_1(\theta)} + \frac{1}{f_1(\theta)}\left(\rho_p^2\omega^4 f_2^2(\theta) + \frac{4\rho_p\omega^2 S^2}{\sqrt{D_{xx}D_{yy}}}f_1(\theta)\right)^{-\frac{1}{2}} \\ & \left(\rho_p\omega^2 f_2^2(\theta) + \frac{2S^2}{\sqrt{D_{xx}D_{yy}}}f_1(\theta)\right)\Bigg\} d\theta, \end{aligned} \tag{1.45}$$

where the coefficients $f_1(\theta)$ and $f_2(\theta)$ are defined in section 1.2.5 equation 1.26.

In recent times, Han et al. [61, 62] have developed a modal density expression of sandwich panels with composite face-sheets and orthotropic sandwich core based on

the improved ordinary sandwich panel theory (IOSPT) presented in subsection 1.2.6. The modal density was expressed in the Han's work with considering the effects of the boundary condition as follows:

$$\begin{cases} N_{CC}(\omega) = \dfrac{ab}{2\pi^2}\displaystyle\int_0^{\frac{\pi}{2}} r^2 d\theta - \left(r|_{\theta=0}\dfrac{a}{\pi} + r|_{\theta=\frac{\pi}{2}}\dfrac{b}{\pi}\right) + 1, \\ N_{FF}(\omega) = \dfrac{ab}{2\pi^2}\displaystyle\int_0^{\frac{\pi}{2}} r^2 d\theta + \left(r|_{\theta=0}\dfrac{a}{\pi} + r|_{\theta=\frac{\pi}{2}}\dfrac{b}{\pi}\right) + 1, \end{cases} \tag{1.46}$$

where N_{CC} and N_{FF} are respectively the mode counts under clamped and free boundary conditions. r^2, $r|_{\theta=0}$ and $r|_{\theta=\frac{\pi}{2}}$ can be obtained by the governing equation 1.31 of the sandwich panel. Subsequently, the modal density of the sandwich panel can be computed via the definition of the modal density (eq. 1.42), as long as the mode counts are given.

1.5 Sound transmission loss through sandwich panels

The control the noise level and vibration is of great interest in either scientific or industrial field for a in-depth understanding of the way in which the sound waves are produced or transmitted through a plate. In general, when a sound wave strikes a plate, a part of its energy is reflected, another part is absorbed and the rest of the power energy is transmitted (see figure 1.10). The sound level of the reflected, absorbed or transmitted part depend directly on the mechanical properties of the plate.

Due to a wide variety of sandwich panels, in terms of configurations of the core, there is a lack of theories which can describe their sound transmission, absorption and reflection characteristics.

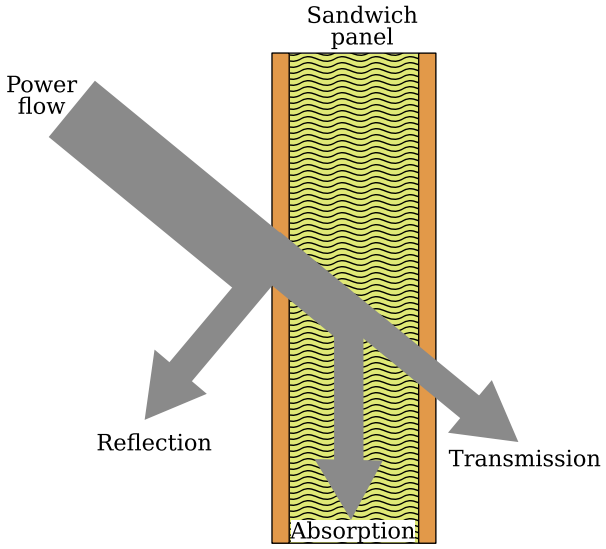

Figure 1.10: Reflection, absorption and transmission of a sound wave strikes a sandwich panel.

The sound transmission loss (TL) is an acoustic indicator used to describe the reduction of sound transmitted through the structure. This indicator [21, 108] is defined as the common logarithm of the ratio between the incident and transmitted powers.

$$TL(\omega) = 10.\log_{10}\left(\frac{1}{\tau(\omega)}\right), \tag{1.47}$$

where $\tau(\omega) = \dfrac{W_T}{W_I}$ is the transmission coefficient, W_I is the incident power, W_T is the transmitted power. The sound transmission loss of a diffuse field for an infinite plate is obtained by averaging the transmission coefficient $\tau\left(\omega,\theta,\varphi\right)$ over all the incident angles θ and the propagation angle φ.

$$\tau(\omega) = \frac{\int_0^{2\pi}\int_0^{\pi/2}\tau(\omega,\theta,\varphi)\sin\theta\cos\theta\ d\theta\ d\varphi}{\int_0^{2\pi}\int_0^{\pi/2}\sin\theta\cos\theta\ d\theta\ d\varphi}. \tag{1.48}$$

As it can be shown in figure 1.11, the TL characteristics for a typical plate can be divided into four distinct regions based on the frequency range under analysis. At very low frequencies, the TL is controlled by the panels stiffness and damping [72]. At lower frequency, the sound transmission loss of the panel is primarily governed by its mass in what is known as the mass controlled region. In this range, the TL expression can be predicted by the mass law :

$$TL = 10.\log_{10}\left[1+\left(\frac{\rho_s \pi f\cos\theta}{\rho_0 c_0}\right)^2\right], \tag{1.49}$$

in which ρ_s is the mass per unit surface area of the panel, f is the frequency, θ is the angle of incidence, ρ_0 and c_0 are the density and the sound speed of in the acoustic medium. For normal incident waves, $\theta = 0°$, the mass law simplifies to the normal incidence mass law which expressed as the following:

$$TL_{(\theta=0)} \approx 20.\log_{10}\left(\rho_s f\right) - 42.5\ [dB], \tag{1.50}$$

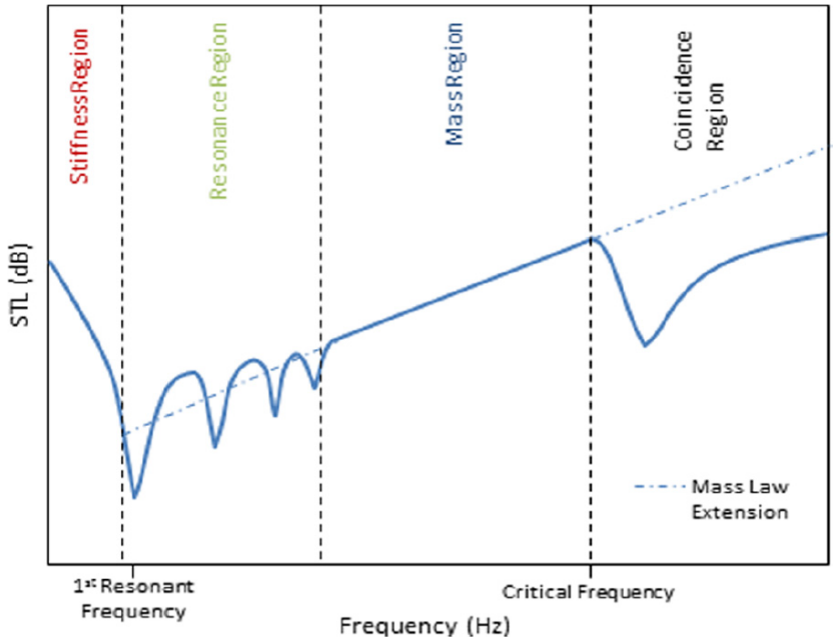

Figure 1.11: Sound transmission regions of a finite panel controlled by stiffness, resonance, mass, and coincidence [58].

For the diffuse field of the mass law, the TL expressed as follows :

$$TL = 10.\log_{10}\left[\frac{0.978\left(\frac{\rho_s \pi f}{\rho_0 c_0}\right)^2}{ln\frac{\left(1+\frac{\rho_s \pi f}{\rho_0 c_0}\right)^2}{1+\left(0.208\frac{\rho_s \pi f}{\rho_0 c_0}\right)^2}}\right], \tag{1.51}$$

The mass law is validated up to the region controlled by the coincidence effect. The critical or coincidence frequency f_c is the frequency at which the speed of bending waves

traveling into the structure equals the speed of sound in the air c_0. Around this frequency, the sound reduction performance is dramatically reduced. After the coincidence region, the TL still increases, but at 9 dB per doubling of frequency. More details about critical and coincidence frequencies are available in Renji et al. work [124].

1.5.1 Statistical Energy Analysis (SEA)

The Statistical Energy Analysis (SEA) method [33, 34, 82, 89] is an approach for modeling the acoustic transmission through a multilayer structure using the relationships of power flow based on the statistical coupling of dynamic modes of the system response.

The SEA approach provides a basis for predicting the average noise especially in the high frequency range where the modal density is high. This method has been developed for the aerospace industry and has been evolved over the last two decades. Lyon, Maidanik [88, 90] and Smith [134] are among the first researchers developing the SEA method where the problem of energy flow between slightly coupled linear oscillators was processed. After this early work, several articles [91, 105, 129, 146] appeared in which improvements and generalizations of this method were presented and discussed.

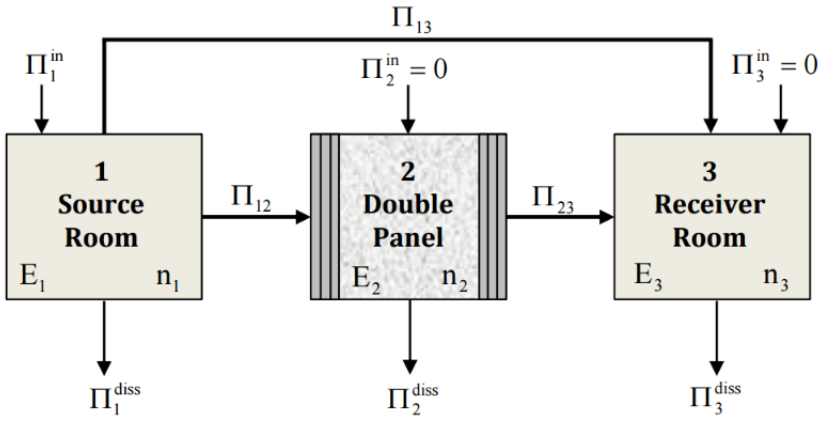

Figure 1.12: Power flow between the three sub-systems of a double composite panel quoted from [133].

The method divides the whole system into subsystems (see figure 1.12) that can either receive, store, or dispel the energy. The energy equilibrium for each subsystem is based on energy conservation. The power flowing from a subsystem to another is assumed to be proportional to the difference in their modal energy, or the vibrational en-

ergy per mode. This is the same principle as that of heat transfer, energy is discharged in a hot subsystem into a cooler subsystem until the temperature difference is equal to zero. In the SEA method, the modal energy is the temperature. If the vibrational energy per mode is equal in the two subsystems, the flow of energy between them is zero. This assumption is called the proportional power coupling.

1.5.2 Transfer matrix method (TMM)

The method of transfer matrices (TMM) [6, 23] allows modeling the acoustic propagation of plane waves in the plies of a layered medium. The media can be of different types: solid, elastic, thin plate, fluid, solid or porous and so on . Each layer is represented by a vector V whose components are the speeds, stresses (solid, porous) or the pressure (fluid) caused by the wave propagating in the medium under consideration.

Figure 1.13 illustrates an incident plane wave with an incident angle θ on a structure having a thickness d. The plate is infinite in x_1 and x_2 directions. The incident wave results in a wave field in a finite media, where the wavenumber along the x_1 direction is equal to the wavenumber in the air following the same direction. The acoustic propagation in the plate is represented by a transfer matrix [T].

$$V(M) = [T]V(M'). \tag{1.52}$$

The transfer matrix method (TMM) can be generalized to be applied to other media such as thick plates, orthotropic plates, sandwich panels and porous materials transversely isotropic [6]. A different excitation field can be modeled (e.g. the plane waves, the point forces,...).

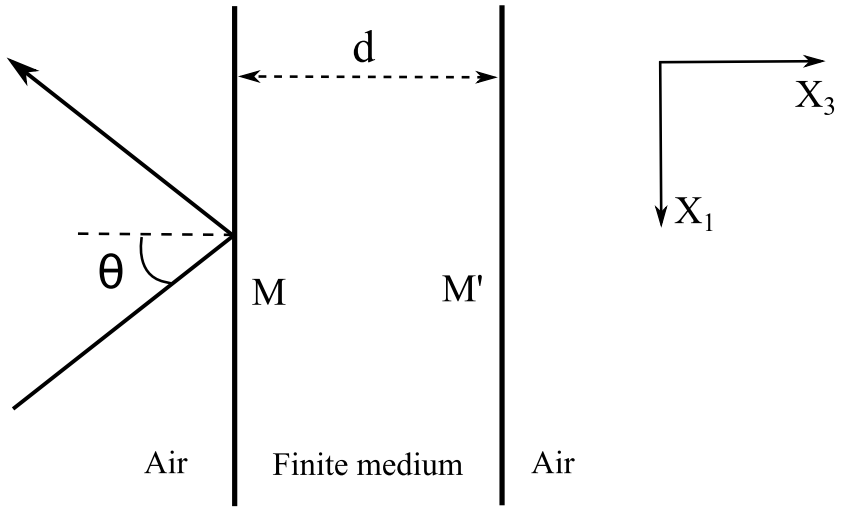

Figure 1.13: Incident plane wave on a plate thickness d, with an incident angle θ.

The acoustic indicators which can obtained via this method are the surface impedance, the coefficients of reflection, absorption and transmission and the loss factor. The classic TMM method assumes a structure with infinite lateral dimensions. This assumption can cause bad results in the low frequencies, especially for the panels of a small size. However, the results can be corrected in order to consider the finite size of the structure [6, 125, 147].

1.5.3 Finite transfer matrix method (FTMM)

Allard and Atalla [6] give an extension of the transfer matrix method, called the finite transfer matrix method (FTMM), similar to the spatial window technique which takes into account the finite size of the structure. The radiation efficiency in this method is calculated differently, but gives similar results to those of the art of spatial window [6]. In the FTMM method, a single spatial window is only used in the incident media side. Allard and Atalla indicate that the use of a dual spatial window to calculate the sound transmission coefficient is contrary to its definition. They have recommended to apply the correction only for the transmitted power. This correction may be necessary to take into account the diffusion of the incident field.

1.5.4 Wang & Lu's approach

This approach developed by Wang and Lu et al. [132, 148, 159] allows predicting the sound transmission loss (TL) for finite sandwich structures with corrugated core that

have been widely used in hull construction of passenger trains. This model is based primarily on replacing the heart with springs of translation and rotation evenly (see figure 1.13) distributed between the two face-sheets of the sandwich structure.

The transmission coefficient of sound power is expressed in this analytical approach as a function of the incident angle θ as follows:

$$\tau(\theta) = \frac{\sum_{m=1}^{\infty} |T_m|^2}{\sum_{m=1}^{\infty} |I_m + R_m|^2}, \tag{1.53}$$

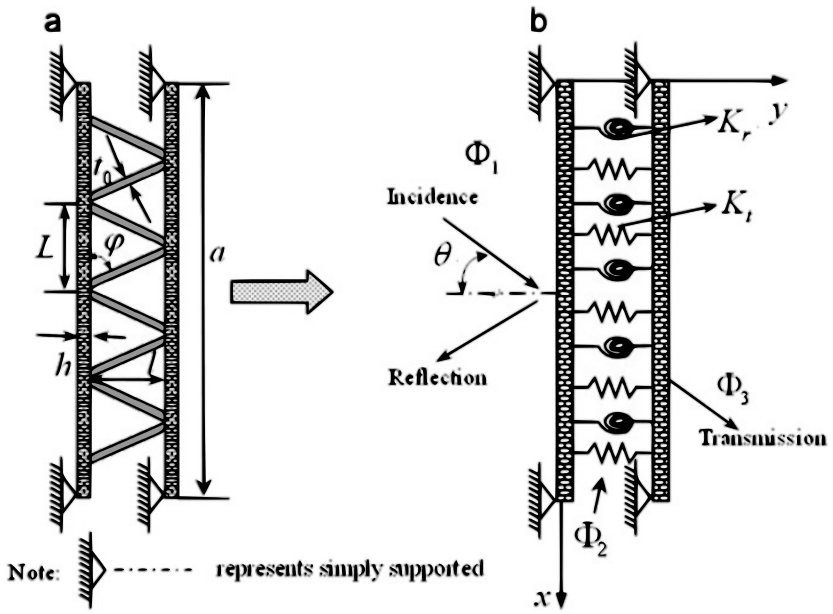

Figure 1.14: (a) Simply-supported sandwich structure with corrugated core; (b) equivalent structure [132].

where T_m and R_m are the amplitude of the transmitted and the reflected acoustic with their expressions are expressed in terms of the amplitude of the incident waves I_m.

$$T_m = \frac{-2j\omega^2\rho_0 Q_{12} I_m e^{jk_y l}}{k_y(Q_{11}Q_{22} - Q_{12}Q_{21})}, \quad R_m = I_m - \frac{2j\omega^2\rho_0 Q_{22} I_m}{k_y(Q_{11}Q_{22} - Q_{12}Q_{21})}, \tag{1.54}$$

with Q_{ij} are coefficients given in reference [132].

1.6 Experimental methods for dispersion analysis

1.6.1 Identification of the wavenumber

Several experimental techniques are available for evaluating the dispersion characteristics. In this subsection, a classical method of spectrum analysis is presented and a promising spectrum estimation approach is then shortly described.

1.6.1.1 Correlation method

The correlation method was developed by Ferguson et al.[51, 69] which deals with windowing the measured normal displacement of a plate for identifying the propagation constants. The method is based on a 2D discrete spatial Fourier transformation.

Similar to the temporal Fourier transform, which allows connecting the time and the frequency, the spatial Fourier transform connects the spatial and wavenumber domain. The formulation of the SFT can be defined as:

$$F(k) = \int_{-\infty}^{\infty} f(x) e^{-jk_x x} dx. \tag{1.55}$$

Also, the inverse spatial Fourier transform is defined as:

$$f(x) = \int_{-\infty}^{\infty} F(k_x) e^{-jk_x x} dk_x. \tag{1.56}$$

Windowing the field allows avoiding the effect of the near field which is caused principally by the sources and the boundary conditions.

1.6.1.2 Inhomogeneous wave correlation (IWC) method

The inhomogeneous wave correlation method was proposed by Berthaut et al. [19] to identify the dispersion characteristics from experimental data. The IWC method not only allows determining the k-space at each frequency but it is also able to identify the corresponding loss factor (i.e. the inhomogeneous wave parts as the near fields induced by the boundary conditions or sources). The main idea behind the IWC method was the computation of the correlation coefficient between the experimental wave field and an inhomogeneous reference wave. Unlike the standard DFT technique, the IWC method is more suitable for real measurements because it requests neither equidistant data grids nor the resolution.

1.6.2 Identification of the sound transmission loss

1.6.2.1 Standard test method

The standard test method [45] is developed by the international standards and testing organization (ASTM) to measure the airborne sound transmission through a partition or partition element in a laboratory. The experimental set-up of this standard method is shown in figure 1.15.

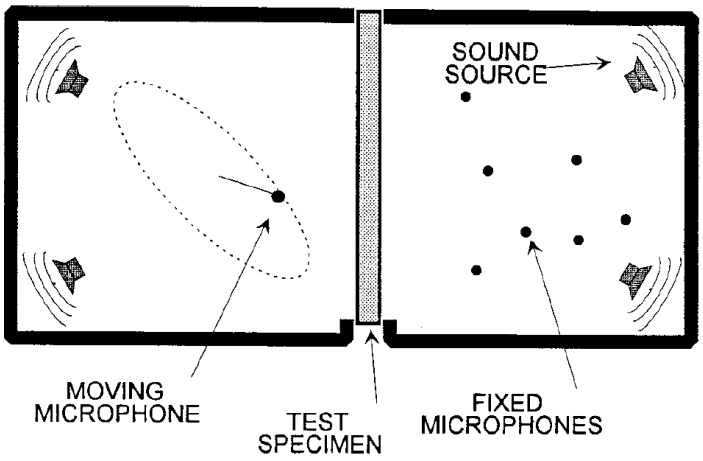

Figure 1.15: Experimental set-up of the sound transmission loss measurement [45].

In the present method, the sound pressure levels in the source and receiving rooms, the sound absorption in the receiving room and the area of the panel are used to determine the sound transmission loss. Different values of the measured sound transmission loss may be expected . So to compensate for this, It is recommended to repeat the whole measurement with reversing the source and receiving rooms and then averaging the final results.

The below equation is used in the experimental method to determine the sound transmission loss (TL) at each frequency f:

$$TL(f) = L_S(f) - L_R(f) + 10\log\left(\frac{S}{A_R(f)}\right), \tag{1.57}$$

where $L_S(f)$ and $L_R(f)$ are respectively the average sound pressure level in the source and receiving rooms. S is the area of the tested panel that is exposed in the receiving room. $A_R(f) = \frac{\sqrt[3]{V^2}}{3}$ is the sound absorption coefficient of the receiving room with V is the receiving room volume. The sound absorption coefficient should be low to achieve the

best possible simulation of the ideal diffuse field condition and to minimize the region dominated by the direct field of the tested panel.

1.6.2.2 Impedance tubes method

The impedance tube method is an experimental method widely used for determining the sound absorption and the acoustic impedance coefficients of the material [1]. This experimental method is exploited by Jung et al. [71] to determine the sound transmission loss of the material.

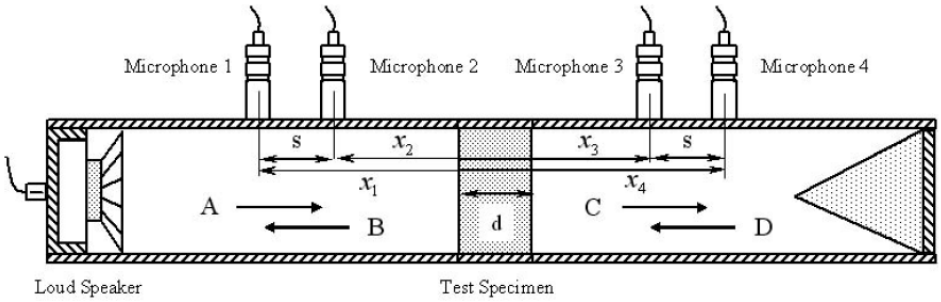

Figure 1.16: Impedance tube for measuring the sound transmission loss [71].

The sound transmission loss of the material can be determined by utilizing the sound pressure measured via the microphones placed at position 1, 2, 3 and 4 (see figure 1.16). The equation used in this method to predict the sound transmission loss experimentally is expressed as the following form:

$$TL = 20\log\left|\frac{e^{jks} - H_{12}}{e^{jks} - H_{34}}\right| - 20\log|H_t|, \tag{1.58}$$

in which $H_{12} = \dfrac{p_1}{p_2}$ and $H_{34} = \dfrac{p_4}{p_3}$ are the transfer function with p_1, p_2, p_3 and p_4 are the Fourier-transform component of the sound pressures at positions 1, 2, 3 and 4 respectively. $H_t = \sqrt{\left|\dfrac{S_d}{S_u}\right|}$ is the square root of the ratio between the auto-spectrums in the downstream tube S_d and the upstream tube S_u.

1.7 Experimental attempts for improving the transmission loss

Over the last decades, many published papers are suggesting different techniques for improving the vibroacoustic performance of the sandwich panel. In this section, it is

tried to present some of the important works published recently.

1.7.1 Palumbo & Klos's work

Palumbo and Klos [110] have established a series of experimental works to improve the sound transmission loss (TL) of the honeycomb sandwich panel while trying at the same time to keep the advantages of this kind of a structure (very high stiffness with low weight). These sandwich structures provide a reasonable alternative to panels stiffened aluminum used currently in most aircraft fuselages and launchers.

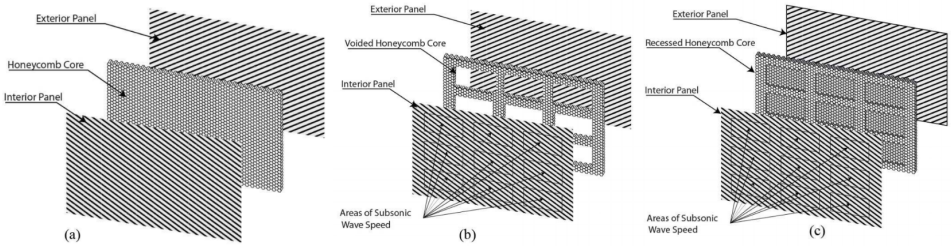

Figure 1.17: Components of full (a), voided (b) and recessed (c) sandwich core [110].

Palumbo et al. have conducted a series of experiments to enhance the vibroacoustic indicator (TL). These experiments are based on creating of reduced stiffness areas (see figure 1.17), which are considered as acoustic damping at the sandwich panel. The reduced stiffness areas were made by creating voids and recesses to the core of the sandwich panel. These areas have resulted in an increase of the sound transmission loss (TL) up to 11 dB in the mid frequency range (see figure 1.18).

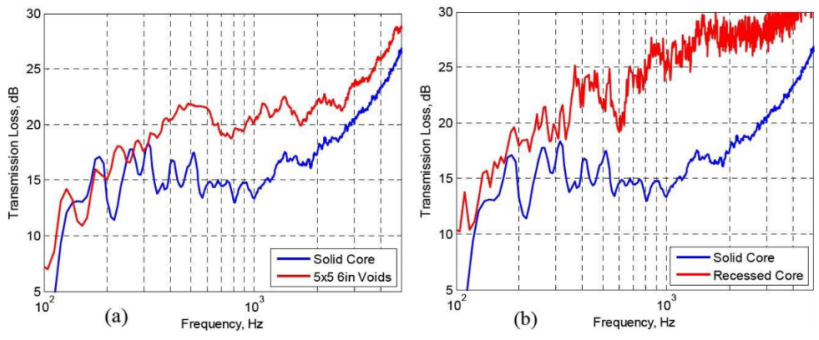

Average Difference in TL Over Frequency Band

100-500	500-1000	1000-2000	2000-5000
1.5	6.5	7.0	5.2

Average Difference in TL Over Frequency Band

100-500	500-1000	1000-2000	2000-5000
5.1	9.7	11.1	7.8

Figure 1.18: Transmission loss curves for (a) voided (b) and recessed sandwich core [110].

Nonetheless, the creation of these acoustic damping areas results in a reduced plate stiffness about 10%. The decrease in the bending stiffness of the modified sandwich panel is still present despite the increase of the core thickness and the improvement of the shape of the voids and recesses in order to avoid the stress concentration.

1.7.2 Attempt of Peters & Nutt

The experimental study carried out by Peters and Nutt [111] aims to identify the influence of different mechanical and geometric parameters (cell size, mass density of the core, shear modulus of the core and so on) on the wave propagation speeds across the honeycomb sandwich structures particularly the shear wave propagation speed.

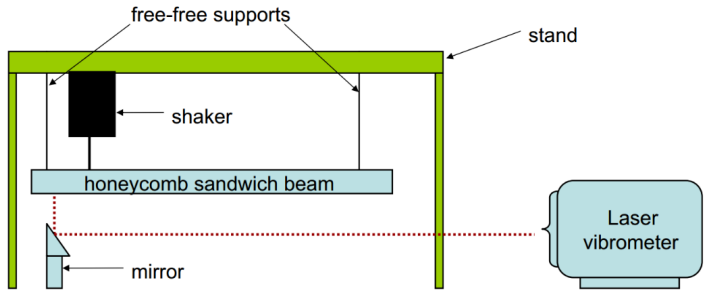

Figure 1.19: Shematic of experimental set-up [111].

The experimental set-up of this study is illustrated in figure 1.19. The experiment measures the bending wave speeds fo the honeycomb sandwich panels with different design parameters and then distinguishes the transition between the panel bending and the shear wave motion . The meseared wave speeds for the honeycomb structure are compared to the TL measurements published [36, 77] for identical structures.

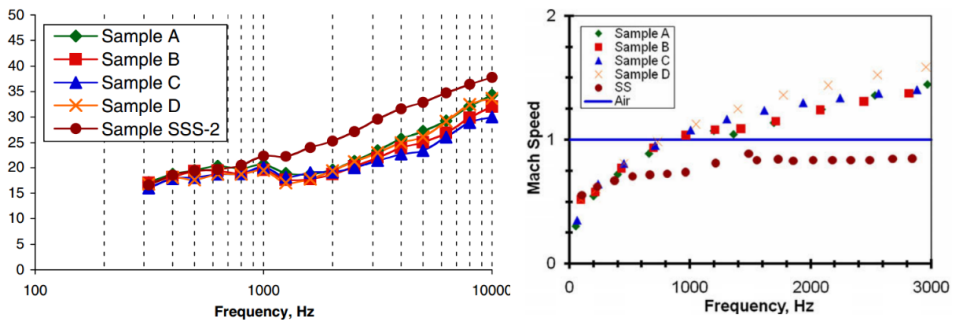

Figure 1.20: Wave speed mesearements [111] and sound transmission loss [124] of carbon fiber laminate face-sheets and a honeycomb core.

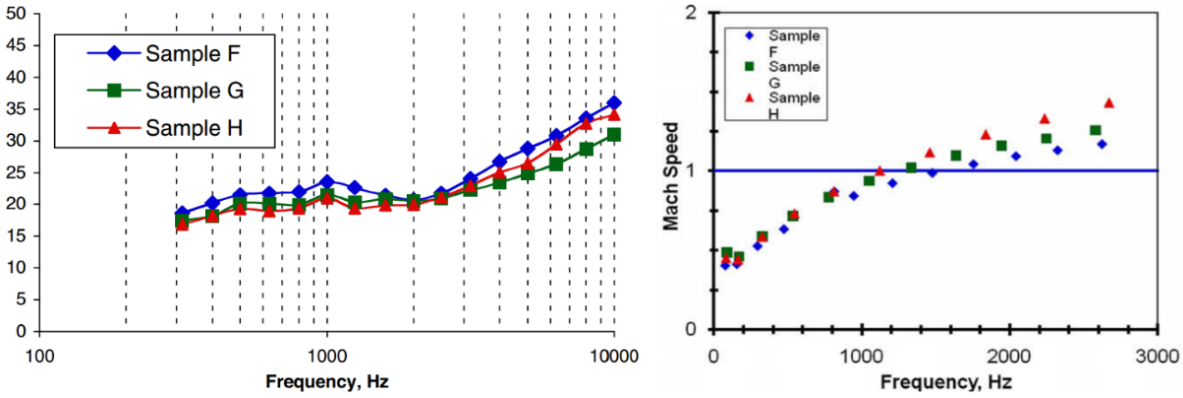

Figure 1.21: Wave speed mesearements [111] and sound transmission loss [124] of glass fiber laminate face-sheets and a honeycomb core.

On the whole, It is shown in the obtained results that the shear modulus of the sandwich core has a significant influence on the waves speed of the tested panels (see figure 1.20 and 1.21), while the cell size has been a negligible effect on either the wave speed or the sound transmission loss (TL).

1.7.3 Attempt of Naify and his co-workers

Naify et al. [103] have proposed a noise reduction strategy by exploiting the difference in acoustic impedance different gasses. The concept of using helium as the gas layers has been studied in many published papers [9, 12, 100, 115] but it has not implemented in an industrial application. As shown in figure 1.22, the concept is based on the impedance mismatch between the air media and the gas layer.

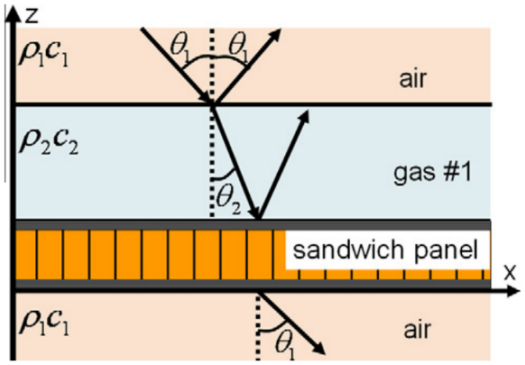

Figure 1.22: Reflection and transmission of sound waves incident on a layered gas panel [103].

The recent paper of Naify et al. [103] is an extension of the impedance mismatch described in figure 1.22. The paper suggests to attach multiple gas layers on the source and receiver sides of the sandwich panel. Figure 1.23 exhibits a comparison of the measured and theoretical sound transmission loss curves between a sandwich panel alone and a sandwich panel with gas layers attaching on the source side or on both source and receiver sides.

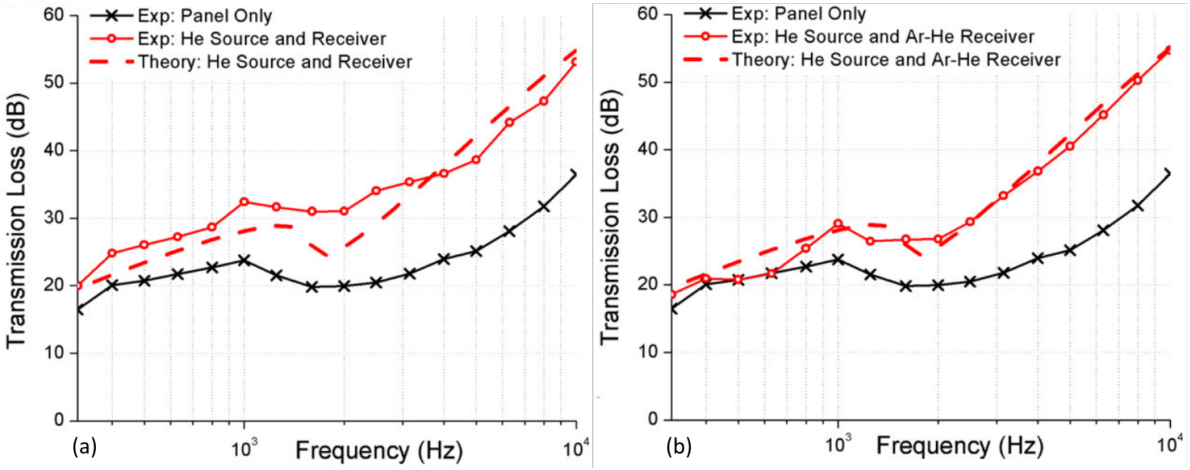

Figure 1.23: (a) Panel with helium layers on the source and receiver sides; (b) Panel with helium on the source side and argon and helium on the receiver side of the panel [103].

Although it is shown in figure 1.23 that the proposed concept for the noise reduction is an effective means to increase the sound transmission loss through a sandwich panel, it should be noted that the concept has some drawbacks. Among them, it can be mentioned that the added layers increase the weight of the reference sandwich panel. Also, after adding the gas layers, the thickness of the sandwich panel is much thicker than the reference panel which can complicate the work of the designers to set a smaller diameter for a cylindrical structure for instance.

1.8 Concluding remarks

Theoretical models and analyses of the vibroacoustic response of sandwich panels are among the central issues of the current engineering research, which are trying to better investigate and reduce the principal drawbacks of such configuration.

In the previous sections and subsections, an overview of the most relevant models able to predict the dynamic characteristics and the vibroacoustic performance of sandwich panels have been cited. Furthermore, some of interesting experimental attempts for improving the acoustic performance of sandwich panels have been presented.

The increasing attention paid to the topic of vibroacoustic models is due to the large variety of core configurations of sandwich panels, arising from different materials and geometrical combinations. This trend spread the research lines rather than focusing on a specific view. This emerges clearly from the presented review in terms of both theoretical modeling and experimental measurements and investigations. In the next chapter, a numerical approach is suggested which can take into account most of the varieties mentioned previously.

CHAPTER 2

IMPLEMENTATION OF THE MESO-MACRO APPROACH

Contents

N this chapter, the development of the meso-macro approach and its results are presented in detail. In general, the suggested approach is able to model the dispersion characteristics for the free wave propagation through complex two-dimensional periodic structures. These characteristics can facilitate the prediction of different vibroacoustic indicators such as the modal density (n), the transition frequency (f_t) and the sound transmission loss (TL). The prediction of the stated indicators allows for a deeper understanding of the vibroacoustic behavior of sandwich

structures by revealing the influence of different geometric parameters of the modeled unit cell via a parametric study, for instance.

2.1 Development of the meso-macro approach

The meso-macro approach, developed in this section, is based on the wave finite element (WFE) method presented in chapter 1, subsection 1.2.9. The WFE method has been presented as a numerical method able to model the vibroacoustic behavior of a periodic structure. This method is then applied here to predict the dynamic behavior of a sandwich panel. It includes the reformulation of the motion equation of a representative elementary cell by introducing the notion of the dynamic stiffness matrix (DSM). This matrix (DSM) involves the mass and stiffness matrices of the two-dimensional periodic cell of the modeled structure. The structural wave motion of the sandwich structure is expressed in terms of the eigenvalues and the eigenvectors of the rewritten dynamic stiffness matrix. The eigenvalues and eigenvectors of the problem formulation represent the wavenumbers and the wavemodes of the studied sandwich panel, respectively.

There are two types of formulation, one- and two-dimensional WFE formulations. The both formulations give the same results for 2D periodic structures. However, the 1D formulation is well recommended for 1D periodic structures. The 2D WFE formulation and a reduction process were further detailed and clarified through the next subsections. The approach, reported here, does not require any homogenization techniques of the sandwich panel. Consequently, the applied approach save up totally the meso-scale information of the considered core.

2.1.1 2D formulation of the WFE method

A rectangular or parallelogram periodic cell of the honeycomb sandwich panel is hereby considered (see figure 2.1) with length L_x and width L_y. Thanks to the structure periodicity, it is sufficient to model just the unit cell representing the periodicity of the sandwich panel by a conventional finite element method [11, 113], instead of the whole structure. The 2D WFE formulation for homogeneous honeycomb sandwich structures was validated and given in many published papers (e.g. Chronopoulos' work [28]). In the present study, the honeycomb sandwich panel was modeled as 3D geometric architecture without using any homogenized values.

According to the 2D WFE method, the motion equation for periodic structural waveguides can be expressed as follows:

$$\begin{pmatrix} D^d_{bdI} & D^d_{bdbd} \\ D^d_{Ibd} & D^d_{II} \end{pmatrix} \begin{pmatrix} U_{bd} \\ U_I \end{pmatrix} = \begin{pmatrix} f_{bd} \\ 0 \end{pmatrix}, \tag{2.1}$$

where D^d_{bdI}, D^d_{bdbd}, D^d_{Ibd}, and D^d_{II} are the block matrices of the dynamic stiffness matrix $D^d = \widetilde{K}(1+j\eta) - \omega^2\widetilde{M}$ of the modeled sandwich panel. $\widetilde{K}$ and $\widetilde{M}$ are respectively the reduced stiffness and mass matrices. η is the damping coefficient. U_{bd} and f_{bd} are respectively the displacement and force vectors of the boundary nodes. U_I represents the displacement vector of internal nodes (see figure 2.2).

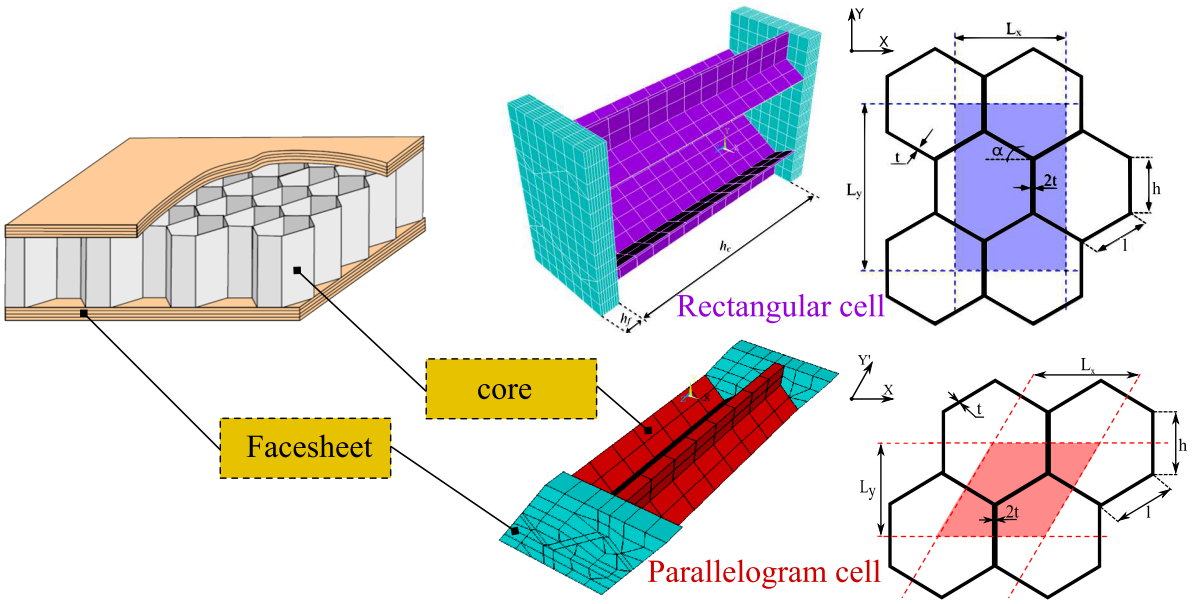

Figure 2.1: Waveguide periodic cell of the honeycomb sandwich panel.

The degrees of freedom (dofs) of the displacement vector related to interior nodes U_I are condensed to the dofs of the displacement vector related to boundary nodes by injecting the bellow expression (2.2) into equation (2.1).

$$U_I = -(D^d_{II})^{-1} D^d_{Ibd} U_{bd}. \tag{2.2}$$

The dofs of the boundary nodes U_{bd} are composed by the dofs of the edge nodes (U_B, U_L, U_R, U_T) and the corner nodes (U_1, U_2, U_3, U_4) (see figure 2.2). In the present numer-

ical approach, it is assumed that each opposite edge and corner nodes must have exactly the same number of dofs. However, there are no mesh constraints for the interior nodes of the periodic cell. Therefore, the FEM mesh inside the waveguide periodic cell can be applied arbitrary.

By using the Floquet-Bloch theory for a periodic rectangular cell and assuming a time harmonic response, the displacements at each edge and corner can be written respectively as a function of the displacements at one single corner U_1 and edges, U_L and U_B.

For the dofs of the corner nodes :

$$U_2 = \lambda_x U_1, \qquad U_3 = \lambda_y U_1, \qquad U_4 = \lambda_x \lambda_y U_1. \tag{2.3}$$

For the dofs of the edge nodes :

$$U_R = \lambda_y U_L; \qquad U_T = \lambda_y U_B, \tag{2.4}$$

with $\lambda_x = e^{i\mu_x}, \lambda_y = e^{i\mu_y}$. $\mu_x = k_x L_x$ and $\mu_y = k_y L_y$ being respectively the propagation constants of a plane harmonic wave in the x- and y-directions, while k_x and k_y are the wavenumbers along the x- and y-directions, respectively. Hence, the total dofs of the boundary and interior nodes can be written in matrix form as follows:

$$\begin{pmatrix} U_1 & U_2 & U_3 & U_4 & U_B & U_L & U_R & U_T & U_I \end{pmatrix}^T = \Lambda_R \begin{pmatrix} U_1 \\ U_B \\ U_L \\ U_I \end{pmatrix}, \tag{2.5}$$

where $\Lambda_R(\lambda_x, \lambda_y)$ is expressed as :

$$\Lambda_R(\lambda_x,\lambda_y)=\begin{pmatrix} I_{n_1} & 0 & 0 & 0 \\ \lambda_x.I_{n_1} & 0 & 0 & 0 \\ \lambda_y.I_{n_1} & 0 & 0 & 0 \\ \lambda_x.\lambda_y.I_{n_1} & 0 & 0 & 0 \\ 0 & I_{n_B} & 0 & 0 \\ 0 & 0 & I_{n_L} & 0 \\ 0 & 0 & \lambda_x.I_{n_L} & 0 \\ 0 & \lambda_y.I_{n_B} & 0 & 0 \\ 0 & 0 & 0 & I_{n_I} \end{pmatrix}. \tag{2.6}$$

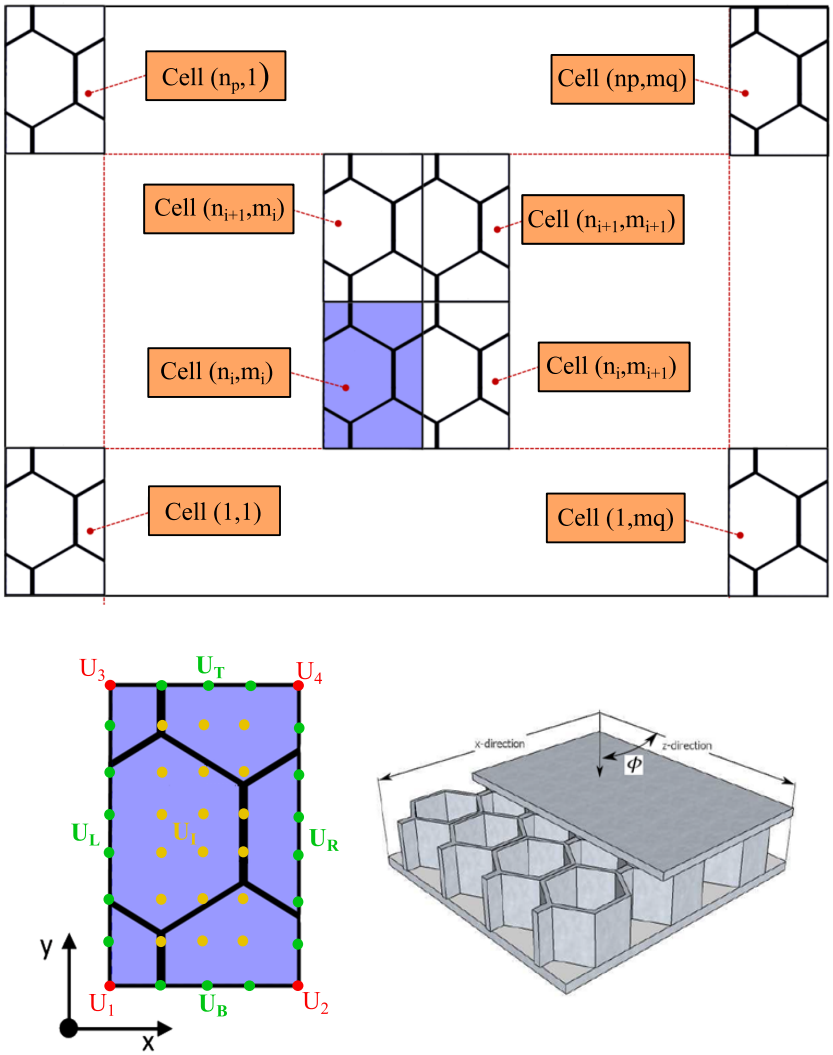

Figure 2.2: Nodes definition of the rectangular unit cell in the 2D WFE method.

It should be mentioned that the propagation constant λ_y has to be replaced in the case of the parallegram cell by $\lambda_{y'} = \lambda_y^{\frac{L_x}{L_y}\cos\alpha}\lambda_x^{\sin\alpha}$ with $\alpha = \frac{\pi}{6}$ which represents the propagation constant in the y'-direction.

In the absence of any external excitation applied to the sandwich panel, the boundary forces equilibrium f_{bd} of the periodic cell for the edges and corner dofs can be expressed as follows:

$$\Lambda_L(\lambda_x,\lambda_y)\begin{pmatrix} f_1 \\ f_B \\ f_L \end{pmatrix} = 0, \tag{2.7}$$

with f_1, f_B and f_L being respectively the applied boundary forces of the periodic cell at the corner node 1, the bottom edge and the left edge, whilst the matrix $\Lambda_L(\lambda_x,\lambda_y)$ is written in the following form :

$$\Lambda_L(\lambda_x,\lambda_y) = \begin{pmatrix} I_{n_1} & \lambda_x^{-1}.I_{n_1} & \lambda_y^{-1}.I_{n_1} & \lambda_x^{-1}.\lambda_y^{-1}.I_{n_1} & 0 & 0 & 0 & 0 & 0 \\ 0 & 0 & 0 & 0 & I_{n_B} & 0 & 0 & \lambda_y^{-1}.I_{n_B} & 0 \\ 0 & 0 & 0 & 0 & 0 & I_{n_L} & \lambda_x^{-1}.I_{n_L} & 0 & 0 \\ 0 & 0 & 0 & 0 & 0 & 0 & 0 & 0 & I_{n_I} \end{pmatrix}. \tag{2.8}$$

Hence, by substituting equation (2.5) into equation (2.1) and multiplying both sides of equation (2.1) by the matrix $\Lambda_L(\lambda_x,\lambda_y)$, the motion equation of the sandwich panel takes the following form:

$$\Lambda_L(\lambda_x,\lambda_y)D^d\Lambda_R(\lambda_x,\lambda_y)\begin{pmatrix} U_1 \\ U_L \\ U_B \end{pmatrix} = 0. \tag{2.9}$$

Many techniques are extensively discussed concerning the solution of the eigenvalue problem developed in equation (2.9) in many published works (e.g. Manconi's work [92]). To calculate the wave propagation along the x-direction, the frequency range ω and the wavenumber k_y across the y-direction are given. So, the non-linear eigenvalue problem of equation (2.9) can be reduced to the following equation:

$$A_j(\omega,\lambda_y).\lambda_x^j.\begin{pmatrix} U_1 \\ U_L \\ U_B \end{pmatrix} = \begin{pmatrix} 0 \\ 0 \\ 0 \end{pmatrix}, \tag{2.10}$$

where $j = 0,...,2$ for the rectangular unit cell and $j = 0,...,6$ for the parallelogram unit cell while the matrices A_j are given in detail in appendix A. Once the matrices A_j are determined, the eigenvalue problem developed in equation 2.10 can be solved using the polyeig function in Matlab.

The propagating wavenumbers k_x and k_y through the honeycomb sandwich panel in the principal directions, x and y, are then given by:

$$k_x = \frac{log(\lambda_x)}{iL_x}, \quad k_y = \frac{log(\lambda_y)}{iL_y}. \tag{2.11}$$

The above eigenvalues k_x and k_y, which stand for the wavenumbers propagating along the x- and y-directions, are complex values. Their real parts $\Re(k_x)$ and $\Re(k_y)$ present the change in phase with respect to the distance, whereas the imaginary parts $\Im(k_x)$ and $\Im(k_y)$ present the decay of the flexural wave amplitude across the sandwich panel.

Reduced computation processes for 1D and 2D WFE formulations were proposed by C. Droz et al. in [41, 43]. The proposed strategy develops a suitable numerical technique to reduce the computation of the wave dispersion in 2D periodic systems by combining the Component Mode Synthesis (CMS) approach and the model order reduction (MOR). the both reduced methods, CMS and MOR, will be presented in detail in the next subsections 2.1.2 and 2.1.3. The total strategy enables us to reduce the simulation time of the modeled structure from a couple of days to just few minutes or even few seconds.

The identification of the flexural wave type of sandwich structural has been realized by using the MAC matrix (Modal Assurance Criterion matrix) which allows distinguishing between different types of waves by comparing the wave shapes Φ of the honeycomb structure.

$$MAC = \frac{\left(\Phi_i^T \overline{\Phi}_j\right)\left(\Phi_j^T \overline{\Phi}_i\right)}{\left(\Phi_i^T \overline{\Phi}_i\right)\left(\Phi_j^T \overline{\Phi}_j\right)}. \tag{2.12}$$

The symbol ^{T} stands for the transpose and the overbar $\overline{\ }$ for the conjugate of the displacement vectors. The correlation coefficient for the MAC criterion with regard to orthotropic structures is typically between 0.4 and 0.8, whilst for isotropic case it can

be reached up to 0.9.

In the two next subsection, the reduction strategy adopted in the present work to reduce the computation cost of the meso-macro approach is presented in detail. The reduction process is based on two reduction methods, the component mode synthesis (CMS) and the model order reduction (MOR). It is worth mentioning that before applying the stated two methods, the execution time of the meso-macro approach was in terms of days.

2.1.2 Component mode synthesis (CMS)

The modal synthesis method (CMS) [32, 60, 162] is a standard method to reduce the size of a large finite element model describing the global response in terms of components for different modes of local substructures. This method is widely used in the aerospace industry to reduce the degrees of freedom of large finite element models. The CMS is considered as an extension approach of CraigBampton procedure [60] in a wave context since the aim here is to capture the local deformed wave shape of the unit cell. The CMS consists of transforming the internal physical dofs of the unit cell into modal internal dofs P_c (see Figure 2.3).

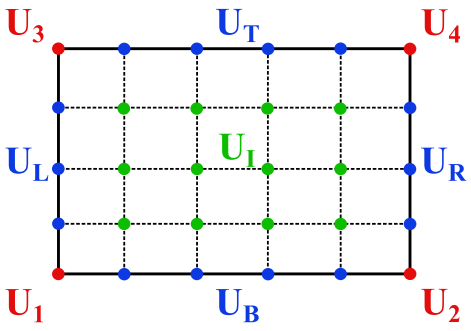

Full cell model with physical internal dofs U_I

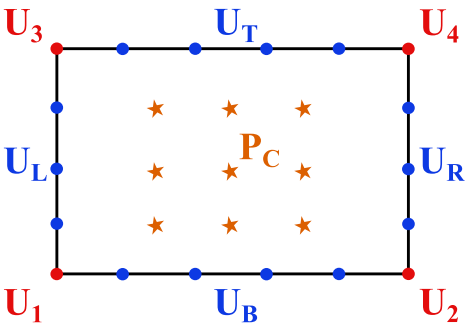

Reduced cell model with modal internal dofs P_c

Figure 2.3: Reduction of the internal dofs by using CMS technique.

The reduction method CMS consists of getting the two reduced mass $\widetilde{M}$ and stiffness $\widetilde{K}$ matrices by multiplying the full matrices, M and K, by a matrix contains two block matrices B and ϕ.

$$\begin{pmatrix} U_{bd} \\ U_I \end{pmatrix} = \begin{pmatrix} B & \phi \end{pmatrix} \begin{pmatrix} U_R \\ q_m \end{pmatrix}, with \qquad m < L \tag{2.13}$$

The subscript bd and I denote the boundary and internal independent elastic nodes of the unit periodic cell. B and ϕ are given as :

$$\begin{pmatrix} B \end{pmatrix} = \begin{pmatrix} I \\ \phi_R \end{pmatrix}, \qquad \begin{pmatrix} \phi \end{pmatrix} = \begin{pmatrix} 0 \\ \phi_L \end{pmatrix}, \tag{2.14}$$

in which ϕ_R and ϕ_L can be obtained by solving the following equations :

$$\begin{cases} [\phi_R] = -[K_{LL}]^{-1}[K_{LR}] \\ \{K_{LL} - \omega_o^2 M_{LL}\}[\phi_L] = 0 \end{cases} \tag{2.15}$$

By introducing the reduction matrices B and ϕ in the motion equation and developing the obtained equation, the motion equation becomes then as follows:

$$\begin{pmatrix} M_{BB} & M_{Bm} \\ M_{mB} & M_{mm} \end{pmatrix} \begin{pmatrix} \ddot{U}_R \\ \ddot{q}_m \end{pmatrix} + \begin{pmatrix} K_{BB} & 0 \\ 0 & K_{mm} \end{pmatrix} = \begin{pmatrix} U_{bd} \\ q_m \end{pmatrix} = \begin{pmatrix} F_{bd} + \phi_R^T F_I \\ \phi_I^T F_I \end{pmatrix}, \tag{2.16}$$

where the coefficients of the mass and stiffness matrices were given in appendix A.

2.1.3 Model order reduction (MOR)

The reduction technique (MOR) proposed by Droz et al. [41, 43] studies the free wave propagation in 1D and 2D composite structures. The main purpose of the stated method is to reduce the matrices A_i developed in equation 2.10 using a subset of eigen-solutions. The main idea of the proposed reduction technique is that a waveguide cross-sectional deformed shape at frequency ω_i can be used to describe the motion of the periodic cell for the same wave in a large frequency range around ω_i.

The first step in the MOR approach is to determine a reduced frequency sample for the wave shape interpolation. The main idea is that a cross-sectional deformed wave shape for a given wave type at a given frequency can be used to model the periodic cell motion for the same wave in a large frequency range around this given frequency. As it is known that in such structures the real wavenumbers remain between $k = 0$ and $k = \frac{\pi}{L}$ (see reference [95]). At the mid frequencies, the wave shapes are then defined by the wavenumber: $k = \frac{\pi}{2L}$. Therefore, the frequency subset can be determined by using

the (k_x, k_y) formulation given in [43].

The reduced wave basis can be identified using the obtained frequency subset $\widetilde{\Omega}$ as described in the system of the following equations:

$$\begin{cases} S(\lambda_x, \lambda_y, \widetilde{\omega}_1)\Psi = 0; \\ \vdots \\ S(\lambda_x, \lambda_y, \widetilde{\omega}_j)\Psi = 0; \quad with \quad \widetilde{\omega}_j \in \widetilde{\Omega} \\ \vdots \\ S(\lambda_x, \lambda_y, \widetilde{\omega}_n)\Psi = 0; \end{cases} \tag{2.17}$$

$$S(\lambda_x, \lambda_y, \widetilde{\omega}_j)\Psi = 0; \quad with \quad \widetilde{\omega}_j \in \widetilde{\Omega} \tag{2.18}$$

where $S(\lambda_x, \lambda_y, \omega)\Psi = 0$ is denoted for the spectral problem equation 2.10 with the solution Ψ is the wave shape on the condensed dofs defined as:

$$\Psi = \begin{pmatrix} U_1 \\ U_L \\ U_B \end{pmatrix} \tag{2.19}$$

So, the final reduced mass $\widetilde{M}$ and stiffness $\widetilde{K}$ matrices introducing in the spectral problem equation and leading to a computation reduction can be written as:

$$\begin{cases} \widetilde{K}_\Psi = B_\Psi^T \widetilde{K} B_\Psi; \\ \widetilde{M}_\Psi = B_\Psi^T \widetilde{M} B_\Psi; \end{cases} \tag{2.20}$$

in which the reduced wave basis B_Ψ is defined as function of the obtained wave shape Ψ as presented in appendix A in detail.

2.2 Validation of the proposed approach

The accuracy of the meso-macro approach and the reduction process presented in the previous section have been checked by a comparison with two published analytical methods presented in the first chapter in subsections 1.2.4 and 1.2.5. The sandwich panel used to check the accuracy of the proposed meso-macro approach is constituted by a honeycomb core made of a Nomex material and isotropic facesheets made of an Aluminum material. The basic mechanical properties of the Nomex material are as follows : Young's modulus $E_c = 3\ GPa$; density $\rho_c = 1380\ kg/m^3$; Poisson ratio $\nu_c = 0.33$. Whilst

the mechanical properties for the facesheet are : Young's modulus $E_f = 72.5\ \ GPa$; density $\rho_f = 2800\ \ kg/m^3$; Poisson ratio $\nu_f = 0.343$.

The effective mechanical properties injected into the two analytical methods are obtained by applying Malek et al. formulations [93] for a honeycomb sandwich core with single and double walls, which have been summarized in appendix A. The effective mechanical properties are then:

$$\rho = 57.637\ kg/m^3, E_x = 0.165\ MPa, E_y = 0.165\ MPa, E_z = 0.125\ GPa;$$
$$G_{xy} = 0.0379\ MPa, G_{xz} = 17.85\ MPa, G_{yz} = 30\ MPa;$$
$$\nu_{xy} = 0.975; \nu_{xz} = 0.00042, \nu_{yz} = 0.00043.$$

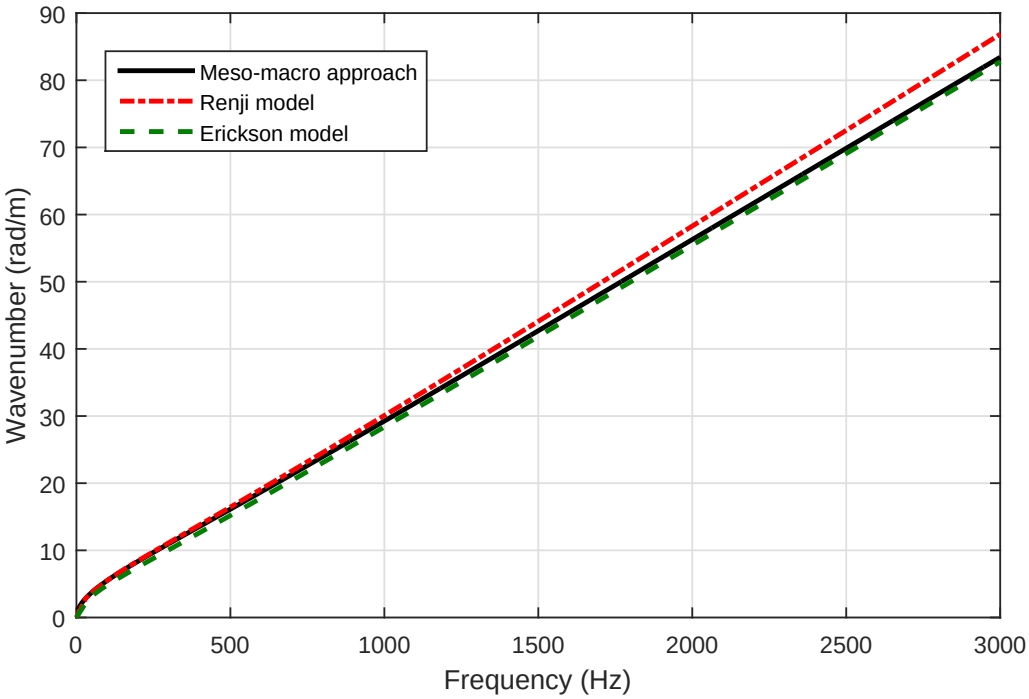

Figure 2.4: Validation of the dispersion curve of the proposed approach.

The averaged equivalent wavenumber over the principal directions, x and y, can be expressed as mentioned in reference [42]:

$$\langle k_f \rangle = \sqrt{k_x^2 + k_y^2}. \tag{2.21}$$

As shown in figure 2.4, the comparison of the dispersion result obtained by the meso-macro approach and the ones obtained by the analytical methods, Renji and Erickson models, shows clearly a good agreement either in the low or mid frequency range.

The modal density with refined angular dispersion sampling $k(\theta,\omega)$ can be expressed [42] as the following form:

$$n(\omega) = \int_0^{\pi} n(\theta,\omega)d\theta, \tag{2.22}$$

where $n(\theta,\omega)$ stands for the angular distribution of the modal density which is given as follows :

$$n(\theta,\omega) = \frac{A}{2\pi^2}\frac{k(\theta,\omega)}{|c_g(\theta,\omega)|}, \tag{2.23}$$

in which A is the surface area and $c_g(\theta,\omega) = \dfrac{\partial\omega}{\partial k}$ is the group velocity along the direction θ. So, the modal density with the averaged equivalent wavenumber $\langle k_f(\omega)\rangle$ can be written as:

$$n(\omega) = \frac{A}{2\pi}\langle k_f(\omega)\rangle \frac{\partial\omega}{\partial\langle k_f(\omega)\rangle}. \tag{2.24}$$

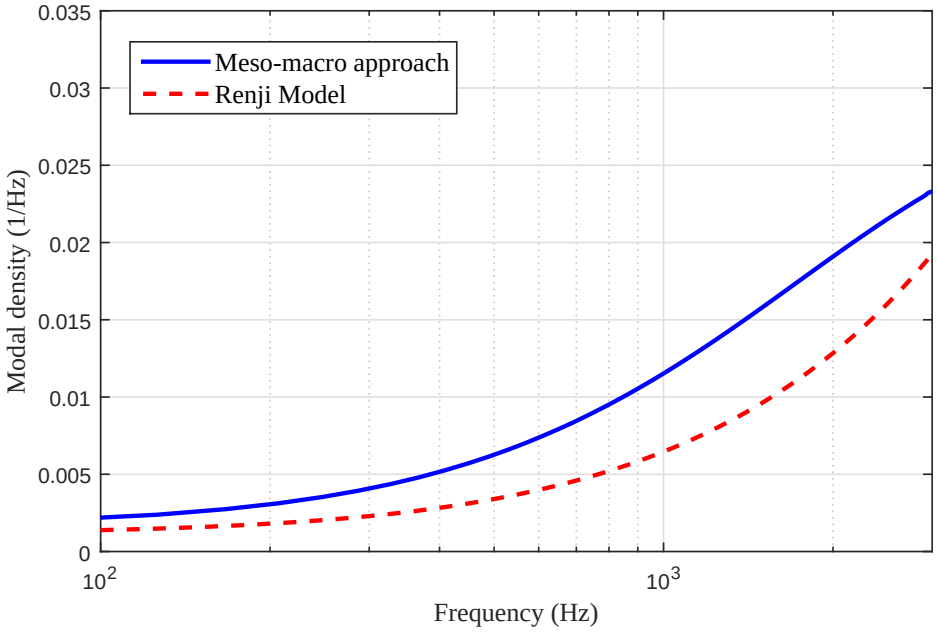

Figure 2.5: Validation of the modal density of the proposed approach.

The result obtained by the previous equation of the modal density has been compared with the formula of the density modal developed and published by Renji in [123]. As shown in figure 2.5, the comparison of the both modal density curves shows generally a good matching in the different frequency ranges.

2.3 Extension for curved sandwich structures

The 2D WFE method has been adapted to model a curved sandwich panel by applying the formulation proposed in references [29, 94]. A curved axisymmetric structure is considered (see figure 2.6) with y, r, and θ the cylindrical coordinates. R is the mean radius and $h_t = h_c + 2h_f$ is the total thickness of the curved sandwich panel.

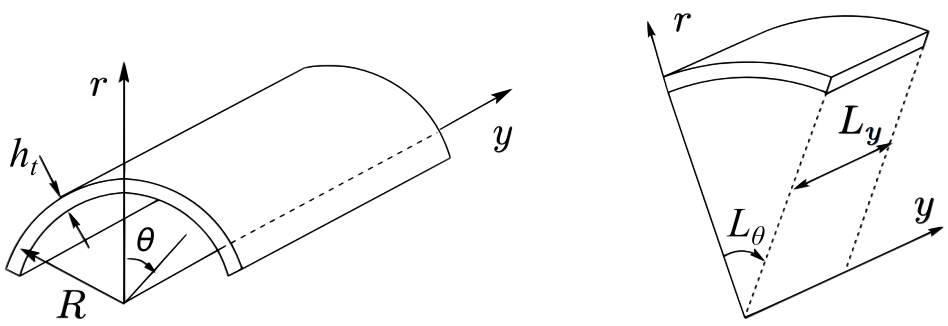

Figure 2.6: Curved structure with cylindrical coordinates and small rectangular prismatic cell [94].

The curved unit cell of the sandwich structure, as illustrated in figure 2.7, is modeled in the classical finite element software as a trapezoid unit cell. A time-harmonic disturbance at a given angular frequency ω is assumed to propagate through a curved structure with a helical pattern so that:

$$w(r,\theta,y,t) = W(r)e^{-i(k_\theta\theta + k_y y - \omega t)}, \tag{2.25}$$

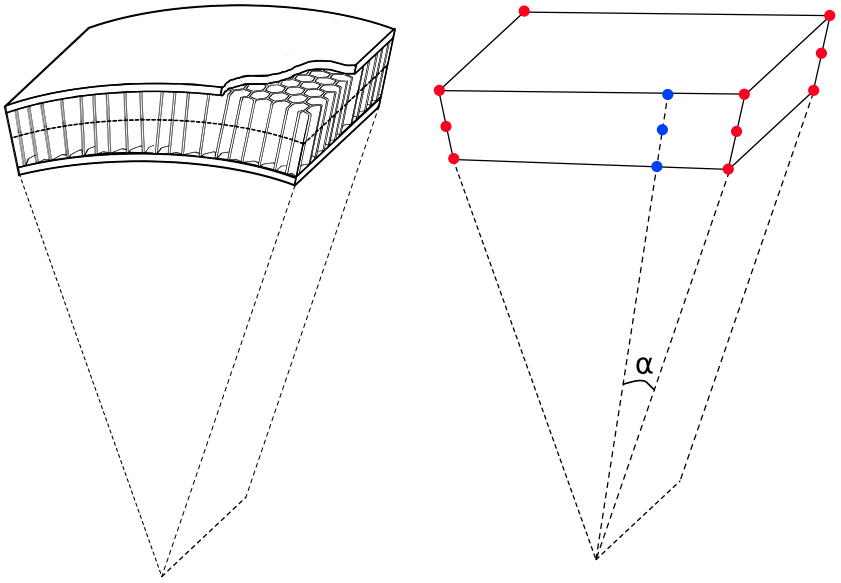

Figure 2.7: FE model of the trapezoid unit cell corresponding to the curved sandwich panel.

in which $W(r)$ being the complex wave amplitude, k_θ and k_y are respectively the wavenumber along the circumferential and axial directions.

Thereafter, the local coordinates have to be rotated for the sake of modeling the desired curvature. A transformation matrix $\overline{R}$ is then defined so that the mass and stiffness matrices M and K of the curved modeled unit cell are rewritten as the following:

$$\begin{cases} M = \overline{R}^T M_L \overline{R} \\ K = \overline{R}^T K_L \overline{R} \end{cases}, \tag{2.26}$$

with M_L and K_L are respectively the mass and stiffness matrices extracted using the trapezoid FE model in the local coordinates. The transformation matrix $\overline{R}$ allows rotating nodes surrounding the mid nodes around y axis through an angle α. The matrix $\overline{R}$ contains, at the diagonal elements, sub-matrices R of the following form :

↬ In the case of the trapezoid unit cell modeled by a 3D structural solid element (Solid185 in ANSYS) with three degrees of freedom, the sub-matrix R is expressed as follows :

$$R = \begin{pmatrix} \cos\alpha & 0 & \mp\sin\alpha \\ 0 & 1 & 0 \\ \pm\sin\alpha & 0 & \cos\alpha \end{pmatrix} \tag{2.27}$$

↬ On the other side the sub-matrix R is expressed in the case of the trapezoid unit cell modeled by a 2D structural shell element (Shell181 in ANSYS) with six degrees of freedom as follows :

$$R = \begin{pmatrix} \cos\alpha & 0 & \mp\sin\alpha & 0 & 0 & 0 \\ 0 & 1 & 0 & 0 & 0 & 0 \\ \pm\sin\alpha & 0 & \cos\alpha & 0 & 0 & 0 \\ 0 & 0 & 0 & \cos\alpha & 0 & \mp\sin\alpha \\ 0 & 0 & 0 & 0 & 1 & 0 \\ 0 & 0 & 0 & \pm\sin\alpha & 0 & \cos\alpha \end{pmatrix} \tag{2.28}$$

The results obtained by the presented extension of the meso-macro approach have been compared with the discrete laminate model (DLM) results published in [54]. The curved sandwich panel has a 2 m radius of curvature and 2.43 $m \times 2.03$ m a projected area of the modeled structure. The thickness of the face-sheet is 1.2 mm and that of the core is 12.7 mm. The curved panel is made up of Graphite/Epoxy face-sheets and of a rigid foam core; the panel orthotropic layout is $[0,0,0]$.

The effective mechanical properties of the sandwich face-sheets are :

$E_x = 0.48x10^{11}\ Pa$, $E_y = 0.48x10^{11}\ Pa$, $G_{xy} = 0.181x10^{11}\ Pa$, $G_{xz} = 0.2757x10^{10}\ Pa$, $G_{yz} = 0.2757x10^{10}\ Pa$, $\nu_{xy} = 0.3$ and , $\rho = 1550\ kg/m^3$.

The effective mechanical properties of the sandwich core are :

$E_x = 0.1448x10^{9}\ Pa$, $E_y = 0.1448x10^{9}\ Pa$, $G_{xy} = 0.5x10^{8}\ Pa$, $G_{xz} = 0.5x10^{8}\ Pa$, $G_{yz} = 0.5x10^{8}\ Pa$, $\nu_{xy} = 0.2$ and , $\rho = 110.44\ kg/m^3$.

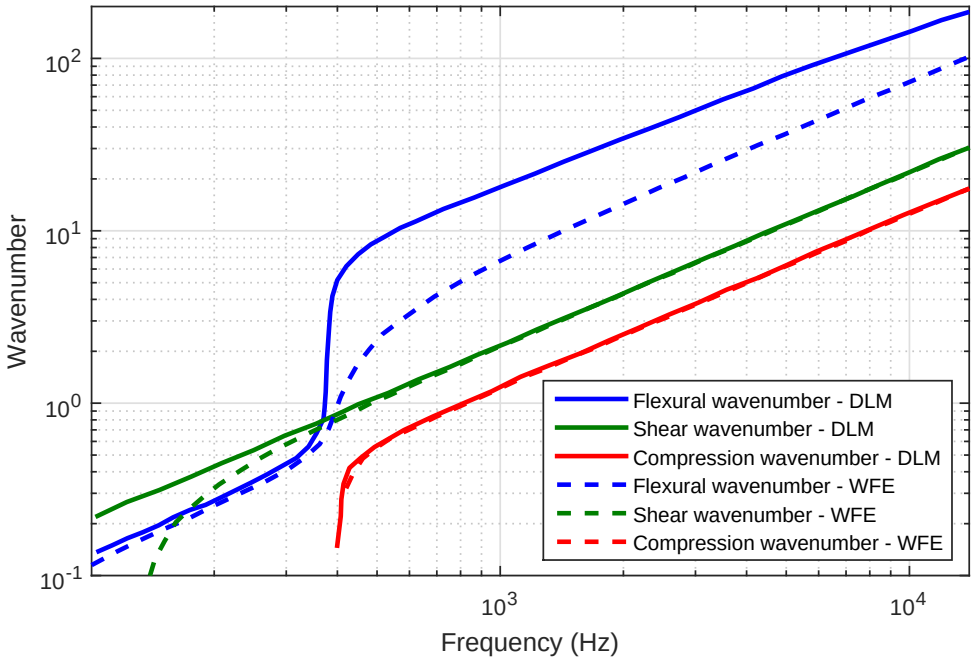

Figure 2.8: Validation of the dispersion curves along the direction θ.

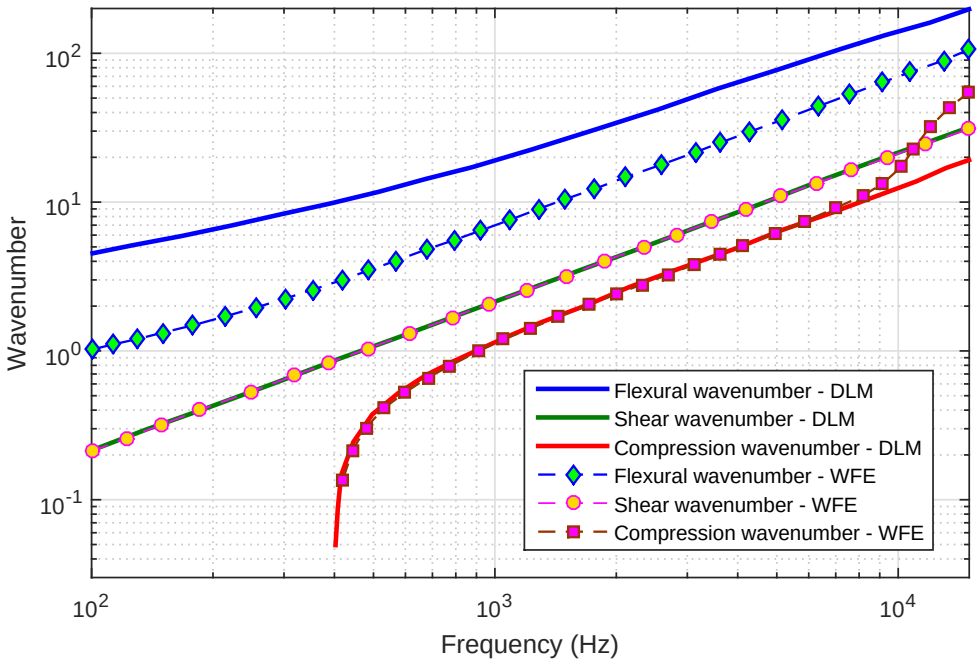

Figure 2.9: Validation of the dispersion curves along the y-direction.

As shown figures 2.8 and 2.9, the comparisons of the dispersion curves for a curved sandwich panel along the circumferential and axial directions show a good agreement regarding to the shear and compression wavenumbers. However, the comparisons for the flexural wavenumber along the both directions exhibit some different features. The gap between the flexural curve obtained by the developed approach and DLM results is due to the lack information concerning the mechanical properties.

2.4 Concluding remarks

In this chapter, an efficient numerical model called the meso-macro approach, based on the wave finite element method, has been proposed to investigate the vibroacoustic behavior for complex 2D periodic structures. A reduction computation process has been also applied to reduce the computation cost. Afterwards, an extension of the developed approach for a curved sandwich panel has been given.

The accuracy of the obtained results for either a flat or curved sandwich panel has been checked by comparisons with different published analytical methods. The comparisons have shown generally a good matching for the different wave types. The developed approach will be used in the next chapters to define the different vibroacoustic responses.

CHAPTER 3

BENDING-SHEAR CORE TRANSITION FOR SANDWICH STRUCTURES

Contents

THe present chapter investigates the vibroacoustics of honeycomb sandwich panels numerical approaches. In a typical sandwich structure, the acoustic transmission in the low and mid frequency ranges is is generally controlled by global bending waves and by core shear effects. This behavior defines two frequency bands of great interest for the vibroacoustic signature. The transition frequency is then an important parameter to predict. In the present work, transition frequency expressions of honeycomb sandwich panels are derived using both a homogenized analytical method and a three-dimensional numerical approach. The expressions obtained show the panel geometry and the core properties influence. Also, they take into account the

orthotropic effect of the entire panel and the transverse shear effect of the sandwich core. The accuracy of the predictions based on the two approaches has been verified by comparing the results obtained with previously published analytical models, showing a good agreement as far as the sandwich panel exhibits an isotropic behavior. However, when the orthotropic behavior of the sandwich panel becomes important, corrections are needed and provided.

3.1 Introduction

The increasing interest devoted recently to sandwich panels in transportation and civil engineering, among other sectors, has led to a growing demand for engineers concerned by the advanced sandwich structures design. This is due to the main advantage of these structures which is the high stiffness-to-weight ratio. Principally, the sandwich structures are made of a moderately thick, lightweight core bonded to a thin isotropic or to an orthotropic face-sheets. Apart from their considerably low ratio of weight to strength, composite sandwich structures benefit from other desirable properties, such as corrosion and thermal resistance and so on. However, a decrease in the panel mass while the stiffness is kept at a high level may have a negative influence on the panel vibroacoustic performance and may lead to unsatisfactory noise transmission.

To clarify the question, researchers have attempted to understand the influence of the structural properties on the sandwich panel vibroacoustic. The modal density, among other vibroacoustic indicators, was often employed to meet this objective. Many authors showed that the vibroacoustic weakness of the honeycomb sandwich structures lies in the effect of the shear core in the mid frequency range [1-4]. For instance, Erickson [47] and Clarkson [31] carried out a study showing the influence of the anisotropy of the core on the modal density. The panel was described by an equivalent shear core and bending face-sheet modulus. In the same way, Renji et al. [123] showed the effect of the transverse shear flexibility on the modal density of a honeycomb sandwich panel wherein the core was characterized by an equivalent transverse shearing. In a more recent work, a study was conducted by Han et al. [61] to investigate the effect of the fiber face-sheet angle, the core shear parameters and the boundary conditions on the modal density.

It seems also relevant to mention different attempts to improve the vibroacoustics

of sandwich panels. For instance, Palumbo et al. [110] conducted an experimental study to improve the honeycomb vibroacoustic behavior by adding voids and recesses to the core in order to create areas of reduced stiffness. This leaded to a notable benefit in the sound transmission loss either in both the low-mid or in the high frequency ranges but to a significant decrease in the panel stiffness. Soon afterwards, Naify et al. [103] performed a theoretical and experimental work to reduce the amount of the sound energy transmitted through the honeycomb panel by attaching additional gas layers.

In this study, the target was aerospace and automotive applications of sandwich structures. The main concern in this case appears in the low-to-mid frequency ranges (up to 1KHz typically). Consequently, the bending and shear effects were examined further in depth. The primary purpose was to predict the transition frequency separating the panel global bending and the shear core effects through analytical and numerical approaches. Optimization of the transition frequency can lead to design rule of the sandwich structure from the vibroacoustic point of view. More precisely, for a typical sandwich panel, there are three dominants wave zones [50]. In the first zone, global bending occurs at a low frequency range. In the second zone, the core shear behavior becomes important, which defines a mid frequency range like behavior. In the last frequency zone, corresponding to higher frequencies, the sandwich panel face-sheets bending is dominant. Expressions of the global bending to shear effect frequency transition for honeycomb sandwich panels are derived in this work. These expressions are controlled by the panel geometry, mass, and the elastic properties of the honeycomb core. In this chapter both analytical and numerical methods are employed. Looking at the open literature, different works using analytical investigations can be mentioned. For instance, Rindel [126] identified the expressions for the transition frequency of a thick plate, called the cross-over frequency. The conclusions of this model were that the cross-over frequency corresponding to the phase speed is twice the cross-over frequency corresponding to the modal density and four times that of the group speed. Evan [48] has determined the transition frequencies of the different zones mentioned in [50] for honeycomb panels using the Kurtze and Waters model [77]. More recently, Guillaumie [59] gave the expression for the transition frequency of symmetric honeycomb sandwich panels with composite faces using the inverse of the mechanical impedance without taking into account the orthotropic effect of the honeycomb panel. In this chapter, the numerical prediction of the transition frequency will be achieved through the Wave Finite Element method (WFE). Several papers, based on the WFE have been published in the last few years to

model the dynamic behavior of one- and two-dimensional periodic structures [13, 32]. The 2D WFE formulation was applied and validated in several works [28, 43, 131] to predict the wave propagation in thin orthotropic structures. In the present work, the 2D WFE method was used to predict the transition frequency of honeycomb sandwich panels with isotropic and orthotropic face-sheets. The main advantage of the last approach is that it models 3D sandwich panels without using any homogenization procedure.

3.2 Analytical identification of the transition frequency

In addition to the transition frequency expression presented in the first chapter, Baho et al. [10] have recently developed an improved analytical expression based on the Renji model [123]. The proposed expression has taken into account the shear effect of the sandwich core as well as the orthotropic effect of the sandwich panel.

Acorrding to reference [10], the transition frequency expression of the sandwich panel developed using the flexural wavenumber is expressed in the following:

$$f_t^w = \frac{K_s}{2\pi\sqrt{\rho_p}} P, \tag{3.1}$$

with

$$P = \left(\int_0^{2\pi} \chi_1(\theta)^{-\frac{1}{2}} d\theta \right) \left(\int_0^{2\pi} \frac{\chi_2(\theta)}{\chi_1(\theta)} d\theta \right)^{-1}.$$

P characterizes the orthotropic properties of a symmetric honeycomb sandwich panel. The developed expression of the transition frequency f_t^w determines the shift from the panel pure bending to the core shear regime for a symmetric honeycomb sandwich panel.

Similarly to the previous development 3.1, the expression of transition frequency f_t^g can be deduced using the group velocity, which indicates the way how the energy flows into the considered structure, as follows:

$$f_t^g = \frac{K_s}{8\pi\sqrt{\rho_p}} P = \frac{1}{4} f_t^w. \tag{3.2}$$

It is noteworthy to mention that the above expression of the transition frequency f_t^g provided by the group velocity analysis is one fourth the one given by the wavenumber domain treatment f_t^w.

It may be deduced from the modal density developed in Renji work the transition frequency f_t^m, which represents the intersection frequency between the asymptotical pure bending modal density and the pure shear modal density. It can be expressed as follows:

$$f_t^m = \frac{K_s}{4\pi\sqrt{\rho_p}} T, \tag{3.3}$$

where T presents the sandwich panel orthotropic effect on the modal density, given by:

$$T = \left(\int_0^{\frac{\pi}{2}} \chi_1(\theta)^{-\frac{1}{2}} d\theta \right) \left(\int_0^{\frac{\pi}{2}} \frac{\chi_2(\theta)}{\chi_1(\theta)} d\theta \right)^{-1}. \tag{3.4}$$

For a symmetric sandwich with regular honeycomb core, we have $T = P$. So, the transition frequency obtained using the modal density equals twice transition frequency found by asymptotical analysis of the wavenumber.

3.3 Numerical identification of the transition frequency

In this section, the transition frequency is predicted using a three dimensional numerical approach called the Wave Finite Element method (WFE). The WFE method combines the periodic structure theory and the classical finite element method (FEM). The present method is applied to predict the dynamic behavior of a periodic structure. It includes the reformulation of the equation of motion by using the dynamic stiffness matrix (DSM). This matrix involves the mass and stiffness matrices of the two dimensional periodic cell of the structure (see figure 3.1). The structural wave motion of the sandwich structure is expressed in terms of the eigenvalues and the eigenvectors of the rewritten dynamic stiffness matrix. The eigenvalues and eigenvectors of the problem formulation represent respectively the wavenumbers and the wavemodes of the honeycomb sandwich panel.

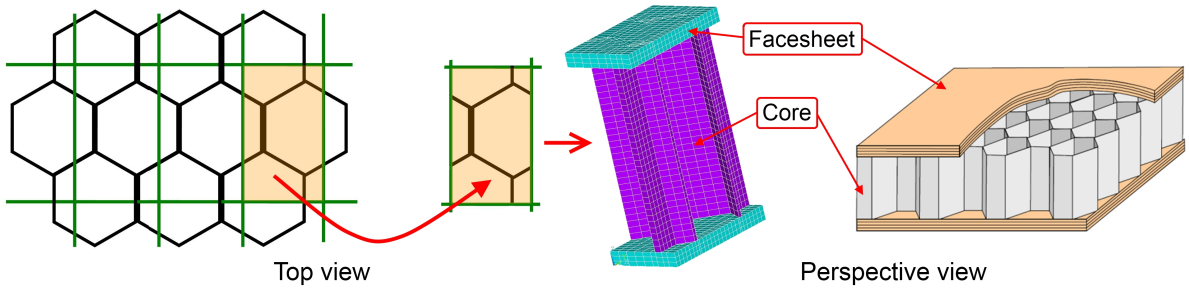

Figure 3.1: Waveguide periodic cell of the honeycomb sandwich panel.

There are two types of formulation, one- and two-dimensional WFE formulations. Referring to the 2D WFE method, the transition frequency is determined by two techniques, namely the bisection and the wavemode energy methods. The both methods do not require any homogenization techniques of the sandwich core. Consequently, the applied techniques save up totally the meso-scale information of the sandwich core. Both techniques were further detailed and clarified through the next subsections.

3.3.1 Transition frequency prediction through the bisection method

The bisection method consists of identifying the transition frequency in the wavenumber, group velocity, and modal density [42] domain by post-treating numerically the output results of the 2D WFE simulation. The equivalent bending and shear properties of the sandwich panel were investigated by applying a non-linear regression.

Once the flexural propagating wave across the honeycomb sandwich panel has been selected by applying the MAC criterion, the asymptotic wavenumbers k_B and k_S were determined and substituted into the group velocity and the modal density expressions.

$$k_B(\omega) = \sqrt[4]{\frac{\omega^2 m_s}{B}}; \quad c_{g_B}(\omega) = \frac{d\omega}{dk_B}; \quad n_B(\omega) = \frac{ab}{2\pi}\frac{\langle k_B(\omega)\rangle}{|c_{g_B}(\omega)|}. \tag{3.5}$$

$$k_S(\omega) = \omega\sqrt{\frac{m_s}{D}}; \quad c_{g_S}(\omega) = \frac{d\omega}{dk_S}; \quad n_S(\omega) = \frac{ab}{2\pi}\frac{\langle k_S(\omega)\rangle}{|c_{g_S}(\omega)|}. \tag{3.6}$$

Where a and b are respectively the length and width of the honeycomb sandwich panel. $\langle k_B(\omega)\rangle$ and $\langle k_S(\omega)\rangle$ are the averaged bending and the shear wavenumbers of the sandwich panel. $c_{g_B}(\omega)$ and $c_{g_S}(\omega)$ are respectively the bending and shear group

velocity of the honeycomb panel.

The transition frequency has been numerically estimated by identifying the intersection between the asymptotic bending wavenumber $k_B(\omega)$ at the low frequencies and the asymptotic shear wavenumber $k_S(\omega)$ in the mid frequency range. The intersection frequency represents, for each vibroacoustic properties, the frequency at which the core shear effect becomes more importance with respect to the panel global bending.

However, the developed technique is too sensitive to the selected frequency band with regard to the WFE simulation. As shown in figure (3.2), in order to obtain the best predicted value of the transition frequency, the WFE frequency range has to belong to the pure bending and shear zone of the sandwich panel. Also, the frequency step in the first zone has to be smaller in comparison to the second zone for the sake of capturing more information in low frequency range.

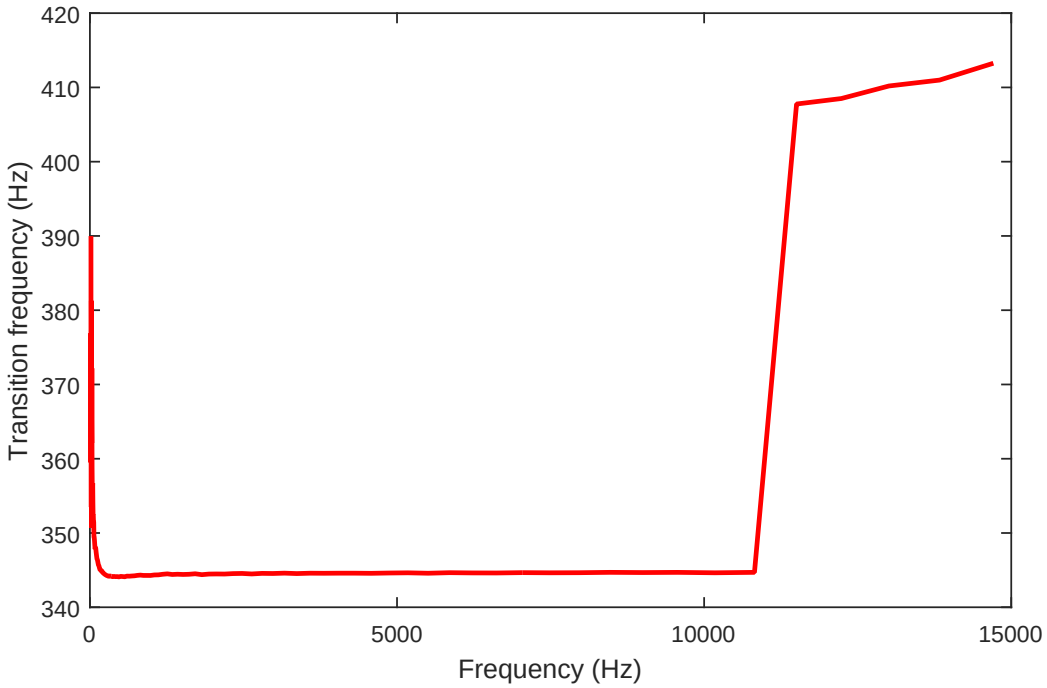

Figure 3.2: Effect of the selected frequency range on the predicted transition frequency.

3.3.2 Transition frequency prediction through the wavemode energy method

The prediction of the transition frequency using the wavemode energy method relies mainly on calculating independently the strain energy of the cell core E_c and the cell face-sheets E_p along the principal directions x and y. Both strain energies were normalized by the total strain energy E_T of the waveguide periodic cell. So, the strain energies E_c and E_p have been calculated by the following expressions:

$$E_c = \frac{\Phi^T K_c \Phi}{E_T} \quad and \quad E_p = \frac{\Phi^T K_p \Phi}{E_T}. \tag{3.7}$$

Where K_c and K_p are the full stiffness matrices of the cell core and face-sheets extracted using a classical FE package. The vector Φ represents the full dofs of the displacement obtained by the 2D WFE simulation. It should be noted that the full dofs of the displacement was obtained by applying the inverse form of the 2D WFE method presented in the development of the meso-macro approach in chapter 2.

The transition frequency has been then determined by identifying the frequency at which the core strain energy E_c becomes more important than the face-sheet strain energy E_p of the sandwich panel along both of the principal directions.

$$f_t = min(f_{tx}, f_{ty}), \tag{3.8}$$

with f_{tx} and f_{ty} being the transition frequencies along the x- and y-directions respectively.

The prediction accuracy depends neither on the mesh size of the periodic unit cell nor on the frequency step of the numerical simulation. Per contra, it extremely depends on the element type (solid or shell element). In view of the thickness of the honeycomb walls ($t = 76.2$ ţm), the use of the solid element to model the core walls gives incorrect predictions of the transition frequency. To avoid these inaccurate predictions, the honeycomb walls have to be well meshed with a very small element size which consequently will increase considerably the simulation time of the periodic cell. CMS and MOR are then of great interest for time consumption reduction.

3.4 Final results and discussions

The numerical and analytical approaches, developed in section 3.2 and 3.3, have been applied to two regular symmetric honeycomb panels (see figure 3.3). The first panel, called model A, is constituted by a Nomex material with isotropic face-sheets, whereas the second one, called model B, is composed also of a Nomex material with orthotropic face-sheets (see table 3.1). The orthotropic face-sheets comprise eight plies with the following angular arrangement $[0°, 30°, 90°, -30°]_S$. The rectangular sandwich panels A and B have the same dimensions of the area : $2.15(x) \times 1.8(y)\ m^2$.

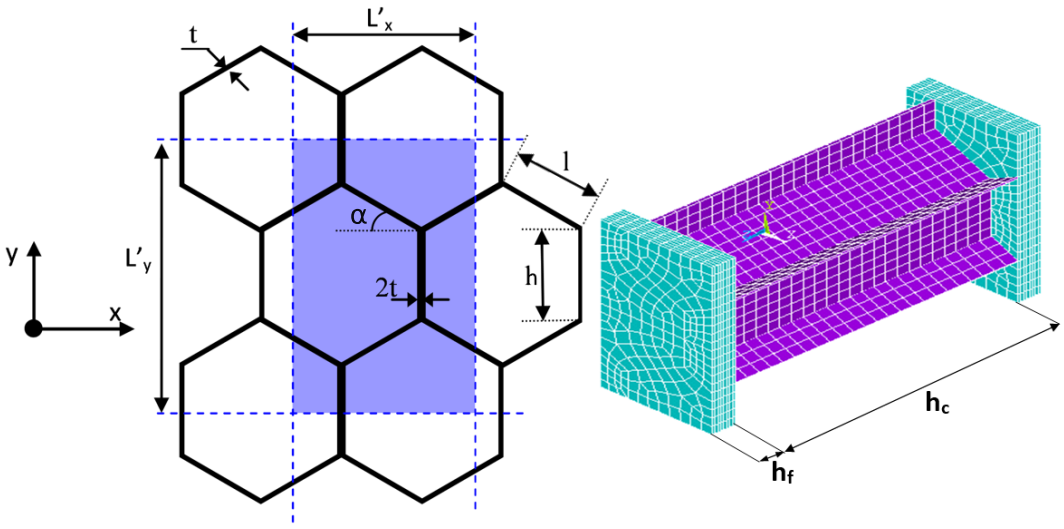

Figure 3.3: Geometric parameters of the unit honeycomb cell.

	Honeycomb core	**Sandwich facesheets**
Model A	*Nomex material* $\rho = 1380\ \ kg/m^3$ $E = 3\ \ GPa$ $\nu = 0.33$	*Aluminum material* $\rho = 2800\ \ kg/m^3$ $E = 72.5\ \ GPa$ $\nu = 0.343$
Model B	*Nomex material* $\rho = 1240\ \ kg/m^3$ $E = 5.5\ \ GPa$ $\nu = 0.33$ $G = 2.07\ \ GPa$	*Epoxy resin with carbon yarn* $\rho = 1550\ \ kg/m^3$ $E_1 = 133.6\ \ GPa;\ \ E_2 = E_3 = 7.7\ \ GPa$ $\nu_{12} = \nu_{13} = 0.29$ $G_{23} = 2.6\ \ GPa;\ \ G_{13} = G_{12} = 3,1\ \ GPa$

Table 3.1: Mechanical properties of the honeycomb sandwich models A and B.

The effective elastic properties of honeycomb core have been calculated analytically

using the homogenized formulations recently developed by Malek et al. [93]. This homogenization technique is an improved version of the work carried out by Gibson and Ashby [57] in 1999. The improvement allows more accurate estimation of the nine elastic constants of the unit cell especially the transverse shear constants. The formulas of these nine elastic were presented in appendix A. The global mechanical properties of the honeycomb core for the models A and B have been summarized in table (3.1), whilst the computed effective elastic constants of the honeycomb cores A and B are summarized in table (3.2).

Model A	**Model B**
$E_x = 0.16\ MPa;\ E_y = 0.165\ MPa$	$E_x = 0.293\ MPa;\ E_y = 0.303\ MPa$
$E_z = 0.125\ GPa;\ G_{xy} = 0.0379\ MPa$	$E_z = 0.229\ GPa;\ G_{xy} = 0.069\ MPa$
$G_{xz} = 17.85\ MPa;\ G_{yz} = 30\ MPa$	$G_{xz} = 32.75\ MPa;\ G_{yz} = 55.04\ MPa$
$\nu_{xy} = 0.975;\ \nu_{xz} = 0.00042$	$\nu_{xy} = 0.975;\ \nu_{xz} = 0.00042$
$\nu_{yz} = 0.00043;\ \rho = 57.637\ kg/m^3$	$\nu_{yz} = 0.00043;\ \rho = 51.82\ kg/m^3$

Table 3.2: Effective elastic properties of the honeycomb core for the models A and B.

The geometrical parameters of the both honeycomb panels A and B are given in figure (3.3) and the corresponding dimensions of the periodic cell are summarized in table 3.3.

Model A	**Model B**
$l = h = 2.75\ mm$	$l = h = 2.75\ mm$
$h_f = 0.6\ mm;\ h_c = 20\ mm$	$h_f = 1.0\ mm;\ h_c = 12\ mm$
$t = 76.2\ \mu m;\ \alpha = \frac{\pi}{6}$	$t = 76.2\ \mu m;\ \alpha = \frac{\pi}{6}$
$a = 2.15\ m;\ b = 1.8\ m$	$t_{layer} = h_f/8 = 0.125\ mm$
	$[0\ 30\ 90\ -30]_s$ (8 layers)
	$a = 2.15\ m;\ b = 1.8\ m$

Table 3.3: Geometric properties of the honeycomb sandwich models A and B.

The rectangular unit cell was meshed using the shell structural elements (Shell181). This element type is a four-noded element with six degrees of freedom at each node. It includes the effect of transverse shear deformation. Also, it allows modeling a layered plate which is the face-sheet case in the model B. In the latter-stated model, the individual composite face-sheets was created as a single layer with 2D elements. The thickness, the layup and the orientation of the face-sheet plies were specified by using the SECTYPE property box in the ANSYS package. The cell nodes were then merged to ensure

the connectivity between the sandwich core and the face-sheets.

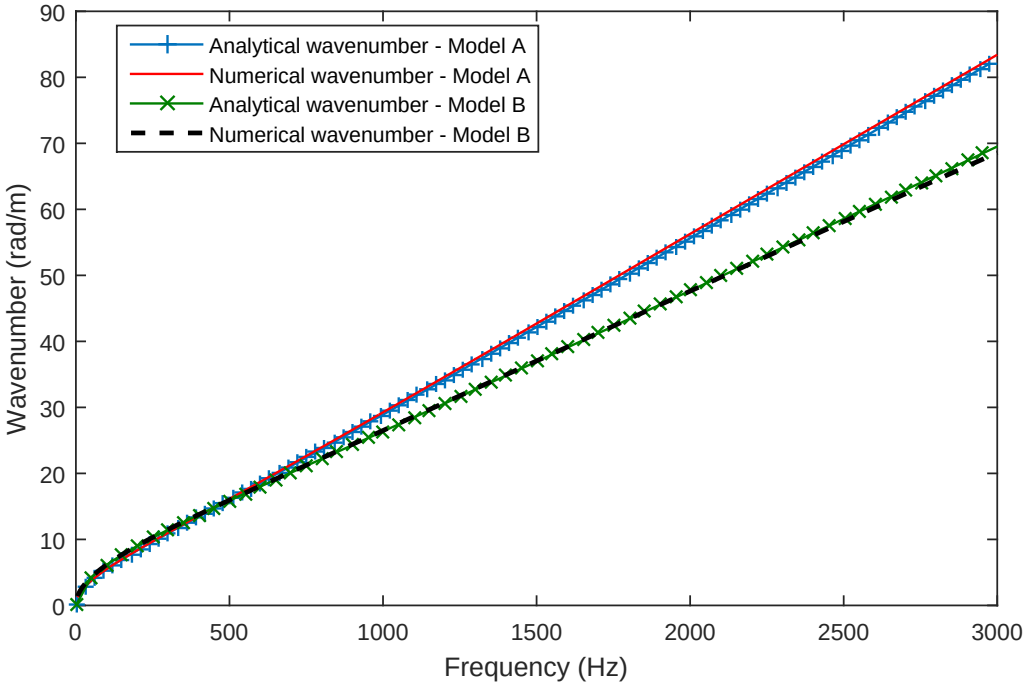

Figure 3.4: Comparison of the numerical and analytical wavenumbers.

In the generation mesh step, the quadrilateral element shape was used with 1086 degrees of freedom (dofs) for the model A (546 internal dofs U_I and 540 boundary dofs U_{bd}) and 3125 dofs for the model B (2274 internal dofs U_I and 876 boundary dofs U_{bd}). After applying the reduce strategy described in subsections 2.1.2 and 2.1.3, the total cell dofs was reduced to 88 dofs for the model A and 96 dof for the model B. Thus, the total computation time spent simultaneously on getting the transition frequency for the both methods was 30 seconds for the model A and 101 seconds for the model B.

The numerical and analytical results, corresponding to the honeycomb panels A and B, are compared in figure (3.4). The comparison of the two sandwich structures, with isotropic face-sheets A and composite face-sheets B, shows clearly a good agreement either in the low or mid frequency range.

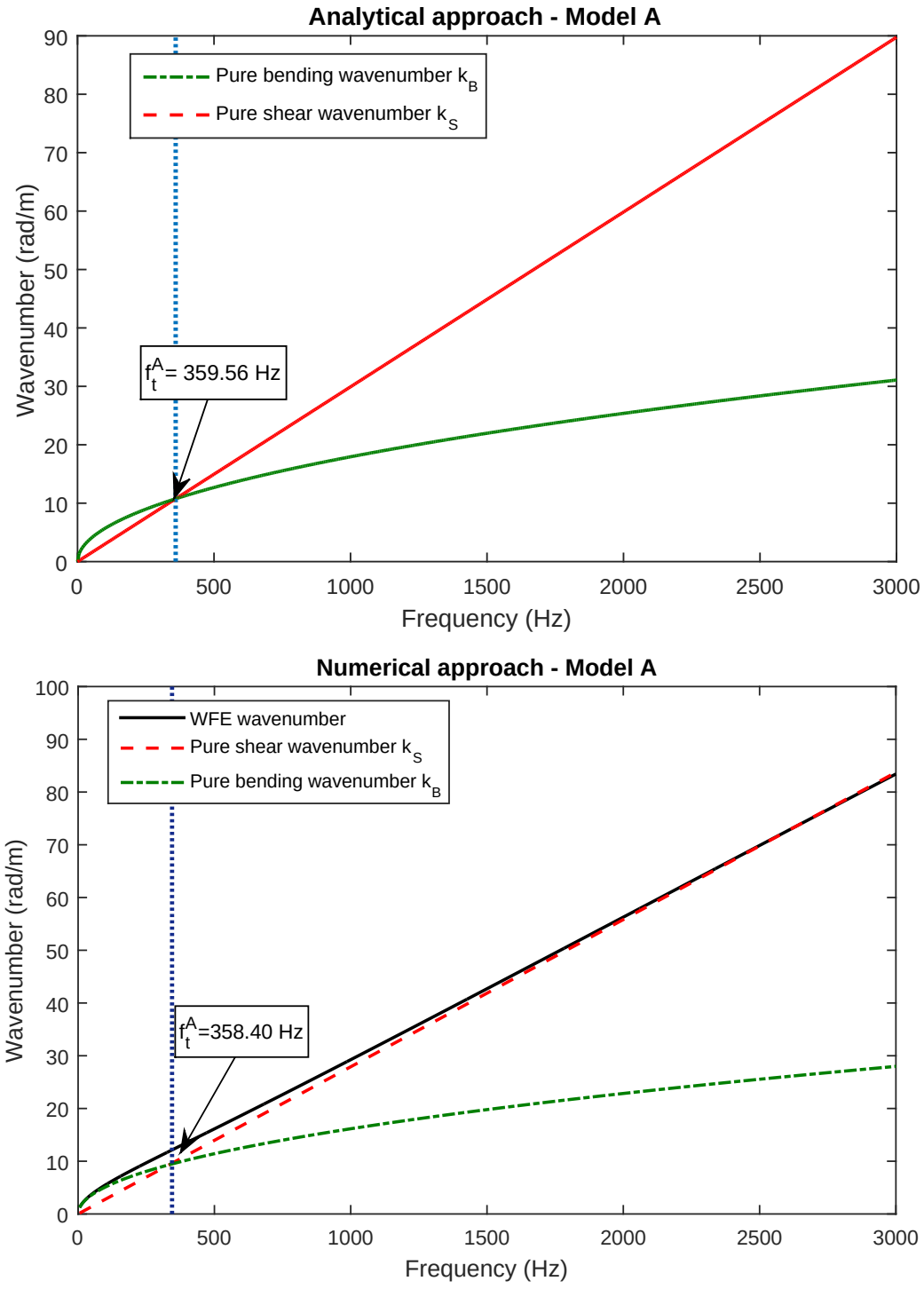

Figure 3.5: Transition frequency using wavenumber curves for the model A.

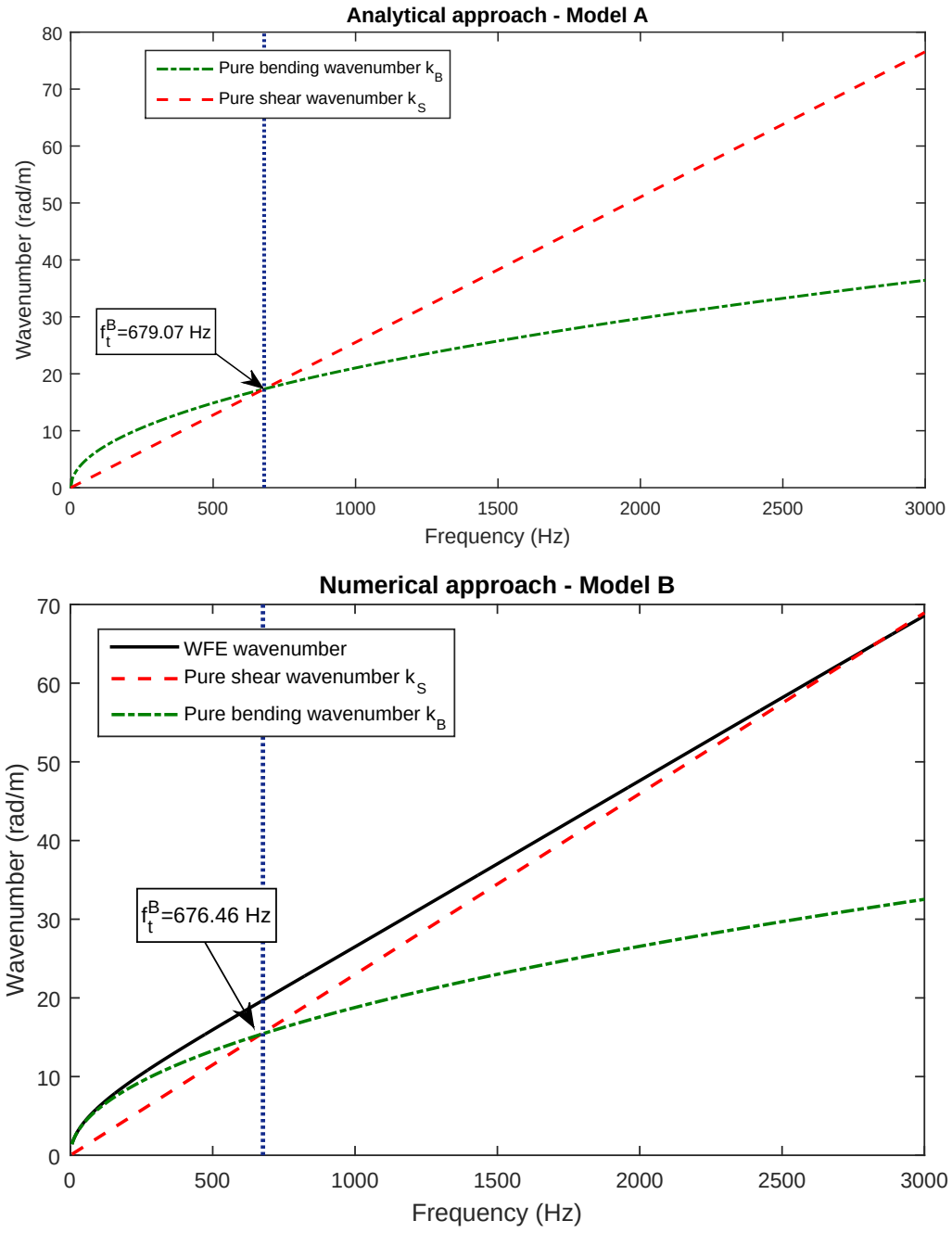

Figure 3.6: Transition frequency using wavenumber curves for the model B.

Figure (3.6) exhibits the flexural wavenumber curves of the honeycomb panels A and B computing by bisection technique based on the 2D WFE method. Likewise, the pure shear curves k_S and the pure bending curves k_B for both models are presented. The predicted transition frequency for the model A is $f_t^A = 358.40\ Hz$, whilst for the model B is $f_t^B = 676.46\ Hz$.

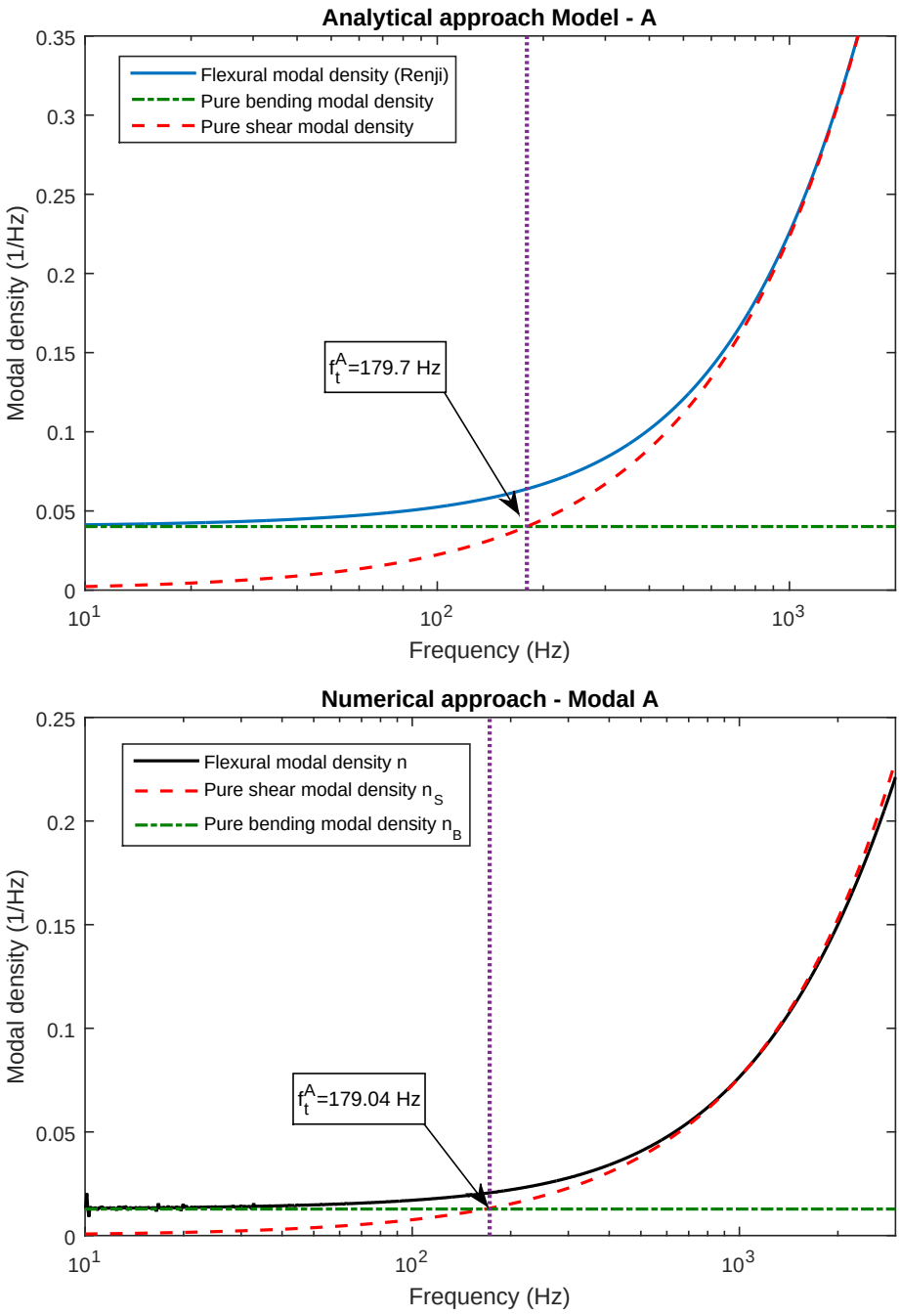

Figure 3.7: Modal density curves of the honeycomb sandwich models A.

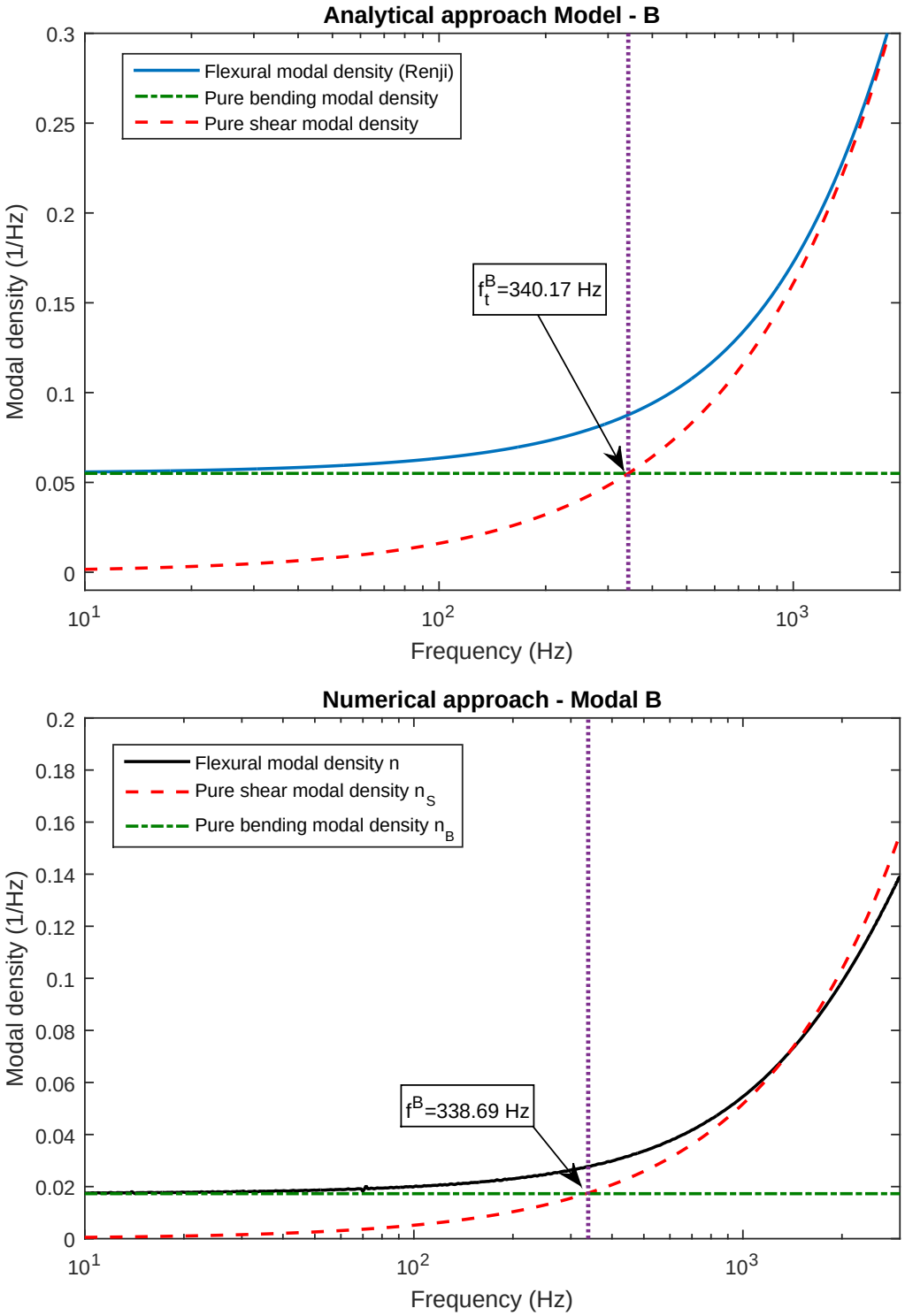

Figure 3.8: Modal density curves of the honeycomb sandwich models B.

The transition frequency based on the modal density of the honeycomb panels A

and B, obtained by using the proposed methods in sections 3.2 and 3.3, are presented in figure 3.8. Both of the numerical and analytical approaches were given the same predicted transition frequency, which is approximately for the model A $f_t^A = 179.78\ Hz$ and $f_t^B = 340.17\ Hz$ for the model B.

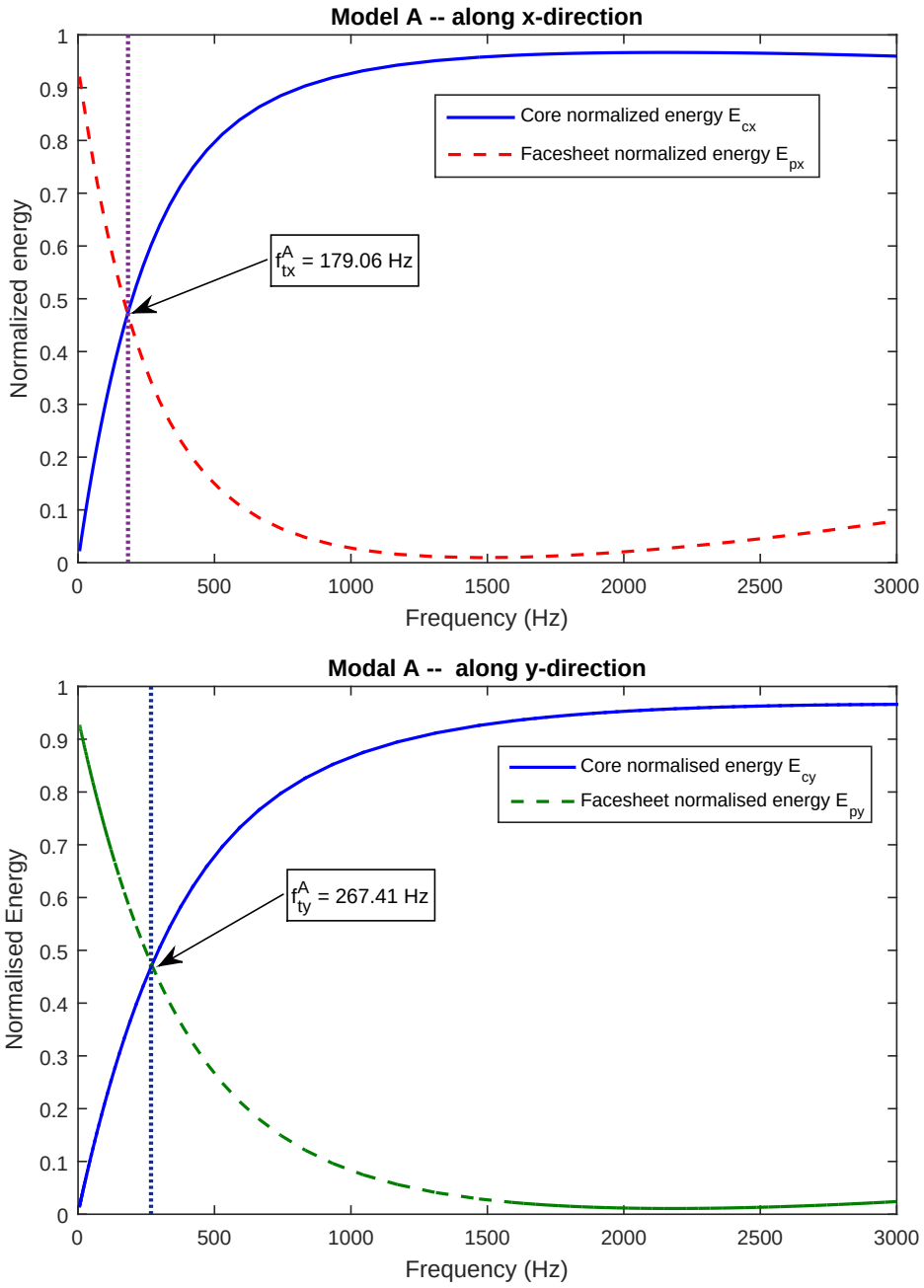

Figure 3.9: Strain energies of the honeycomb sandwich models A.

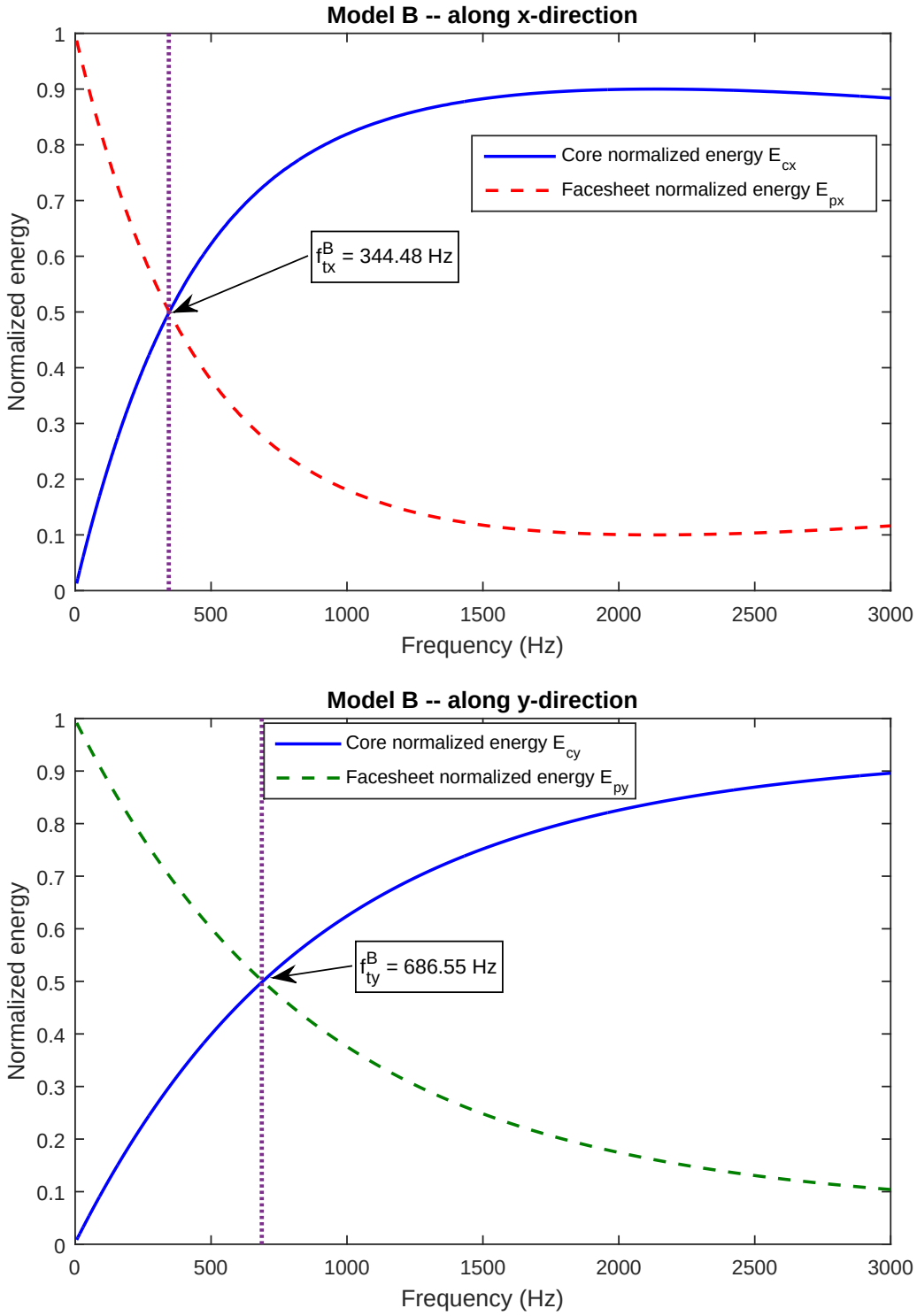

Figure 3.10: Strain energies of the honeycomb sandwich models B.

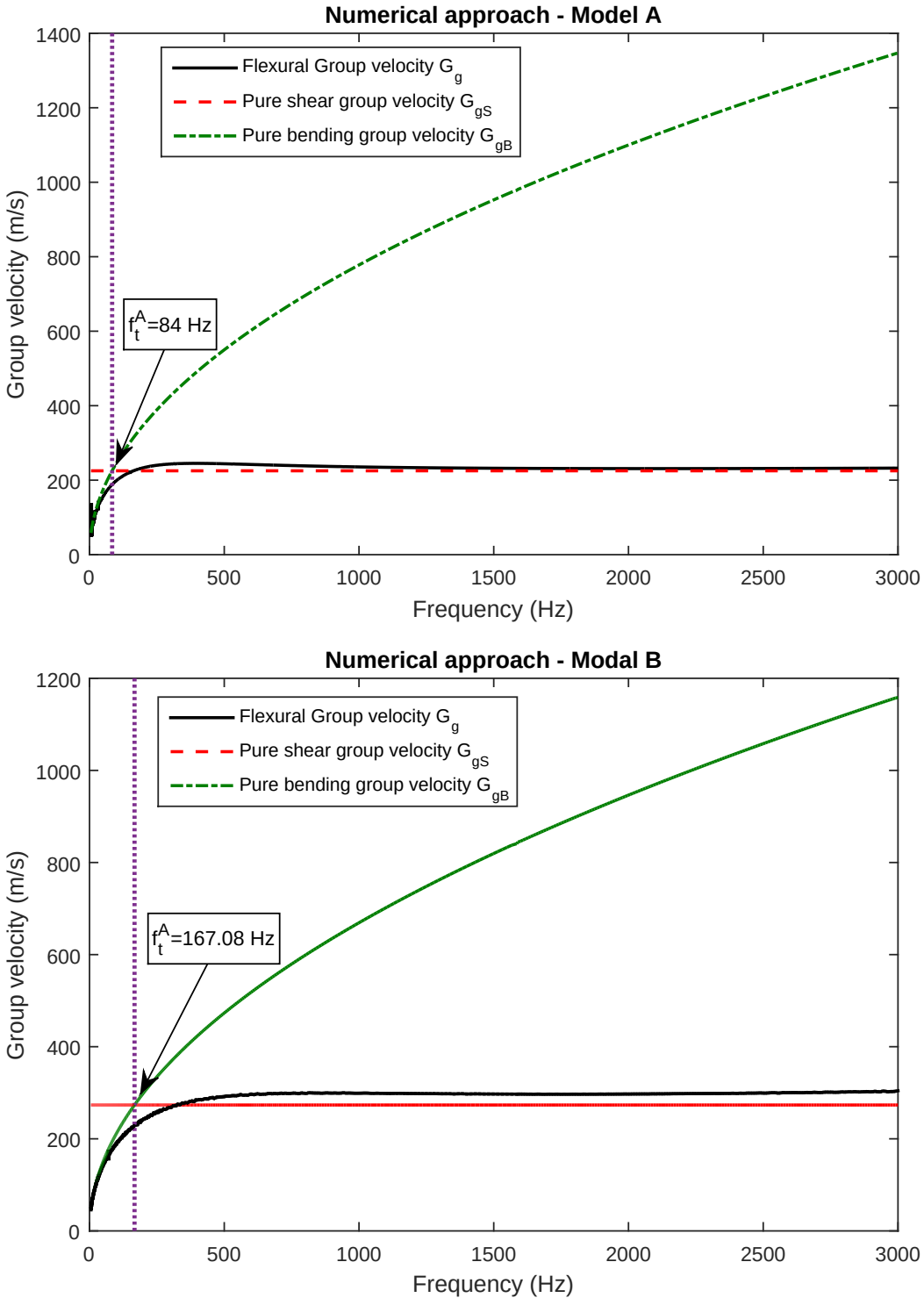

Figure 3.11: Group velocities of the honeycomb sandwich models A and B.

In table 3.4, a comparison is made between the transition frequencies of honeycomb

		Pane A $\Gamma_A = 1$	Panel B $\Gamma_B = 0.8$
Wavenumber	Baho's method [10]	359.56 Hz	680.08 Hz
	Evan's method [48]	339.08 Hz	–
	Rindel's method [126]	359.25 Hz	–
	Bisection method	358.40 Hz	676.46 Hz
Modal density	Baho's method [10]	179.78 Hz	340.17 Hz
	Guillaumie's method [59]	179.78 Hz	354.40 Hz
	Bisection method	179.04 Hz	338.69 Hz
	Energy method	179.06 Hz	344.48 Hz
Group velocity	Baho's method [10]	89.89 Hz	170.08 Hz
	Bisection method	89.02 Hz	167.08 Hz

Table 3.4: Summary of the obtained transition frequency using different methods.

panels A and B identified by the different methods presented in the present work and those previously published [48, 59]. As illustrated in the table and as stated in sections 3.1 and 3.2, it is noticed practically that the transition frequency predicted by the wavenumber of the honeycomb panels A and B is approximately twice the transition frequency obtained using the modal density of the structures, while in group velocity is roughly four time the transition frequency estimated by the wavenumber domain. Moreover, when the honeycomb panel with composite face-sheets presents an orthotropic coefficient Γ (e.g. $\Gamma > 1$ or $\Gamma < 1$), the published methods are less accurate than the methods proposed here because of the orthotropic effect which is not taken into account in Evan's and Guillaumie's models.

On the other hand, it is noticed that, in table 3.4, there is a noteworthy difference between the transition frequency predicted using Evan's method [48] $f_t^A = 339.08\ Hz$ and the obtained one using the others methods $f_t^A = 359.56\ Hz$ (the difference is approximately 20 Hz). The prediction error is due to mainly the shear stiffness formula used in the shear wave speed expression c_{ms}.

3.5 Concluding remarks

In the present study, analytical and numerical approaches are proposed for predicting the transition frequency of the honeycomb sandwich panel with either isotropic or orthotropic face-sheets. In general, the transition frequency exists, if and only if, the shearing effect of the sandwich core cannot be neglected, which actually is the case for

honeycomb sandwich panel. By definition, the transition frequency separates two main domains. The first domain is controlled by the total panel pure bending at the low frequencies, whilst the second regime is controlled by the sandwich core shear in the mid frequency range.

With respect to the sandwich panel modal density, the transition frequency is the frequency at which the number of modes begins to increase dramatically with the frequency. From this special frequency, the sandwich panel becomes gradually less stiff, compared to what it was at the previous frequencies, due to the core shear effect, which enters into play. It is noticed that the predicted transition frequency, based on use of the dispersion relation of the sandwich panel, is approximately twice the transition frequency corresponding to the modal density, while it is four times the transition frequency corresponding to the group speed.

In view of the results obtained and the expressions developed, it may be noticed that the transition frequency is very much dependent to mechanical and geometric properties of honeycomb sandwich panel. Also, and as mentioned before, it is shown that the orthotropic behavior of the honeycomb sandwich panel has a significant influence on the predicted transition frequency which increases with increasing the orthotropic coefficient Γ of the sandwich panel. Therefore, the assumption often adopted in the literature (i.e. an equivalent isotropic plate) for predicting the transition frequency for an orthotropic plate may lead to large errors.

Finally, the numerical results obtained by the bisection and wavemode energy techniques are in agreement with the transition frequency predicted using the analytical approach. As the main advantage of the numerical techniques is that they are not based on any homogenization procedure, they may be very useful in the 3D modeling of any strange architecture of the sandwich core.

CHAPTER 4

EVALUATION OF THE EFFECTS OF DIFFERENT SHAPED SANDWICH CORES ON THE TRANSITION FREQUENCY

Contents

THe present chapter evaluates the influence of the core geometry on the transition frequency of a sandwich panel involving orthotropic composite facesheets. The bending-shear transition occurs when the transverse shear stiffness has a significant influence on the flexural motion, compared to the bending stiffness of a sandwich panel. It should be noted that the modal density and the acoustic radiation increase considerably above the transition. The periodic waveguide is modeled at the meso-scale as a 3D finite element model of the unit cell. Consequently, the

used approach does not require any homogenization of the core to provide the wave dispersion characteristics. Although, the core shapes compared, in this chapter, share the same stiffness-to-mass ratio, a significant alteration of the transition frequency and modal density can be observed compared to honeycomb cores. A periodic octagonal core is designed, providing up to 70 % increase of the transition frequency and a significant reduction of the modal density.

4.1 Introduction

Sandwich panels are widely used in automotive, naval and aerospace industry. These structures have a high stiffness-to-weight ratio and are usually made of a moderately thick, lightweight core surrounded by glass or carbon-fibre composite skins. The core can be made of polymer foam or more complex structures involving aluminum or resin honeycomb constructions. Although the material and geometrical properties of the panel are usually designed to provide specific stiffness and density characteristics, structural optimization also concerns acoustic radiation efficiency in order to improve the acoustic comfort. Therefore, there is an increasing need for reliable optimization tools for design engineers, providing a fast vibroacoustic evaluation of large-scaled structures involving composite components.

In this context, the knowledge of accurate wave dispersion characteristics in two laminated orthotropic skins connected by 3D cellular honeycomb core is a key information for the prediction of the acoustic transmission parameters. Numerical methods for analysing the vibrational behaviour of complex composite or periodic panels in a broadband frequency range were extensively investigated in the last decade. Honeycomb sandwich panels were usually modelled using classical laminate plate (CPLT) of Reissner–Mindlin (FSDT) theories involving three homogeneous layers. An extensive number of analytical formula for analysing wave dispersion characteristics in two-dimensional waveguides can be found in the literature (see Reddy [116]), starting with the asymptotic model for analysing wave dispersion in thick symmetric sandwich panels developed by Kurtze and Watters [77], then later in the classic work of Wilkinson [157] and Erickson [47]. The prediction of wave propagation characteristics of structurally advanced structures using analytical models has been a subject of intense research over the past years. Renji et al. [123] introduced a new analytical formulation providing a core transverse shear stiffness and bending matrices in both directions for orthotropic

honeycomb sandwich panels. Ghinet and Atalla [54] also used an analytical model based on Discrete Laminate Theory (DLT) to compute the dispersion characteristics of layered structures and obtain their acoustic parameters.

Recently, Guillaumie [59] proposed an analytical solution for the eigenmodes and modal densities of symmetric sandwich panels involving composite skins and honeycomb core. This model was found to be effective in the low- and medium-frequency range for moderately thick sandwich structures and was confirmed by experiments. Florence and Renji [52] also derived explicit solutions for the modal density of composite cylinders.

However, these analytical solutions require a homogenisation of the hexagonal cells of the core based on Gibson and Ashby formulations [57]. These analytical approaches therefore suffer some drawbacks in the medium-frequency range, since they cannot handle arbitrarily shaped 3D cells for the core. Besides, these models are often inaccurate when compared to experimental characterizations in higher frequency range, especially when dealing with complex industrial products involving thick, multi-layered constructions made of anisotropic glass or carbon fibres skins.

Therefore, numerical methods were recently developed to perform wave analysis in complex periodic waveguides defined using classical finite element packages (FEM). Among others, the wave finite element method (WFEM) [92, 98] has been successfully applied to predict the radiation efficiency of numerous thick layered structures. Nevertheless, these models involve homogeneous orthotropic layers for the honeycomb construction, and may become inaccurate when the wavelengths are reaching the periodic cells dimensions. Although the design optimisation of honeycomb cells has received a lot of attention recently [5, 25], the dispersion characteristics of sandwich panels involving realistic composite skins and arbitrarily shaped cores was not investigated to the author's knowledge.

This chpter focuses on the influence of the meso-scale parameters of the core's construction on the vibroacoustic response of the sandwich panel. A special interest is given to the modal density, a typical vibroacoustic parameter and the transition frequency, associated with the passage from a behaviour where the flexural wave is ruled by the skins stiffness to a behaviour where the core's transverse shear parameters governs the

flexural motion. First, finite element models are developed for the periodic cells. The WFEM, which combines FEM and the Periodic Structures Theory (PST) is applied to evaluate the wave dispersion characteristics. Since numerous degrees of freedom are usually involved to ensure accuracy in a broadband frequency range, reduced order modelling (ROM) was recently investigated for periodic [24, 163] and large-scaled [41] waveguides. A hybrid wave-mode ROM is therefore applied to provide suitable computational efficiency. When dealing wit hexagonal cores, the equivalent orthotropic material can be described using Gibson and Ashby formulations, and the analytical expression of the wavenumber can be derived for the symmetric sandwich. The possibility to use a regression on the wavenumber function is therefore examined for various core's configurations, in order to derive an analytical expression of the transition frequency from the equivalent bending and shear parameters. Finally, the effects of several geometrical parameters of the core on the modal density and the transition frequency are investigated.

4.2 Evaluation of the transition frequency of sandwich structures

The dynamic characteristics used to identify the bending-shear transition have been determined the meso-macro approach presented in chapter 2. In sandwich structures, one can discriminate between three frequency domains associated with different kinetic energy distributions. In low frequency, the structure has a classical isotropic plate behavior. The asymptotic wavenumber modulus $k(f \to 0)$ and modal density $n(f \to 0)$ are written:

$$k(f \to 0) = \left(\frac{\rho_s}{D}\right)^{1/4} \sqrt{\omega} \quad ; \quad n(f \to 0) = \frac{A}{2}\sqrt{\frac{\rho_s}{D}}, \tag{4.1}$$

where A, D, ρ_s denote the area, equivalent bending rigidity and mass per unit area of the plate, respectively.

In a medium frequency (usually acoustic) range, the transverse vertical shear rigidity S, increases and influences the dynamical behaviour. The asymptotic solutions for the orthotropic plate are:

$$k(f)_{\text{M.F.}} \simeq \omega\sqrt{\frac{\rho_s}{S}} \quad ; \quad n(f)_{\text{M.F.}} \simeq A\left(\frac{\rho_s}{S}\right)\omega \tag{4.2}$$

In terms of waves, higher frequencies are associated with fully localised propagation, meaning that flexural waves can propagate independently in both skins. The transition frequency considered here refers specifically to the passage from the isotropic plate behaviour to a motion governed by the out-of-plane shear rigidity. In Guillaumie [59], this frequency is calculated as the intersection between the asymptotic wavenumbers: $k(f \to 0)$ and $k(f)_{\text{M.F.}}$. The influence of a core's shear rigidity on the modal density and transition frequency of a sandwich plate was well analysed by Renji et al. [123]. Above the transition frequency the modal density increases linearly with frequency and produces higher levels of acoustic radiation. In the following, the possibility to shift the transition frequency by using different cores geometries is investigated.

The modal density can be written using classical Statistical Energy Analysis (SEA) expression [82]:

$$n(\omega) = \int_0^{\pi} n(\theta,\omega) d\theta, \tag{4.3}$$

where $n(\theta,\omega)$ denotes the angular distribution of the modal density:

$$n(\theta,\omega) = \frac{A}{2\pi^2} \frac{k(\theta,\omega)}{|c_g(\theta,\omega)|}. \tag{4.4}$$

A is the surface area and $c_g(\theta,\omega) = \dfrac{\partial\omega}{\partial k}$ is the group velocity in the direction θ. An equivalent wavenumber $\langle k_f(\omega)\rangle$ is defined so that the modal density can be written:

$$n(\omega) = \frac{A}{2\pi} \langle k_f(\omega)\rangle \frac{\partial\omega}{\partial \langle k_f(\omega)\rangle}. \tag{4.5}$$

This expression enables the comparison of scalar solutions of the dispersion relation while ensuring the accurate computation of the modal density in the 2D structure, since the directivity is taken into account. The averaged wavenumber can be expressed in terms of the angular wavenumber:

$$\langle k_f(\omega)\rangle = \sqrt{\frac{1}{2\pi}\int_0^{2\pi} k_f^2(\theta,\omega) d\theta}. \tag{4.6}$$

The modal density can be also determined by the area integration of the wavenumber space (see Langley [78]). In case of an elliptic orthotropy along x- and y-directions, the equivalent wavenumber can be defined so that the k-space areas remain the same: $\pi k_x k_y = \pi \langle k_f \rangle^2$. It yields $\langle k_f \rangle = \sqrt{k_x k_y}$.

For a sake of clarity, the equivalent flexural wavenumber $\langle k_f(\omega)\rangle$ and group velocity $\dfrac{\partial\omega}{\partial\langle k_f(\omega)\rangle}$ are simply denoted k and c_g in the following.

4.3 Dispersion characteristics in different shaped sandwich panels

4.3.1 Core geometry and material properties

A symmetric sandwich plate involving composite face-sheets made of carbon reinforced epoxy resin is considered here. The core is assumed isotropic made of Nomex paper (aramid fibre and phenolic resin) of thickness 76.2 μm. The skins are made with two plies of transverse isotropic, 0.25 mm-thick, unidirectional composite (UD) with the staking sequence [0^o, 90^o]. The thickness of the core is h_T = 25 mm and the material properties are detailed in Table 4.1.

Material	**Nomex core**	**UD laminate**
Density (kg/m^3)	ρ_c = 1240	ρ_f = 1550
Young modulus ($\times 10^9$ Pa)	E_c = 5.5	E_1 = 133.6
		E_2 = 7.7
		E_3 = 7.7
Shear modulus ($\times 10^9$ Pa)	G_c = 2.7	G_{23} = 2.6
		G_{13} = 3.1
		G_{12} = 3.1
Poisson ratio	ν_c = 0.33	ν_{23} = 0.49
		ν_{13} = 0.29
		ν_{12} = 0.29

Table 4.1: Mechanical properties of Nomex paper and UD fibre.

The influence of a core's geometry on the transition frequency and modal density is the concern of this chapter. Consequently, the mechanical properties and thicknesses of the skins, core and Nomex paper are identical in all the models. The sandwich panels developed below only differ in the geometry of their cores and the dimensions L_x, L_y of their unit-cells.

The cores are created from the parametrized models shown in figure 4.1. The rectangular boxes describe the periodic cell's dimensions, while the inner lines describe the

top-view position of the Nomex paper in the core. A parametrized hexagonal core is proposed in figure 4.1.a. The core construction is designed using the three points M, P_1, P_2 and the corner parameters A_x, A_y, B_x and B_y. The other parameters are imposed by the compatibility requirement between the unit-cells. It can be seen that triangular, squares and pentagonal geometries can be obtained by setting coincident points $M = P_1$, $P_1 = P_2$ or $A_x = B_x$ and $A_y = B_y$.

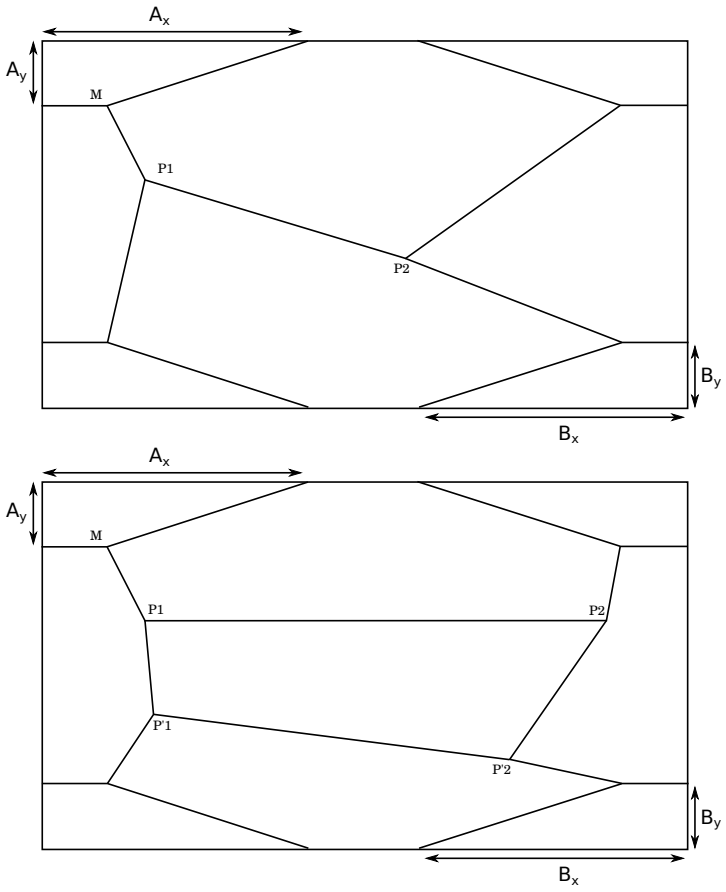

Figure 4.1: Top view of the 2D parametrized cores. Hexagonal (a) and octagonal (b) constructions.

In figure 4.1b, two additional points P_1' and P_2' are used for the construction of octagonal cores. Although this model can be easily generalized to create more complex shapes, it is reminded that the computational cost associated with optimization procedures depends on the number of design parameters.

The finite element model of five unit-cells obtained using the first parametrized model is shown in figure 4.2. These models involve linear block elements having 3 de-

grees of freedom per node. Case (a) is a classical hexagonal model (honeycomb). Case (b) is a rectangular, Case (c) is triangular, Case (d) is a pentagonal core and Case (e) is a parallelogram. An finely meshed octagonal core was also designed in figure 4.3. It should be noted that all the models are converged in the considered frequency range, but refined meshes such as in figure 4.3 would be necessary in higher frequencies to describe the local dynamics at the cell's scale.

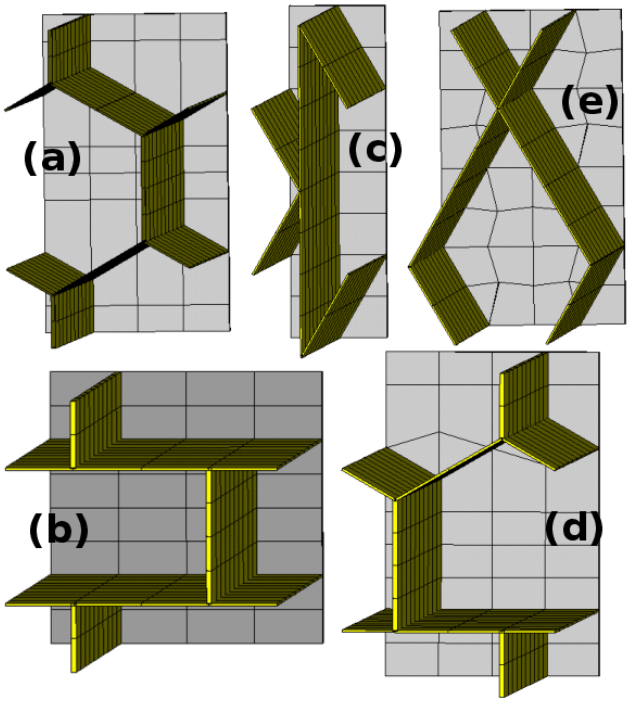

Figure 4.2: 3D Finite element models of the considered periodic cells.

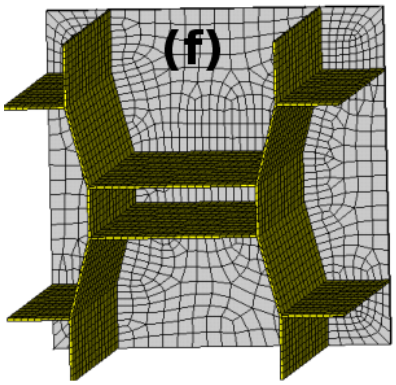

Figure 4.3: 3D Finite element model of the octagonal construction.

Besides, the geometry of the core has a noticeable influence on the Nomex distribution, hence on the surface density of the sandwich panel. For this reason, the dimensions of the cellular core is chosen so that the overall bending stiffness-to-mass ratio remains constant in the sandwich. It means that the modal density is expected to be identical for all the considered models at low frequency. The size of the unit-cells, L_x and L_y are detailed in table 4.2.

Case	**a**	**b**	**c**	**d**	**e**	**f**
$L_x\ (mm)$	6.93	8	4.29	6.93	13.85	20
$L_y\ (mm)$	12	8	14.48	10.53	8	20

Table 4.2: Size of the rectangular unit-cells in the six cases.

4.3.2 Effects of the core geometry on the transition frequency

The wave dispersion characteristics of the periodic waveguides defined by unit-cells (a)-(f) are obtained using the method described in section 4.2. The flexural wavenumbers k are compared in figure 4.4. It is seen that the core geometry has a significant influence on the wavenumbers of the sandwich panel. More precisely, the flexural behaviours remain similar due to the constant bending rigidity and differ above the transition frequency. A 95% difference can then be observed between the (c) and (f) wavenumbers at 1800 Hz.

The transition frequency is located at the intersection between the asymptotic shear and bending curves. The method is shown in figure 4.5 for the core geometry (b), where the bending k_b and shear k_s wavenumbers are both derived from the WFEM solution. It should be noted that an accurate bending wavenumber requires a refined frequency sampling in the lower frequencies. For the considered models, it can be seen that a clear bending behaviour is observed below 200 Hz, while the shear behavior occurs above 600 Hz except for case (f).

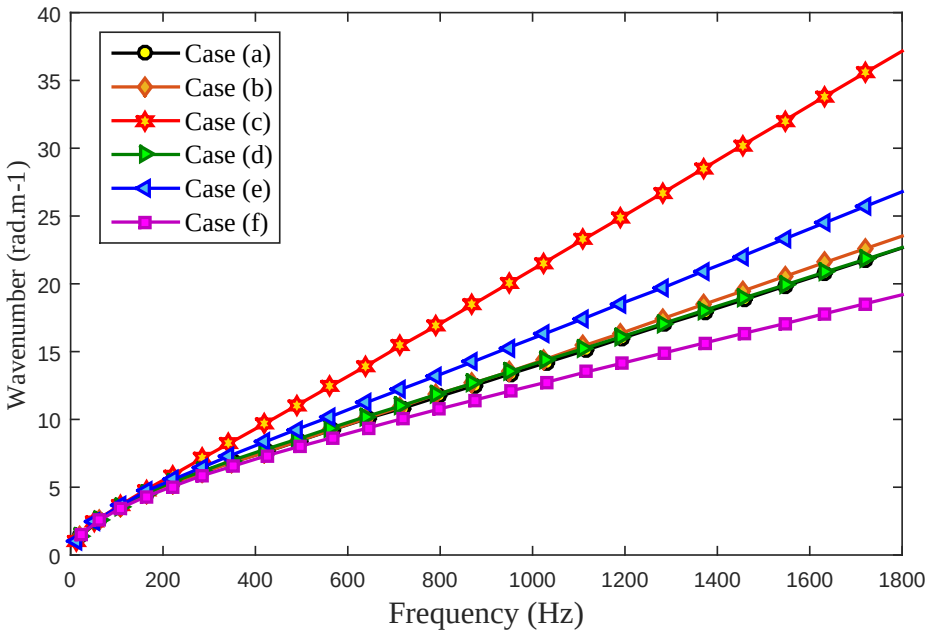

Figure 4.4: Flexural wavenumbers for the five core configurations.

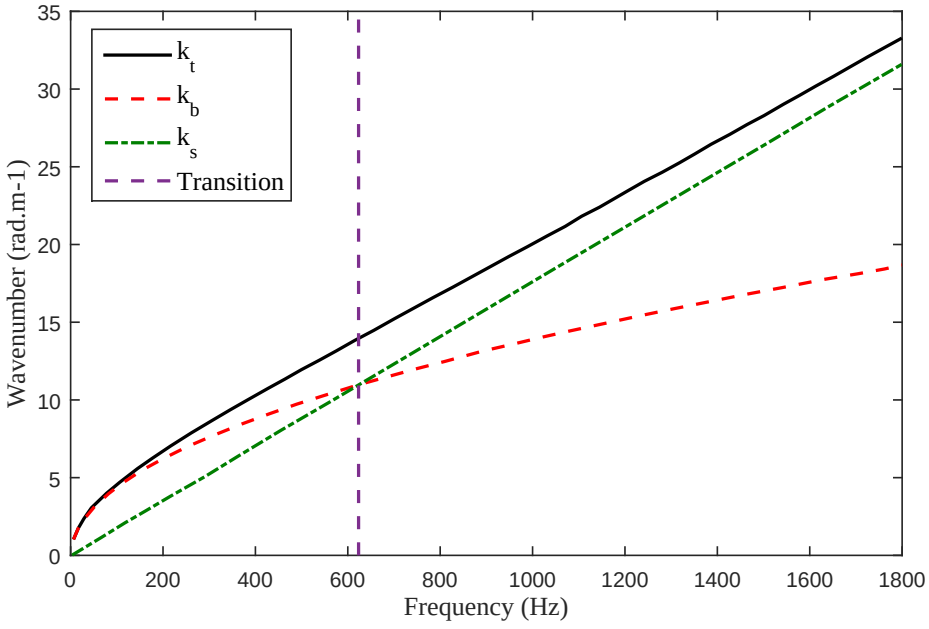

Figure 4.5: Definition of the transition frequency : intersection between asymptotic shear and bending waves in the case (b).

For the honeycomb core (a), an exact analytical expression can be derived for the

transition frequency. The dispersion relation in the sandwich can be written in terms of the mass per unit area m_s, the equivalent transverse shear stiffness S and bending rigidity D of the plate [59]:

$$k^2 = \frac{m_S}{2S}\left(\omega^2 + \omega\sqrt{\omega^2 + \frac{4S^2}{m_S D}}\right) \tag{4.7}$$

Therefore, equalizing the asymptotic solutions defined equations (4.1) and (4.2) yields:

$$\omega_{\mathrm{T}} = \frac{S}{\sqrt{m_S D}} \tag{4.8}$$

The transition frequency ω_{T} can therefore be expressed analytically in terms of the equivalent bending, shear and mass parameters.

For other cores' geometries, it should be noted that the transition frequency can be only approximated using equations (4.1) and (4.2), since Gibson and Ashby homogenisation is no longer valid. The equivalent parameters $\tilde{m}_S$,$\tilde{D}$ and $\tilde{S}$ are obtained from equation(4.7) and the numerical solution $k_t(\omega)$ evaluated using non-linear least-square regression. The error on the regression function is written:

$$\varepsilon_{\mathrm{reg}}(\omega) = \left|\frac{k_t(\omega) - k_{\mathrm{reg}}(\omega, \tilde{D}, \tilde{m}_S, \tilde{S})}{k_t(\omega)}\right| \tag{4.9}$$

The values of $\varepsilon_{\mathrm{reg}}$ are compared in figure 4.6. The regression appears in very good agreement with the WFEM solutions, except for Case (c) which exhibits up to 3% error in the considered frequency range. On the other hand Case (d) and (f) fit very well with the honeycomb model described in equation (4.7). It should be noted that the regression accuracy may depends on the chosen frequency range for f_{reg}.

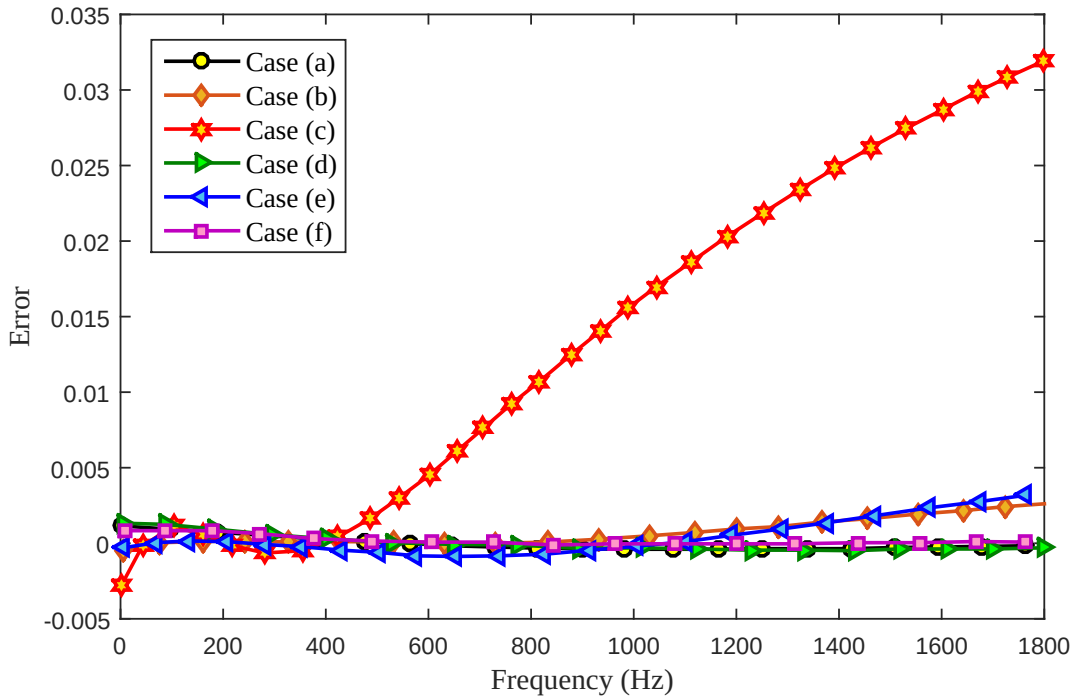

Figure 4.6: Difference between WFEM solutions and approximated wavenumbers.

To summarize, the transition frequency can be determined from the asymptotic wavenumbers k_s and k_b derived from the WFEM solutions. In order to reduce the sensitivity to sampling for the determination of $k_b(\omega \to 0)$, the equivalent shear, bending and mass parameters can be obtained through a regression model. An analytical expression can therefore be derived for ω_{T} with a good accuracy, except for case (c).

4.3.3 Effects of the core geometry on the modal density

The transition can be observed on the averaged group velocity c_g, as the passage from a square to linear function. The velocities are compared in figure 4.7. It can be seen that the cores have a significant influence on the energy velocity in the panel, and the waves are still dispersive above the transition frequency. Noteworthy, the maximal group velocity is obtained around the transition, meaning that reduced wave attenuations are expected in this frequency range.

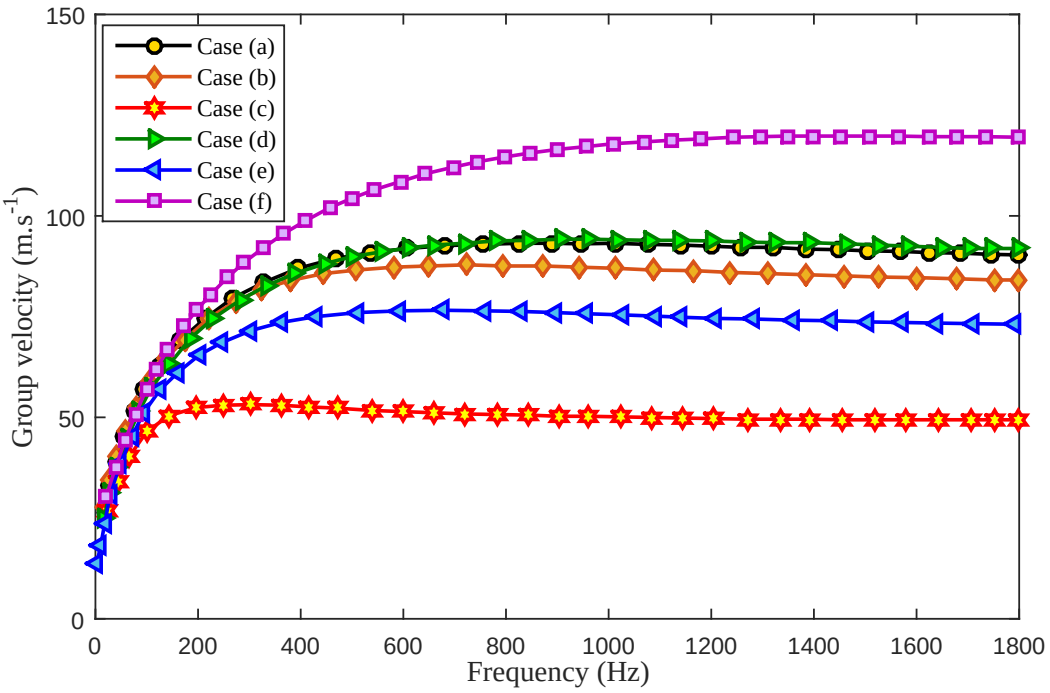

Figure 4.7: Averaged energy velocity in the sandwich waveguide.

The transition frequencies are detailed in table 4.3 and compared with the honeycomb model (a). Case (c), associated with triangular construction has the lowest shear rigidity. The rectangular and parallelogram cores, cases (b) and (e) are associated with reduced transition frequencies compared to the hexagonal (a) core. The pentagonal core (d), produces a slight increase (9.11 %) of the transition frequency compared with honeycomb. On the other hand, the octagonal core (f) provides a considerable increase (70 %) of the transition frequency. Therefore, this geometry can postpone the transition frequency while maintaining the stiffness-to-mass ratio.

Cases	Transition frequency (Hz)	Variation with honeycomb
a	765.79	/
b	624.03	- 18.5 %
c	244.64	- 68 %
d	835.54	**+ 9.11 %**
e	570.29	- 25.5 %
f	1302.5	**+ 70.05 %**

Table 4.3: Transition frequency in the panel for different cores geometries.

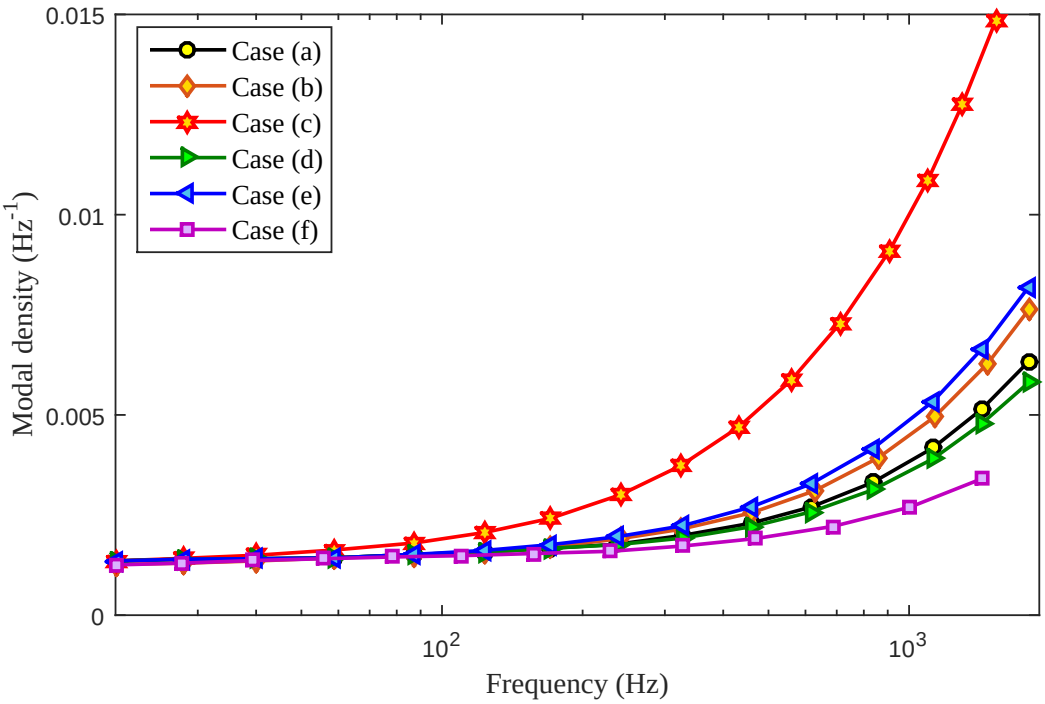

Figure 4.8: Modal density in the sandwich panels with different cores.

The modal density in the sandwich panel is calculated from the propagating wavenumbers and group velocities as mentioned above. The WFEM solutions are compared in figure 4.8 for a surface S=1 m^2, although it is reminded that the transition frequency does not depend on the panel's surface. The scaling procedure to preserve the mass-to-stiffness ratios is validated since the modal densities $n(\omega \to 0)$ are the same for the six models. It can be seen that $n(\omega)$ critically increases above ω_{T} for each model. It should be noted that the influence of the core's geometry on the overall flexural behavior will increase if the ratio between the core h_T and the skins h_s increases.

4.4 Concluding remarks

This chapter is concerned with the design of sandwich panels with improved vibroacoustic parameters. Although honeycomb constructions provide excellent compressional strength to density ratio, other types of periodic cores can be used to increase the transition frequency and reduce the modal density in a given frequency range.

In this work, the meso-macro approach presented in chapters 2 and 3 was employed to compare various types of core constructions for a given sandwich panel. This approach does not suffer the limitations associated with core homogenization and provides accurate wave dispersion characteristics with a reasonable computational cost. It was shown that a 70 % increase of the transition frequency can be obtained by using an octagonal core geometry, while maintaining the same bending stiffness-to-mass ratio, as well as the skin and core materials. As a consequence of the increased equivalent shear modulus, the octagonal core also produces significantly higher group velocity and reduced modal density.

This transition frequency can be used as a relevant output for optimization procedures oriented toward improving vibroacoustic parameters. It should be noted that the proposed application is restrained to 2D geometric parameters (the core is unchanged along its thickness), since a reduced number of design parameters is required for sensitivity of optimization procedures. An interesting development would be to understand how 3D cores could be designed in order to significantly postpone the bending to shear transition to higher frequencies.

CHAPTER 5

TRANSMISSION LOSS THROUGH SANDWICH STRUCTURES : PARAMETRIC SURVEY

Contents

THe current chapter presents a parametric analysis on the sound transmission loss. An expression of the latter indicator was derived wherein the shear core effect of the sandwich panel are taken into account. The developed expression is based on a two-scale approach described in detail in chapter 1. The vibroacoustic indicators of interest, in this study, are primarily the sound transmission loss (TL) and the bending-shear transition frequency presented in chapter 3. The stated indicators depend mainly on the geometrical and mechanical parameters of the studied case. The proposed parametric survey, therefore, reveals the effects of the different

meso-scale parameters on the macro-scale responses of the sandwich panels by performing three-dimensional model of a representative elementary cell. The obtained results were compared with different analytical methods and an experimental result to check the accuracy of the prediction and showed a good agreement.

5.1 Introduction

Most industrial applications are seeking for innovative structures, which are characterized by high mechanical and chemical performances as well as they could be as light as possible. Nowadays, the most suitable structure that can combine all these properties is known as a sandwich structure. This kind of structure is widely used in several sectors especially in the high-speed transportation industries such as launcher, plans, trains and so on and so forth. This trend is thanks to their great global mechanical properties with respect to their micro mechanical properties [57, 93, 161]. Nevertheless, from the vibroacoustic side, increasing stiffness to weight ratio could have a harmful effect on the vibroacoustic performance of the structure which then might lead to unsatisfactory sound insulation performance.

Theoretically, the root cause of the poor acoustic transparency of sandwich panels is due mainly to the shear core effect of sandwich panels at the mid frequencies. Fahy et al. [50] defined three dominant zones for a typical sandwich panel: global panel bending, core shear and individual face-sheet bending. The frequency separating the first two zones, known as the transition frequency, is of great interest [10, 42]. The main idea of the latter papers was to increase the transition frequency of a sandwich panel with a goal of shifting the shear core effect to the high-frequency range wherein the acoustic transparency can be easily controlled by adding a porous material for instance. Many published papers [10, 36, 59, 126] propose developments of the transition frequency expression. In the present study, a survey has been carried out to reveal the influence of an increasing transition frequency on the sound transmission loss (TL) of sandwich panel with orthoropic face-sheets.

Over the past several decades, Various methods have been proposed for predicting the sound transmission loss (TL) across composite sandwich structure. In the Kurtze and Watters study [77], it has been proved that TL is controlled by three physical characteristics, the mass per unit area, the dynamic bending stiffness and the internal

damping of the structure. The latter model was improved by Ford [53] by introducing compressible core and dilatational motions which enables to study foam sandwich core panels. Few years later, Statistical Energy Analysis (SEA) has been used by Crocker [35] to predict the sound transmission loss, the radiation resistance and the vibration amplitude of a partition. In 2005, Renji [122] has derived an analytical transmission loss expression in terms of the coincidence frequency considering also the shear core flexibility. Griese et al. [58] carried out a parametric study on the transmission loss and the vibration properties of in-plane loaded honeycomb sandwich panels using structural acoustic finite element method by varying the honeycomb cellular core geometries. Recently, Mejdi et al. [97] has developed a semi-analytical approach, called a wave spectral finite element model, that can capture the stretch information through the thickness of the sandwich core.

On the other hand, many experimental attempts have been performed to understand and enhance the vibroacoustic flexural behavior of the honeycomb sandwich panel. Palumbo and his co-workers [110] carried out an experimental analysis by creating different forms and size of areas with reduced stiffness in the honeycomb core. The created areas led to a notable benefit on the sound transmission loss either in the low-mid frequency or in the high frequency ranges but to a significant decrease in the panel stiffness as well. A year later, Peters and Nutt [112] established an experimental parametric study using a sturcture-borne excitation. The main purpose was to validate the influence of the shear wave speeds on the sound transmission loss revealed analytically by Kurtze and Watters in [77] and Davis in [36]. Similarly, Naify et al. [103] has performed theoretical and experimental surveys to reduce the amount of sound energy transmitted through the honeycomb panel by attaching additional gas layers. Impedance mismatch of gasses was shown to be an efficient means to relatively decrease the noise transmitted across a honeycomb sandwich panel.

The main purpose of this study is to investigate the shear core and the transition frequency effects of the sandwich panel on the sound transmission loss (TL) through a multi-scale like numerical method. A parametric analysis was then conducted to reveal the influence of the increasing transition frequency. The proposed two-scale approach is based on a numerical method known as the Wave Finite Element Method (WFE). The WFE method combines the classical finite element method (FEM) and the periodic structure theory (PST) developed in [109]. The main advantage of the developed approach is

that it keeps into consideration the periodicity of the structure, which allows to model typically just one elementary cell instead of the whole structure. Accordingly, the calculations cost is hugely reduced. Moreover, this numerical model keeps the meso-scale parameters of the periodic cell.

5.2 Sound transmission loss expression through sandwich panels

We consider here a sandwich panel of infinite boundary, separating two semi-infinite incident and transmitted medium (see figure 5.1).

The external excitation of the incident sound wave strikes the sandwich panel's surface causing it to vibrate and radiate sound to the transmitted side. The flexural vibroacoustic behavior of the full structure are governed by Renji's model [123]

$$D_X \frac{\partial^4 W}{\partial x^4} + 2D_{XY} \frac{\partial^4 W}{\partial x^2 \partial y^2} + D_Y \frac{\partial^4 W}{\partial y^4} + \rho_p \frac{\partial^2}{\partial t^2} \left(\frac{D_X}{N_x} \frac{\partial^2 W}{\partial x^2} + \frac{D_Y}{N_y} \frac{\partial^2 W}{\partial y^2} \right) + \rho_p \frac{\partial^2 W}{\partial t^2} = q, \quad (5.1)$$

with D_X and D_Y are the bending stiffness along the x- and y-directions. $D_{XY} \cong \sqrt{D_X D_Y}$ is the cross-bending stiffness of the sandwich panel.

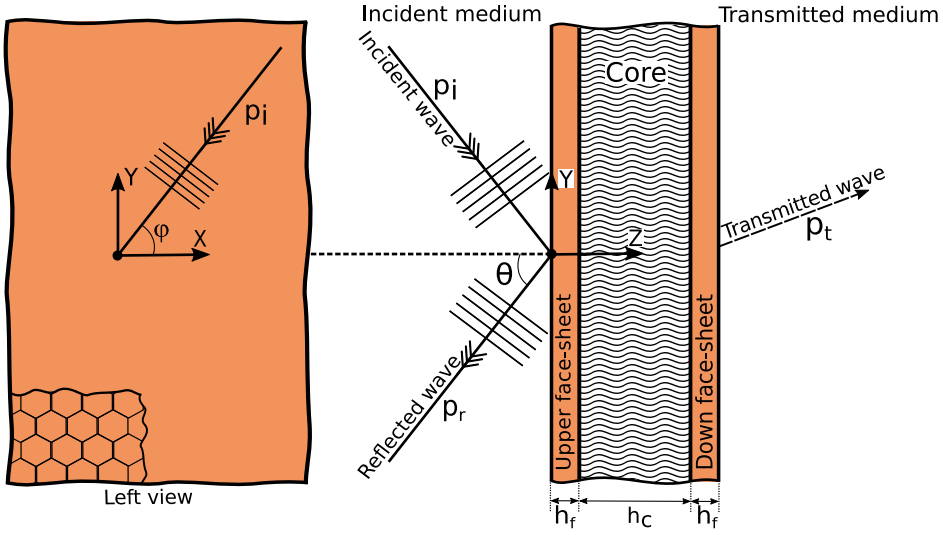

Figure 5.1: Transmetted and reflected plane wave at an infinite sandwich panel

It is assumed that the variation of the sound pressure through the sandwich panel is only along the z-direction. So, the vertical displacement $W(x,y,z,t)$ of the sandwich panel is only considered.

$$W(x,y,z,t) = W_o.e^{-(k_x x + k_y y \pm k_z z - \omega t)} \tag{5.2}$$

$$k_x = k_o sin\theta cos\varphi, \;\; k_y = k_o sin\theta sin\varphi, \;\; k_z = k_o cos\varphi,$$

where $k_o = \dfrac{\omega}{c_o}$ is the acoustic wavenumber with c_o is the sound speed in air.

A harmonic motion is assumed in the present study. Thus, the plane acoustic pressure incident on the sandwich panel at an heading angle θ and at a wave heading direction φ is represented by :

$$p_i(x,y,z,t) = p_{io}.e^{-i(k_x x + k_y y + k_z z - \omega t)} \tag{5.3}$$

While the corresponding expressions for the reflected and transmitted waves are :

$$\begin{cases} p_r(x,y,z,t) = p_{ro}.e^{-i(k_x x + k_y y - k_z z - \omega t)}, \\ p_t(x,y,z,t) = p_{to}.e^{-i(k_x x + k_y y + k_z z - \omega t)} \end{cases} \tag{5.4}$$

By considering the continuity of the acoustic pressure and the acoustic velocity at the sandwich panel and by applying Newton's third law, we obtain :

$$\begin{aligned} &p_{io} + p_{ro} - p_{to} = \Delta p = i\omega\rho_s v_o, \\ &v_o = (p_{io} - p_{ro})\frac{\cos\theta}{\rho_o c_o} = p_{to}\frac{\cos\theta}{\rho_o c_o}, \end{aligned} \tag{5.5}$$

where ρ_s is the mass per unit area of the sandwich panel, ρ_o and c_o are respectively the density and the speed of sound in the surrounding medium which is in our case the air. By combining equations (5.1 - 5.5), the transmission coefficient $\tau(\omega,\theta,\varphi)$ for sandwich panels takes the following form :

$$\tau(\omega,\theta,\varphi) = \left|\frac{p_{to}}{p_{io}}\right|^2 = \left\{\left[1 + \eta\frac{\rho_s\omega cos\theta}{2\rho_0 C_0}\left(\frac{k_0^4 sin^4\theta}{k_{eq1}^4} + \frac{k_0^2 sin^2\theta}{k_{eq2}^2}\right)\right]^2 + \left[\frac{\rho_s\omega cos\theta}{2\rho_0 C_0}\left(1 - \frac{k_0^4 sin^4\theta}{k_{eq1}^4} - \frac{k_0^2 sin^2\theta}{k_{eq2}^2}\right)\right]^2\right\}^{-1}, \tag{5.6}$$

where k_{eq1} and k_{eq2} are the equivalent wave-numbers of the sandwich panel which can be expressed as the following form:

$$\begin{cases} \dfrac{1}{k_{eq1}^2} = \dfrac{sin^2\varphi}{k_{bx}^2} + \dfrac{cos^2\varphi}{k_{by}^2}. \\ \dfrac{1}{k_{eq2}^2} = \dfrac{sin^2\varphi}{k_{bx}^4} k_{sx}^2 + \dfrac{cos^2\varphi}{k_{by}^4} k_{sy}^2. \end{cases}$$

The sound transmission loss (TL) through a sandwich panel is then given by the following expression :

$$TL = 10\log_{10}\left(\frac{1}{\tau(\omega)}\right) = 10\log_{10}\left(\left|\frac{p_{io}}{p_{to}}\right|^2\right), \tag{5.7}$$

where, the acoustic diffuse field transparency $\tau(\omega)$ is calculated by averaging all the possible incidents θ and the wave heading directions φ.

$$\tau(\omega) = \frac{\int_0^{2\pi}\int_0^{\pi/2} \tau(\omega,\theta,\varphi)\sin\theta\cos\theta \; d\theta \; d\varphi}{\int_0^{2\pi}\int_0^{\pi/2} \sin\theta\cos\theta \; d\theta \; d\varphi}. \tag{5.8}$$

The proposed modeling strategy for sandwich panels is generally illustrated in figure 5.2. The procedure can be summarized as follows :

↬ Extract, reorder and reduce the size of the mass and stiffness matrices for the periodic sandwich cell.

↬ Solve the non-linear polynomial equation 2.10 depending on the chosen unit sandwich cell.

↬ Compute the vibroacoustic indicators of the sandwich panel which are, in the current paper, the sound transmission loss (TL) and the transmission frequency f_t.

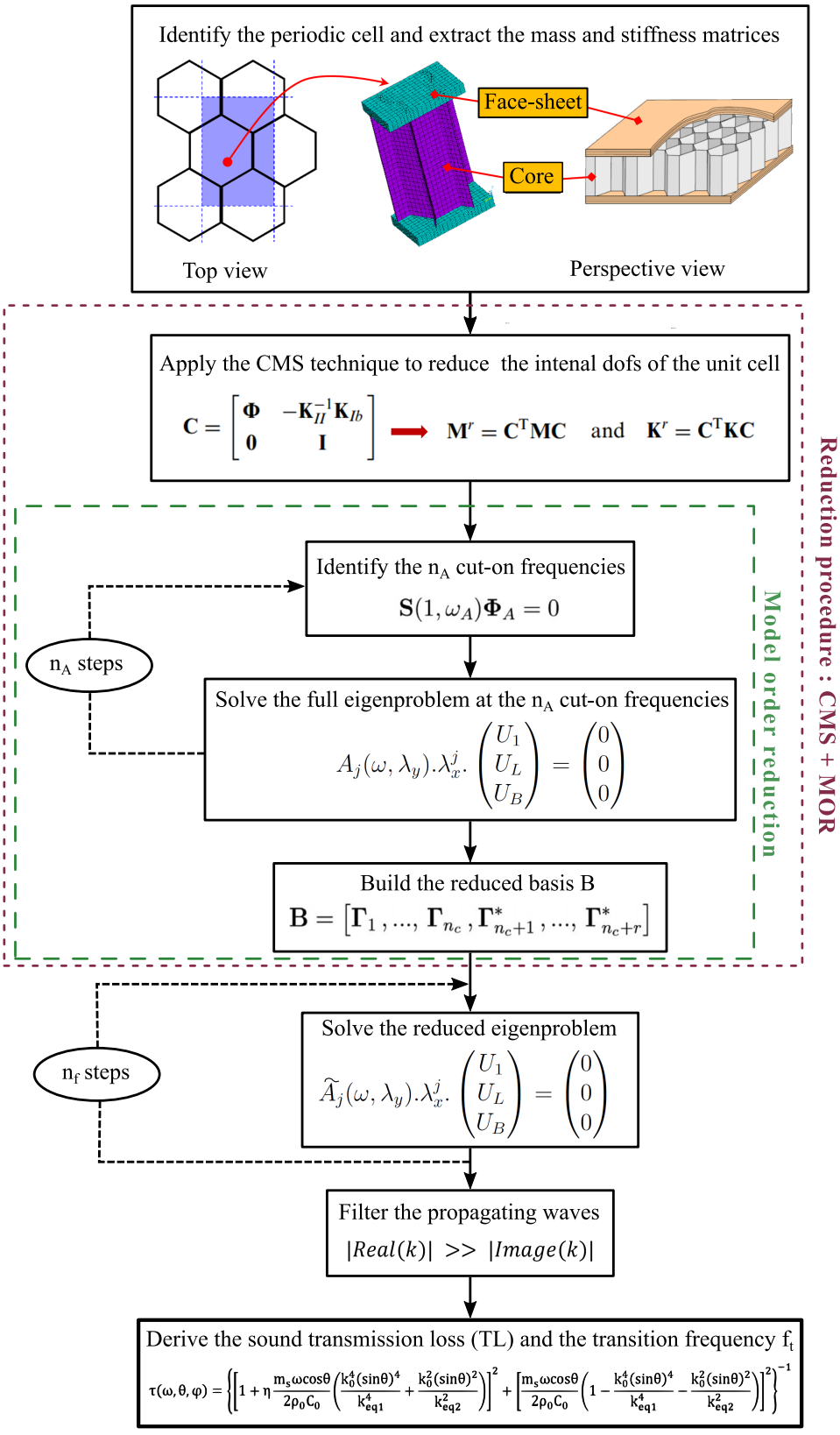

Figure 5.2: Procedure of the proposed parametric analysis for sandwich panels

5.3 Validation and parametric survey

The prediction accuracy of the meso-macro approach, described in the previous sections, was assessed by checking the obtained result against two semi-analytical models (the discrete laminate model (DLM) [54] and the wave spectral finite element model (WS-FEM) [97]) and an experimental data [44] as shown in Figure 5.3. The measurement data and the semi-analytical results were digitalized from figure 2 in reference [97].

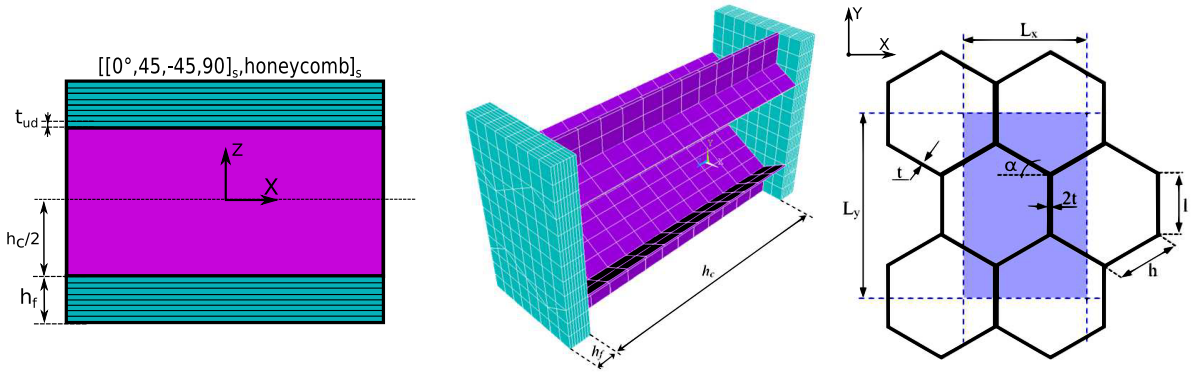

Figure 5.3: Comparison of the sound transmison loss of the sandwich panel

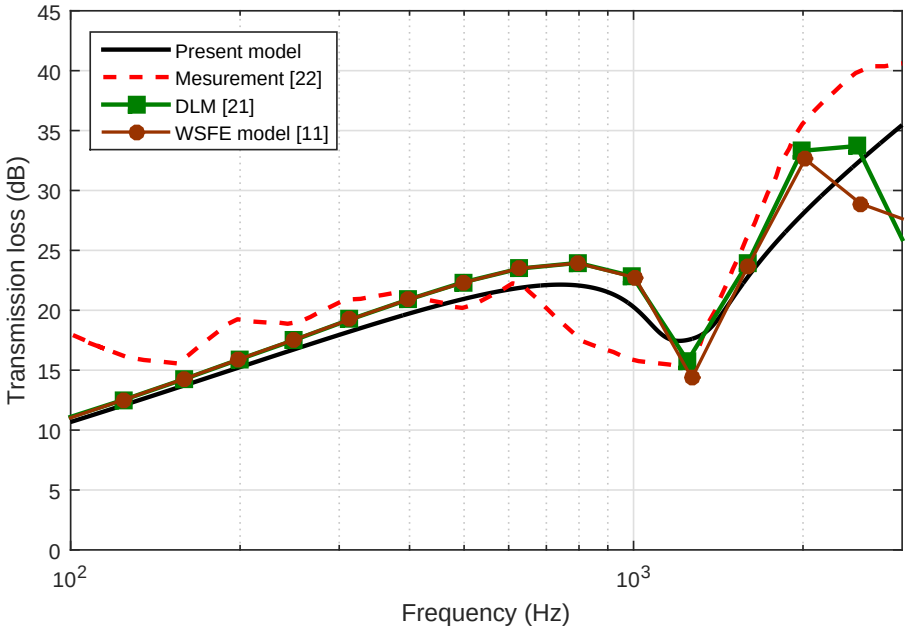

Figure 5.4: Comparison of the sound transmison loss of the sandwich panel

The effective mechanical properties and the geometric dimensions of the sandwich panel used to check the accuracy are given in [97] (case 2). As clearly noticed in figure 5.4, the results obtained using the proposed approach is in good agreement with the semi-analytical models and the experimental measurement.

Sandwich core *Nomex material*	**Sandwich face-sheets** *Epoxy resin with carbon yarn*
$\rho = 1240\ \ kg/m^3$	$\rho = 1550\ \ kg/m^3$
$E = 5.5\ \ GPa$	$E_1 = 133.6\ \ GPa;\ \ E_2 = E_3 = 7.7\ \ GPa$
$\nu = 0.33$	$\nu_{12} = \nu_{13} = 0.29$
$G = 2.07\ \ GPa$	$G_{12} = 3.1\ \ GPa;\ \ G_{13} = G_{12} = 3,1\ \ GPa$

Table 5.1: Mechanical properties of the sandwich panel.

In the next subsections, parametric analyses have been performed to quantify the effect of the geometric parameters and the architecture of the sandwich core on the sound transmission loss as well as on the transition frequency. The used sandwich structures are symmetric panels made up of Nomex (paper of aramid fiber with phenolic resin) in the center layer and epoxy resin with carbon yarn in the sandwich face-sheets. The reference sandwich panel has a core thickness $h_c = 0.012\ m$ and a total face-sheet thickness $h_f = 0.001\ m$ with angular arrangement $[0,45,90,-45]_S$. The typical geometric parameters utilized to define the unit periodic cell topology are described in figure 3.2. In the parametric analyses, it is tried to keep the unit cell mass constant by changing two geometric parameters at the same time. The finite element software used for extracting the full mass and stiffness matrices of the unit periodic cell was Ansys software with shell elements. It should be also noted that the damping loss factor used throughout the parametric analyses is $\eta = 0.01$.

A useful representation proposed by De Rosa and his co-workers in [38] was used for the obtained curves with a dimensionless frequency axis. The proposed representation allows removing the mass effect for more efficient analyses. This frequency f^* is defined as follows:

$$f^* = f\frac{\rho_s}{\rho_0 c_0}, \tag{5.9}$$

in which ρ_s is the equivalent mass per unit area of the sandwich panel. $\rho = 1.164\ kg/m^3$ and $c_0 = 349.2\ m/s$ are the air density and the sound speed in the air, respectively.

5.3.1 Honeycomb core case

In the first subsection, a parametric survey was carried out for a hexagonal cell by changing the conventional geometric parameters described in figure 5.3 and using the same core and face-sheets materials.

The transmission loss curves for a symmetric sandwich panel with different cell angle values α are presented in figure 5.5. It is noticed from the stated figure that there is a negligible improvement on the sound transmission loss (TL) in the mid frequency range. However, the bending stiffness value D of the sandwich panel, in the present case, is maximal at the cell angle $\alpha = 28$ °.

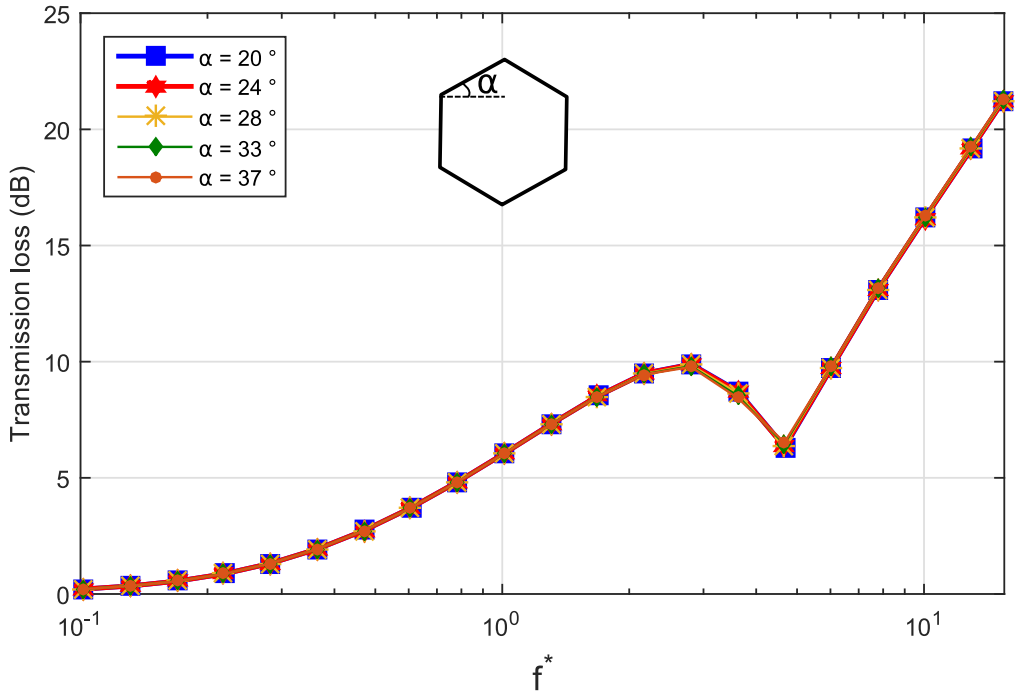

α	**Transition frequency** f_t	**Bending stiffness** D	**mass per unit area** ρ_s
20 °	346.7 Hz	4664.7 $N.m$	3.7 kg/m^2
24 °	320.9 Hz	4674.9 $N.m$	3.7 kg/m^2
28 °	292.7 Hz	4777.8 $N.m$	3.7 kg/m^2
33 °	276.4 Hz	4629.7 $N.m$	3.7 kg/m^2
37 °	250.7 Hz	4678.9 $N.m$	3.7 kg/m^2

Figure 5.5: Effect of the sandwich core angle α

The effect of the ratio $R = t/h_c$ (the wall hexagonal thickness t and the core thickness

h_c) on the sound transmission loss is illustrated in figure 5.6. As it has been shown, the increase of the ratio $R = t/h_c$ has led to a notable improvement of the sound transmission loss in the mid frequency range. The enhancement observed on the TL indicator was arrived up approximately to 6 dB. On the contrary, it is noticed that this increase of the ratio $R = t/h_c$ has led to a significant decreasing of the equivalent bending stiffness D of the sandwich panel as well. It is also noticed a decrease of the TL indicator in the high frequency range.

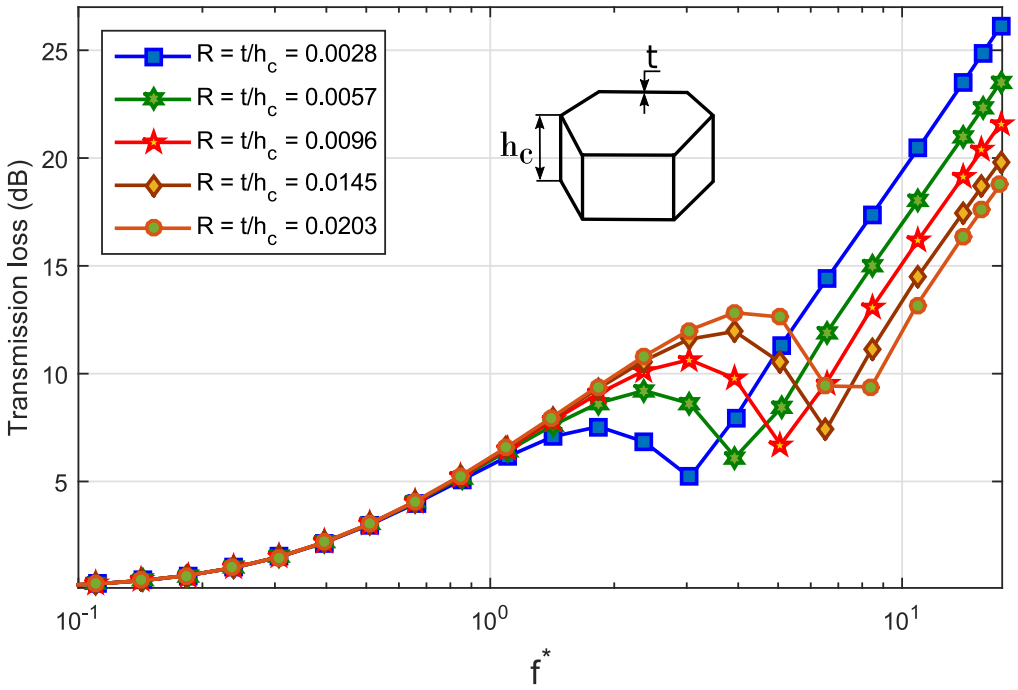

$R = t/h_c$	**Transition frequency** f_t	**Bending stiffness** D	**mass per unit area** ρ_s
0.0028	193.3 Hz	9728.1 $N.m$	3.72 kg/m^2
0.0057	271.7 Hz	5196.6 $N.m$	3.71 kg/m^2
0.0096	364.0 Hz	3208.8 $N.m$	3.71 kg/m^2
0.0145	671.9 Hz	2307.0 $N.m$	3.70 kg/m^2
0.0203	812.6 Hz	1712.5 $N.m$	3.70 kg/m^2

Figure 5.6: Effect of the wall and panel thicknesses t and h_c

The effect of the ratio $R = t/l$, the wall thickness t and the angled member length l on the sound transmission loss is presented in Figure 5.8. It is shown that the increase of the ratio $R = t/h$ leads to an improvement of TL and to a raise of the frequency transition f_t in the mid frequency. However, the improvement, in the low frequency, is due

to the increase the mass per unit area ρ_s (approximately 15%). The bending stiffness D of the sandwich dropped by approximately 4%.

Figure 5.7 illustrates the effect of the ratio $R = t/h$ (the wall thickness t and the vertical member length h) on the sound transmission loss (TL). In the mid frequency, it is observed that the increase of the wall thickness t with respect to the vertical member length h has led to a moderate improvement in the TL curves (roughly 4 dB) and to a rise of the frequency transition f_t as well. It is also noticed that the equivalent bending stiffness D of the sandwich panel was dropped by approximately 4%.

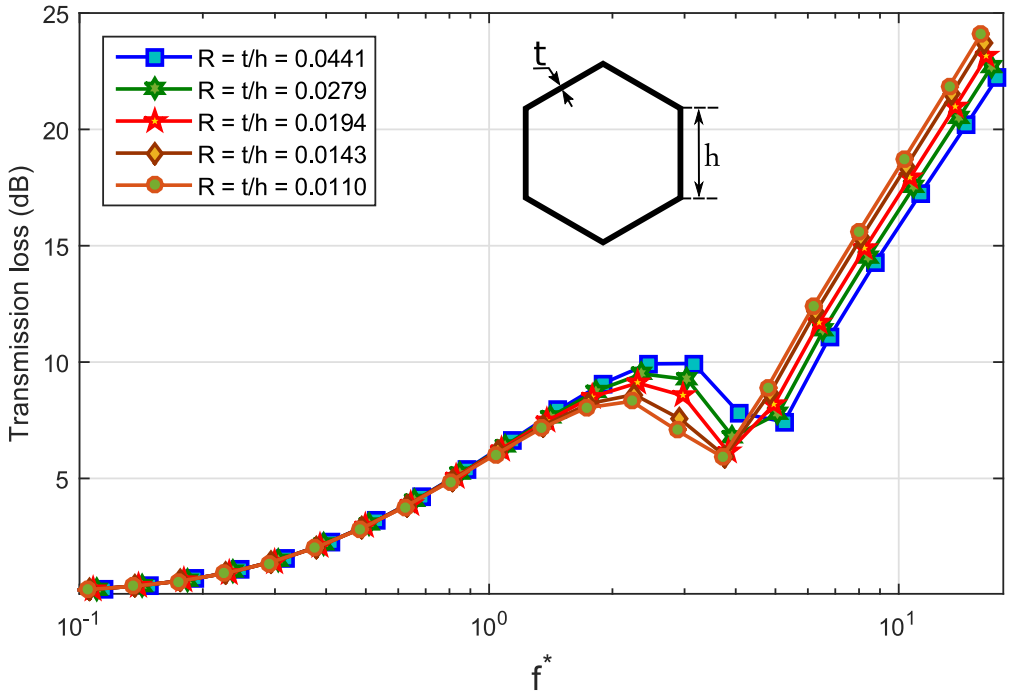

$R = t/h$	**Transition frequency** f_t	**Bending stiffness** D	**mass per unit area** ρ_s
0.0441	398.9 Hz	4674.8 $N.m$	3.84 kg/m^2
0.0279	293.3 Hz	4629.2 $N.m$	3.71 kg/m^2
0.0194	227.6 Hz	4617.9 $N.m$	3.62 kg/m^2
0.0143	178.6 Hz	4792.5 $N.m$	3.55 kg/m^2
0.0110	150.5 Hz	4656.5 $N.m$	3.50 kg/m^2

Figure 5.7: Effect of the wall thickness t and the vertical member length h

The effect of the ratio $R = t/l$ (the wall thickness t and the angled member length l) on the sound transmission loss is presented in figure 5.8. It is shown that the increase

of the ratio $R = t/h$ has led to an improvement of TL and to a rise of the frequency transition f_t in the mid frequency. However, a slump of the equivalent bending stiffness D of the sandwich (about 4%) is noticed.

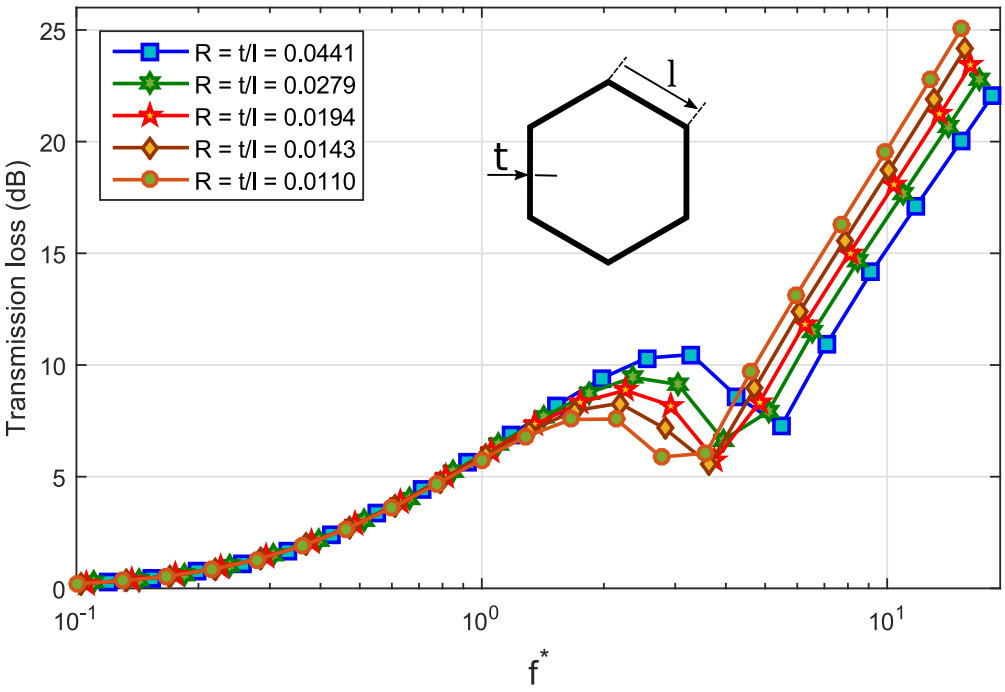

$R = t/l$	**Transition frequency** f_t	**Bending stiffness** D	**mass per unit area** ρ_s
0.0441	354.6 Hz	4614.5 $N.m$	4.01 kg/m^2
0.0279	285.4 Hz	4732.3 $N.m$	3.71 kg/m^2
0.0194	245.3 Hz	4619.5 $N.m$	3.55 kg/m^2
0.0143	208.9 Hz	4612.6 $N.m$	3.44 kg/m^2
0.0110	169.0 Hz	4802.4 $N.m$	3.37 kg/m^2

Figure 5.8: Effect of the wall thickness t and the angled member length l

Figure 5.9 shows in general a slight improvement of the sound transmission loss and the transition frequency f_t in the mid frequency range. This slight improvement is due to the increase of the vertical member length h with respect to the pane thickness h_c. However, a significant slump of the equivalent bending stiffness D (about 60%) is observed.

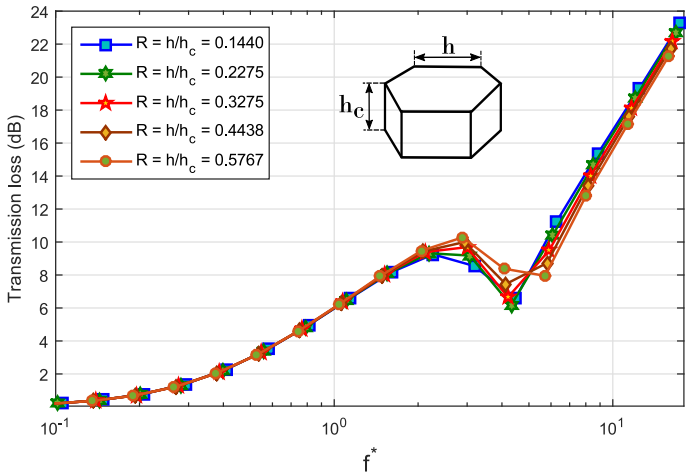

$R = h/h_c$	**Transition frequency** f_t	**Bending stiffness** D	**mass per unit area** ρ_s
0.1440	341.3 Hz	6066.6 $N.m$	3.85 kg/m^2
0.2275	291.1 Hz	4668.3 $N.m$	3.71 kg/m^2
0.3275	262.8 Hz	3645.8 $N.m$	3.62 kg/m^2
0.4438	240.3 Hz	2960.4 $N.m$	3.55 kg/m^2
0.5767	229.0 Hz	2432.2 $N.m$	3.50 kg/m^2

Figure 5.9: Effect of the panel thickness h_c and the vertical member length h

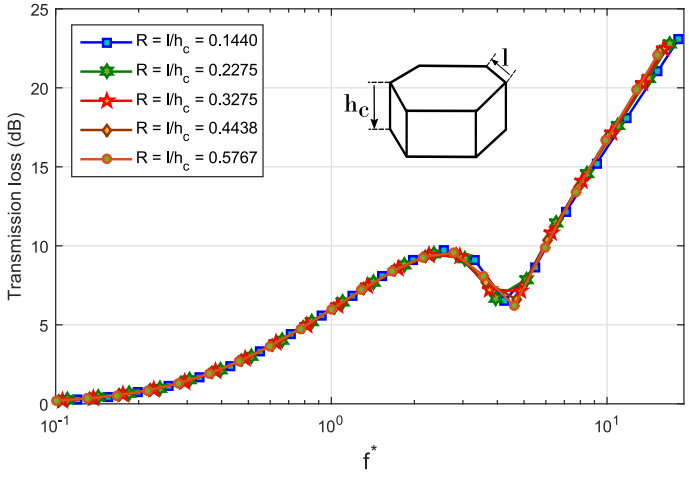

$R = l/h_c$	**Transition frequency** f_t	**Bending stiffness** D	**mass per unit area** ρ_s
0.1440	300.1 Hz	6082.2 $N.m$	4.01 kg/m^2
0.2275	288.1 Hz	4696.0 $N.m$	3.72 kg/m^2
0.3275	285.1 Hz	3681.1 $N.m$	3.55 kg/m^2
0.4438	270.2 Hz	3000.6 $N.m$	3.44 kg/m^2
0.5767	246.0 Hz	2486.5 $N.m$	3.37 kg/m^2

Figure 5.10: Effect of the panel thickness h_c and the angled member length l

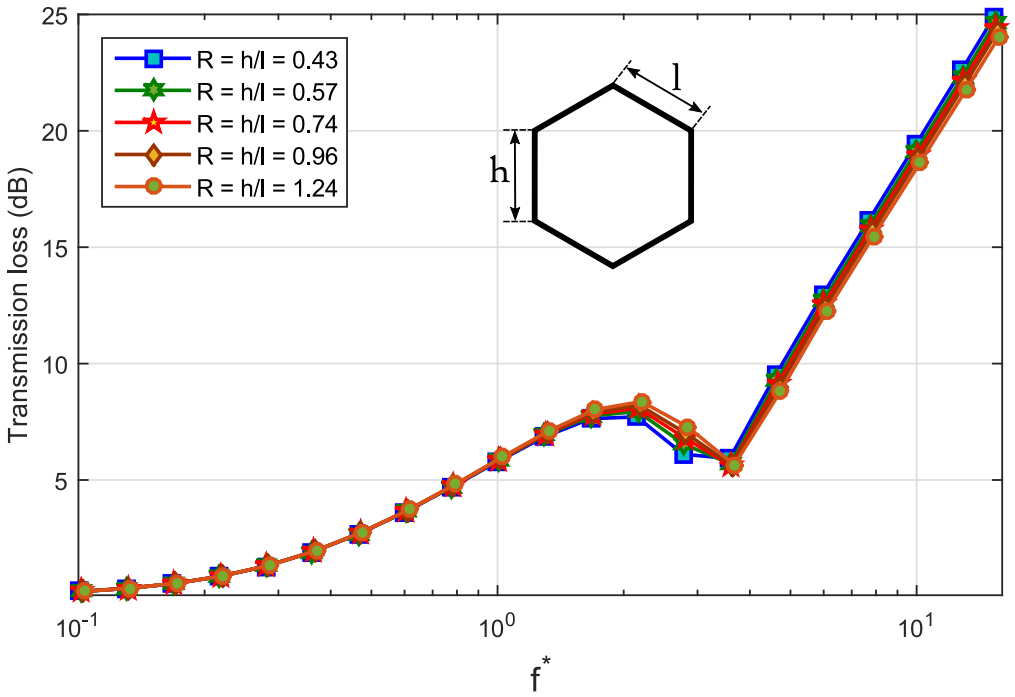

$R = h/l$	**Transition frequency** f_t	**Bending stiffness** D	**mass per unit area** ρ_s
0.4285	161.0 Hz	4735.5 $N.m$	3.38 kg/m^2
0.5702	184.2 Hz	4590.8 $N.m$	3.39 kg/m^2
0.7431	187.8 Hz	4606.9 $N.m$	3.41 kg/m^2
0.9587	177.3 Hz	4585.4 $N.m$	3.43 kg/m^2
1.2352	172.3 Hz	4548.3 $N.m$	3.46 kg/m^2

Figure 5.11: Effect of the vertical member length h and the angled member length l

On the other hand, the increase of the ratio $R = l/h_c$ in figure 5.10 has not led to any important improvement of the sound transmission loss. While it is shown that the equivalent bending stiffness D was dropped considerably.

The effect of the ratio $R = h/l$ on the transmission loss is presented in figure 5.11. The increase of the angled member length l (about 25%) with respect to the vertical member length h has led to a slight improvement on the TL indicator at the mid frequencies. Whilst there is a slight decrease of the equivalent bending stiffness D of the sandwich panel.

5.3.2 Other forms for the sandwich core

In the second subsection, other forms for the sandwich core were examined and compared with the hexagonal core. The topologies of the sandwich core presented in figure 5.13 were obtained by introducing other geometric core parameters as shown in figure 5.12.

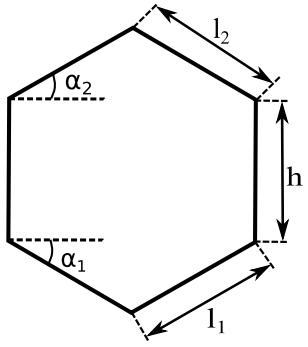

Figure 5.12: Geometric parameters of periodic unit cell of the sandwich panel

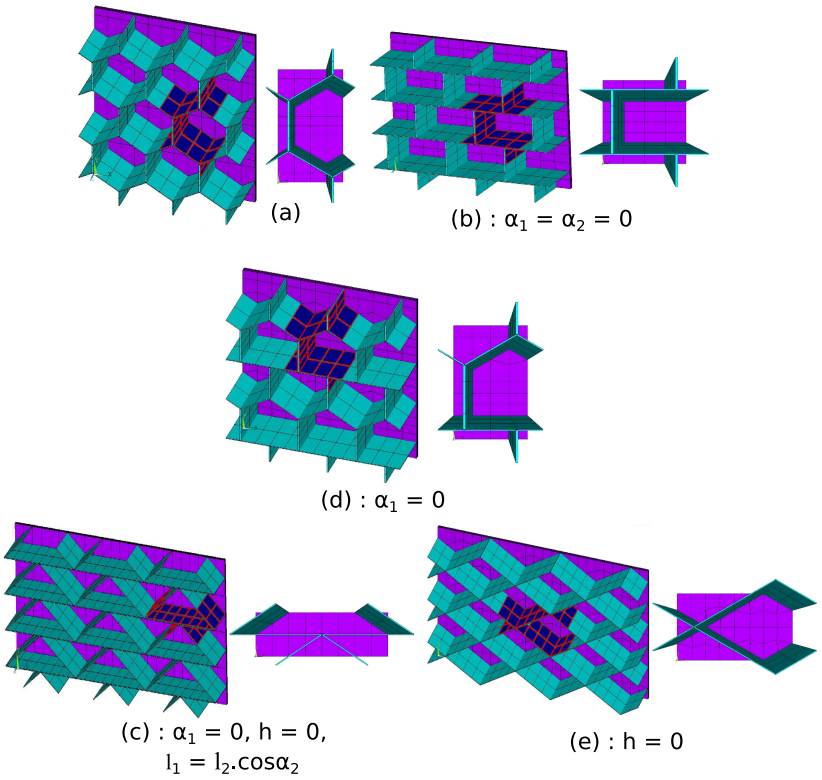

Figure 5.13: Studied core forms of the sandwich panels

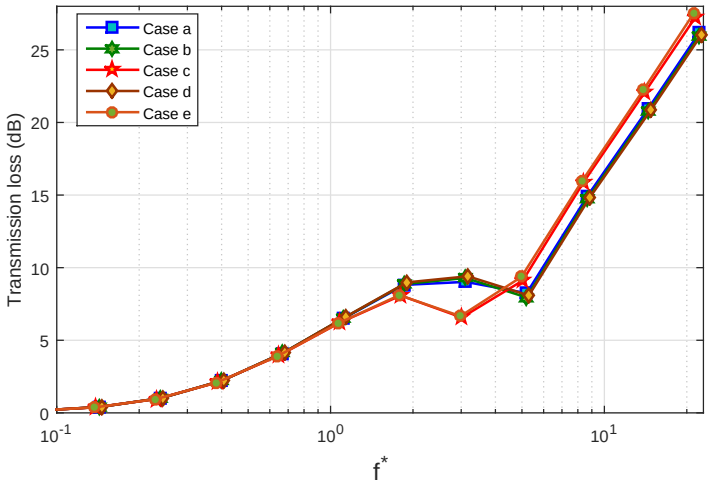

Cases	**Transition frequency** f_t	**Bending stiffness** D	**mass per unit area** ρ_s
a	280.9 Hz	4708.1 $N.m$	3.72 kg/m^2
b	274.9 Hz	4462.0 $N.m$	3.72 kg/m^2
c	092.1 Hz	4232.9 $N.m$	3.60 kg/m^2
d	344.0 Hz	4693.6 $N.m$	3.79 kg/m^2
e	139.3 Hz	4953.8 $N.m$	3.56 kg/m^2

Figure 5.14: Effect of changing topology for the unit cell on TL

Figure 5.14 presents the comparison in terms of TL for the different topologies presented in figure 5.13. According to figure 5.14, the best topologies among the presented cases in terms of TL are the cases a, b and d. On the other hand, the bending stiffness D of the sandwich panel remain approximately constant.

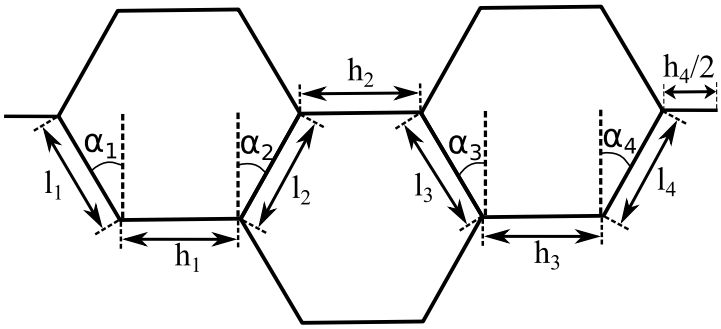

Figure 5.15: Studied core forms of the sandwich panels

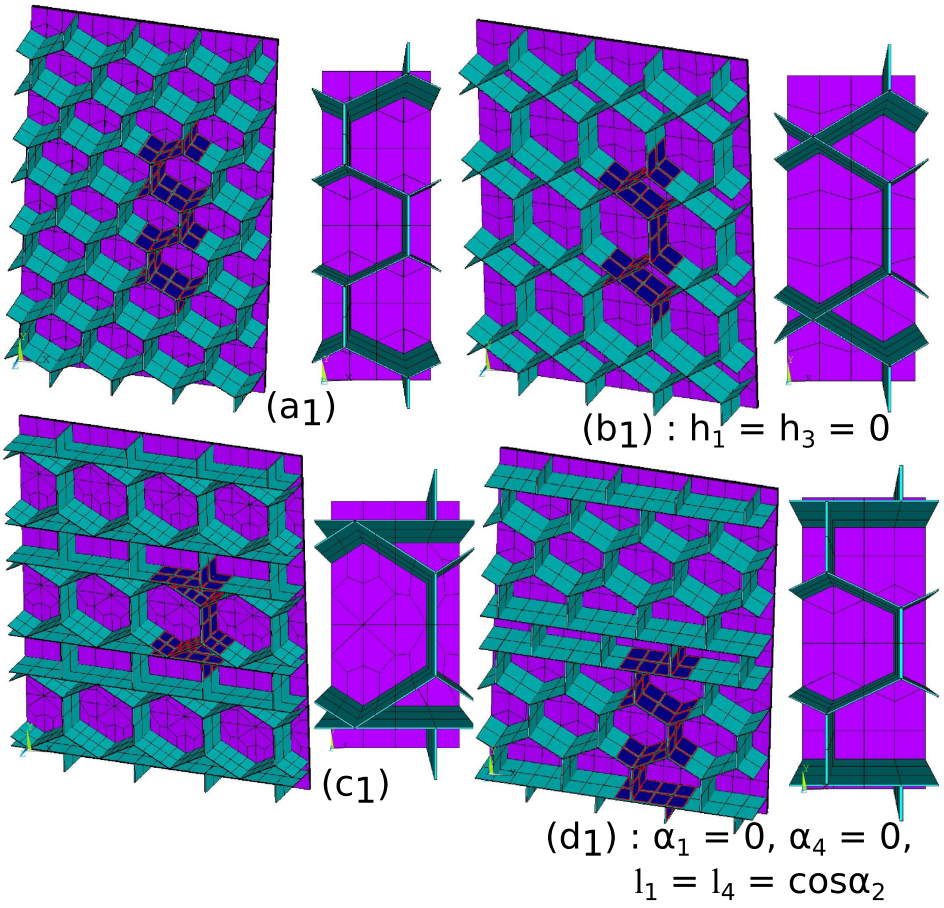

Figure 5.16: Studied core forms of the sandwich panels

In the second part of the second subsection, we tried to introduce more than one form in the unit periodic cell in order to compared them with the hexagonal core. The proposed topologies of the sandwich core presented in figure 5.16 were obtained by adding another geometric core parameters as shown in figure 5.15.

The comparison of the generated topologies presented in figure 5.16 is exhibited in figure 5.17. As shown in this figure, the preferred topologies among the presented cases in terms of TL are the cases a_1 and d_1 with a satisfactory bending stiffness D for the sandwich panel.

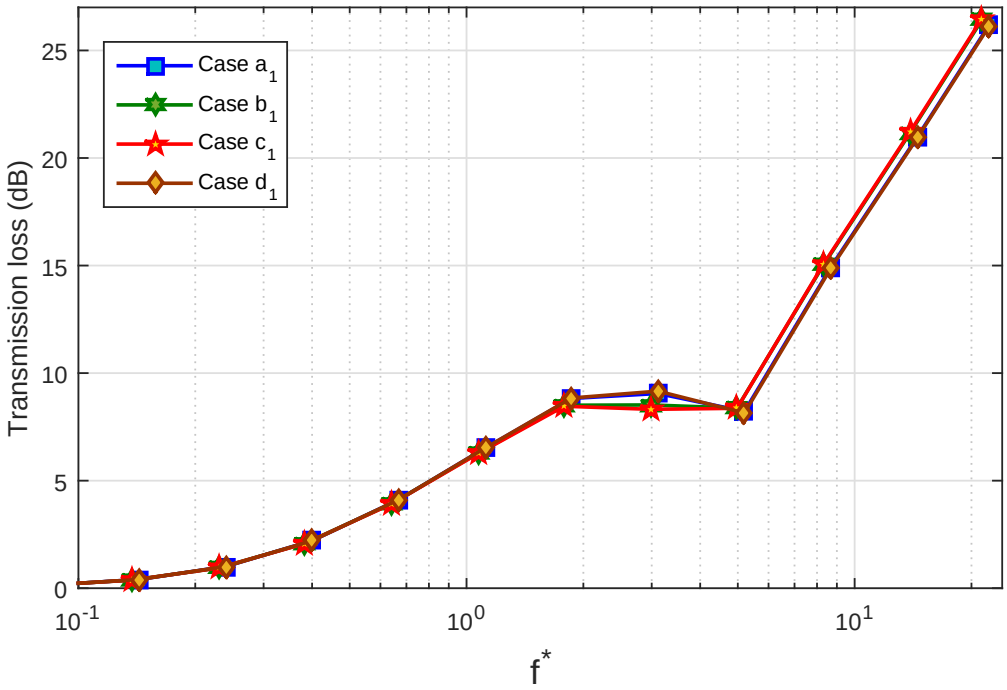

Cases	**Transition frequency** f_t	**Bending stiffness** D	**mass per unit area** ρ_s
a_1	282.0 Hz	4685.6 $N.m$	3.72 kg/m^2
b_1	297.5 Hz	4604.7 $N.m$	3.56 kg/m^2
c_1	211.5 Hz	4479.1 $N.m$	3.56 kg/m^2
d_1	321.6 Hz	4611.3 $N.m$	3.72 kg/m^2

Figure 5.17: Effect of introducing more than one form in the unit cell on TL.

5.4 Concluding remarks

A parametric analysis has been carried out to reveal the effect of the conventional geometric parameters of a sandwich panel on the sound transmission loss (TL) and on the transition frequency f_t and also to reveal the relationship between the two latter indicators. The numerical model was validated with two semi-analytical models (DLM and WSFE model) and a digitalized measurement result.

As conclusion, it is apparent through the previous parametric analysis that the cell angle α of the sandwich panel does not have any effect on the transmission loss. It is also shown that the increase of the panel thickness h_c lead to a significant improvement of the TL and an increase of the transition frequency f_t but also to a remarkable drop of the stiffness-weight ratio of the sandwich panel. Moreover, it is clearly observed that

increasing the angled member length l with respect to the vertical member length h can enhance the transmission loss in the mid frequency range. In addition, it is noticed that the increased transition frequency reflects generally an improvement on the sound transmission loss (TL) across the sandwich panel.

Ultimately, the two-scale approach developed herein might be introduced in a numerical optimization process which serves to identify the optimal geometrical parameters, either for a hexagonal cell or any other form cell, that can enhance the macro vibroacoustic responses for the sandwich panel. The optimization process, which can be the next project paper, allows to treat simultaneously all the geometric parameter combinations while considering the weight and stiffness constrains.

CHAPTER 6

EXPERIMENTAL SURVEY OF THE TRANSITION FREQUENCY FOR SANDWICH PANELS

Contents

THrough the current chapter, the Inhomogeneous Wave Correlation (IWC) technique developed by Berthaut et al. in [19] has been described in detail. Afterwords, the experimental test allows obtaining the harmonic displacement field of the sandwich panel with white noise excitation was presented. Then, the validation of the experimental wavenumber space obtained by the IWC technique has been checked. Finally, the identification of the modal density and the transition frequency of the test sandwich panels have been presented and compared.

6.1 Development of the IWC method

The inhomogeneous Wave Correlation (IWC) method proposed by Berthaut et al. [19, 30, 66, 67, 164] was developed to identify the dispersion characteristics of complex structures from experimental data. The IWC method is not only allow the determination of the k-space but is also able to identify the corresponding loss factor. The loss factor represents inhomogeneous wave parts which can be as mentioned in subsection 1.6.1.2, near fields induced by boundary conditions or sources. The key idea behind the IWC method is to calculate the correlation coefficient between the experimental wave field $\widehat{w}(\omega,x,y)$ and an inhomogeneous reference wave given as :

$$\widehat{o}_{(k,\gamma,\theta)}(x,y) = e^{-jk(\theta)(x\cos\theta+y\sin\theta)(1+j\gamma(\theta))}, \tag{6.1}$$

Lyon and Dejong [89] was expressed the relationship between the inhomogeneous wave attenuation γ and the classical damping loss factor η as the following:

$$\gamma = \frac{\eta c_\alpha}{2c_g}, \tag{6.2}$$

with c_α and c_g being respectively the phase and group velocities. The correlation between the inhomogeneous wave $\widehat{o}_{(k,\gamma,\theta)}$ and the complete wave field $\widehat{w}(\omega)$ on a surface area A is determined like a Modal Assurance Criterion (MAC) technique [49] which compares a measured mode shape with a predicted one, using the following expression:

$$IWC(\omega,k,\gamma,\theta) = \frac{\left|\iint_A \widehat{w}(\omega,x,y).\widehat{o}^*_{(k,\gamma,\theta)}(x,y)dxdy\right|}{\sqrt{\iint_A |\widehat{w}(\omega,x,y)|^2 dxdy.\iint_A \left|\widehat{o}_{(k,\gamma,\theta)}(x,y)\right|^2 dxdy}}, \tag{6.3}$$

with the subscript * stands for the complex conjugate. In practice, it is assumed that the displacement wave field $\widehat{w}(\omega,x,y)$ is known on arbitrary data points. The integration $\iint_A dxdy$ over the whole surface area A in equation 6.3 are replaced by a finite weighted sum $\sum_{i=1}^{n} \kappa^2_{M_0,M_i} A_i$:

$$IWC(\omega,k,\gamma,\theta) = \frac{\left|\sum_{i=1}^{n} \widehat{w}_i(\omega).\widehat{o}^*_{(k,\gamma,\theta),i}.\kappa^2_{M_0,M_i}A_i\right|}{\sqrt{\left(\sum_{i=1}^{n} |\widehat{w}(\omega)|^2.\kappa^2_{M_0,M_i}A_i\right)\left(\sum_{i=1}^{n}\left|\widehat{o}_{(k,\gamma,\theta)}\right|^2.\kappa^2_{M_0,M_i}A_i\right)}}, \tag{6.4}$$

with κ_{M_0,M_i} is the coherence coefficient between the measurement data at point M_j and the excitation point at M_0 (if the coherence coefficient is not available, it can be set to $\kappa_{M_0,M_i} = 1$) and A_i is the surface area around the point M_j. So, the dispersion characteristics of such structures can then be identified by determining the values k_i and γ_i at which the value of the IWC method is maximized for a given frequency ω and an angular direction θ.

6.2 Experimental set-up and post-processing

In addition to the geometrical and mechanical properties of the sandwich panel, the IWC technique needs additional input information in order to identify the wave propagation. The needed input information are the displacement field of the test sandwich panel which can be obtained by conducting experiments. There are different ways to obtain the requested information for the IWC technique either in terms of excitement, or measurement. As has been mensionned in reference [66, 68], the excitation can be made either by a loudspeaker or a shaker, while for the measurement, either a microphone or a laser vibrometer can be used.

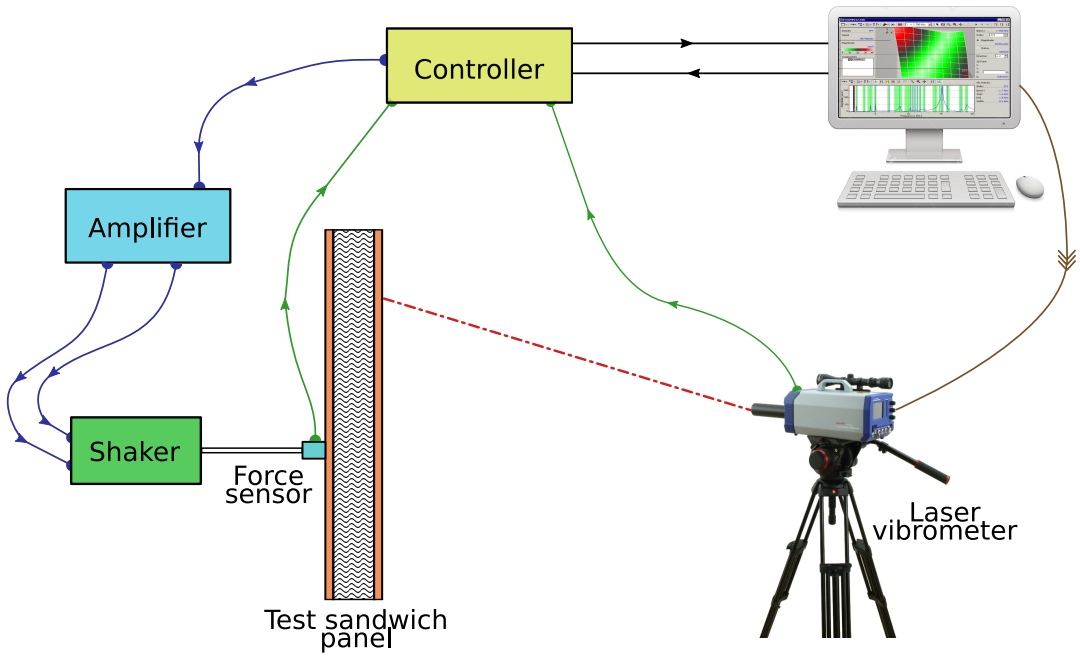

Figure 6.1: Schema of the experimental set-up.

The experimental set-up used in the present thesis framework is as the same as that used in reference [19], i.e. a shaker (Brüel & Kjaer type 4810) has been used as the excitation device and a laser vibrometer (Brüel & Kjaer type 8330) as the measurement device (see figure 6.1). The stated devices has several advantages as the author mentioned in [19]. The used shaker allows exciting the test sandwich panel at frequencies up to 3.2 kHz. Also, it allows controlling the quality of the generated force thanks to the force sensor (Brüel & Kjaer type 8001) placed between the shaker and the test sandwich panel (see figure 6.1). Similarly for the measurement, the used laser vibrometer allows measuring the displacement field without any direct contact with the test plate. In addition, the vibrometer allows the possibility for scanning automatically the whole of the measurement points, which can be very handy when the test has to be repeated several times or when the number of the measurement points is important.

Figure 6.2: Testbed realized to measure the displacement field of the sandwich panels.

The testbed used for the IWC technique (see figure 6.2) has also some disadvantages. First, it is impossible to identify the speeds beyond 3.2 kHz due to the cutoff frequency of the shaker. So to extend the frequency limit of the testbed, other excitation means is needed to be tested. Second, the position accuracy of the scanning doppler laser vibrometer is very low for the identification at high frequencies. To avoid this, it would

be better to use a fixed laser vibrometer and move it with a micrometer displacement system, however, this technique can be expensive to achieve.

6.3 Numerical and experimental investigations on the sandwich panels

The present section is devoted to study the characteristics of the wave propagation through two sandwich panels with different cell size. The dimensions of the two sandwich panels are summarized and given in table 6.1. Both of the sandwich panels have carbon epoxy (reference Hexcel 43199) as facesheet material with resin-fibre ratio of 50 % while the sandwich core material is Nida NOMEX.

	Panel A	**Panel B**
Surface area A	$1 \times 1\ m^2$	$1 \times 1{,}01\ m^2$
Core thickness h_c	$13\ mm$	$13\ mm$
Facesheet thickness h_f	$0.5\ mm$	$0.5\ mm$
Cell size	3,2	4,8

Table 6.1: Geometrical properties of the panel A and B.

The principle mechanical and geometric properties needed for treating the experimental data extracted from the experimental set-up presented in section 6.2 of the both sandwich panels A and B have been summarized in table 6.2. Also, additional information about the mesh measured points and the excitation position have been shown in figure 6.3.

	Panel A	**Panel B**
G_{xz}	$30e^{+06}\ Pa$	$28e^{+06}\ Pa$
G_{yz}	$40e^{+06}\ Pa$	$40e^{+06}\ Pa$
E_x	$141e^{+09}\ Pa$	$141e^{+09}\ Pa$
References	ECA-3.2-48 (51)	ECA-4.8-48 (51)

Table 6.2: Mechanical properties of the panel A and B.

In the next subsections, the experimental data and the available information about the sandwich panel A and B will be used in the code matlab to identify the k-space, the averaged wavenumber, the modal density and then the transition frequency.

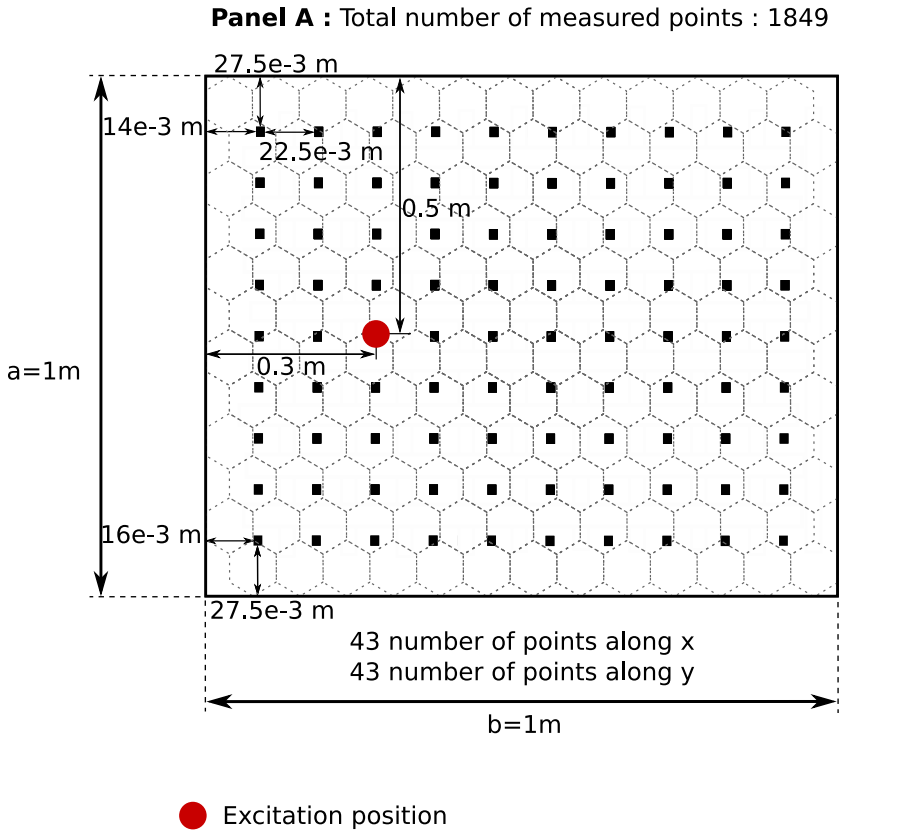

Figure 6.3: Mesh of the panels A and B.

6.3.1 Identification of the k-space

The dispersion results of the sandwich panel A and B obtained via the inhomogeneous Wave Correlation (IWC) method, presented in the previous sections, have been averaged using the following expression 6.5.

$$\langle k(\omega)\rangle = \frac{1}{2\pi}\int_{0}^{2\pi} k(\omega,\theta)\,d\theta, \tag{6.5}$$

in which $k(\omega)$ is an angular sampling of the wavenumber at defined frequency range. The angular sampling have to be well refined for the case of orthotropic or anisotropic structures. These kind of behavior structures can exhibit high directivity. So, figure 6.4 represents the averaged wavenumbers of the sandwich panels A and B obtained by the expression 6.5.

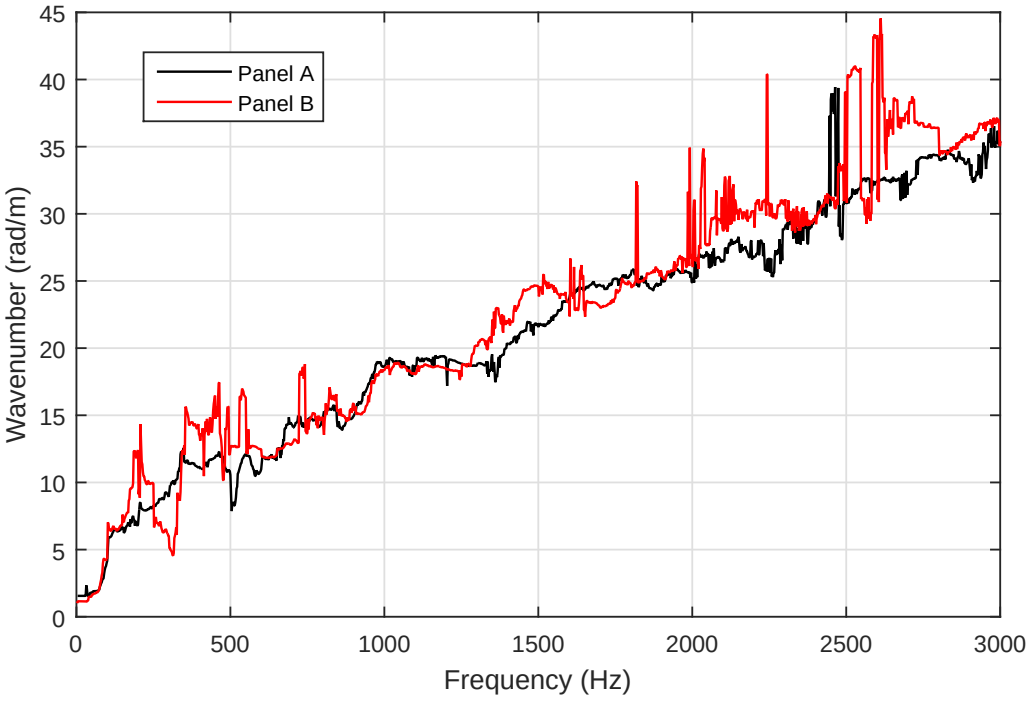

Figure 6.4: Dispersion curves for the panels A and B identifying by IWC.

6.3.2 Identification of the modal density

The angular distribution of the modal density of the sandwich panels A and B can be generally calculated in terms of the ratio of the structural wavenumber $k(\omega,\theta)$ and the

group velocity $c_g(\omega,\theta)$:

$$n(\omega,\theta) = \frac{A}{2\pi}\frac{k(\omega,\theta)}{|c_g(\omega,\theta)|}, \tag{6.6}$$

with A the surface area of the sandwich panel. $k(\omega,\theta)$ and $c_g(\omega,\theta)$ have been deduced from the experimental data treated by the IWC technique.

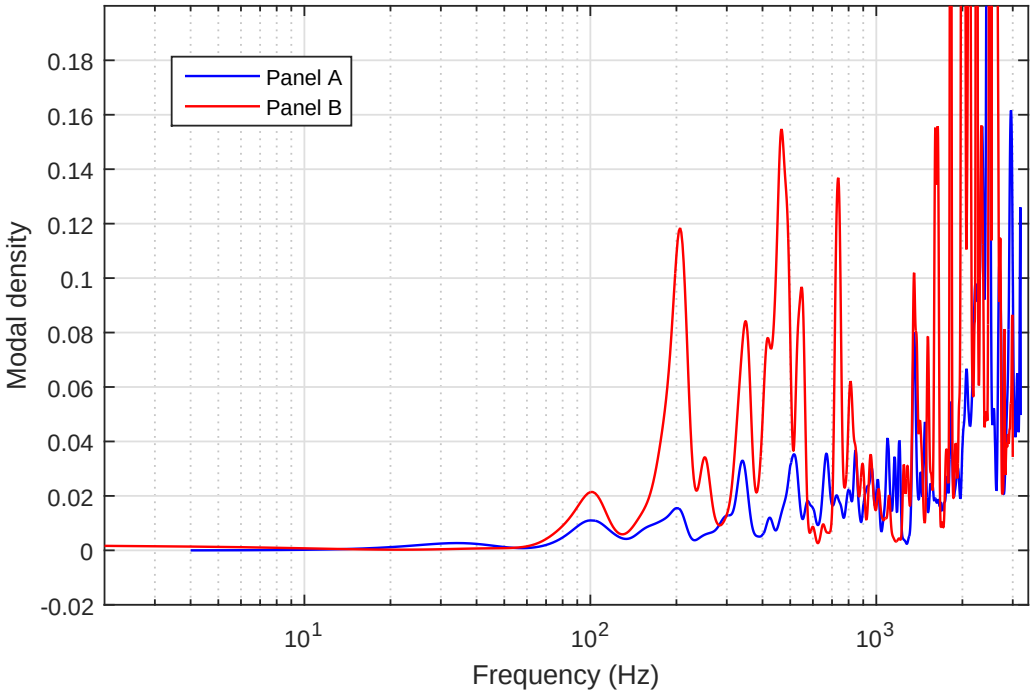

Figure 6.5: Modal density for the panels A and B identifying by IWC.

In general, there are two methods to calculate the modal density, whether we calculate it without the IWC treatment by counting the peaks in each 1/3 Octave Bands or using the previous formulation 6.6. The both techniques give approximately the same result.

6.3.3 Experimental identification of the transition frequency

The averaged wavenumbers of the sandwich panels A and B obtained in the previous sections have been readjusted by an analytical model for the sake of defining the equivalent bending and shear wavenumbers. The stated wavenumbers can then help to identify the transition frequency of the both sandwich panel.

	Equivalent shear rigidity S	**Equivalent bending stiffness D**	**Mass per unit area ρ_s**
Panel A	$5.32e^{+05}\ Pa$	$6.42e^{+03}\ N.m$	$1.93\ kg/m^2$
Panel B	$4.69e^{+05}\ Pa$	$6.42e^{+03}\ N.m$	$1.94\ kg/m^2$

Table 6.3: Equivalent mechanical properties of the panel A and B.

The analytical model used for the readjustment of the experimental results is the Guillaumie model [59]. The equivalent mechanical properties obtained have been given in table 6.3. The readjusted curves have obtained with prediction errors of 8% for the panel A and 10% for the panel B with respect to the experimental curves.

As shown in figures 6.6 and 6.7, The cell size change demonstrates clearly the core geometric effect on the transition frequency which has been already proof theoretically in chapters 3 and 5. The change lead to a gain of approximately 90 Hz in the transition frequency ($f_t^A = 760,21\ Hz$ and $f_t^B = 670,44\ Hz$).

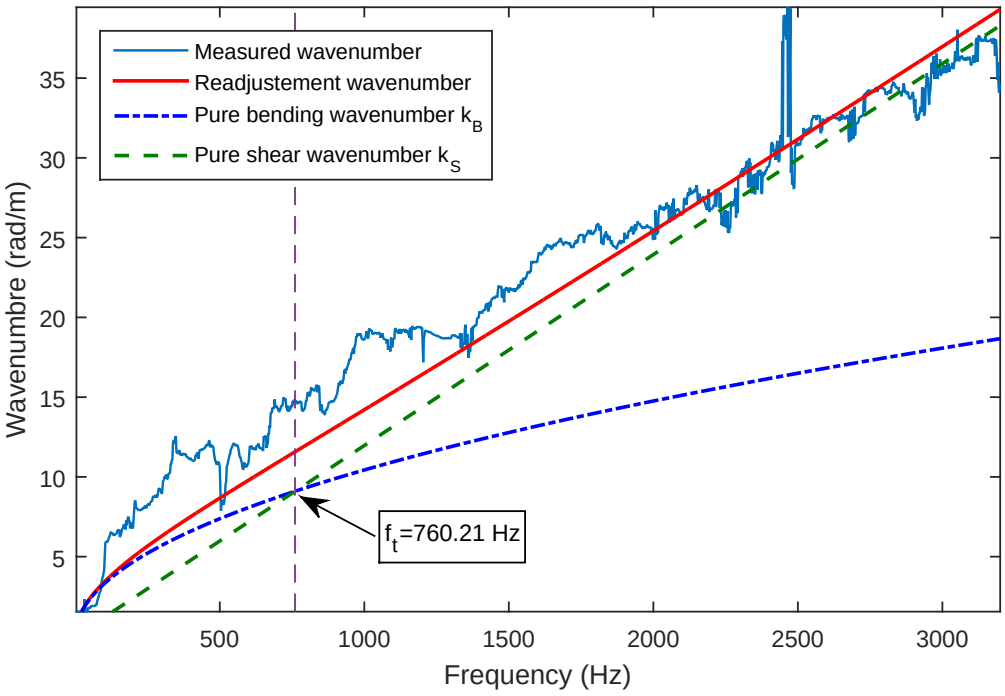

Figure 6.6: Identification of the transition frequency for the panel A.

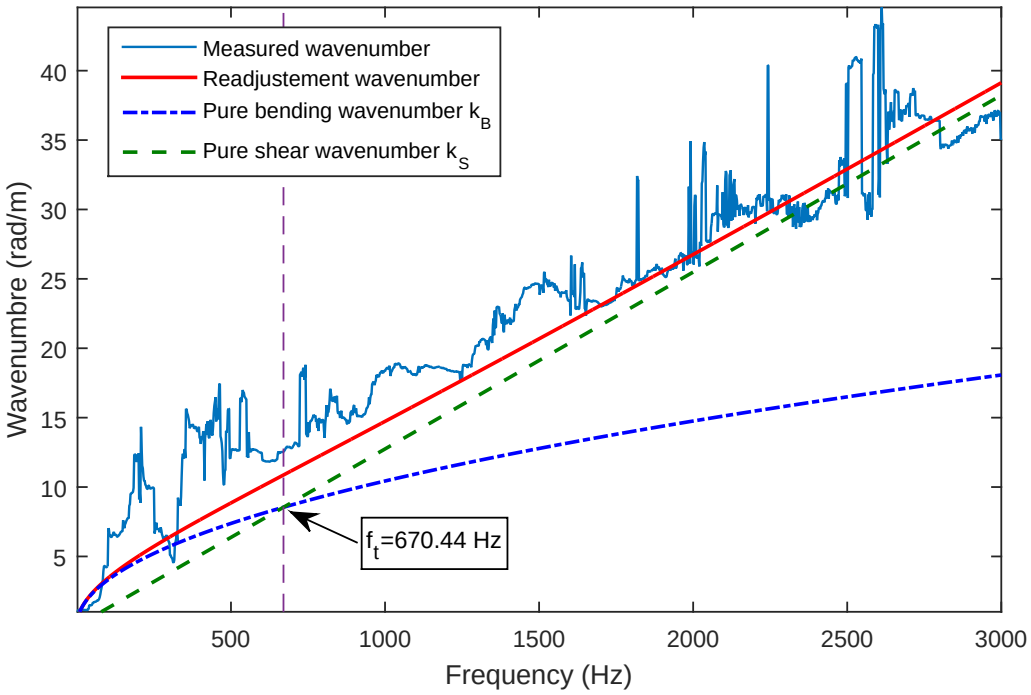

Figure 6.7: Identification of the transition frequency for the panel B.

6.4 Concluding remarks

In this chapter, the inhomogeneous Wave Correlation (IWC) method and its experimental set-up have been presented in detail. The latter experimental method was applied on two sandwich panels, A and B, with the same material for the core and facesheets while their cell sizes are different. The known mechanical properties and the averaged wavenumbers of the both sandwich panels have been introduced into a non-linear regression model in order to determine the asymptotic wavenumbers.

According to the obtained results, it is shown experimentally via the identified dispersion characteristics that the cell size of the honeycomb sandwich core has an effect on the transition frequency which confirms the results deduced from the parametric analysis established in chapter 5.

CHAPTER 7

NONLINEAR FREE VIBRATIONS OF C-C-SS-SS SYMMETRICALLY LAMINATED CARBON FIBER REINFORCED PLASTIC (CFRP) RECTANGULAR COMPOSITE PLATES

Contents

THe purpose of this chapter is to apply the theoretical model developed in references [15–17, 63–65] in order to analyze the geometrically nonlinear

free dynamic response of C-C-SS-SS rectangular CFRP symmetrically laminated plates so as to investigate the effect of non-linearity on the nonlinear resonance frequencies, the nonlinear fundamental mode shape and associated bending stress patterns at large vibration amplitudes. Various values of the plate aspect ratio and the amplitude of vibrations will be considered, and useful numerical data also are provided.

7.1 Introduction

The geometrically nonlinear vibration of structures is of continuing interest, due to the tendency to build more reliable structures, with high strength, high stiffness, and low weight such as composites. Such new materials have a more accentuated nonlinear behavior [15–17, 63–65], It is then necessary to develop new design concepts, taking into account the nonlinear behavior induced by large vibration amplitudes, which may occur for example in severe environments. The large displacement amplitudes induce geometrical nonlinearity that is mainly caused by the development of in-plane membrane stresses. In such cases, one of the basic assumptions of the linear vibration theory, i.e. small displacement amplitudes compared to the plate thickness is violated. Therefore, it is of crucial theoretical and practical interest, to develop new approaches which take into account the membrane stress effect, neglected in the classical treatment of plate vibrations. Even though the vibration of plates overall has interested researchers for a long time, the exact linear solutions are known only for the six cases having two opposite edges simply supported corresponding to a square plate or a rectangular plate [79, 80]. Also, as has been mentioned in the study made by Leissa in 1973 [80], it was pointed out that until 1954, when Warburton derived his formulae based on a single-term representation of the deflection shapes for the natural frequencies of plates with various boundary conditions, no solution, even approximate, was known for six boundary condition cases. The general accuracy of Warburtons formulae is discussed in references [79, 80].

A great deal of studies and a wide program of experimental work carried out by White and his co-workers [14, 18, 106, 150–155, 158] has been developed in order to understand the dynamic behavior of homogeneous and CFRP beams and plates. In Chias book [26], an extensive information is given on the nonlinear analysis of plates, with presentation of a variety of geometrically nonlinear static and dynamic problems. Also, a survey was presented of the literature on the geometrical nonlinear analysis of laminated composite elastic plates in reference [27]. In Sathyamoorthys work [128], a review

was presented which deals with analytical, numerical and experimental methods used in the geometrically nonlinear dynamic analysis of plates.

In recent published carried out by F. Alijani and M. Amabili [3, 4] in 2013, nonlinear vibrations of completely free laminated and sandwich rectangular plates are investigated using multimodal energy approach based on Lagrange equations and by using classical and higher-order shear deformation theories [119] with von Karman type nonlinearities [104].

In several engineering applications, large vibration amplitudes of plate-type structures are encountered especially in the aerospace sector. The plates are assumed to be whether fully or partially free, simply supported, or clamped. The clamped boundary conditions assume that both displacements and rotations are prevented. In exchange, the simply supported boundary conditions assume that displacements are al-lowed, but rotations are not. In practice, it is extremely hard to achieve both cases [2]. Because of the real plate boundaries are neither completely clamped nor simply supported. So, in most cases, the real boundary conditions are a combination of clamped, simply supported, or free conditions. As a real illustration example of combination boundary conditions, aircraft wing panels [140].

The purpose of this chapter is to apply the theoretical model developed in references [15, 16] in order to analyze the geometrically nonlinear free dynamic response of C-C-SS-SS rectangular CFRP symmetrically laminated plates so as to investigate the effect of non-linearity on the nonlinear resonance frequencies, the nonlinear fundamental mode shape and associated bending stress patterns at large vibration amplitudes. Various values of the plate aspect ratio and the amplitude of vibrations will be considered, and useful numerical data will be provided.

7.2 General formulation of the geometrically nonlinear free vibration of C-C-SS-SS symmetrically laminated rectangular composite plates

7.2.1 Constitutive equation at large deflections

Consider the transverse vibration W of the plate of dimensions a, b and H shown in figure 7.1 with a coordinate system taken such that the xy plane coincides with the mid-

plane of the plate.

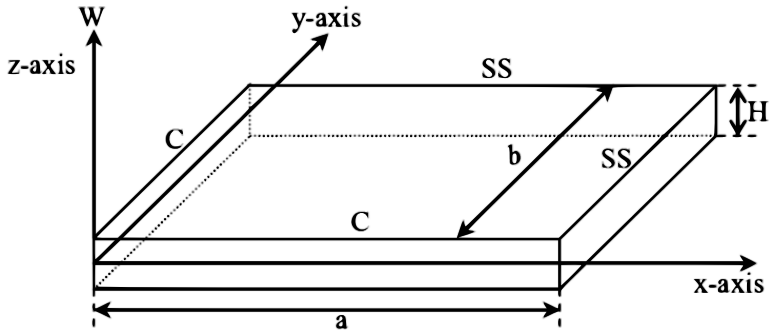

FIGURE 7.1. The plate notation.

The strain-displacement relationship for large deflections, considering the classical plate laminated theory [8], are given by the expression taken from the reference [141] which assume that the plate is thin (the thickness H is much smaller than the typical plate dimension, $H << a$, b) and the magnitude of the transverse deflection W is of the same order as the thickness of plate as well as the in-plane displacements U and V are a linear function of the z-coordinate :

$$\{\epsilon\} = \{\epsilon^0\} + z\{k\} + \{\lambda^0\} \tag{7.1}$$

Where $\{\epsilon^0\}$, $\{k\}$, and $\{\lambda^0\}$ are given by [15–17, 63, 64]:

$$\{\epsilon^0\} = \begin{pmatrix} \epsilon_x^0 \\ \epsilon_y^0 \\ \epsilon_z^0 \end{pmatrix} = \begin{pmatrix} \dfrac{\partial U}{\partial x} \\ \dfrac{\partial V}{\partial y} \\ \dfrac{\partial U}{\partial y} + \dfrac{\partial V}{\partial x} \end{pmatrix}, \quad \{k\} = \begin{pmatrix} k_x \\ k_y \\ k_{xy} \end{pmatrix} = \begin{pmatrix} \dfrac{-\partial^2 W}{\partial x^2} \\ \dfrac{-\partial^2 W}{\partial y^2} \\ \dfrac{\partial^2 W}{\partial xy} \end{pmatrix}, \quad and \quad \{\lambda\} = \begin{pmatrix} \lambda_x^0 \\ \lambda_y^0 \\ \lambda_z^0 \end{pmatrix} = \begin{pmatrix} \dfrac{1}{2}\left(\dfrac{\partial W}{\partial x}\right) \\ \dfrac{1}{2}\left(\dfrac{\partial W}{\partial y}\right) \\ \dfrac{\partial W}{\partial x}\dfrac{\partial W}{\partial y} \end{pmatrix}. \tag{7.2}$$

Where U, V, and W are the displacements of the plate mid-plane, in the x, y and z directions respectively. In the development of the nonlinear energy expression, the transverse displacement W of the plate mid-plane has been taken into consideration while the in-plane displacements U and V have been neglected. Therefore, the strain energy (eq. 7.3 and 7.4) of an elastic solid is written in Cartesian coordinates as follows [15–17, 63, 64]:

$$V_b = \frac{1}{2}\iint \left[D_{11}\left(\frac{\partial^2 W}{\partial x^2}\right)^2 + 2D_{12}\frac{\partial^2 W}{\partial x^2}\frac{\partial^2 W}{\partial y^2} + D_{22}\left(\frac{\partial^2 W}{\partial y^2}\right)^2 + 4D_{16}\frac{\partial^2 W}{\partial x^2}\frac{\partial^2 W}{\partial xy} + 4D_{26}\frac{\partial^2 W}{\partial x^2}\frac{\partial^2 W}{\partial xy} + 4D_{66}\left(\frac{\partial^2 W}{\partial xy}\right)^2 \right] dxdy . \tag{7.3}$$

$$V_a = \frac{1}{2}\iint \left[\frac{A_{11}}{4}\left(\frac{\partial W}{\partial x}\right)^4 + \frac{A_{22}}{4}\left(\frac{\partial W}{\partial y}\right)^4 + \left(\frac{A_{22}}{2} + A_{66}\right)\left(\frac{\partial W}{\partial y}\right)^2\left(\frac{\partial W}{\partial x}\right)^2 A_{16}\left(\frac{\partial W}{\partial x}\right)^3\frac{\partial W}{\partial y} + A_{26}\left(\frac{\partial W}{\partial y}\right)^3\frac{\partial W}{\partial x} \right] dxdy. \tag{7.4}$$

The kinetic energy of a structure may be written as [15–17, 63, 64]:

$$T = \frac{1}{2}\rho H \iint \left(\frac{\partial W}{\partial t}\right)^2 dxdy. \tag{7.5}$$

In which the in-plane and rotary inertia terms are neglected.

7.2.2 Numerical model for the nonlinear mode shapes and resonance frequencies of C-C-SS-SS rectangular CFRP symmetrically laminated plates

The transverse displacement function W may be written as in references [141, 142] in the form of a double series as follows:

$$W(x,y,t) = w(x,y)\sin\omega t = \sum_{i=1}^{N}\sum_{j=1}^{N} a_{ij} w_{ij}(x,y)\sin\omega t. \tag{7.6}$$

Where ij is the contribution coefficient of the function obtained as product of the i^{th} clamped simply-supported beam mode shape in the x-direction, with the jth clamped simply-supported beam mode shape in the y-direction for the case of CCSSSS rectangular plates, and vice versa.

The discretization of the strain and kinetic energy expressions (eq. 7.3, 7.4, 7.5) can be carried out leading to [15–17, 63, 64]:

$$\begin{cases} V_b = \dfrac{1}{2} a_i a_j k_{ij} \sin^2 \omega t, \\ V_a = \dfrac{1}{2} a_i a_j b_{ijkl} \sin^4 \omega t, \\ T = \dfrac{1}{2} a_i a_j \omega^2 m_{ij} \cos^2 \omega t. \end{cases} \tag{7.7}$$

Where m_{ij}, k_{ij}, and b_{ijkl} are respectively the mass tensor, the rigidity tensor and geometrical non-linearity tensor. The expressions for these tensors are defined as follows:

$$\begin{cases} m_{ij} = \rho H^5 a b m^*_{ij}, \\ k_{ij} = \dfrac{a H^5 E}{b^3} k^*_{ij}, \\ b_{ijkl} = \dfrac{a H^5 E}{b^3} b^*_{ijkl}. \end{cases} \tag{7.8}$$

Where the non-dimensional tensors m^*_{ij}, k^*_{ij}, and b^*_{ijkl} have the below form:

$$\mathrm{m^*_{ij}} = \iint \mathrm{w^*_i w^*_j dx^* dy^*} \tag{7.9}$$

$$\begin{aligned} k^*_{ij} = \iint \Bigg[& D^*_{11} \alpha^4 \left(\frac{\partial^2 w^*_i}{\partial x^{*2}} \frac{\partial^2 w^*_j}{\partial x^{*2}} \right) + D^*_{12} \alpha^2 \left(\frac{\partial^2 w^*_i}{\partial x^{*2}} \frac{\partial^2 w^*_j}{\partial y^{*2}} + \frac{\partial^2 w^*_i}{\partial y^{*2}} \frac{\partial^2 w^*_j}{\partial x^{*2}} \right) + D^*_{22} \left(\frac{\partial^2 W^*_i}{\partial y^{*2}} \frac{\partial^2 W^*_j}{\partial y^{*2}} \right) \\ & + 2 D^*_{16} \alpha^3 \left(\frac{\partial^2 w^*_i}{\partial x^{*2}} \frac{\partial^2 w^*_j}{\partial x^* y^*} + \frac{\partial^2 w^*_i}{\partial x^* y^*} \frac{\partial^2 w^*_j}{\partial x^{*2}} \right) + 2 D^*_{26} \alpha \left(\frac{\partial^2 w^*_i}{\partial y^{*2}} \frac{\partial^2 w^*_j}{\partial x^* y^*} + \frac{\partial^2 w^*_i}{\partial x^* y^*} \frac{\partial^2 w^*_j}{\partial y^{*2}} \right) \\ & + 4 D^*_{66} \alpha^2 \left(\frac{\partial^2 w^*_i}{\partial x^* y^*} \frac{\partial^2 w^*_j}{\partial x^* y^*} \right)^2 \Bigg] dx^* dy^*. \end{aligned} \tag{7.10}$$

$$\begin{aligned} b^*_{ijkl} = \iint \Bigg[& \frac{A^*_{11}}{4} \alpha^4 \left(\frac{\partial w^*_i}{\partial x^*} \frac{\partial w^*_j}{\partial x^*} \frac{\partial w^*_k}{\partial x^*} \frac{\partial w^*_l}{\partial x^*} \right) + \frac{A^*_{22}}{4} \left(\frac{\partial w^*_i}{\partial y^*} \frac{\partial w^*_j}{\partial y^*} \frac{\partial w^*_k}{\partial y^*} \frac{\partial w^*_l}{\partial y^*} \right) + \left(\frac{A^*_{12}}{4} + \frac{A^*_{66}}{2} \right) \alpha^2 \\ & \left\{ \left(\frac{\partial w^*_i}{\partial y^*} \frac{\partial w^*_j}{\partial y^*} \frac{\partial w^*_k}{\partial x^*} \frac{\partial w^*_l}{\partial x^*} \right) + \left(\frac{\partial w^*_i}{\partial x^*} \frac{\partial w^*_j}{\partial x^*} \frac{\partial w^*_k}{\partial y^*} \frac{\partial w^*_l}{\partial y^*} \right) \right\} + \frac{A^*_{16}}{2} \alpha^3 \left\{ \left(\frac{\partial w^*_i}{\partial x^*} \frac{\partial w^*_j}{\partial x^*} \frac{\partial w^*_k}{\partial x^*} \frac{\partial w^*_l}{\partial y^*} \right) \right. \\ & \left. + \left(\frac{\partial w^*_i}{\partial x^*} \frac{\partial w^*_j}{\partial x^*} \frac{\partial w^*_k}{\partial y^*} \frac{\partial w^*_l}{\partial x^*} \right) \right\} + \frac{A^*_{26}}{2} \alpha \left\{ \left(\frac{\partial w^*_i}{\partial x^*} \frac{\partial w^*_j}{\partial y^*} \frac{\partial w^*_k}{\partial y^*} \frac{\partial w^*_l}{\partial y^*} \right) + \left(\frac{\partial w^*_i}{\partial y^*} \frac{\partial w^*_j}{\partial x^*} \frac{\partial w^*_k}{\partial y^*} \frac{\partial w^*_l}{\partial y^*} \right) \right\} \Bigg] dx dy \end{aligned} \tag{7.11}$$

Applying Hamiltons principle to the vibration problem gives:

$$3 a_i a_j a_k b^*_{ijkr} + 2 a_i k^*_{ir} - 2 \omega^* 2 a_i m^*_{ir} = 0, \quad r = 1, \ldots, n. \tag{7.12}$$

In matrix form, the above expression (18) is rewritten as the following form:

$$3\left[B^*(A)\right]\{A\}+2\left[K^*\right]\{A\}-2\omega^*2\left[M^*\right]\{A\}=\{0\}, \tag{7.13}$$

where ω^* is the non-dimensional nonlinear frequency parameter, the expression of which can be obtained by pre-multiplying equation (7.12) by $[A]^T$ from the left-hand side, which leads to the following equation:

$$\omega^{*2}=\frac{a_i a_j k^*_{ij}+\frac{3}{2}a_i a_j a_k a_l b^*_{ijkl}}{a_i a_j m^*_{ij}} \tag{7.14}$$

The set of nonlinear algebraic equations (7.14), in which the parameters b^*_{ijkl}, k^*_{ij} and m^*_{ij} were computed numerically by using Simpsons rule, has been solved numerically by using the Harwell library routine NS01A. This routine is based on a hybrid method combining the steepest descent and Newtons methods, to obtain the numerical results presented for the first nonlinear mode of a C-C-SS-SS anisotropic rectangular plate.

7.3 Applications to C-C-SS-SS rectangular laminated CFRP composite panels

The following table 1 shows the geometric and material properties of the CFRP rectangular composite plates, they have been taken from the reference [46], which are treated here in this work.

In the present work, the set of admissible functions concerning C-C-SS-SS anisotropic rectangular plates are obtained as products of linear clamped simply-supported beam mode shapes in the x- and y-directions beam functions, corresponding to clamped clamped end conditions have been used and shown to be ap-propriate in previous studies on linear and nonlinear vibrations [17, 64].

Number of layers	**Orientation of principal axes**	**a (mm)**	**b (mm)**	**H (mm)**
8	$[90,45,-45,0]_S$	480	320	1
$E_x(Gpa)$	$E_y(Gpa)$	$G_{xy}(Gpa)$	vxy	$\rho(kg/m^3)$
120.5	9.63	3.58	0.32	1540

Table 7.1: Geometric and material properties of the rectangular plate.

The beam functions used, whose analytical expressions are given in Appendix, in the present work satisfy all of the C-C-SS-SS theoretical boundary conditions, i.e. zero displacement along the four edges, zero slope along the two clamped edges, and zero moment with respect to x and y along the two simply sup-ported edges.

7.3.1 Linear analysis

In order to verify the accuracy of the results obtained in the present work corresponding to the C-C-SS-SS rectangular plate, we will compare the solution of the equation (7.15), that is considered as an eigenproblem which will be solved by using MATLAB software, with the previous published results.

$$a_j k^*_{ir} = a_i \omega^* 2 m^*_{ir}, \qquad r = 1, \ldots, n. \tag{7.15}$$

The calculation was made by using 36 basic functions obtained as products of the first six clamped simply-supported beam functions, leading to square mass and rigidity matrices of dimension 25.

	Aspect ratio α				
	0.4	**0.5**	**0.667**	**1.0**	**1.5**
ω^*_l	9.12141	11.462242	17.89957	46.447142	166.25531
ω^*_{nl} ($a_{11} = 0.001$)	9.121334	11.462156	17.89945	46.446766	166.25356
ω^*_{nl} ($a_{11} = 0.15$)	9.8864237	12.339166	19.123762	49.411693	176.96215

Table 7.2: Comparison of non-dimensional frequency parameters.

In the table 7.2, the nonlinear frequency parameters obtained from the nonlinear analysis at too small vibration amplitudes ($a_{11} = 0.001$ and 0.15) corresponding to various values of the plate aspect ratio, are com-pared with results obtained from linear analysis. Consequently, the results are showing the convergence of the nonlinear model to the linear approach at very small vibration amplitudes.

7.3.2 Nonlinear analysis

Table 7.3 listed the summary of the first nonlinear mode shape of C-C-SS-SS rectangular plate corresponding to $\alpha = 0.667$ for $a_{11} = 0.001$ and 0.15, which are calculated here using 25 basic functions.

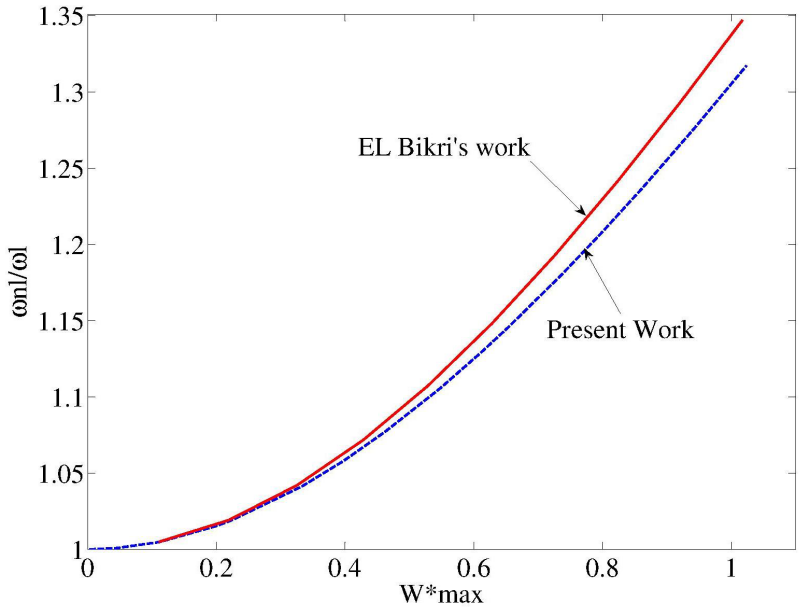

FIGURE 7.2. Comparison of the nonlinear frequency parameters of the first nonlinear mode of C-C-SS-SS rectangular plate, — present work, - - - with the linear value taken from [46] corresponding to $\alpha = 0.4$.

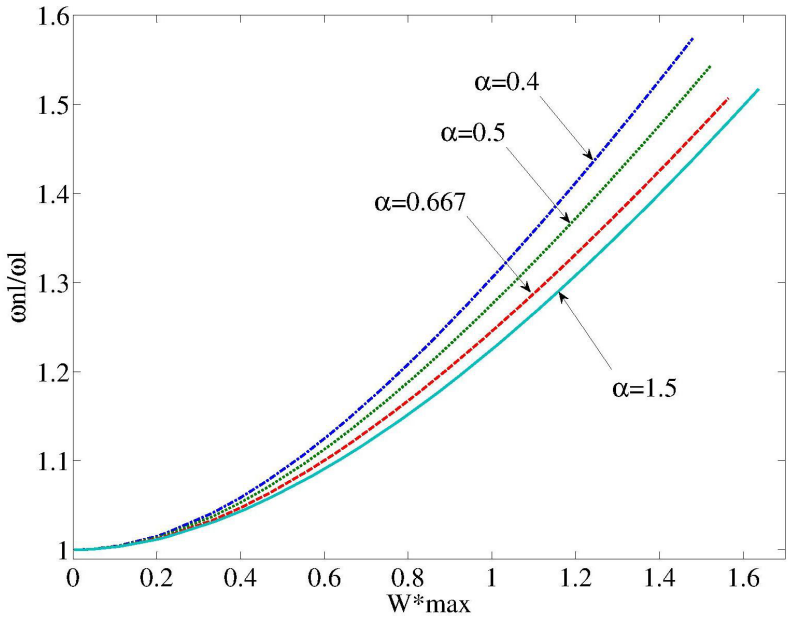

FIGURE 7.3. Comparison of the change frequency of the first mode for $\alpha = 0.4$, 0.5, 0.667, and 1.5.

The comparison in term of quality that is done in the figure 7.2 of the nonlinear frequency parameters of the first nonlinear mode, between the results obtained here and those are obtained in the reference [46] for an isotropic square plate at the similar boundary conditions showed that the curved continuous line of El Bikris work increases speedily more than the curved dashed one of present work. On the other hand, the comparison done with Work of B. Harras et al. in figure 7.4 showed that the fully clamped anisotropic rectangular plate exhibits less non-linearity than the case of the present work.

		$W_{max} = 0.11173319E-01$	$W_{max} = 0.26809814$
	(a) $\omega_l^* = 17.89957$	(b) $\omega_{nl}^* = 17.89945$	(c) $\omega_{nl}^* = 19.123762$
a_{11}	1	0.001	0.15
a_{12}	0.034640933	0.34693649E-04	0.71160884E-02
a_{13}	0.007849452	0.78612035E-05	0.10368977E-02
a_{14}	0.002492575	0.24964054E-05	0.61552283E-03
a_{15}	0.000990265	0.99177280E-06	0.21810887E-03
a_{21}	0.040354981	0.40415664E-04	0.62294442E-02
a_{22}	-0.001785123	-0.17877778E-05	-0.14783568E-03
a_{23}	-0.001032162	-0.10337164E-05	-0.14807638E-03
a_{24}	-0.000468162	-0.46886538E-06	-0.63046742E-04
a_{25}	-0.00021805	-0.21837845E-06	-0.32070459E-04
a_{31}	0.009393579	0.94078473E-05	0.18552141E-02
a_{32}	-0.001170972	-0.11727421E-05	-0.18827547E-03
a_{33}	-0.000763724	-0.76482717E-06	0.33978506E-04
a_{34}	-0.000396506	-0.39711893E-06	-0.10327654E-03
a_{35}	-0.000203788	-0.20409761E-06	-0.44565495E-04
a_{41}	0.003032144	0.30366964E-05	0.42418279E-03
a_{42}	-0.000565483	-0.56632875E-06	-0.67252538E-04
a_{43}	-0.000425984	-0.42663248E-06	-0.87193658E-04
a_{44}	-0.000250132	-0.25050635E-06	-0.31356367E-04
a_{45}	-0.000140975	-0.14118626E-06	-0.19236005E-04
a_{51}	0.001214007	0.12158334E-05	0.18055087E-03
a_{52}	-0.000273669	-0.27407930E-06	-0.34861000E-04
a_{53}	-0.000229392	-0.22973835E-06	-0.36839827E-04
a_{54}	-0.000148152	-0.14837451E-06	-0.21774339E-04
a_{55}	-9.01E-05	-0.90258064E-07	-0.13305140E-04

(a) Linear results calculated here; (b) present results obtained from nonlinear analysis for $a_{11} = 0.001$; (c) present results obtained from nonlinear analysis for $a_{11} = 0.15$

Table 7.3: Comparison of non-dimensional frequency parameters using 25 basic functions.

In the figure 7.3 are plotted the nonlinear frequency on the maximum non-dimensional

amplitude for the first nonlinear mode shape of C-C-SS-SS rectangular plate for various values of the plate aspect ratio. All curves are similar to that mentioned in reference [46, 64].

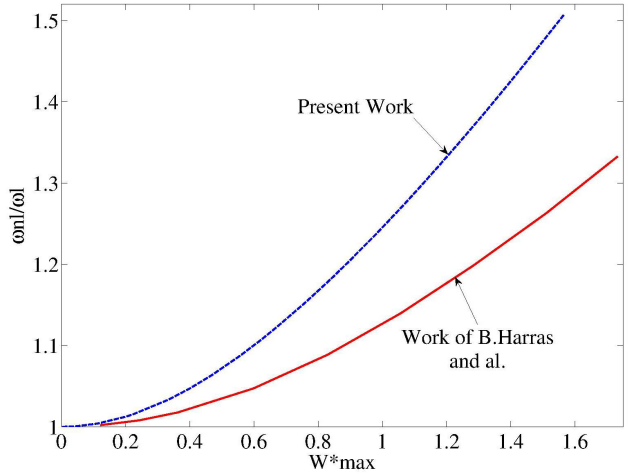

FIGURE 7.4. Comparison of the nonlinear frequency parameters of the first nonlinear mode with anisotropic fully clamped rectangular plate [64] corresponding to $\alpha = 0.667$.

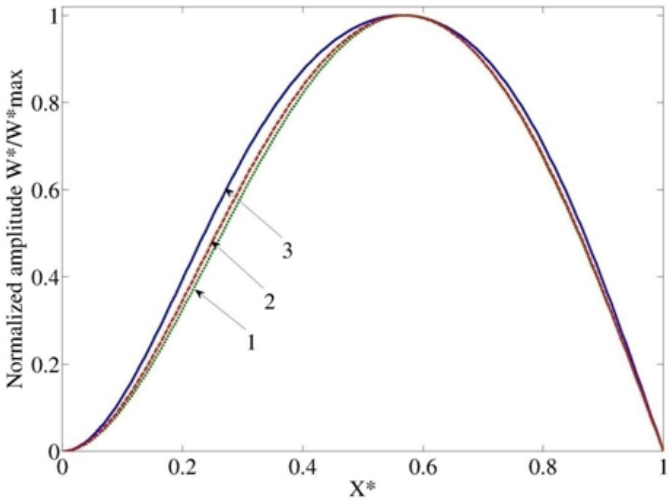

FIGURE 7.5. Normalized first nonlinear mode of a C-C-SS-SS rectangular plate corresponding to X^*_{max} and $\alpha = 1.0$. Curve 1, lowest amplitude ; Curve 3, highest amplitude.

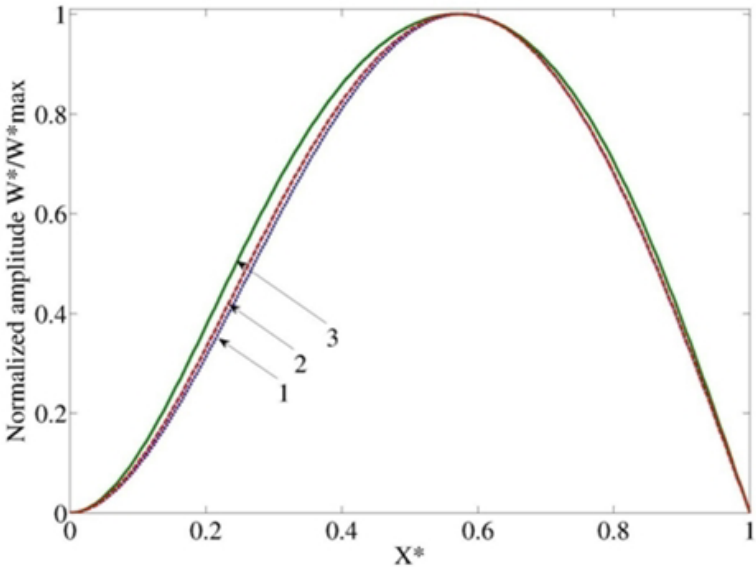

FIGURE 7.6. Normalized first nonlinear mode of a C-C-SS-SS rectangular plate corresponding to X^*_{max} and $\alpha = 1.5$. Curve 1, lowest amplitude ; Curve 3, highest amplitude.

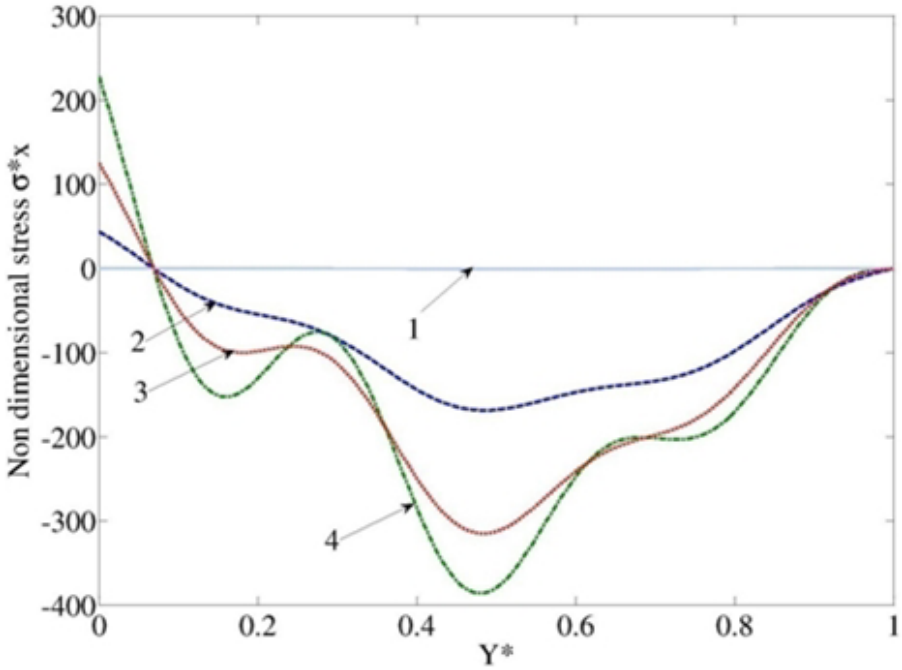

FIGURE 7.7. Non-dimensional bending stress distribution associated with C-C-SS-SS rectangular plate first nonlinear mode along $Y^* = 0.5$ for $\alpha = 0.667$. Curve 1, lowest amplitude ; Curve 4 highest amplitude.

The curves in figures 7.5 and 7.6, obtained via the present model, are plotted respectively for the values of the maximum non-dimensional amplitudes $W^*_{max}(\alpha = 1.0) = 0.22321327E{-}02, 1.3602697, 2.5601464$, and $W^*_{max}(\alpha = 1.5) = 0.22250147E{-}02, 1.3861804, 2.6043763$ along the y-direction of the nonlinear fundamental mode shape of a rectangular plate ($\alpha = 1.0$ and 0.5) corresponding to X^*_{max}. They show that the amplitude of the nonlinear mode shape and an increase of curvatures near to the clamped edges, on the other hand no changes concerning the simply supported ones, thereby, we suppose that the flexural stresses will increase non-linearly near to the clamped edges accompanying increase of the vibration amplitudes.

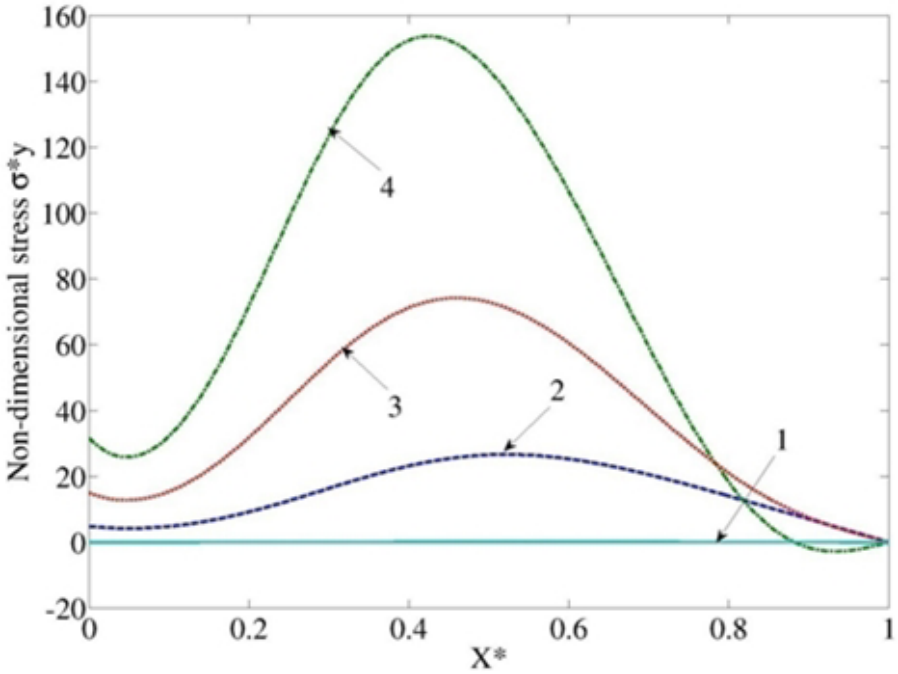

FIGURE 7.8. Non-dimensional bending stress distribution associated with C-C-SS-SS rectangular plate first nonlinear mode along $Y^* = 0.25$ for $\alpha = 0.667$. Curve 1, lowest amplitude ; Curve 4 highest amplitude.

The figures 7.7 and 7.8 represent the non-dimensional flexural stress distributions associated to the first non-linear mode shape of a C-C-SS-SS rectangular plate, which show the effect of large vibration amplitudes along the x and y directions, corresponding to $Y^* = 0.5$ and $X^* = 0.25$ for $\alpha = 0.667$. Besides, all curves show that the flexural stress is equal to zero close to the edge where the rectangular plate is simply supported, but on the other side the flexural stress exhibit a higher increase which has been proved in the linear vibration approach.

7.4 Concluding remarks

The nonlinear free vibrations of C-C-SS-SS rectangular symmetrically laminated plates are studied in this chapter using a theoretical model developed previously in references [63–65] for geometrically non-linear free vibrations of thin elastic structures. The objective was to determine the effects of large vibration amplitudes on the first mode shape, the fundamental natural frequency, and the associated flexural stress distribution. The model, based on Hamiltons principle, reduces the nonlinear free vibration problem to solution of a set of nonlinear algebraic equations involving the classical rigidity, mass tensors and a fourth order tensor due to the geometrical non-linearity.

The study of the first nonlinear mode shape for the CFRP plates considered has shown that the curvature near the edge increases very rapidly with increase of the vibration amplitude. In addition, the mode shape close to the center of the plate becomes flatter when the mode amplitude increases as well as it was also noticed that the deformation of the mode shape, for a given value of the normalized amplitude of vibration, increases as the aspect ratio α increases. The non-dimensional bending stress distribution associated with the CFRP rectangular plate first nonlinear mode shows an increase with increasing a_{11} which is much higher than that obtained for a linear vibration for CFRP plates of identical aspect ratio. As a consequence of the deformation of the mode shape, it was shown that the rate of increase in the induced bending stresses in a region close to the clamped edges. Furthermore, the non-dimensional bending stress distribution associated with the CFRP rectangular plate first nonlinear mode for different amplitudes of vibration show a non-symmetry along the length of the section considered because of the influence of the fiber orientation. It is worth noting here that further investigations are needed in order to check the distribution of the nonlinear bending stresses obtained at very high amplitudes of vibration.

At last, this present work enabled us to find out how the thin elastic structures behave at the large vibration amplitude by plotting different spectrum analysis. In addition, as far as quality is concerned, the comparison has been done with the results of an isotropic rectangular plate at the similar boundary conditions obtained in reference [46] and which of anisotropic rectangular plate obtained in reference [64] showed good and satisfactory results.

NOMENCLATURE:

$\{\varepsilon\}$	Column matrix of total strains
$\{\varepsilon^0\}$	Column matrix of strains due to the in-plane displacements u, v, w
x, y, z	Point co-ordinates
$\{K\}$	Column matrix of bending or twisting
$\{\lambda^0\}$	Column matrix of strains induced by large displacements W
ε_x, ε_y, γ_{xy}	Tensor strain components
$\sigma_x^{(k)}$, $\sigma_y^{(k)}$, $\sigma_{xy}^{(k)}$	Stresses in the k_{th} layer
$[\bar{Q}]$	6x6 matrix of transformed stiffness
$[\bar{Q}]_k$	6x6 matrix of transformed stiffness for the k_{th} layer
$N_x^{(k)}$, $N_y^{(k)}$, $N_{x,y}^{(k)}$	Force resultant for the k_{th} layer
$M_x^{(k)}$, $M_y^{(k)}$, $M_{x,y}^{(k)}$	Moment resultant for the k_{th} layer
h_k	Distance from the mid-plane to the layer surface of the k_{th} layer
A_{ij}, B_{ij}, D_{ij}	Extensional, coupling and bending stiffness coefficients for the laminated plate
${A_{ij}}^*$, ${D_{ij}}^*$	Non-dimensional extensional and bending stiffness coefficients
$\{A_k\}^T$	Matrix of coefficients corresponding to the k_{th} harmonic
$\{W\}^T$	Basic spatial functions matrix
a_{ij}	Contribution coefficient of the plate deflection function as a product of the i_{th} and j_{th} beam mode shapes in the x and y directions respectively
a, b	Length, width of the plate
E	Young's modulus
H	Plate thickness
K_{ij}, m_{ij}, b_{ijkl}	General term of the rigidity tensor, the mass tensor and the non-linearity tensor respectively
${K_{ij}}^*$, ${m_{ij}}^*$, ${b_{ijkl}}^*$	General term of the non-dimensional rigidity tensor, mass tensor and non-linearity tensor respectively
U(x, y, t), V(x, y, t)	In-plane displacements at point (x, y) of the plate
V_b, V_a and V	Bending, axial and total strain energy respectively
T	Kinetic energy
W(x, y, t)	Transverse displacement at point x on the plate
$W^*(x, y, t)$	Non-dimensional transverse displacement at point x on the plate
W^*_{max}	Maximum of the non-dimensional transverse displacement
α	Non-dimensional parameter (aspect ratio) given by $\alpha = b/a$

ν_{xy}	Major Poisson's ratio
E_x	Longitudinal modulus
E_y	Transverse modulus
G_{xy}	Shear modulus
ρ	Mass density per unit volume of the plate
ω, ω^*	Frequency and non-dimensional frequency parameter respectively
ω_l, ω_{nl}	Linear frequency and non-linear frequency respectively
σ_{xy}, σ_{yx}	Dimensional bending stresses
${\sigma_{xy}}^*, {\sigma_{yx}}^*$	Non-dimensional bending stresses

The clamped simply-supported beam functions $P_i^*(x)$ are defined as follows:

$$P_i^*(x) = \left[\cos\left(\frac{\lambda_i x}{a}\right) - \cosh\left(\frac{\lambda_i x}{a}\right)\right] - \gamma_i \left[\sin\left(\frac{\lambda_i x}{a}\right) - \sinh\left(\frac{\lambda_i x}{a}\right)\right], \tag{7.16}$$

where

$$\gamma_i = \frac{ch(\lambda_i) - \cos(\lambda_i)}{sh(\lambda_i) - \sin(\lambda_i)}, \tag{7.17}$$

In which λ_i for $i = 1,2,\ldots$ are the eigenvalue parameters for a clamped simply-supported beam. Besides the values of the parameters λ_i were computed solving numerically the transcendental equation $\tanh\lambda_i - \tan\lambda_i = 0$ by using Newtons method.

$$w_i^* = \frac{1}{G} P_{\alpha i}^*\left(x^*\right) P_{\beta i}^*(x), \tag{7.18}$$

where

$$x^* = \frac{x}{a} \ , \ y^* = \frac{y}{b} \ , \ w_i^*\left(x^*, y^*\right) = \frac{w_i}{H(x^*, y^*)}.$$

G is a normalization scaling factor given by:

$$G = \sqrt{\iint \left(X_{\alpha i}^*(x^*) Y_{\beta i}^*(x)\right)^2 dx^* dy^*}. \tag{7.19}$$

i	λ_i	i	λ_i
1	3.926990817	9	29.059732046
2	7.068583471	10	32.201324700
3	10.210176124	11	35.342917353
4	13.351768778	12	38.484510006
5	16.493361431	13	41.626102660
6	19.634954085	14	44.767695314
7	22.776546739	15	47.909287967
8	25.918139392	16	51.050880621

Table 7.4: The eigenvalue parameters for a C-C-SS-SS beam.

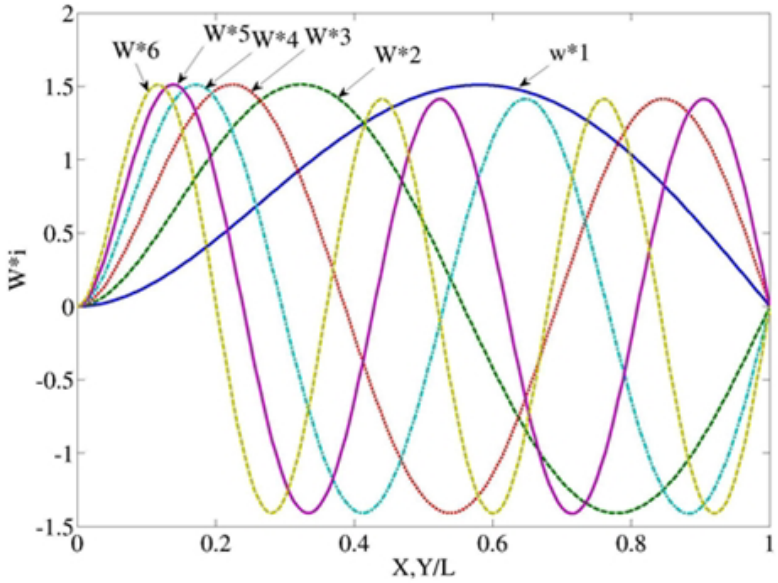

FIGURE 7.9. Clamped simply-supported beam functions for i=1, 2, 3, 4, 5, and 6.

Conclusion & Outlooks

The main purpose of the project thesis was addressed to develop a modeling strategy which can be able to take into account the different scale variety of the sandwich structure. The developed numerical model can help to clarify the effect of the core properties on the vibroacoustic behavior.

The implement of the proposed numerical approach has been presented in detail in the first chapter with reduction computation methods. The approach has been validated by comparing the obtained results with analytical method either for the dispersion curve or for the modal density of the sandwich panel. An extension for the prediction of the dispersion characteristics for curved sandwich panel was also validated.

The transition frequency separates the global panel bending and core shear regimes has been identified by two numerical methods, bisection and wavemode energy methods. The obtained results have been compared with existing analytical expressions. The comparison showed that the transition frequency identified via the two proposed methods is taken into consideration the orthotropic effect of the sandwich panel.

In chapter 5, a semi-analytical expression of the sound transmission loss has been developed. The proposed expression was validated with experimental and analytical data. A parametric study has been Then performed for different core configurations with a goal of revealing the effect of the geometric core of the vibroacoustic behavior. Overall, it was shown in the parametric survey that the change of the transition frequency by changing the geometric parameters of the core has influence on the sound transmission loss in the low-mid frequency range.

Finally, in the last part of the study, experimental analyses have been put in place to validate the remarks deduced from the developed meso-macro approach. For this reason, the Wave Inhomogeneous correlation (IWC) technique has been applied with a view

to identifying the transition frequency. So, the obtained results via the IWC method confirm the effect of the core cell size on the vibroacoustic behavior of the sandwich structure.

To finalize the vibroacoustic study starting in this project's thesis for sandwich structures, some perspectives have been planned :

- Extend the present numerical model for predicting the sound transmission loss through curved sandwich panels and determining their corresponding first transition frequency;
- Identify the second transition frequency which separates the shear core and the individual face-sheet bending regimes for more efficient control of the vibroacoustic behavior for sandwich panels;
- Develop a numerical optimization process which serves to identify the optimal geometrical parameters, either for a hexagonal cell or other core configurations;
- Extend the Wave Inhomogeneous correlation (IWC) for measuring the wave propagation characteristics through curved sandwich panels.

PUBLICATIONS DURING THE THESIS

✧—☞ *International Journals*

↬ **Z. Zergoune**, M. N. Ichchou, O. Bareille, B. Harras, R. Benamar, and B. Troclet, Assessments of shear core effects on sound transmission loss through sandwich panels using a two-scale approach, Computers & Structures, 10.1016/j.compstruc.2016.11.017.

↬ O. Baho, **Z. Zergoune**, M.N. Ichchou, B. Harras, R. Benamar, B. Troclet, and O. Bareille, On global bendingshear core transition effects for the vibroacoustic of sandwich structures: Analytical and numerical investigations, Composite Structures, 2016, 154, 453-463, 10.1016/j.compstruct.2016.07.062.

↬ C. Droz, **Z. Zergoune**, R. Boukadia, O. Bareille, and M.N. Ichchou, Vibro-acoustic optimisation of sandwich panels using the wave/finite element method, Composite Structures, 2016, 10.1016/j.compstruct.2016.01.025.

↬ **Zakaria Zergoune**, Bilal Harras, and Rhali Benamar, Nonlinear Free Vibrations of C-C-SS-SS Symmetrically Laminated Carbon Fiber Reinforced Plastic (CFRP) Rectangular Composite Plates, World Journal of Mechanics, 2015, 5, 20-32, 10.4236/wjm.2015.52003.

✧—☞ *International Conferences*

↬ **Z. Zergoune**, M. N. Ichchou, B. Harras, R. Benamar, and B. Troclet, Sound Transmission Loss through honeycomb sandwich panels: prediction and parametric survey, ECSSMET 2016 - The 14th European Conference on Spacecraft Structures, Materials and Environmental Testing, 27-30 September 2016 in Toulouse, France.

↬ C. Droz, **Z. Zergoune**, O. Baho, J.-L Christen, and M. Ichchou, Vibro-acoustic optimization of sandwich panels involving hexagonal honeycomb cores, ICCS18 -

18th International Conference on Composite Structures, 15-18 June 2015, Lisbon, Portugal.

- **Z. Zergoune**, M. N. Ichchou, O. Bareille, B. Harras, and R. Benamar, A two-scale approach for assessment of the honeycomb core shear effects on the transmission loss, DYNCOMP2015 - International Conference on Dynamics of Composite Structures, 2-4 June 2015, Arles - France.

- **Z. Zergoune**, B. Harras and R. Benamar, Non-Linear Steady State, Forced, Composites Periodic Vibrations of CCSSSS Symmetrically Laminated Carbon Fiber Reinforced PEEK (AS4/APC2) Rectangular Composite Plates, ARCACHON 2014. 4th International Conference on Carbon Composites (IC3). 12-14 Mai Arcachon-France.

- **Z. Zergoune**, B Harras, and Rhali Benamar,Non-linear free vibrations of CCSSSS symmetrically laminated carbon fiber reinforced peek (AS4/APC2) rectangular composite plates, MEDYNA 2013: 1st Euro-Mediterranean Conference on Structural Dynamics and Vibroacoustics. 23-25 April 2013 Marrakech Morocco.

National/ Regional Conferences

- **Z. Zergoune**, M. Ichchou, B. Harras, and R. Benamar, Parametric analysis on the transmission loss of honeycomb structure using a meso-macro approach , JJCAB 2015. 5-6 novembre 2015 Besançon France.

- J.-L. Christen, **Z. Zergoune**, M. Ichchou et B. Troclet, Analyse de sensibilité globale pour la transmission acoustique de structures composites, CSMA 2015, 12 Colloque National en Calcul des Structures. 18-22 Mai 2015, Presqu'île de Giens (Var) France.

- **Z. Zergoune**, M. Ichchou, B. Harras, R. Benamar, and B. Troclet, A meso-macro analysis of honeycomb structure using wave finite element method, JJCAB 2014. 6-7 novembre 2014 Lyon France.

- **Z. Zergoune**, C. Droz, M. Ichchou, B. Harras, R. Benamar and B. Troclet, On the vibro-acoustic honeycomb design through a meso-macro analysis, VISHNO 19th Conference, Aix-en-Provence, France, June 2014.

APPENDIX A

APPENDIX A

Chapter 1:

The coefficients a_i (with $i = 1,...,7$) (eq. 1.8) for the dispersion relation (eq. 1.7) obtained using the classical laminated plate theory (CLPT) presented in chapter 1, subsection 1.2.1.1 are defined in the following forms:

$$\begin{cases} a_1 = (A_{11}.(i.\cos\theta)^2 + 2.A_{16}.(i.\cos\theta).(i.\sin\theta) + A_{66}.(i.\sin\theta)^2).k^2; \\ a_2 = -\rho_s.(-i.\omega)^2; \\ a_3 = A_{16}.(i.\cos\theta)^2 + (A_{12} + A_{66}).(i.\cos\theta).(i.\sin\theta) + A_{26}.(i.\sin\theta)^2; \\ a_4 = -B_{11}.(i.\cos\theta)^3 - 3.B_{16}.(i.\cos\theta)^2.(i.\sin\theta) - (B_{12} + 2.B_{66}).(i.\cos\theta).(i.\sin\theta)^2 - B_{26}.(i.\sin\theta)^3; \\ a_5 = A_{66}.(i.\cos\theta)^2 + 2.A_{26}.(i.\cos\theta).(i.\sin\theta) + A_{22}.(i.\sin\theta)^2; \\ a_6 = -B_{16}.(i.\cos\theta)^3 - (B_{12} + 2.B_{66}).(i.\cos\theta)^2.(i.\sin\theta) - 3.B_{26}.(i.\cos\theta).(i.\sin\theta)^2 - B_{22}.(i.\sin\theta)^3; \\ a_7 = D_{11}.(i.\cos\theta)^4 + D_{16}.(i.\cos\theta)^3.(i.\sin\theta) + 2.(D_{12} + 2.D_{66}).(i.\cos\theta)^2.(i.\sin\theta)^2; \\ \qquad + 4.D_{26}.(i.\cos\theta).(i.\sin\theta)^3 + D_{22}.(i.\sin\theta)^4; \end{cases} \tag{A.1}$$

Chapter 2:

Matrices A_j (with $j = 0,...,6$) for the parallelogram unit cell of the sandwich panel in chapter 2 can be expressed in terms of the matrix block of the dynamic matrix $\widetilde{D}$ as the following form:

$$A_0 = \begin{pmatrix} \tilde{D}_{41} & \tilde{D}_{4B} & \tilde{D}_{4L} \\ 0 & 0 & 0 \\ 0 & 0 & 0 \end{pmatrix} \tag{A.2}$$

$$A_1 = \begin{pmatrix} b(\tilde{D}_{21}+\tilde{D}_{43}) & b(\tilde{D}_{2B}+\tilde{D}_{4T}) & b\tilde{D}_{2L} \\ 0 & 0 & 0 \\ b\tilde{D}_{R1} & b\tilde{D}_{RB} & b\tilde{D}_{RL} \end{pmatrix} \tag{A.3}$$

$$A_2 = \begin{pmatrix} b^2\tilde{D}_{23}+(\tilde{D}_{42}+\tilde{D}_{31}) & b^2\tilde{D}_{2T}+\tilde{D}_{3B} & \tilde{D}_{3L}+\tilde{D}_{4R} \\ \tilde{D}_{T1} & \tilde{D}_{TB} & \tilde{D}_{TL} \\ b^2\tilde{D}_{R3} & b^2\tilde{D}_R T & 0 \end{pmatrix} \tag{A.4}$$

$$A_3 = \begin{pmatrix} b(\tilde{D}_{11}+\tilde{D}_{22}+\tilde{D}_{33}+\tilde{D}_{44}) & b(\tilde{D}_{B1}+\tilde{D}_{3T}) & b(\tilde{D}_{1L}+\tilde{D}_{2R}) \\ b(\tilde{D}_{B1}+\tilde{D}_{T3}) & b(\tilde{D}_{BB}+\tilde{D}_{TT}) & b\tilde{D}_{BL} \\ b(\tilde{D}_{L1}+\tilde{D}_{R2}) & b\tilde{D}_{LB} & b(\tilde{D}_{LL}+\tilde{D}_{RR}) \end{pmatrix} \tag{A.5}$$

$$A_4 = \begin{pmatrix} \tilde{D}_{23}+b^2(\tilde{D}_{13}+\tilde{D}_{24}) & b^2\tilde{D}_{1T} & \tilde{D}_{3R} \\ b^2\tilde{D}_{B3}+\tilde{D}_{T2} & b^2\tilde{D}_{BT} & \tilde{D}_{TR} \\ b^2(\tilde{D}_{L3}+\tilde{D}_{R4}) & b^2\tilde{D}_{LT} & 0 \end{pmatrix} \tag{A.6}$$

$$A_5 = \begin{pmatrix} b(\tilde{D}_{12}+\tilde{D}_{34}) & 0 & b\tilde{D}_{1R} \\ b(\tilde{D}_{B2}+\tilde{D}_{T4}) & 0 & b\tilde{D}_{BR} \\ b\tilde{D}_{L2} & 0 & b\tilde{D}_{LR} \end{pmatrix} \tag{A.7}$$

$$A_6 = \begin{pmatrix} b^2.\tilde{D}_{14} & 0 & 0 \\ b^2.\tilde{D}_{B4} & 0 & 0 \\ b^2.\tilde{D}_{L4} & 0 & 0 \end{pmatrix} \tag{A.8}$$

in which $b = \lambda_y^{\frac{L_x}{L_y}\cos\alpha}$ with $\alpha = \frac{\pi}{6}$.

Matrices A_j (with $j = 0,...,2$) for the rectangular unit cell of the sandwich panel in chapter 2 can be expressed in terms of the matrix block of the dynamic stiffness matrix $\tilde{D}$ as the following form:

↬ For the constant term A_0:

$$\begin{cases} A_{11}^{\{0\}} = \widetilde{D}_{21} + \widetilde{D}_{43} + \widetilde{D}_{41}\lambda_y^{-1} + \widetilde{D}_{23}\lambda_y; \\ A_{1B}^{\{0\}} = \widetilde{D}_{2B} + \widetilde{D}_{4T} + \widetilde{D}_{4B}\lambda_y^{-1} + \widetilde{D}_{2T}\lambda_y; \\ A_{1L}^{\{0\}} = \widetilde{D}_{2L} + \widetilde{D}_{4L}\lambda_y^{-1}; \end{cases}$$

$$\begin{cases} A_{B1}^{\{0\}} = 0; \\ A_{BB}^{\{0\}} = 0; \\ A_{BL}^{\{0\}} = 0; \end{cases} \tag{A.9}$$

$$\begin{cases} A_{L1}^{\{0\}} = \widetilde{D}_{R1} + \widetilde{D}_{R3}\lambda_y; \\ A_{LB}^{\{0\}} = \widetilde{D}_{RB} + \widetilde{D}_{RT}\lambda_y; \\ A_{LL}^{\{0\}} = \widetilde{D}_{RL}; \end{cases}$$

↬ For the coefficients of the first order matrix A_1:

$$\begin{cases} A_{11}^{\{1\}} = \left(\widetilde{D}_{11} + \widetilde{D}_{22} + \widetilde{D}_{33} + \widetilde{D}_{44}\right) + \left(\widetilde{D}_{31} + \widetilde{D}_{42}\right)\lambda_y^{-1} + \left(\widetilde{D}_{13} + \widetilde{D}_{24}\right)\lambda_y; \\ A_{1B}^{\{1\}} = \widetilde{D}_{1B} + \widetilde{D}_{3T} + \widetilde{D}_{3B}\lambda_y^{-1} + \widetilde{D}_{1T}\lambda_y; \\ A_{1L}^{\{1\}} = \widetilde{D}_{1L} + \widetilde{D}_{2R} + \left(\widetilde{D}_{4L} + \widetilde{D}_{1L}\right)\lambda_y^{-1}; \end{cases}$$

$$\begin{cases} A_{B1}^{\{1\}} = \widetilde{D}_{B1} + \widetilde{D}_{T3} + \widetilde{D}_{T1}\lambda_y^{-1} + \widetilde{D}_{B3}\lambda_y; \\ A_{BB}^{\{1\}} = \widetilde{D}_{BB} + \widetilde{D}_{TT} + \widetilde{D}_{TB}\lambda_y^{-1} + \widetilde{D}_{BT}\lambda_y; \\ A_{BL}^{\{1\}} = \widetilde{D}_{BL} + \widetilde{D}_{TL}\lambda_y^{-1}; \end{cases} \tag{A.10}$$

$$\begin{cases} A_{L1}^{\{1\}} = \widetilde{D}_{L1} + \widetilde{D}_{R2} + \left(\widetilde{D}_{L3} + \widetilde{D}_{R4}\right)\lambda_y; \\ A_{LB}^{\{1\}} = \widetilde{D}_{LB} + \widetilde{D}_{LT}\lambda_y; \\ A_{LL}^{\{1\}} = \widetilde{D}_{LL} + \widetilde{D}_{RR}; \end{cases}$$

↬ For the coefficients of the second order matrix A_2:

$$\begin{cases} A_{11}^{\{2\}} = \widetilde{D}_{12} + \widetilde{D}_{34} + \widetilde{D}_{32}\lambda_y^{-1} + \widetilde{D}_{14}\lambda_y; \\ A_{1B}^{\{2\}} = 0; \\ A_{1L}^{\{2\}} = \widetilde{D}_{1R} + \widetilde{D}_{3R}\lambda_y^{-1}; \end{cases}$$

$$\begin{cases} A_{B1}^{\{2\}} = \widetilde{D}_{B2} + \widetilde{D}_{T4} + \widetilde{D}_{T2}\lambda_y^{-1} + \widetilde{D}_{B4}\lambda_y; \\ A_{BB}^{\{2\}} = 0; \\ A_{BL}^{\{2\}} = \widetilde{D}_{BR} + \widetilde{D}_{TR}\lambda_y^{-1}; \end{cases} \tag{A.11}$$

$$\begin{cases} A_{L1}^{\{2\}} = \widetilde{D}_{L2} + \widetilde{D}_{L4}\lambda_y; \\ A_{LB}^{\{2\}} = 0; \\ A_{LL}^{\{2\}} = \widetilde{D}_{LR}; \end{cases}$$

The coefficients of the reduced mass and stiffness matrices in equation 2.16 obtained by developping the CSM are as follows :

$$M_{BB} \equiv B^T M B = \begin{pmatrix} I \\ \phi_R \end{pmatrix}^T \begin{pmatrix} M_{bdbd} & M_{bdI} \\ M_{IbdR} & M_{II} \end{pmatrix} \begin{pmatrix} I \\ \phi_R \end{pmatrix} = M_{bdbd} + M_{bdI}\phi_R + \phi_R^T M_{Ibd} + \phi_R^T M_{II}\phi_R \tag{A.12}$$

$$M_{Bm} \equiv B^T M \phi = \begin{pmatrix} I \\ \phi_R \end{pmatrix}^T \begin{pmatrix} M_{bdbd} & M_{bdI} \\ M_{Ibd} & M_{II} \end{pmatrix} \begin{pmatrix} 0 \\ \phi_L \end{pmatrix} = [M_{bdI} + \phi_R^T M_{II}]\phi_L \tag{A.13}$$

$$M_{mB} \equiv \phi^T M B = \begin{pmatrix} 0 \\ \phi_L \end{pmatrix}^T \begin{pmatrix} M_{bdbd} & M_{bdI} \\ M_{Ibd} & M_{II} \end{pmatrix} \begin{pmatrix} I \\ \phi_R \end{pmatrix} = \phi_L^T [M_{Ibd} + M_{II}\phi_R] \tag{A.14}$$

$$M_{mm} \equiv \phi^T M \phi = \begin{pmatrix} 0 \\ \phi_L \end{pmatrix}^T \begin{pmatrix} M_{bdbd} & M_{bdI} \\ M_{Ibd} & M_{II} \end{pmatrix} \begin{pmatrix} 0 \\ \phi_L \end{pmatrix} = \phi_L^T M_{II}\phi_L \tag{A.15}$$

$$\begin{aligned} K_{BB} \equiv B^T K B = \begin{pmatrix} I \\ \phi_R \end{pmatrix}^T \begin{pmatrix} K_{bdbd} & K_{bdI} \\ K_{Ibd} & K_{II} \end{pmatrix} \begin{pmatrix} I \\ \phi_R \end{pmatrix} &= K_{bdbd} + K_{bdI}\phi_R + \phi_R^T [K_{Ibd} + K_{II}\phi_R] \\ &= K_{bdbd} + K_{bdI}\phi_R \end{aligned} \tag{A.16}$$

$$K_{Bm} \equiv B^T K \phi = \begin{pmatrix} I \\ \phi_R \end{pmatrix}^T \begin{pmatrix} K_{bdbd} & K_{bdI} \\ K_{Ibd} & K_{II} \end{pmatrix} \begin{pmatrix} 0 \\ \phi_L \end{pmatrix} = [K_{bdI} + \phi_R^T K_{II}]\phi_L = 0 \tag{A.17}$$

$$K_{mB} \equiv \phi^T K B = \begin{pmatrix} 0 \\ \phi_L \end{pmatrix}^T \begin{pmatrix} K_{bdbd} & K_{bdI} \\ K_{Ibd} & K_{II} \end{pmatrix} \begin{pmatrix} I \\ \phi_R \end{pmatrix} = \phi_L^T [K_{Ibd} + K_{II}\phi_R] = 0 \tag{A.18}$$

$$K_{mm} \equiv \phi^T K \phi = \begin{pmatrix} 0 \\ \phi_L \end{pmatrix}^T \begin{pmatrix} K_{bdbd} & K_{bdI} \\ K_{Ibd} & K_{II} \end{pmatrix} \begin{pmatrix} 0 \\ \phi_L \end{pmatrix} = \phi_L^T K_{II} \phi_L \tag{A.19}$$

The reduced wave basis matrix B_Ψ is expressed as the following form :

$$B_\Psi = \begin{vmatrix} \widetilde{B}_\Psi & 0 \\ 0 & I \end{vmatrix}, \tag{A.20}$$

where the matrix $\widetilde{B}_\Psi$ is defined as function of the associated vectors Γ to the global displacement:

$$\widetilde{B}_\Psi = \begin{vmatrix} \Gamma^{(1)} & & & & & & & & \\ & \Gamma^{(2)} & & & & 0 & & & \\ & & \Gamma^{(3)} & & & & & & \\ & & & \Gamma^{(4)} & & & & & \\ & & & & \Gamma^{(B)} & & & & \\ & & & & & \Gamma^{(L)} & & & \\ & & 0 & & & & \Gamma^{(T)} & & \\ & & & & & & & \Gamma^{(R)} & \end{vmatrix}, \tag{A.21}$$

with $\Gamma = \dfrac{\widetilde{\Psi}(i)}{\Psi(i)}$ is the normalized vector associated to the global displacement field.

The expressions of the effective mechanical parameters of honeycombs with double thickness vertical walls, used in chapter 2 and developed in [93], are described as follows (the geometrical parameters used for developping the formulas are presented in figure A.1) :

$$\rho^* = \rho_p \left(1 - \frac{l\cos\theta\,(h_b + l\sin\theta)}{(l\cos\theta + t)(h + l\sin\theta)}\right), \tag{A.22}$$

with the superscript $*$ denotes the effective mechanical properties of the sandwich panel. l_b and h_b are expressed as follows:

$$\begin{cases} l_b = l - t\tan\left(\dfrac{\pi}{4} - \dfrac{\theta}{2}\right), \\ h_b = h - t\tan\left(\dfrac{\pi}{4} - \dfrac{\theta}{2}\right), \end{cases} \tag{A.23}$$

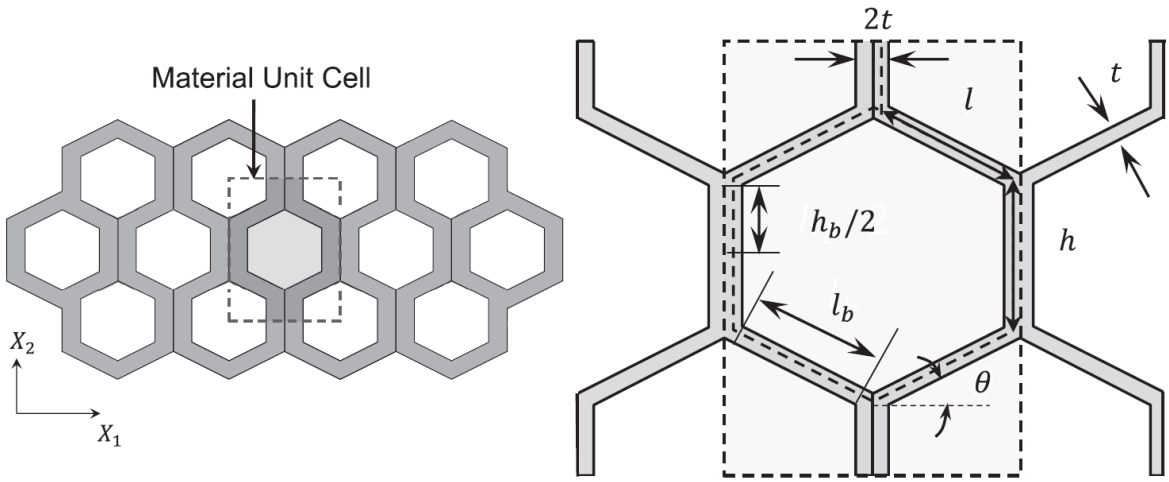

Figure A.1: Geometrical parameters for honeycombs with double thickness vertical cell walls as defined in [93].

↬ The effective Young's modulus of the sandwich core are given as:

$$\begin{cases} E_3^* = E_c\left(\dfrac{\rho^*}{rho_p}\right), \\ E_1^* = E_c\left(\dfrac{t}{l_b}\right)^3 \dfrac{\cos\theta}{\left(\dfrac{h}{l}+\sin\theta\right)\sin^2\theta}\left[\dfrac{1}{1+\left(2.4+1.5\nu_c+\cot^2\theta\right)\left(\dfrac{t}{l_b}\right)^2}\right], \\ E_2^* = E_c\left(\dfrac{t}{l_b}\right)^3 \dfrac{\left(\dfrac{h}{l}+\sin\theta\right)}{\cos^3\theta}\left[\dfrac{1}{1+\left(2.4+1.5\nu_c+\tan^2\theta+\dfrac{\left(\dfrac{h_b}{l_b}\right)}{\cos^2\theta}\right)\left(\dfrac{t}{l_b}\right)^2}\right], \end{cases} \tag{A.24}$$

↬ The effective shear modulus of the sandwich core are given as:

$$\begin{cases} G_{12}^{*} = E_c \left(\dfrac{t}{l_b}\right)^3 \dfrac{\left(\dfrac{h}{l}+\sin\theta\right)}{\left(\dfrac{h_b}{l_b}\right)^2 \cos\theta} \left(\dfrac{1}{B}\right), \\ G_{13}^{*} = C\left[\cos^2\theta\left(\dfrac{l_b}{l}\right)+2\left(\dfrac{t}{l}\right)\tan\left(\dfrac{\pi}{4}-\dfrac{\theta}{2}\right)\right], \\ G_{23}^{*} = C\left[\sin^2\theta\left(\dfrac{l_b}{l}\right)+\dfrac{h}{l}+\left(\dfrac{t}{l}\right)\tan\left(\dfrac{\pi}{4}-\dfrac{\theta}{2}\right)\right], \end{cases} \tag{A.25}$$

with B and C are expressed as follows

$$\begin{cases} B = \left[1+2\left(\dfrac{h_b}{l_b}\right)+\left(\dfrac{t}{l_b}\right)^2\left(\dfrac{2.4+1.5\nu_c}{\dfrac{h_b}{l_b}}\left(4+\dfrac{h}{l}+\sin\theta\right)+\dfrac{\dfrac{h}{l}+\sin\theta}{\left(\dfrac{h_b}{l_b}\right)^2}\left[\left(\dfrac{h}{l}+\sin\theta\right)\tan^2\theta+\sin\theta\right]\right)\right], \\ C = G_c\left(\dfrac{\dfrac{t}{l}}{\left(\dfrac{h}{l}+\sin\theta\right)\left(\cos\theta+\dfrac{t}{l}\right)}\right), \end{cases} \tag{A.26}$$

Chapter 5:

The spatial frequency response function (FRF) of the sandwich panel A at different measured points :

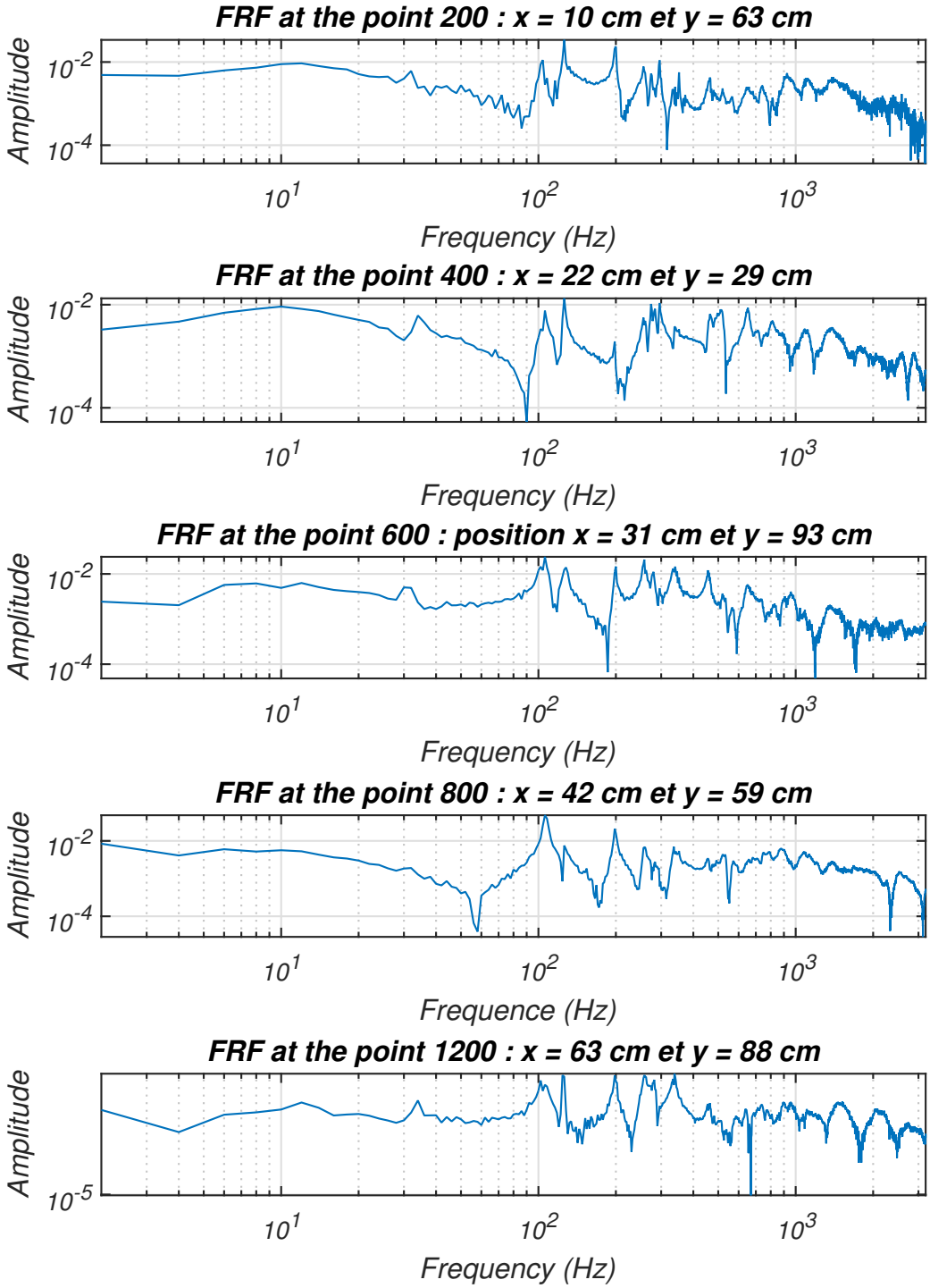

Figure A.2: Spatial FRF at different point for the panel A.

BIBLIOGRAPHY

[1] ISO 10534-2. *Acoustics – Determination of sound absorption coefficient and impedance in impedance tubes – Part 2: Transfer-function method*. ISO/TC 43/SC 2, 1998. URL: http://www.iso.org/iso/catalogue_detail.htm?csnumber=22851.

[2] S. Abrate and G. Schoeppner. *Identification of Support Conditions for Composite Beams and Plates from Natural Frequencies*. 29 International SAMPE (Society for the Advancement of Materials and Process Engineering) Technical Conference, Orlando, 28 October-1 November, 725-732, 1997.

[3] F. Alijani and M. Amabili. Nonlinear vibrations of laminated and sandwich rectangular plates with free edges. part 1: Theory and numerical simulations. *Composite Structures*, 105:422–436, 2013. doi:10.1016/j.compstruct.2013.05.034.

[4] F. Alijani, M. Amabili, G. Ferrari, and V. DAlessandro. Nonlinear vibrations of laminated and sandwich rectangular plates with free edges. part 2: Experiments & comparisons. *Composite Structures*, 105:437–445, 2013. doi:10.1016/j.compstruct.2013.05.020.

[5] M. Alkhader, S. Iyer, W. Shi, and T. Venkatesh. Low frequency acoustic characteristics of periodic honeycomb cellular cores: The effect of relative density and strain fields. *Composite Structures*, 133:7784, December 2015. doi:10.1016/j.compstruct.2015.07.102.

[6] J. F. Allard and N. Atalla. *Propagation of sound in porous media: Modeling sound absorbing materials*. John Wiley & Sons Ltd, 2nd edition, 2009. doi:10.1002/9780470747339.

[7] S. A. Ambartsumyan. *On the theory of bending of anisotropic plates (in Russian)*. Investiia Akademiia Nauk SSSR Otdelenie Tekhnicheska nauk 4, 1958.

[8] J.E. Ashton and J.M. Whitney. *Theory of Laminated Plates*. Technomic Publication, Stanford, 1970.

[9] M. S. Atwal and M. J. Crocker. *Use of helium gas to reduce acoustic transmission*. New York, Noise Control Foundation, 1985, p. 187-192. NASA-supported research., 1985. URL: http://adsabs.harvard.edu/abs/1985nce..conf..187A.

[10] O. Baho, Z. Zergoune, M. N. Ichchou, B. Harras, R. Benamar, B. Troclet, and O. Bareille. On global bendingshear core transition effects for the vibroacoustic of sandwich structures: Analytical and numerical investigations. *Composite Structures*, 154:453463, 2016. doi:10.1016/j.compstruct.2016.07.062.

[11] K. J. Bathe. *Finite element procedures in engineering analysis*. Prentice-Hall, Inc, 1982. URL: https://fr.scribd.com/doc/38610682/eBook-Finite-Element-Procedures-in-Engineering-Analysis-Bathe-1982.

[12] J. G. Belvins and L. L. Hansen. *Use of helium gas to reduce acoustic transmission*. 6th Structures, Structural Dynamics, and Materials Conference, Structures, Structural Dynamics, and Materials and Co-located Conferences, 1985. doi:10.2514/6.1985-601.

[13] M. A. Ben Souf, O. Bareille, M.N. Ichchou, B. Troclet, and M. Haddar. Variability of coupling loss factors through a wave finite element technique. *Journal of Sound and Vibration*, 332:2179–2190, 2013. doi:10.1016/j.jsv.2012.07.003.

[14] R. Benamar. *Non-linear dynamic behaviour of fully clamped beams and rectangular isotropic and laminated plates*. Ph.D. Thesis, Institute of Sound and Vibration Research, Southampton, 1990.

[15] R. Benamar, M.M.K. Bennouna, and R.G. White. *The effects of large vibration amplitudes on the fundamental mode shape of a fully clamped, symmetrically laminated rectangular plate*. Proceedings of the 4th International Conference on Recent Advances in Structural Dynamics, Southampton, 1990.

[16] R. Benamar, M.M.K. Bennouna, and R.G. White. The effects of large vibration amplitudes on the fundamental mode shape of thin elastic structures. part i: simply supported and clamped clamped beams. *Journal of Sound and Vibration*, 149(2):179–195, 1991. doi:10.1016/0022-460X(91)90630-3.

[17] R. Benamar, M.M.K. Bennouna, and R.G. White. The effects of large vibration amplitudes on the fundamental mode shape of thin elastic structures. part ii: fully clamped rectangular isotropic plates. *Journal of Sound and Vibration*, 164(2):295–316, 1993. doi:10.1006/jsvi.1993.1215.

[18] M.M.K. Bennouna. *Non-linear behaviour of a clamped-clamped beam with consideration of fatigue life*. Ph.D. Thesis, Institute of Sound and Vibration Research, Southampton, 1981.

[19] J. Berthaut, M. N. Ichchou, and L. Jezeque. K-space identification of apparent structural behaviour. *Journal of Sound and Vibration*, 280(3-5):11251131, 2005. doi:10.1016/j.jsv.2004.02.044.

[20] A. Bhimaraddi. Dynamic response orthotropic, homogeneous, and laminated cylindrical shells. *AIAA Journal*, 11(27):1834–1837, 1985. doi:10.2514/3.9182.

[21] J. S. Bolton, N. M. Shiau, and Y. J. Kang. Sound transmission through multi-panel structures lined with elastic porous materials. *Journal of Sound and Vibration*, 191(3):317–347, April 1996. doi:10.1006/jsvi.1996.0125.

[22] L. Brillouin. *Wave Propagation in Periodic Structures (Second edition)*. Dover, 1953.

[23] B. Brouard, D. Lafarge, and J. F. Allard. A general method of modelling sound propagation in layered media. *Journal of Sound and Vibration*, 183(1):129–142, 1995. doi:10.1006/jsvi.1995.0243.

[24] F. Casadei, J. Rimoli, and M. Ruzzene. Multiscale finite element analysis of wave propagation in periodic solids. *Finite Elements in Analysis and Design*, 108:81–95, January 2016. doi:10.1016/j.finel.2015.10.002.

[25] A. Catapano and M. Montemurro. A multi-scale approach for the optimum design of sandwich plates with honeycomb core. part ii: the optimisation strategy. *Composite Structures*, 133:677690, December 2014. doi:10.1016/j.compstruct.2014.07.058.

[26] C.Y. Chia. *Nonlinear Analysis of Plates*. McGraw-Hill, New York, 1980.

[27] C.Y. Chia. Geometrically nonlinear behavior of composite plates: A review. *Applied Mechanics Reviews*, 41(12):439–451, 1988. doi:10.1115/1.3151873.

[28] D. Chronopoulos, B. Troclet, O. Bareille, and M. Ichchou. Modeling the response of composite panels by a dynamic stiffness approach. *Composite Structures*, 96:111120, September 2013. doi:10.1016/j.compstruct.2012.08.047.

[29] D. Chronopoulos, B. Troclet, M. N. Ichchou, and J.P. Lainé. A unified approach for the broadband vibroacoustic response of composite shells. *Composites Part B: Engineering*, 43(4):18371846, June 2012. doi:10.1016/j.compositesb.2012.01.059.

[30] Dimitrios Chronopoulos. *Prediction of the vibroacoustic response of aerospace composite structures in a broadband frequency range*. Thesis of École centrale de Lyon, 2012. URL: http://bibli.ec-lyon.fr/exl-doc/TH_T2301_dchronopoulos.pdf.

[31] B. L. Clarkson and M. F. Ranky. Modal density of honeycomb plates. *Journal of Sound and Vibration*, 91(1):103–118, 1983. doi:10.1016/0022-460X(83)90454-6.

[32] V. Cotoni, R. S. Langley, and P. J. Shorter. A statistical energy analysis subsystem formulation using finite element and periodic structure theory. *Journal of Sound and Vibration*, 318(3-5):10771108, 2008. doi:10.1016/j.jsv.2008.04.058.

[33] R. J. M. Craik. Non-resonant sound transmission through double walls using statistical energy analysis. *Applied Acoustics*, 64(3):325–341, March 2003. doi:10.1016/S0003-682X(02)00051-8.

[34] R. J. M. Craik and R. Wilson. Sound transmission through masonry cavity walls. *Journal of Sound and Vibration*, 179(1):79–96, January 1995. doi:10.1006/jsvi.1995.0005.

[35] M. J. Crocker and A. J. Price. Sound transmission using statistical energy analysis. *Journal of sound and vibration*, 9:469–486, July 1969. doi:10.1016/0022-460X(69)90185-0.

[36] E. B. Davis. Designing honeycomb panels for noise control. *American Institute of Aeronautics and Astronautics*, 31:792801, 1999. doi:10.2514/6.1999-1917.

[37] M. De Rochambeau. *Analyse des interactions fluide-structure en moyennes fréquences sous chargement aérodynamique*. Thèse de doctorat, École Centrale de Lyon, 2010. URL: http://bibli.ec-lyon.fr/exl-doc/mrochambeau.pdf.

[38] S. De Rosa, M. Capobianco, G. Nappo, and G. Pagnozzi. Models and comparisons for the evaluation of the sound transmission loss of panels. *Proceedings of the Institution of Mechanical Engineers, Part C: Journal of Mechanical Engineering Science*, 228(18):3343–3355, May 2014. doi:10.1177/0954406214530597.

[39] S. B. Dong, K. S. Pister, and R. L. Taylor. On the theory of laminated anisotropic shells and plates. *Journal of Aeronautical Science*, (2):969–975, 1966. doi:10.2514/8.9668.

[40] S. B. Dong and F. K. W. Tso. On a laminated orthotropic shell theory including transverse shear deformation. *Journal of Applied Mechanics*, (39):1091–1097, 1972. doi:10.1115/1.3422834.

[41] C. Droz, J.-P. Lainé, M.N. Ichchou, and G. Inquiété. A reduced formulation for the free-wave propagation analysis in composite structures. *Composite Structures*, 113:134144, March 2014. doi:0.1016/j.compstruct.2014.03.017.

[42] C. Droz, Z. Zergoune, R. Boukadia, O. Bareille, and M. N. Ichchou. Vibro-acoustic optimization of sandwich panels using the wave/finite element method. *Composite Structures*, 2016. doi:10.1016/j.compstruct.2016.01.025.

[43] C. Droz, C. Zhou, M. N. Ichchou, and J.-P. Lainé. A hybrid wave-mode formulation for the vibro-acoustic analysis of 2d periodic structures. *Journal of Sound and Vibration*, 363:285–302, November 2016. doi:10.1016/j.jsv.2015.11.003.

[44] C. L. Dym and D. C. Lang. Transmission loss of damped asymmetric sandwich panels with orthotropic cores. *Journal of Sound and Vibration*, 118:299319, September 1983. doi:10.1016/0022-460X(83)90690-9.

[45] ASTM E90. Standard test method for laboratory measurement of airborne sound transmission loss of building partitions and elements. *ASTM E90-09*. URL: https://www.astm.org/Standards/E90.htm.

[46] K. El Bikri, R. Benamar, and M. Bennouna. Geometrically non-linear free vibrations of clamped simply supported rectangular plates. part 1: The effects of large vibration amplitudes on the fundamental mode shape. *Computers & Structures*, 81(20):2029–2043, 2003.

[47] L. L. Erickson. Modal density estimates for sandwich panels: theory and experiment. *NASA technical note D-5771, September*, 1970. URL: http://ntrs.nasa.gov/archive/nasa/casi.ntrs.nasa.gov/19700031338.pdf.

[48] D. Evan. *Designing honeycomb panels for noise control*. 5th AIAA/CEAS Aeroacoustics Conference and Exhibit, Aeroacoustics Conferences, 1999. doi:10.2514/6.1999-1917.

[49] D. J. Ewins. *Modal Testing: Theory and Practice*. Research Studies Press, New York, 1984. URL: https://fr.scribd.com/doc/133501854/D-J-Ewins-Modal-Testing-Theory-and-Practice.

[50] F. Fahy and P. Gardonio. *Sound and Structural Vibration: Radiation, Transmission and Response*. pages 135241, Academic Press, second edition, 2007. doi:10.1016/B978-012373633-8/50007-7.

[51] N. S. Ferguson, C. R. Halkyard, B. G. Mace, and K. H. Heron. *The estimation of wavenumbers in two dimensional structures*, volume II. Proceedings of ISMA 2002: International Conference on Noise and Vibration Engineering, Leuven, Belgium, 2002. URL: http://eprints.soton.ac.uk/10023/.

[52] S. J. K. Florence and K. Renji. Modal density of thin composite cylindrical shells. *Journal of Sound and Vibration*, 365:157171, March 2015. doi:10.1016/j.jsv.2015.11.030.

[53] R. D. Ford, P. Lord, and A. W. Walter. Sound transmission through sandwich constructions. *Journal of Sound and Vibration*, 5:9–21, March 1967. doi:10.1016/0022-460X(67)90173-3.

[54] S. Ghinet, N. Atalla, and H. Osman. The transmission loss of curved laminate and sandwich composite panels. *Journal of the Acoustical Society of America*, 118:774–90, April 2005. doi:10.1121/1.1932212.

[55] S. Ghineta and N. Atalla. Vibro-acoustic behaviors of flat sandwich composite panels. *Transactions of the CSME / de la SCGM*, 30(4):473493, 2006. URL: http://www.tcsme.org/Papers/Vol30/Vol30No4Paper2.pdf.

[56] S. Ghineta, N. Atalla, and H. Osman. Diffuse field transmission into infinite sandwich composite and laminate composite cylinders. *Journal of Sound Vibration*, (289):745778, 2006. doi:10.1016/j.jsv.2005.02.028.

[57] L. J. Gibson and M. F. Ashby. *Cellular solids: structure and properties*. Cambridge university press, 2nd edition, 1999. URL: http://www.cambridge.org/se/academic/subjects/engineering/materials-science/cellular-solids-structure-and-properties-2nd-edition?format=PB.

[58] D. Griese, J. D. Summers, and L. Thompson. The effect of honeycomb core geometry on the sound transmission performance of sandwich panels. *Journal of Vibration and Acoustics*, October 2014. doi:10.1115/1.4029043.

[59] L Guillaumie. Vibroacoustic flexural properties of symmetric honeycomb sandwich panels with composite faces. *Journal of Sound and Vibration*, 343:71–103, January 2015. doi:10.1016/j.jsv.2014.12.026.

[60] W. B. Haile. *Primer on the Craig-Bampton method*. Young, J. T., 2000. URL: http://www.vibrationdata.com/tutorials2/Primer_on_the_Craig-Bampton_Method.pdf.

[61] J. Han, K. Yu, X. Li, and R. Zhao. Modal density of sandwich panels based on an improved ordinary sandwich panel theory. *Composite Structures*, 131:927–938, July 2015. doi:10.1016/j.compstruct.2015.06.039.

[62] J. Han, K. Yu, X. Li, and R. Zhao. Modal density and mode counts of sandwich panels in thermal environments. *Composite Structures*, 153:69–80, June 2016. doi:10.1016/j.compstruct.2016.05.109.

[63] B. Harras, R. Benamar, and R.G. White. Experimental and theoretical investigation of the linear and nonlinear dynamic behavior of a glare 3 hybrid composite panel. *Journal of Sound and Vibration*, 252(2):281–315, 2002. doi:10.1006/jsvi.2001.3962.

[64] B. Harras, R. Benamar, and R.G. White. Geometrically non-linear free vibration of fully clamped symmetrically laminated rectangular composite plates. *Journal of Sound and Vibration*, 251(4):579–619, 2002. doi:10.1006/jsvi.2001.3713.

[65] B. Harras, R. Benamar, and R.G. White. Investigation of non-linear free vibrations of fully clamped symmetrically laminated carbon-fibre-treinforced peek (as4/apc2) rectangular composite panels. *Composite Science and Technology*, 62(5):719–727, 2002. doi:10.1016/S0266-3538(01)00133-6.

[66] Carsten Hoever. *Experimental evaluation of dispersion characteristics*. Thesis of Institut für Strömungsmechanik undTechnische Akustik, 2007. URL: https://www.researchgate.net/publication/266224510.

[67] Tianli Huang. *Multi-modal propagation through finite elements applied for the control of smart structures*. Thesis of École centrale de Lyon, 2012. URL: http://bibli.ec-lyon.fr/exl-doc/TH_T2344_thuang.pdf.

[68] Guillaume Inquiété. *Simulation numérique de la propagation des ondes dans les structures composites stratifiées*. Thesis of École centrale de Lyon, 2008. URL: http://bibli.ec-lyon.fr/exl-doc/ginquiete.pdf.

[69] N. Iwama and T. Tsukishima. A correlation method for estimating wave-number spectrum moments of fluctuations. *Applied Physics Letters*, 31(11):783–785, 1977. doi:10.1063/1.89547.

[70] R. M. Jones. *Mechanics of Composite Materials*. New York: McGraw-Hill, 1975. URL: https://fr.scribd.com/doc/134187856/Mechanics-of-Composite-Materials-RM-JONES.

[71] S. S. Jung, Y. T. Kim, and Y. B. Lee. Measurement of sound transmission loss by using impedance tubes. *Journal- Korean Physical Society*, 53(2):S59, 2008. doi:10.3938/jkps.53.596.

[72] A. C. Kenneth. The science and applications of acoustics. *The Journal of the Acoustical Society America*, 126(4):16711680, 2009. doi:10.1121/1.3177255.

[73] E. M. Kerwin. Damping of flexural waves by a constrained viscoelastic layer. *Journal of the Acoustical Society of America*, 7(31):952–962, 1959. doi:10.1121/1.1907821.

[74] A. A. Khdeir, J. N. Reddy, and L. Libreseu. Analytical solution of a refined shear deformation theory for rectangular composite plates. *International Journal of Solids and Structures*, 10(23):1447–1463, 1987. doi:10.1016/0020-7683(87)90009-6.

[75] G. R. Kirchhoff. *Über des Gleichgewicht und die Bewegung einer elastischen Scheibe*. Journal für die reine und angewandte Mathematik (Crelles Journal), 1850. URL: http://www.degruyter.com/view/j/crll.1850.issue-40/crll.1850.40.51/crll.1850.40.51.xml.

[76] H. Kraus. *Thin elastic shells: an introduction to the theoretical foundations and the analysis of their static and dynamic behavior*. John Wiley and Sons, 1967. URL: https://books.google.co.ma/books/about/Thin_elastic_shells.html?id=HNo8AAAAIAAJ&redir_esc=y.

[77] G. Kurtze and B. G. Watters. New wall design for high transmission loss or high damping. *Journal of the Acoutical Society of America*, 31:739748, June 1959. doi:10.1121/1.1907780.

[78] R. Langley. The modal density and mode count of thin cylinders and curved panels. *Journal of Sound and Vibration*, 169(1):43–53, January 1994. doi:10.1006/jsvi.1994.1005.

[79] A.W. Leissa. *Vibration of plates*. NASA-SP-160. US Government Printing Office, Washington DC, 1969.

[80] A.W. Leissa. Free vibrations of rectangular plate. *Journal of Sound and Vibration*, 31(3):257–293, 1973. doi:10.1016/S0022-460X(73)80371-2.

[81] S. G. Lekhnitskii. *Strength calculation of composite beams*. Vestnik Inzhenerov i Tekhnikov 9, 1935.

[82] C. Lesueur. *Rayonnement acoustique des structures Vibroacoustique, interactions fluide-structure*. Eyrolles, first edition, 1988. URL: http://www.eyrolles.com/Sciences/Livre/rayonnement-acoustique-des-structures-0000000057035.

[83] C. Libove and S. B. Batdorf. A general small-deflection theory for flat sandwich plates. *NACA report 899*, 1948. URL: http://naca.central.cranfield.ac.uk/reports/1948/naca-report-899.pdf.

[84] L. Librescu. The elasto-kinetic problems in the theory of anisotropic shells and plates, part ii : Plates theory. *Revue Roumaine des Sciences Techniques, Série de Mecanique Appliquée*, 3(7), 1969.

[85] L. Librescu, A. A. Khdeir, and J. N. Reddy. A comprehensive analysis of the state of elastic anisotropic flat plates using refined theories. *International Journal of Solids and Structures*, (70):57–81, 1987. doi:10.1007/BF01174647.

[86] K. H. Lo, R. M. Christensen, and E. M. Wu. A higher order theory of plate deformation, part 2 : laminated plates. *Journal of Applied Mechanics*, (44):669–676, 1977. doi:10.1115/1.3424155.

[87] A. E. H. Love. The small free vibrations and deformations of elastic shells. *Philosophical Transactions of the Royal Society (London)*, A 179:491–546, 1888. doi:10.1098/rsta.1888.0016.

[88] R. H. Lyon. *Statistical energy analysis of dynamical systems : theory and applications*. M.I.T. Press, 1975. URL: https://mitpress.mit.edu/books/statistical-energy-analysis-dynamical-systems.

[89] R. H. Lyon and R. G. DeJong. *Theory and application of statistical energy analysis*. Butterworth-Heinemann, Boston, 2nd edition, 1995. doi:10.1016/B978-0-7506-9111-6.50005-1.

[90] R. H. Lyon and G. Maidanik. Statistical methods in vibration analysis. *AIAA Journal*, 2(6):1015–1024, June 1964. doi:10.2514/3.2492.

[91] R. H. Lyon and T. D. Scharton. Vibrational energy transmission in a three element structure. *Journal Acoustical Society of America*, 2(38):253–261, march 1965. doi:10.1121/1.1909649.

[92] B. R. Mace, D. Duhamel, M. J. Brennan, and L. Hinke. Finite element prediction of wave motion in structural waveguides. *The Journal of the Acoustical Society America*, 117:2835–2843, Avril 2005. doi:10.1121/1.1887126.

[93] S. Malek and L. Gibson. Effective elastic properties of periodic hexagonal honeycombs. *Mechanics of Materials*, 91:226240, July 2015. doi:10.1016/j.mechmat.2015.07.008.

[94] E. Manconi and B. R. Mace. Wave characterization of cylindrical and curved panels using a finite element method. *Journal of the Acoustical Society of America*, 125(1):154163, September 2009. doi:10.1121/1.3021418.

[95] D. Mead and S. Parthan. Free wave propagation in two-dimensional periodic plates. *Journal of Sound and Vibration*, 64(3):325348, June 1979. doi:10.1016/0022-460X(79)90581-9.

[96] D. J. Mead. A general theory of harmonic wave propagation in linear periodic systems with multiple coupling. *Journal of Sound and Vibration*, 27(2):235–260, 1973. doi:10.1016/0022-460X(73)90064-3.

[97] A. Mejdi, N. Atalla, and S. Ghinet. Wave spectral finite element model for the prediction of sound transmission loss and damping of sandwich panels. *Computers & Structures*, 158:251258, June 2015. doi:10.1016/j.compstruc.2015.06.014.

[98] J. M. Mencik and M. N. Ichchou. Multi-mode propagation and diffusion in structures through finite elements. *European Journal of Mechanics - A/Solids*, 24(5):877–898, Octobe 2005. doi:10.1016/j.euromechsol.2005.05.004.

[99] R. D. Mindlin. Influence of rotatory inertia and shear on flexural motions of isotropic elastic plates. *Journal of Applied Mechanics*, (18):31–38, 1951.

[100] A. K. Mohanty, C. C. Oliver, and K. R. Purdy. Acoustic measurements in low-density gases. *Acoustic measurements in low-density gases*, 8(10):11981201, 1975. URL: http://iopscience.iop.org/article/10.1088/0022-3727/8/10/006.

[101] A. V. K. Murty. Higher-order theory for vibration of thick plates. *AIAA Journal*, 12(15):1823–1824, 1977. doi:10.2514/3.7490.

[102] M. V. V. Murty. An improved transverse shear deformation theory for laminated anisotropic plates. *NASA Technical Paper 1903*, pages 1–37, 1981. URL: http://ntrs.nasa.gov/archive/nasa/casi.ntrs.nasa.gov/19820003615.pdf.

[103] C. J. Naify, C. Huang, M. Sneddon, and S. Nutt. Transmission loss of honeycomb sandwich structures with attached gas layers. *Applied Acoustics*, 72:71–77, September 2010. doi:10.1016/j.apacoust.2010.09.005.

[104] A.H. Nayfeh and P. Frank Pai. *Linear and Nonlinear Structural Mechanics*. John Wiley & Sons, Inc., Hoboken, 2004. doi:10.1002/9783527617562.

[105] D. E. Newland. Calculation of power flow between coupled oscillators. *Journal of Sound Vibration*, 3(3):262–276, May 1966. doi:10.1016/0022-460X(66)90095-2.

[106] C.F. Ng and R.G. White. Dynamic behaviour of postbuckled isotropic plates under in-plane compression. *Journal of Sound and Vibration*, 120(2):1–18, 1988. doi:10.1016/0022-460X(88)90331-8.

[107] A. K. Noor and W. S. Burton. Assessment of computational models for multilayered shells. *Ing. Arch.*, (43):67–97, 1990. doi:10.1115/1.3119162.

[108] M. Norton and D. Karczub. *Fundamentals of Noise and Vibration Analysis for Engineers*. Cambridge University Press, 2nd edition, 2003. doi:10.1017/CBO9781139163927.

[109] R. M. Orris and M. Petyt. A finite element study of harmonic wave propagation in periodic structures. *Journal of Sound and Vibration*, 33:223236, 1974. doi:10.1016/S0022-460X(74)80108-2.

[110] D. L. Palumbo and J. Klos. Development of quiet honeycomb panels. *Langley Research Center, Hampton, Virginia, NASA/TM-2009-215954*, 2009. URL: http://ntrs.nasa.gov/archive/nasa/casi.ntrs.nasa.gov/20090042975.pdf.

[111] P. Peters and S. Nutt. Wave speeds of honeycomb sandwich structures: An experimental approach. *International Journal of Non-Linear Mechanics*, 71(2):115–119, 2010. doi:10.1016/j.apacoust.2009.07.017.

[112] P. Peters and S. Nutt. Wave speeds of honeycomb sandwich structures: An experimental approach. *Applied Acoustics*, 71:115119, September 2010. doi:10.1016/j.apacoust.2009.07.017.

[113] M. Petyt. *Introduction to finite element vibration analysis*. Cambridge University Press, 1990. doi:10.1017/CBO9780511624292.

[114] C. N. Phan, Y. Frostig, and G. A. Kardomateas. Free vibration of unidirectional sandwich panels, part ii: Incompressible core. *Journal of Sandwich Structures and Materials*, 15(4):412–428, June 2013. doi:10.1177/1099636213485520.

[115] P. K. Raju and M. J. Crocker. Prediction of sound transmission through double walled systems containing helium. *The Journal of the Acoustical Society of America*, 78(1):S59, 1985. doi:10.1121/1.2022899.

[116] J. N. Reddy. *Mechanics of laminated composite plates and shells: Theory and analysis*. Boca Raton, FL: CRC Press, 1997. URL: http://www.tamu.edu/faculty/jnreddy/acml_old/Books/Book-9_FM.pdf.

[117] J. N. Reddy. *Energy Principles and Variational Methods in Applied Mechanics*. John Wiley, 2002. URL: http://eu.wiley.com/WileyCDA/WileyTitle/productCd-047117985X.html.

[118] J. N. Reddy and D. H. Robbins. Theories and computational models for composite laminates. *Applied Mechanics Review*, 6(47):147–167, 1994. doi:10.1115/1.3111076.

[119] J.N. Reddy. *Mechanics of Laminated Composite Plates: Theory and Analysis*. CRC Press, Boca Raton, 1996.

[120] E. Reissner. On the theory of bending of elastic plates. *Journal of Mathematics and Physics*, 23(1-4):184–191, 1944. doi:10.1002/sapm1944231184.

[121] E. Reissner and Y. Stavsky. Bending and stretching of certain types of anisotropic elastic plates. *Journal of Applied Mechanics*, (28):402–408, 1961.

[122] K. Renji. Sound transmission loss of unbounded panels in bending vibration considering transverse shear deformation. *Journal of Sound and Vibration*, 283:478–486, 2005. doi:10.1016/j.compstruct.2010.04.014.

[123] K. Renji and P. S. Nair. Modal density of composite honeycomb sandwich panels. *Journal of Sound and Vibration*, 195(5):687–699, January 1996. doi:10.1006/jsvi.1996.0456.

[124] K. Renji, P. S. Nair, and S. Narayanan. Critical and coincidence frequencies of flat panels. *Journal of Sound and Vibration*, 205(1):1932, 1997. doi:10.1006/jsvi.1997.0992.

[125] D. Rhazi and N. Atalla. A simple method to account for size effects in the transfer matrix method. *Journal of the Acoustical Society of America*, 127(2):EL30–EL36, 2010. doi:10.1121/1.3280237.

[126] J.H. Rindel. Dispersion and absorption of structure-borne sound in acoustically thick plates. *Applied Acoustics*, 41(2):97–111, 1994. doi:10.1016/0003-682X(94)90063-9.

[127] Y. V. K. Sadasiva Rao and B. C. Nakra. Vibrations of unsymmetrical sandwich beams and plates with viscoelastic cores. *Journal of Sound and Vibration*, 3(34):309–326, 1974. doi:10.1016/S0022-460X(74)80315-9.

[128] M. Sathyamoorthy. Nonlinear vibration analysis of plates: A review and survey of current developments. *Applied Mechanics Reviews*, 40(11):1553–1561, 1987. doi:10.1115/1.3149544.

[129] T. D. Scharton and R. H. Lyon. Power flow and energy sharing in random vibration. *Journal Acoustical Society of America*, 6(43):1332–1343, May 1968. doi:10.1121/1.1910990.

[130] M. D. Sciuva. An improved shear-deformation theory for moderately thick multilayered anisotropic shells and plates. *Journal of Applied Mechanics*, 3(54):589–596, 1987. doi:10.1115/1.3173074.

[131] Q. Serra, M.N. Ichchou, and J.-F. Deü. Wave properties in poroelastic media using a wave finite element methods. *Journal of Sound and Vibration*, 335:125146, 2015. doi:10.1016/j.jsv.2014.09.022.

[132] C. Shen, F. X. Xin, and T. J. Lu. Theoretical model for sound transmission through finite sandwich structures with corrugated core. *International Journal of Non-Linear Mechanics*, 47(10):1066–1072, 2012. doi:10.1016/j.ijnonlinmec.2011.09.014.

[133] M. H. Shojaeefard, R. Talebitooti, R. Ahmadi, and Ranjbar B. A study on acoustic behavior of poroelastic media bonded between laminated composite panels. *Latin American Journal of Solids and Structures*, 11(13):2379–2407, June 2014. doi:10.1590/S1679-78252014001300004.

[134] P. W. Smith. Responses and radiation of structural modes excited by sound. *Acoustical Society of America*, 34(5):640–647, May 1962. doi:10.1121/1.1918178.

[135] Y. Stavsky. Bending and stretching of laminated anisotropic plates. *Journal of Engineering Mechanics*, EM6(87):31–56, 1961.

[136] M. Stein and J. Mayers. A small-deflection theory for curved sandwich plates. *NACA report 1008*, 1951. URL: http://ntrs.nasa.gov/archive/nasa/casi.ntrs.nasa.gov/19930091092.pdf.

[137] J. W. S. Strutt and B. Rayleigh. *The theory of sound*. second edition, vol.1, 1877. URL: https://archive.org/details/theorysound06raylgoog.

[138] C. T. Sun. Theory of laminated plates. *Journal of Applied Mechanics*, (38):231–238, 1971. doi:10.1115/1.3408748.

[139] C. T. Sun and J. M. Whitney. Theories for the dynamic response of laminated plates. *AIAA Journal*, 2(11):178–183, 1973. doi:10.2514/3.50448.

[140] C.E. Teh. *Dynamic Behaviour and Acoustic Fatigue of Isotropic and Anisotropic Panels under Combined Acoustic Excitation and Static in Plane Compression*. Ph.D. Thesis, Institute of Sound and Vibration Research, Southampton, 1989.

[141] S. Timoshenko. *Theory of Plates and Shells*. McGraw-Hill, New York, 416, 1959.

[142] S. Timoshenko, S. Weinsowsky-Krieger, and R.M. Jones. *Theory of Plates and Shells*. Mechanics of Composite Materials. International Student Edition, McGraw-Hill Kogakusha, Ltd., Tokyo, 51, 1975.

[143] B. Troclet, S. Vanpeperstraete, and M. O. Schott. *Experimental analysis of lift-off and aerodynamic noise on the Ariane 5 launch vehicle*. In Proceedings of First Joint CEAS/AIAA Aeroacoustics Conference, Munich, Allemagne, Juin 1995.

[144] Bernard Troclet. *Analyse énergétique des vibrations sous sollicitations aéroacoustiques et validation dans lindustrie spatiale*. Mémoire dHabilitation à diriger des Recherches, 2007. URL: http://w3.lmt.ens-cachan.fr/PDFs/TROCLET.2007.1.pdf.

[145] Y. S. Uflyand. The propagation of waves in the transverse vibrations of bars and plates (in russian). *Akademii Nauk SSSR, Prikladnaya Matematika i Mekhanika*, pages 287–300, 1948.

[146] E. E. Ungar. Statistical energy analysis of vibrating systems. *ASME : Journal of Manufacturing Science and Engineering*, 89(4):626–632, August 1967. doi:10.1115/1.3610123.

[147] M. Villot, C. Guigou, and L. Gagliardini. Predicting the acoustical radiation of finite size multi-layered structures by applying spatial windowing on infinite structures. *Journal of Sound and Vibration*, 245(3):433–455, 2001. doi:10.1006/jsvi.2001.3592.

[148] J. Wang, T. J. Lu, J. Woodhouse, R. S. Langley, and J. Evans. Sound transmission through lightweight double-leaf partitions: theoretical modelling. *Journal of Sound and Vibration*, 286(4-5):817–847, 2005. doi:10.1016/j.jsv.2004.10.020.

[149] G. B. Warburton. *The Dynamical Behaviour of Structures*. Oxford: Pergamon Press, 1964. URL: http://www.sciencedirect.com/science/book/9780080203645.

[150] R.G. White. Effects of non-linearity due to large deflections in the resonance testing of structures. *Journal of Sound and Vibration*, 16(2):255–267, 1971. doi:10.1016/0022-460X(71)90486-X.

[151] R.G. White. Some measurements of the dynamic mechanical properties of mixed, carbon fiber reinforced plastic beams and plates. *Aeronautical Journal*, 79(2):318–325, 1975.

[152] R.G. White. A comparison of some statistical properties of the responses of aluminum and cfrp plates to acoustic excitation. *Composites*, 9(4):251–258, 1978. doi:10.1016/0010-4361(78)90178-7.

[153] R.G. White. *The acoustic excitation and fatigue of composite plates*. Proceedings of the 29th AIAA/ASME Structures, Structural Dynamics and Materials Conference, Williamsburg, Paper 88-2242, 253-260, 1988.

[154] R.G. White and E.M.Y. Abdin. Dynamic properties of aligned short carbon fiber-reinforced plastics in flexure and torsion. *Composites*, 16(2):293–306, 1985. doi:10.1016/0010-4361(85)90282-4.

[155] R.G. White and R.F. Mousley. *Dynamic response of CFRP plates under the action of random acoustic loading*. Proceedings of the Fourth International Conference on Composite Structures, Paisley College of Technology, 1519-1535, 1987.

[156] J. M. Whitney and A. W. Leissa. Analysis of heterogeneous anisotropic plates. *Journal of applied mechanics*, 2(36):261–266, 1969. doi:10.1115/1.3564618.

[157] J. P. D. Wilkinson. Modal densities of certain shallow structural elements. *The Journal of the Acoustical Society of America*, 43(2):245251, 1968. doi:10.1121/1.1910773.

[158] H. Wolfe. *An experimental investigation of non-linear behaviour of beams and plates excited to high levels of dynamic response*. Ph.D. Thesis, University of Southampton, Southampton, 1995.

[159] F. X. Xin and T. J. Lu. Analytical modeling of sound transmission through clamped triple-panel partition separated by enclosed air cavities. *European Journal of Mechanics A/Solids*, 30(6):770–782, 2011. doi:10.1016/j.euromechsol.2011.04.013.

[160] P. C. Yang, C. H. Norris, and Y. Stavsky. Elastic wave propagation in heterogeneous plates. *International Journal of Solids and Structures*, (2):665–684, 1966. doi:10.1016/0020-7683(66)90045-X.

[161] Q. Zhang, X. Yang, P. Li, G. Huang, S. Feng, C. Shen, B. Han, X. Zhang, F. Jin, F. Xu, and T. J. Lu. Bioinspired engineering of honeycomb structure using nature to inspire human innovation. *Progress in Materials Science*, 74:332400, July 2015. doi:10.1016/j.pmatsci.2015.05.001.

[162] C. Zhou, M. N. Ichchou, J.-P. Lainé, and A. M. Zine. *Application of wave finite element method on reduced models for the analysis of flexural waves in periodic beams, April 2013 Marrakech - Maroc*. Medyna 2013 1st Euro-Mediterranean Conference on Structural Dynamics and Vibroacoustics. URL: http://medyna2013.sciencesconf.org/12875.

[163] C. Zhou, J. Lainé, M. Ichchou, and A. Zine. Multi-scale modelling for two-dimensional periodic structures using a combined mode/wave based approach. *Computers and Structures*, 145:145–162, July 2015. doi:10.1016/j.compstruc.2015.03.006.

[164] Changwei Zhou. *Wave and modal coupled approach for multiscale analysis of periodic structures*. Thesis of École centrale de Lyon, 2014. URL: http://bibli.ec-lyon.fr/exl-doc/TH_T2431_czhou.pdf.